LEVEL II

(12) 294 p.

(6) PROCEEDINGS OF LOW-SPEED BOUNDARY-LAYER TRANSITION WORKSHOP. II,

(10) William S. King
Mari Yokota

(11) Jan[redacted]78

(15) N00014-76-C-0852 NR

APPROVED FOR PUBLIC RELEASE; DISTRIBUTION UNLIMITED

(14) RAND/R-P-6119

notes

The Rand Paper Series

Papers are issued by The Rand Corporation as a service to its professional staff. Their purpose is to facilitate the exchange of ideas among those who share the author's research interests; Papers are not reports prepared in fulfillment of Rand's contracts or grants. Views expressed in a Paper are the author's own, and are not necessarily shared by Rand or its research sponsors.

The Rand Corporation
Santa Monica, California 90406

PREFACE

This paper contains the proceedings of the Low-Speed Boundary-Layer Transition Workshop: II, held at the offices of The Rand Corporation, Santa Monica, California, September 13-15, 1976. The Workshop was jointly sponsored by the Defense Advanced Research Projects Agency and the Office of Naval Research, and organized by The Rand Corporation. The proceedings, which have been given a limited circulation to ARPA and ONR, are here reproduced in Rand's Paper series for worldwide distribution.

The primary goal of the Workshop was to provide a forum to exchange current research results, to assess recent progress in laminar-flow technology, and to establish new, viable research goals. Consistent with this principal theme was the desire to provide an opportunity for researchers and engineering designers to interact and to develop a mutual appreciation of their respective efforts in improving the knowledge of transition. This paper was prepared from the camera-ready abstracts provided by the authors, and should be useful to hydrodynamicists, designers of submersibles, and others engaged in fluid mechanics research. Other related Rand publications include:

R-1752-ARPA/ONR, *Low-Speed Boundary-Layer Transition Workshop*, June 1975.

R-1789-ARPA, *Controlling the Separation of Laminar Boundary Layers in Water: Heating and Suction*, September 1975.

R-1863-ARPA, *The Effects of Wall Temperature and Suction on Laminar Boundary-Layer Stability*, April 1976.

R-1898-ARPA, *"e^9": Stability Theory and Boundary-Layer Transition*, February 1977.

R-1966-ARPA, *The Buoyancy and Variable Viscosity Effects on a Water Laminar Boundary Layer Along a Heated Longitudinal Horizontal Cylinder*, February 1977.

R-2111-ARPA, *Entry Flow in a Heated Tube*, June 1977.

R-2165-ARPA, *Approximate Methods for Calculating the Properties of Laminar Boundary Layers in Water* (to be published).

ACKNOWLEDGMENTS

The generous support of this Workshop by the Defense Advanced Research Projects Agency and the Office of Naval Research is acknowledged. A grateful acknowledgment is extended to Drs. George Donahue and P. Selwyn of ARPA and Mr. Ralph Cooper and Mr. Stanley Doroff of ONR for their helpful suggestions and ideas on the Workshop program. The notable contributions of the session chairmen, Professor Mark V. Morkovin, Illinois Institute of Technology, Dr. A. M. O. Smith, University of California at Los Angeles, Dr. Leslie Mack of the Jet Propulsion Laboratory, and Dr. J. Aroesty of The Rand Corporation, and the keynote speaker, Professor Eli Reshotko, of Case Western Reserve University, merit recognition. Special thanks are due to N. Lippert and L. Chansler of The Rand Corporation for assistance in organizing and running the Workshop.

CONTENTS

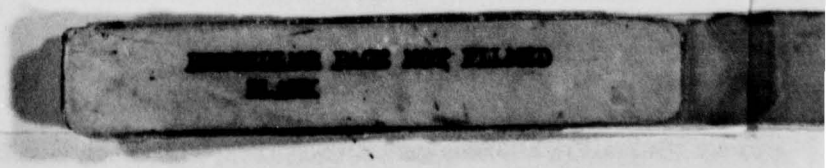

Major subject areas discussed include: Numerical Investigations of Navier-Stokes Equation; Transition and Stability Theory;

(cont'd p viii)

SECTION VI - THE DESIGN AND PARAMETRIC STUDIES OF LAMINAR FLOW BODIES

INFORMAL PRESENTATIONS

INTRODUCTION

The Low-Speed Boundary-Layer Transition Workshop was held on September 13 to September 15, 1976 at the Rand Corporation, Santa Monica. The purpose of the Workshop was to provide a forum to exchange current research results, to assess recent progress in laminar-flow technology and to establish viable new research goals. In support of these goals, one specific aim was to provide an opportunity for researchers and engineering designers to interact and to develop a mutual appreciation of their respective efforts in improving our knowledge of transition.

Research into the fundamental aspects of boundary-layer transition has advanced relatively rapidly during recent years. Improved experimental protocol is providing a wealth of data that both substantiates and even surpasses available theory. The catalyst for the rapid development in theoretical research has been improved analytical techniques and faster, larger computers. The large number of research papers presented at the Workshop attest to the vigor of the current revival in transition research.

Concurrent with advances in research have been advances in the engineering art of applied laminar-flow technology. A principal reason for this renewed interest is the reduced availability of energy. Consequently the desire to improve performance and reduce energy consumption for both civilian and military applications has inspired design and development studies of long-range aircraft, high speed ground transportation, and high performance underwater vehicles. Designs are available that would exploit laminar flow technology, and performance estimates have been made. However, this still appears to be an area of highly specialized expertise and intuition. What is needed is a routine procedure for designing laminar-flow vehicles and estimating their performance. Several such procedures were introduced at the Workshop.

The Workshop was the second low-speed boundary-layer transition workshop with joint sponsorship of ARPA and ONR and organized by Rand. Attendance was by invitation, and there were 110 participants and 32

invited papers were presented in the six sessions. The papers were divided according to subject matter and this resulted in the following sessions:

I. Numerical Investigations of Navier-Stokes Equation

II. Transition and Stability Theory

III. Predictions of Transition by Model Equations

IV. The Effects of Free Stream Disturbances and Surface Roughness on Transition

V. Experimental Investigations of Transition

VI. The Design and Parametric Studies of Laminar Flow Bodies

This proceedings volume includes the meeting program, list of attendees, and abstracts of the papers.

Program

LOW-SPEED BOUNDARY-LAYER TRANSITION WORKSHOP: II

Monday, September 13, 1976

8:30 a.m. WELCOME: Dr. E. C. Gritton, Head, Physical Sciences Department, The Rand Corporation

Laminar-Flow Research
Dr. G. L. Donohue, Defense Advanced Research Projects Agency

9:00 a.m. KEYNOTE SPEAKER: Dr. E. Reshotko, Case Western Reserve University

Morning Section: I. NUMERICAL INVESTIGATIONS OF NAVIER-STOKES EQUATIONS
Chairman: W. S. King, The Rand Corporation

I-1 *Numerical Investigation of Nonlinear Wave Interaction in a Two-Dimensional Boundary Layer*, J. W. Murdock and T. D. Taylor, The Aerospace Corporation

I-2 *Numerical Simulation of Transition Phenomena in Incompressible Flows*, H. Fasel, Institut A für Mechanik, Universität Stuttgart

I-3 *Fundamental Dynamical Aspects of Indeterminacy and Incompleteness of the Navier-Stokes Equations Bearing on Transition*, P. Lieber, K. S. Wen, and J. S. Marks, University of California, Berkeley

Afternoon Section: II. TRANSITION AND STABILITY THEORY
Chairman: L. M. Mack, Jet Propulsion Laboratory

II-1 *Numerical Simulation of Transition*, S. A. Orszag, Massachusetts Institute of Technology

II-2 *The Effects of Acceleration on the Growth Rate of Small Disturbances in a Laminar Boundary Layer*, C. von Kerczek, Naval Ship Research and Development Center

II-3 *On Boundary-Layer Transition Studies*, S. I. Cheng, Princeton University

II-4 *Transition, Pressure Gradient, Suction, Separation, and Stability Theory*, J. L. van Ingen, Delft University of Technology, The Netherlands

II-5 *Nonparallel Stability of Boundary Layers*, W. S. Saric and A. H. Nayfeh, Virginia Polytechnic Institute and State University

II-6 *Wave Mechanical Aspects of Transition*, M. T. Landahl, Massachusetts Institute of Technology

Tuesday, September 14, 1976

Morning Section: III. PREDICTIONS OF TRANSITION BY MODEL EQUATIONS
Chairman: M. V. Morkovin, Illinois Institute of Technology

III-1 *Theoretical and Experimental Transition Studies at ONERA/CERT*, R. Michel, ONERA-CERT-DERAT

III-2 *Turbulence-Model Predicted Effects of Surface Heat Transfer on Boundary-Layer Transition*, D. C. Wilcox and T. L. Chambers, DCW Industries, Inc.

III-3 *On the Application of Second-Order Closure Models to Boundary-Layer Transition*, M. L. Finson, Physical Sciences, Inc.

IV. THE EFFECTS OF FREESTREAM DISTURBANCES AND SURFACE ROUGHNESS ON TRANSITION
Chairman: M. V. Morkovin, Illinois Institute of Technology

IV-1 *An Analytical Study of the Effect of Surface Roughness on the Stability of a Heated Water Boundary Layer*, D. R. S. Ko and M. Kosecoff, Physical Dynamics, Inc.

IV-2 *On the Effect of Freestream Turbulence on Boundary-Layer Transition*, L. M. Mack, Jet Propulsion Laboratory

IV-3 *The Effects of Finite-Amplitude Disturbances on the Mean Flow Profiles in a Laminar Boundary Layer*, C. L. Merkle, D. R. S. Ko, and T. Kubota, Flow Research, Inc.

IV-4 *Fluctuations in a Boundary Layer Introduced by Traveling-Wave Irrotational Freestream Disturbances*, H. L. Rogler, Case Western Reserve University

Afternoon Section: V. EXPERIMENTAL INVESTIGATIONS OF TRANSITION
Chairman: A. M. O. Smith, University of California, Los Angeles

V-1 *Stability of a Heated Water Boundary Layer for Non-Uniform Wall Temperature Distributions*, A. Strazisar and E. Reshotko, Case Western Reserve University

V-2 *Transition in an Axisymmetric Boundary Layer with Wall Heating*, S. J. Barker, Poseidon Research and University of California, Los Angeles

V-3 *Pressure Fluctuations in the Transition Regions of Forebodies of Revolution*, T. T. Huang, Naval Ship Research and Development Center

V-4 *A Comparison between Measured and Computed Locations of Transition on Nine Forebodies of Revolution*, J. L. Power, Naval Ship Research and Development Center

Wednesday, September 15, 1976

VI. THE DESIGN AND PARAMETRIC STUDIES OF LAMINAR FLOW BODIES
Chairman: J. Aroesty, The Rand Corporation

VI-1 *The Combined Effects of Pressure Gradient and Heating on Boundary-Layer Stability and Transition*, A. R. Wazzan and C. Gazley, Jr., The Rand Corporation

VI-2 *Laminarization of Water Boundary Layers over Bodies of Revolution*, A. M. O. Smith and A. R. Wazzan, University of California, Los Angeles

VI-3 *A Study of Heat Addition Effects on Laminar, Water Boundary Layers of Axisymmetric Bodies*, J. J. Eisenhuth, Pennsylvania State University

VI-4 *Design of a Laminar, Low-Drag Research Vehicle*, R. S. Scotti, B. H. Carmichael, and D. A. King, Rockwell International

VI-5 *Axisymmetric Vehicle System Design for Total Propulsion Power Optimization*, F. R. Goldschmied, Westinghouse Research Laboratories

INFORMAL PRESENTATIONS

"Simple Relations for the Stability of Heated Laminar Boundary Layers in Water: Modified Dunn-Lin Method," J. Aroesty, et al., The Rand Corporation.

"Primary and Secondary Instabilities in Unstably Stratified Shear Flows," R. E. Kelly and R. M. Clever, University of California, Los Angeles.

"September 1976 Status Report on BLCS Research," T. G. Lang, Naval Undersea Center.

"Roughness Effects on Transition on an Ellipsoid," M. M. Reischman and G. L. Donohue, Naval Undersea Center.

LOW-SPEED BOUNDARY-LAYER TRANSITION WORKSHOP: II
September 1976

LIST OF ATTENDEES

ACOSTA, Professor Allan J.
Department of Mechanical Engineering
California Institute of Technology
Pasadena, California 91125
(213) 795-6841

AROESTY, Dr. Jerome
Physical Sciences Department
The Rand Corporation
1700 Main Street
Santa Monica, California 90406

BAKER, Richard
Aerospace Corporation
P. O. Box 92957
Los Angeles, California 90009
(213) 648-6103

BARKER, Professor Steven J.
Mechanics and Structures Department
School of Engineering
5731 Boelter Hall
University of California
Los Angeles, California 90024
(213) 825-7724

BEDDINI, Mr. Robert A.
Aeronautical Research Associates
of Princeton, Inc.
50 Washington Road
Princeton, New Jersey 08540
(609) 452-2950

CAGLE, Mr. Ben
Department of the Navy
Office of Naval Research
1030 East Green Street
Pasadena, California 91106
(213) 681-5264

CEBECI, Dr. Tuncer
McDonnell-Douglas Corporation
3855 Lakewood Boulevard
Long Beach, California 90801
(213) 593-5511

CHANG, Dr. I-Shih
Autonetics Division
Rockwell International Corporation
3370 Miraloma Avenue
P. O. Box 3105
Anaheim, California 92803

CHAPMAN, Mr. Robert M.
Office, Director of Defense, Research,
and Engineering
Department of Defense
Washington, D. C. 20301
(202) 697-2205

CHARWAT, Professor Andrew F.
School of Engineering and Applied Science
University of California
Los Angeles, California 90024
(213) 825-4197

CHENG, Professor Sin-I
Department of Aerospace and Mechanical
Sciences
Engineering Quadrangle
Princeton University
Princeton, New Jersey 08540

COX, Captain Henry, USN
ARPA/TTO
Defense Advanced Research Projects Agency
1400 Wilson Boulevard
Arlington, Virginia 22209

CRIMINALE, Professor William O., Jr.
Department of Oceanography
University of Washington
Seattle, Washington 98195

CROW, Professor Steven
School of Engineering and Applied Science
University of California
Los Angeles, California 90024
(213) 825-5653 or 825-2591

CULP, Mr. Claude R.
Deputy Vice President
National Security Division
The Rand Corporation
1700 Main Street
Santa Monica, California 90406

LOW-SPEED BOUNDARY-LAYER TRANSITION WORKSHOP: II (List of Attendees)

DONOHUE, Dr. George L.
Tactical Technology Office
Defense Advanced Research Project Agency
1400 Wilson Boulevard
Arlington, Virginia 22209
(202) 694-1903

DOROFF, Mr. Stanley W.
Office of Naval Research
Department of the Navy
Arlington, Virginia 22217
(202) 692-4021

EISENHUTH, Dr. Joseph J.
Applied Research Laboratory
The Pennsylvania State University
P. O. Box 30
State College, Pennsylvania 16801

ELLINGWOOD, Dr. John W.
Aerospace Corporation
P. O. Box 92957
Los Angeles, California 90009
(213) 648-7391

ELLISON, Dr. William
Cambridge Acoustical Associates, Inc.
1033 Massachusetts Avenue
Cambridge, Massachusetts 02138

FASEL, Dr. Hermann F.
Institut A. für Mechanik
University of Stuttgart
Keplerstrasse 17
Stuttgart 1
West Germany
(0711) 2073-2109

FINSON, Dr. Michael L.
Physical Sciences, Inc.
30 Commerce Way
Woburn, Massachusetts 01801

FITZGERALD, Dr. Thomas M.
Physical Sciences Department
The Rand Corporation
1700 Main Street
Santa Monica, California 90406

FRANZ, Mr. Gerald J.
Silencing Technology Associates
P. O. Box 695
Bayview, Idaho 83803
(208) 683-2845

FURUYA, Mr. Okitsugu
Tetra-Tech, Inc.
630 North Rosemead Boulevard
Pasadena, California 91107
(213) 449-6400

GAZLEY, Dr. Carl, Jr.
Physical Sciences Department
The Rand Corporation
1700 Main Street
Santa Monica, California 90406

GLOVER, Mr. Lynn W.
Undersea Systems Division
McDonnell Douglas Astronautics Corporation
5301 Bolsa Avenue
Huntington Beach, California 92647
(714) 896-3311

GODDARD, Dr. Frank Eber, Jr.
Jet Propulsion Laboratory
Building 180-701
4800 Oak Grove Drive
Pasadena, California 91103

GOLDSCHMIED, Fabio R.
Advisory Scientist
Heat Transfer and Fluid Dynamics Research
Westinghouse Electric Corporation
Research and Development Center
Beulah Road
Pittsburgh, Pennsylvania 15235
(412) 256-7634

GOODRICH, Mr. David
Naval Underwater Systems Center
Code SB323
Newport, Rhode Island 02840
(401) 841-2553

GRAN, Dr. Robert
Dynamics Technology, Inc.
3838 Carson Street
Torrance, California 90503
(213) 540-5557

LOW-SPEED BOUNDARY-LAYER TRANSITION WORKSHOP: II (List of Attendees)

GRANVILLE, Mr. Paul S. (Code 1541)
David Taylor Naval Ship Research and Development Center
Department of the Navy
Carderock Laboratory
Bethesda, Maryland 20034
(202) 227-1411

GRITTON, Dr. Eugene C., Head
Physical Sciences Department
The Rand Corporation
1700 Main Street
Santa Monica, California 90406

HAIGH, Mr. Wayne W.
Dynamics Technology, Inc.
3838 Carson Street
Torrance, California 90503
(213) 540-5557

HANSEN, Dr. Robert J.
Code 8441
Naval Research Laboratory
Washington, D. C. 20375
(202) 767-2904

HARLAND-WHITE, Mr. Todd B.
Westinghouse Electric Corporation
Oceanic Division
Box 1488
Annapolis, Maryland 21404
(301) 765-5508

HARPOLE, Mr. George
Physical Sciences Department
The Rand Corporation
1700 Main Street
Santa Monica, California 90406

HUANG, Thomas
David Taylor Naval Ship Research and Development Center
Department of the Navy
Bethesda, Maryland 20034
(202) 227-1340

HUGHES, Thomas
Mail Code 104-44
Division of Engineering and Applied Science
California Institute of Technology
Pasadena, California 91125
(213) 795-6811

JENNINGS, Mr. Carl G.
Autonetics Division
Rockwell International Corporation
3370 Miraloma Avenue
P. O. Box 4921
Anaheim, California 92803

JUNCOSA, Dr. Mario L.
Physical Sciences Department
The Rand Corporation
1700 Main Street
Santa Monica, California 90406

KAPLAN, Professor Richard E.
Department of Aerospace Engineering
University of Southern California
Los Angeles, California 90007
(213) 746-2511

KAUPS, Dr. Kalle
McDonnell-Douglas Corporation
3855 Lakewood Boulevard
Long Beach, California 90801
(213) 593-5511

KELLER, Professor Herbert
Department of Applied Mathematics
California Institute of Technology
Pasadena, California 91125
(213) 795-6811

KELLY, Dr. Robert E.
Mechanics and Structures Department
School of Engineering
University of California
Los Angeles, California 90024
(213) 825-5515

KENDALL, Dr. James M.
Jet Propulsion Laboratory
4800 Oak Grove Drive
Pasadena, California 91103
(213) 354-4321

KING, Dr. William S.
Physical Sciences Department
The Rand Corporation
1700 Main Street
Santa Monica, California 90406

LOW-SPEED BOUNDARY-LAYER TRANSITION WORKSHOP: II (List of Attendees)

KING, Mr. Douglas A.
Autonetics Division
Rockwell International Corporation
3370 Miraloma Avenue
P. O. Box 4921
Anaheim, California 92803

KLEBANOFF, Dr. Philip S.
Chief, Fluid Mechanics Section
Mechanics Division, IBS
U.S. Department of Commerce
National Bureau of Standards
Washington, D. C. 20234
(301) 921-3684

KNIGHT, Dr. Doyle
Applied Mathematics Department
California Institute of Technology
Pasadena, California 91125
(213) 795-6811

KO, Dr. Denny R. S.
Vice President
Dynamics Technology, Inc.
3838 Carson Street
Torrance, California 90503
(213) 540-5557

KOSECOFF, Dr. Michael A.
Physical Dynamics, Inc.
P. O. Box 2895
Torrance, California 90509
(213) 540-5557

KRALL, Mr. Kenneth M.
Vought Corporation
Advanced Technology Center, Inc.
P. O. Box 6144
Dallas, Texas 75222
(214) 266-7488

LANDAHL, Professor Marten T.
Department of Aeronautics and
Astronautics
School of Engineering
Massachusetts Institute of Technology
Cambridge, Massachusetts 02139
(617) 253-2261

LANG, Dr. Thomas G. (Code 251)
Head, Advanced Concepts Division
Department of the Navy
Navy Undersea Center
San Diego, California 92132
(714) 225-6495

LAUCHLE, Dr. Gerald C.
Applied Research Laboratory
The Pennsylvania State University
P. O. Box 30
State College, Pennsylvania 16801

LAUFER, Professor John
Head, Department of Aerospace Engineering
University of Southern California
Los Angeles, California 90007
(213) 746-2511

LEE, Mr. Richard S.
Undersea Systems Division
McDonnell-Douglas Corporation
5301 Bolsa Avenue
Huntington Beach, California 92647
(714) 896-3311

LEEHEY, Professor Patrick
Department of Ocean Engineering
Massachusetts Institute of Technology
Room 5-222
Cambridge, Massachusetts 02139
(617) 253-4337

LEWIS, Dr. John E.
Poseidon Research
Suite 641
11777 San Vicente Boulevard
Los Angeles, California 90049
(213) 826-5543

LIEBER, Professor Paul
Department of Mechanical Engineering
College of Engineering
University of California
Berkeley, California 94720
(415) 642-2863

LIN, Dr. Wen-Chin
David Taylor Naval Ship Research and
Development Center
Carderock, Maryland 20034
(202) 227-1574

LIU, Mr. Tony
Dynamics Technology, Inc.
3838 Carson Street
Torrance, California 90503
(213) 540-5557

LOW-SPEED BOUNDARY-LAYER TRANSITION WORKSHOP: II (List of Attendees)

McCARTHY, Mr. Justin H.
David Taylor Naval Ship Research and Development Center
Carderock, Maryland 20034
(202) 227-1865

MACK, Dr. Leslie M.
Jet Propulsion Laboratory
4800 Oak Grove Drive
Pasadena, California 91103
(213) 354-4321

MAGER, Dr. Artur
Aerospace Corporation
P. O. Box 95085
Los Angeles, California 90009

MANNING, Mr. Robert W.
Naval Sea Systems Command
PMS-395-A412
Washington, D. C. 20362
(202) 692-3920

MARKS, Mr. Jerry S.
Mechanical Engineering Department
University of California
Berkeley, California 94720

MENG, Dr. James C-S.
Science Applications, Inc.
1200 Prospect Street
P. O. Box 2351
La Jolla, California 92037
(714) 459-0211

MERKLE, Dr. Charles
Dynamics Technology, Inc.
3838 Carson Street
Torrance, California 90503
(213) 540-5557

MICHEL, M. Roger
Chef du Département d'Aérothermodynamique
ONERA/CERT
2, avenue Edouart Belin
31055 - Toulouse
FRANCE

MILLER, Dr. Richard T.
Associate Professor of Mathematics
Michigan State University
East Lansing, Michigan 48823

MINDAK, Mr. Robert J.
Office of Naval Research
Code 438
Arlington, Virginia 22217
(202) 692-4305

MONS, Dr. Robert F.
Westinghouse Electric Corporation
Oceanic Division
P. O. Box 1488
Annapolis, Maryland 21404
(301) 765-5515

MORKOVIN, Professor Mark V.
Department of Mechanics and Mechanical and Aerospace Engineering
Illinois Institute of Technology
3300 South Federal Street
Chicago, Illinois 60616
(312) 225-9600

MURDOCK, Dr. John W.
Aerospace Corporation
P. O. Box 92957
Los Angeles, California 90009
(213) 648-6103

MURMAN, Dr. Earll M.
Flow Research, Inc.
1819 South Central Avenue
Kent, Washington 98031
(206) 854-9590

NADOLINK, Richard H.
Naval Underwater Systems Center
Code SB323
Newport, Rhode Island 02840
(401) 841-2553

NELSON, David
Naval Undersea Center
San Diego, California 92132

LOW-SPEED BOUNDARY-LAYER TRANSITION WORKSHOP: II (List of Attendees)

ORMAND, Lt. Col. Lowell
Office of Scientific Research
AFOSR/NA Building 410
Bolling Air Force Base, D. C. 20332
(202) 693-0022

ORSZAG, Dr. Steven A.
Department of Mathematics
Massachusetts Institute of Technology
Cambridge, Massachusetts 02139
(617) 253-4987

PARKIN, Professor Blaine R.
Applied Research Laboratory
Pennsylvania State University
P. O. Box 30
State College, Pennsylvania 16801
(814) 865-1741

PEIRCE, Dr. Thomas E. (NSEA-0351)
Director, Research and Technology
Naval Sea Systems Command
Department of the Navy
Arlington, Virginia 20362
(202) 692-1151

REDA, Dr. Daniel C.
Code WA 42
Naval Surface Weapons Center
Silver Spring, Maryland 20910
(202) 394-2323

REISCHMAN, Dr. Michael M.
Naval Undersea Center
Code 2542
San Diego, California 92132
(714) 225-2461

RESHOTKO, Professor Eli
Case Western Reserve University
Cleveland, Ohio 44106
(216) 368-2940

ROBINSON, Mr. James H.
Code 1522
David Taylor Naval Ship Research and
Development Center
Carderock Laboratory
Bethesda, Maryland 20034
(202) 227-1347

ROGERS, Kenneth H.
Northrup Corp., Ventura Division
1515 Rancho Conejo Boulevard
Newbury Park, California 91320
(805) 498-3131

ROGERS, Dr. Milton S.
Directorate of Aeromechanics and
Energetics
Office of Scientific Research
Headquarters, United States Air Force
1400 Wilson Boulevard
Arlington, Virginia 22209
(202) 693-0016

ROGLER, Dr. Harold L.
Case Institute of Technology
Glennan Building, University Circle
Case Western Reserve University
Cleveland, Ohio 44106
(216) 368-2000

SAFFMAN, Professor Philip G.
Applied Mathematics Department
California Insitute of Technology
Pasadena, California 91125
(213) 795-6811

SARIC, William S.
College of Engineering
Virginia Polytechnic Institute and
State University
Blacksburg, Virginia 24061
(703) 951-6871

SCOTTI, Mr. Richard S.
Marine Systems Division
Autonetics Division
Rockwell International Corporation
3370 Miraloma Avenue, P. O. Box 4921
Anaheim, California 92803
(714) 632-4431

SELWYN, Dr. Philip A.
Institute for Defense Analyses
400 Army-Navy Drive
Arlington, Virginia 22202
(703) 558-1615

LOW-SPEED BOUNDARY-LAYER TRANSITION WORKSHOP: II (List of Attendees)

SHEN, Dr. John T. C.
David Taylor Naval Ship Research and Development Center
Mail Code 1942
Department of the Navy
Bethesda, Maryland 20034
(202) 227-1555

SMITH, Dr. A. M. O.
School of Engineering and Applied Science
University of California
Los Angeles, California 90024

SMITH, Lt. Col. Robert C.
Office of Scientific Research
AFOSR/NA, Building 410
Bolling Air Force Base, D. C. 20332
(202) 693-0016

SROKOWSKI, Mr. Andrew
Langley Research Center
National Aeronautics and Space Administration
Hampton, Virginia 23665
(804) 827-3735

STRAZISAR, Professor Anthony
Department of Fluid Thermal Sciences
Case Western Reserve University
Cleveland, Ohio 44106
(216) 368-2000

STEWARTSON, Professor Keith
Department of Mathematics
University College
Gower Street
London WC1E6BT
ENGLAND

STUHMILLER, Dr. James H.
JAYCOR
1401 Camino Del Mar
Del Mar, California 92014
(714) 453-6580

SWIGART, Mr. Rudy
Aerospace Corporation
P. O. Box 92957
Los Angeles, California 90009

TAYLOR, Dr. Thomas D.
Aerospace Corporation
P. O. Box 92957
Los Angeles, California 90009
(213) 648-6103

VAGLIO-LAURIN, Dr. Robert
General Applied Science Laboratory
Merrick and Stewart
Westbury, New York 11590
(516) 832-2554

van DRIEST, Dr. Edward R.
Physical Sciences Department
The Rand Corporation
1700 Main Street
Santa Monica, California 90406

van INGEN, Professor Jan L.
Department of Aeronautical Engineering
Delft University of Technology
1 Kluyverweg, Delft 2209
THE NETHERLANDS

VICTORIA, Dr. Keith J.
Science Applications, Inc.
1200 Prospect Street
P. O. Box 2351
La Jolla, California 92037
(714) 459-0211

von KERCZEK, Dr. Christopher
David Taylor Naval Ship Research and Development Center
Department of the Navy
Bethesda, Maryland 20034

WAGNER, Mr. Richard D.
Langley Research Center
National Aeronautics and Space Administration
Hampton, Virginia 23665
(804) 827-2045

WEN, Dr. Kwan Sun
Department of Mechanical Engineering
University of California
Berkeley, California 94720

LOW-SPEED BOUNDARY-LAYER TRANSITION WORKSHOP: II (List of Attendees)

WHITEHEAD, Mr. Robert E.
Vehicle Technology Program
Office of Naval Research
Department of the Navy
Arlington, Virginia 22217
(202) 692-4424

WHITNEY, Mr. Arthur K.
Lockheed Missiles and Space
Company, Inc.
3251 Hanover Street
Palo Alto, California 94304

WILCOX, Dr. David C.
President
DCW Industries, Inc.
4367 Troost Avenue
Studio City, California 91604
(213) 769-7571

WILMARTH, Professor William W.
University of Michigan
Department of Aerospace Engineering
College of Engineering
Ann Arbor, Michigan 48104
(313) 764-1817

WOLF, Dr. Calvin J.
Aerotherm
Division of Acurex Corporation
485 Clyde Avenue
Mountain View, California 94042
(415) 964-3200

WOOLLEY, Mr. James P.
Nielsen Engineering and Research
510 Clyde Avenue
Mountain View, California 94043

WORTMAN, Dr. Andrew
Northrup Corporation
Ventura Division
1515 Rancho Conejo Boulevard
Newbury Park, California 91320
(805) 498-3131

WYGNANSKI, Professor I.
(Until April 1977)
Department of Aerospace Engineering
University of Southern California
University Park
Los Angeles, California 90007

WYGNANSKI, Professor I.
(Permanent address)
Tel-Aviv University
School of Engineering
Ramat-Aviv, Tel-Aviv 69978
ISRAEL

YAO, Dr. Lun-Shin
Physical Sciences Department
The Rand Corporation
1700 Main Street
Santa Monica, California 90406

XERIKOS, James
Undersea Systems Division
McDonnell Douglas Corporation
5301 Bolsa Avenue
Huntington Beach, California 92647
(714) 896-3311

ZAKANYCZ, Dr. Stephen
Defense Advanced Research Projects Agency
Strategic Technology Office
1400 Wilson Boulevard
Arlington, Virginia 22209

Section I

NUMERICAL INVESTIGATION OF NONLINEAR WAVE INTERACTION IN A TWO-DIMENSIONAL BOUNDARY LAYER

I-1 Numerical Investigation of Nonlinear Wave Interaction in a Two-Dimensional Boundary Layer

John W. Murdock and Thomas D. Taylor
The Aerospace Corporation
P. O. Box 92957
Los Angeles, California 90009

The present work is the initial phase of a study whose purpose is to develop a computer code to solve the Navier-Stokes equations (or an appropriate simplified version of same) in the Reynolds number range of transition and to study the various stages of boundary layer transition. The unsteady, two-dimensional, Navier-Stokes equations as well as parabolized vorticity equations have been solved for flow over a flat plate. (The parabolized vorticity equations were obtained from the Navier-Stokes equations by neglecting the fourth order streamwise derivative of the stream function.) The physical problem considered is equivalent to that frequently used in wind tunnel investigations of linear stability and transition in which a two-dimensional, time-periodic, disturbance is introduced with a vibrating ribbon in the boundary layer. This situation is achieved numerically by imposing an upstream boundary condition, at a fixed location on a plate, which consists of the sum of the Blasius solution and a time-periodic solution to the Orr-Sommerfeld equation.

The dependent variables in the study were the stream function and vorticity; the independent variables were orthogonal parabolic coordinates. The equations were solved with a so-called spectral scheme which was selected because it can be more accurate for comparable machine storage than a finite difference method. The spectral scheme was implemented by expanding the dependent variables in Chebyshev polynomials in both space dimensions. The solution was developed by substituting the expansion into the flow equations and equating the coefficients of equal order polynomials. Since the coefficients are a function of time the result is a set of coupled ordinary differential equations. These equations have been solved by both implicit and explicit integration schemes for the complete equations and the parabolized equations.

There are four main results or conclusions which have been achieved to date. The first is that it is possible to solve the two-dimensional Navier-Stokes equations with non-trivial boundary conditions using an orthogonal function

expansion in both space dimensions. (A complete description of the numerics will be contained in a forthcoming paper.)

The second conclusion reached in this study is that for the type of flows considered the parabolized vorticity equations are an adequate model of the flow. This conclusion is substantiated by the fact that these equations were used to derive a modified Orr-Sommerfeld equation, the solution of which agreed with the solution of the usual Orr-Sommerfeld equation to 4 significant figures for a typical test case. This is not surprising if the order of magnitude of the various terms in the Orr-Sommerfeld equation is considered. (See for example Gaster (1).) Figure 1 shows a comparison of the Navier-Stokes calculations of Fasel (2) with the present parabolized vorticity computations. The agreement is excellent; similar agreement has been found between the present Navier-Stokes and parabolized vorticity solutions. This result is important since it has been possible to generate solutions to the parabolized vorticity equations in as much as one-twentieth the time required to solve the same physical problem with the Navier-Stokes equations. The saving arises because the additional boundary condition which must be imposed on the Navier-Stokes equations in general creates a thin boundary region at the downstream boundary of the computation. For numerical stability this boundary region must be resolved; this requires a fine spatial resolution and an associated decrease in the time step which, in general, substantially increases running time.

The third result of this work is that the nonlinear effects are initially destabilizing relative to the linear effects. That is to say that the boundary layer is more unstable to large disturbances than to small ones. This is an important result since previous analytic nonlinear stability analyses apply only to parallel flow and, in addition, are series expansions about the critical point. The present results are for a non-parallel boundary layer and may be obtained for arbitrary Reynolds number and disturbance wave form.

The nonlinear stability effects have been investigated by inputing Orr-Sommerfeld disturbances of an amplitude of about five percent of the mean flow at $R_x = 10^5$ and solving for the steady state disturbance downstream. In Figure 2 the computed linear ($A = 0.001$) and non linear ($A = 0.08$) wave forms are compared. Although the terms "linear" and "non linear" are used to distinguish between the two computations described herein, both results are solutions of the non linear parabolized vorticity equations. Figure 2 shows significant distortion from a modulated sinusoidial wave form by nonlinear effects as the wave propagates from $R_x = 10^5$ to 2.2×10^5.

Inspection of Figure 2 demonstrates that it is difficult to physically interpret the nonlinear effect by simply inspecting the variation of velocity as a function of R_x. (Note, however, that the broadened positive peaks and large narrow negative peaks are qualitatively similar to the hot wire measurements of Klebanoff and Tidstrom (3) taken in a boundary layer excited with a large amplitude Tollmien-Schlicting wave.) Because the boundary layer is being excited at a fixed dimensionless frequency, $\omega = 13.19$, it may be Fourier transformed in time once all transient effects are washed downstream. The Fourier amplitude of the perturbation velocity is illustrated in Figure 3 at the same station in the boundary layer as Figure 2. Figures 2 and 3 are at a station well down in the shear layer ($\eta = 0.2$); the Fourier amplitude at a station near the maximum of the input Orr-Sommerfeld solution is shown in Figure 4. The nonlinear curves ($A = 0.08$) in Figures 3 and 4 show that up to $R_x = 1.3 \times 10^5$ the primary mode is changed only slightly from the linear behavior while the second mode grows dramatically. Thus, in this range the nonlinear effects are destabilizing. Beyond this point the relative stability becomes to some extent a matter of definition.

The magnitude of the mean perturbation from the Blasius is also shown at selected points in Figures 3 and 4. It is clearly less important than the second harmonic. Higher harmonics are smaller than the mean and are therefore not shown.

Figures 3 and 4 show the Fourier amplitude of the perturbation as a function of R_x; it is also of interest to consider the variation across the boundary layer. As a point of reference consider first the linear behavior. Figure 5 shows the disturbance amplitude as input at $R_x = 10^5$; the corresponding curve at $R_x = 2.2 \times 10^5$ shows the peak is shifted in η-space as the wave propagates downstream and is amplified. The Fourier amplitudes of the various nonlinear modes at $R_x = 1.3 \times 10^5$ are shown in Figure 6. The primary mode shape is changed only slightly from the linear one. The general shape of the secondary is similar to the primary but the peak and phase reversal point are closer to the wall. The amplitude of the mean is positive near the wall with a smaller negative region adjacent. (Only absolute values are shown in the figure.) Figure 7 shows a similar result at $R_x = 2.2 \times 10^5$. In this case the normalized amplitude of the nonlinear primary is changed somewhat from the linear curve. The mean contribution again has a positive region near the wall followed by a now significant negative region.

Up to this point the results have emphasized the Fourier amplitude; it is also of interest to look at the phase relationship between the primary and

secondary disturbance. The usual analytic studies of nonlinear stability theory assume that the secondary is a harmonic in space as well as in time. Figure 8 shows a typical phase relationship between the two disturbances (where for convenience both amplitudes are normalized to unity). The results show that the secondary is very nearly a spatial harmonic of the primary. However, a particularly interesting feature of this curve is the rather abrupt change in the relative phase at about $R_x = 1.7 \times 10^5$ which is about the location of the change in shape of the secondary disturbance. Although this point needs further study, a tentative finding of this work is that small changes in the relative phase appear to be associated with significant changes in the growth/decay behavior of the secondary wave.

References

1. Gaster, M., "On the Effects of Boundary-Layer Growth," J. Fluid Mech., 66, 1974, p. 465.

2. Fasel, H. F., "Numerical Solution of the Unsteady Navier-Stokes Equations for the Investigation of Laminar Boundary Layer Stability," Proceedings of 4th International Conference on Numerical Methods in Fluid Mechanics, 1974.

3. Klebanoff, P. S. and K. D. Tidstrom, "Evolution of Amplified Waves Leading to Transition in a Boundary Layer with Zero Pressure Gradient," NASA TN D-195, 1959.

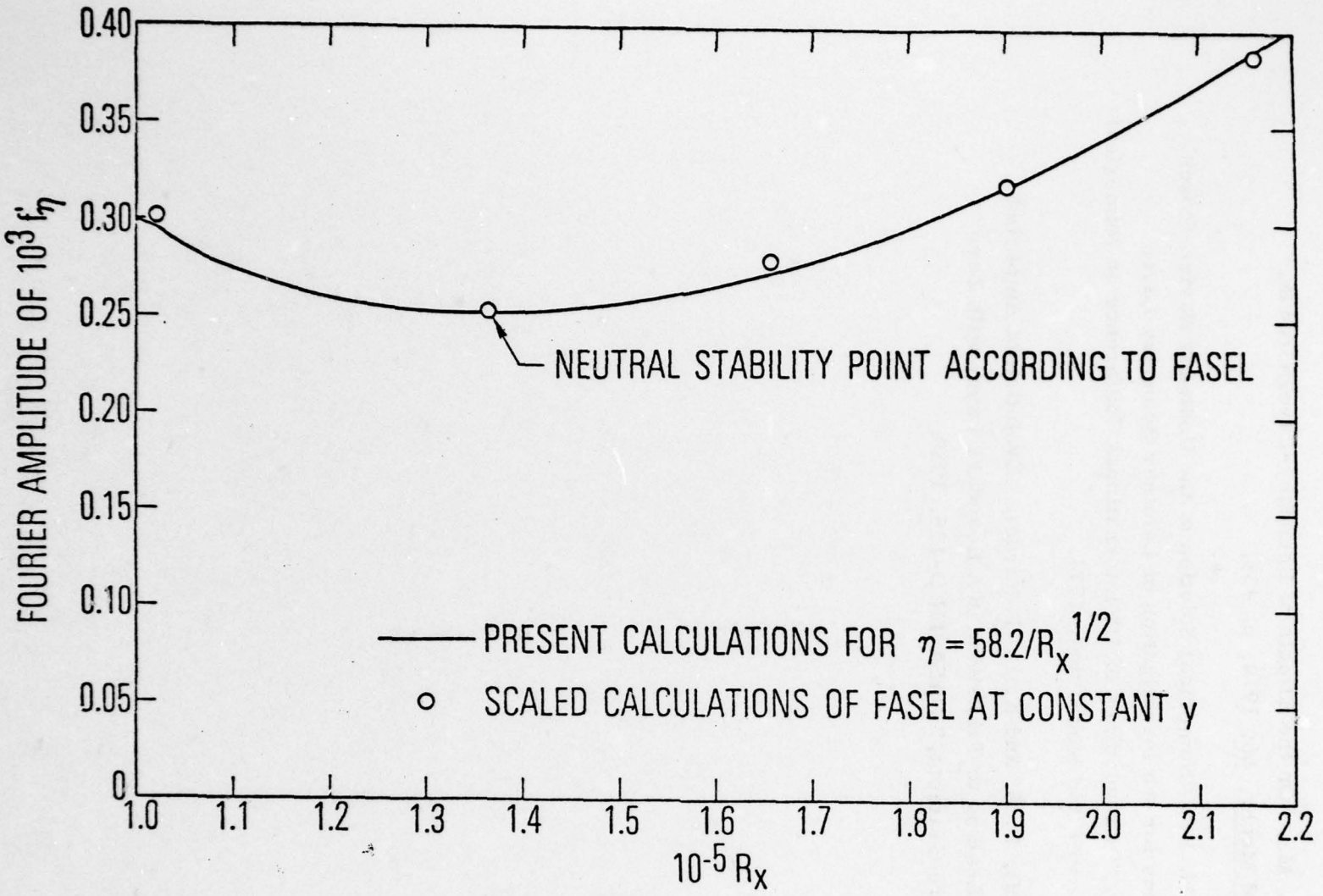

Fig. 1. Comparison of Amplitude of u with Results of Fasel

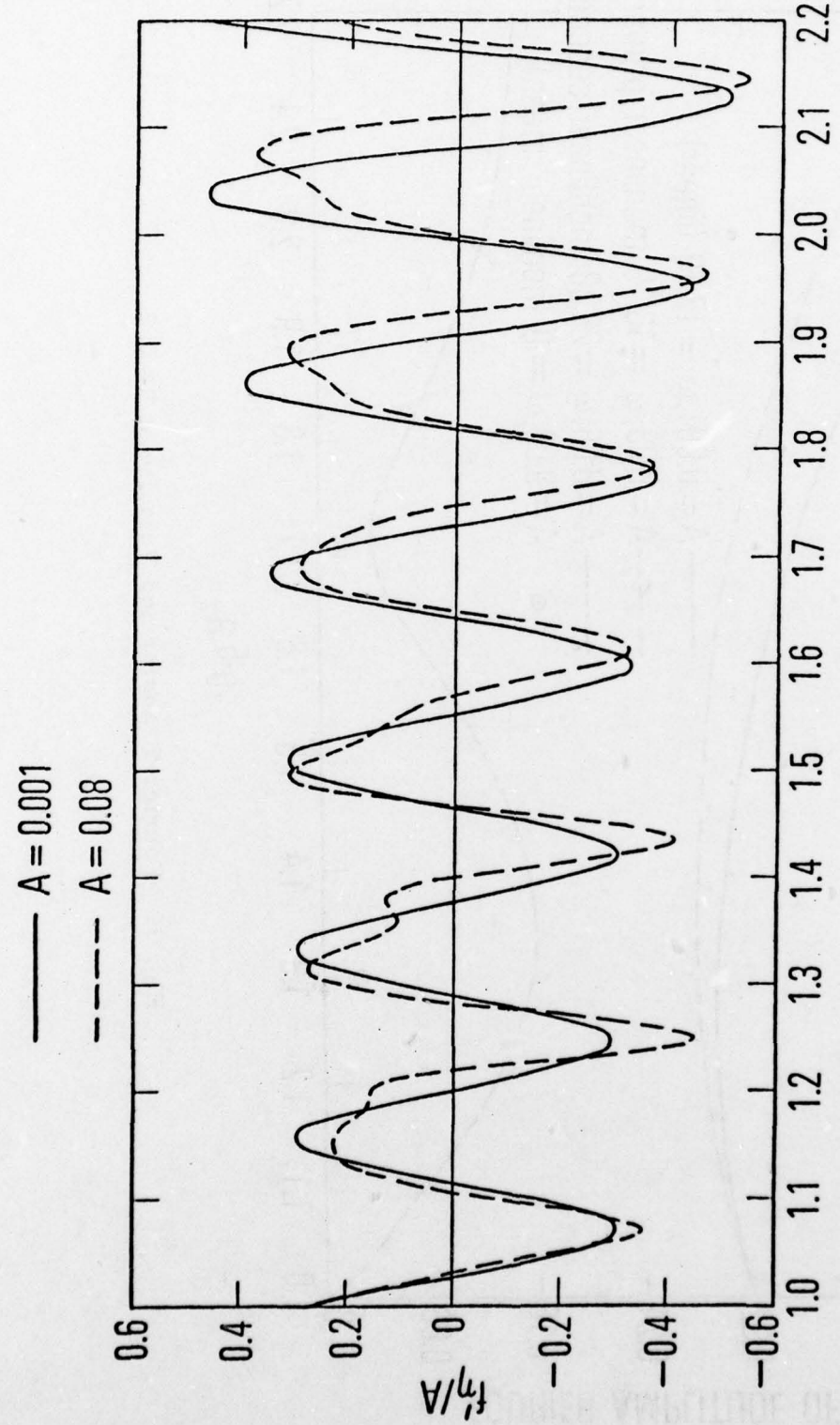

Fig. 2. Perturbation Velocity at $\eta = 0.2$, $\tau = 4.2265$

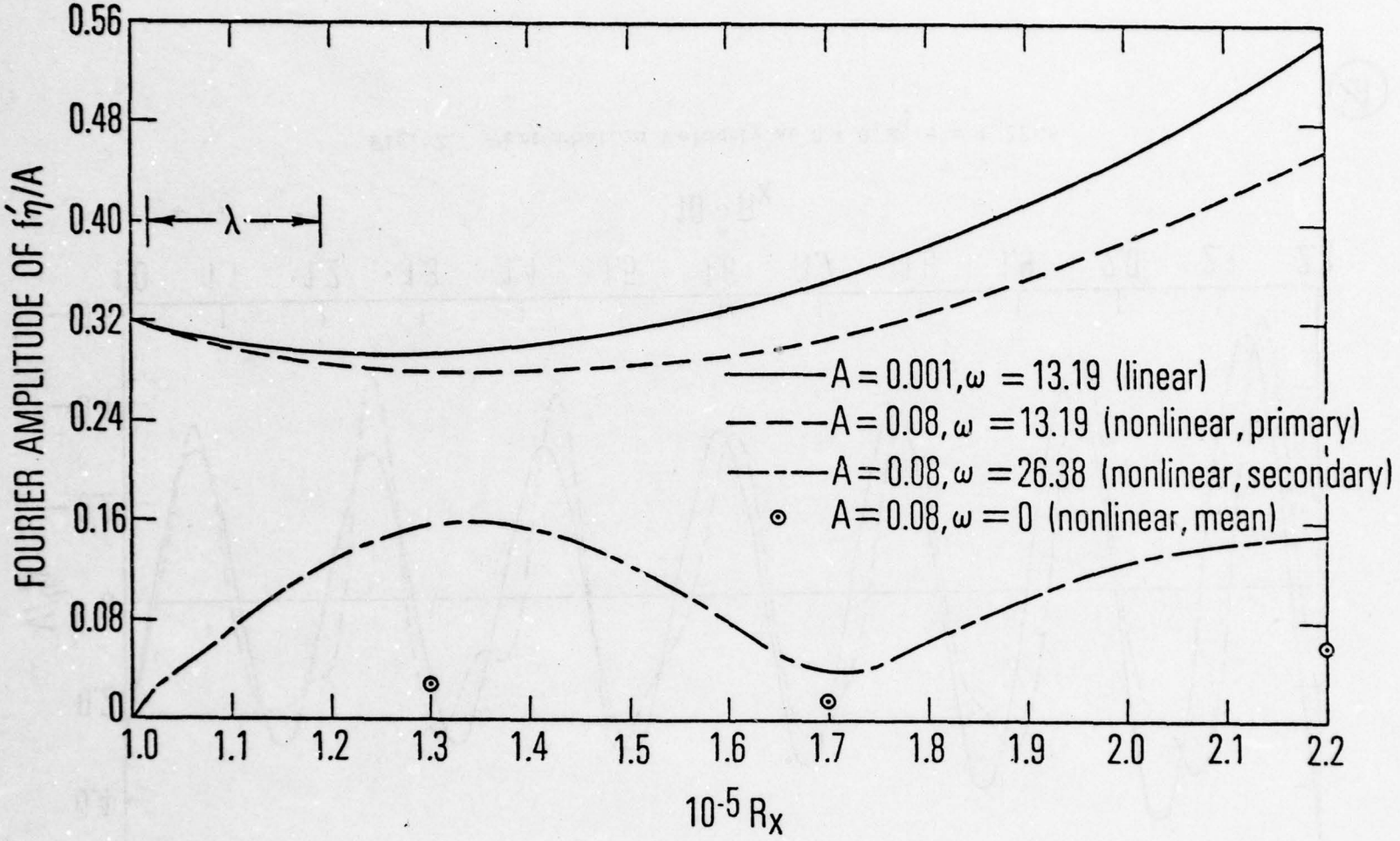

Fig. 3. Fourier Transformed Velocity at $\eta = 0.2$

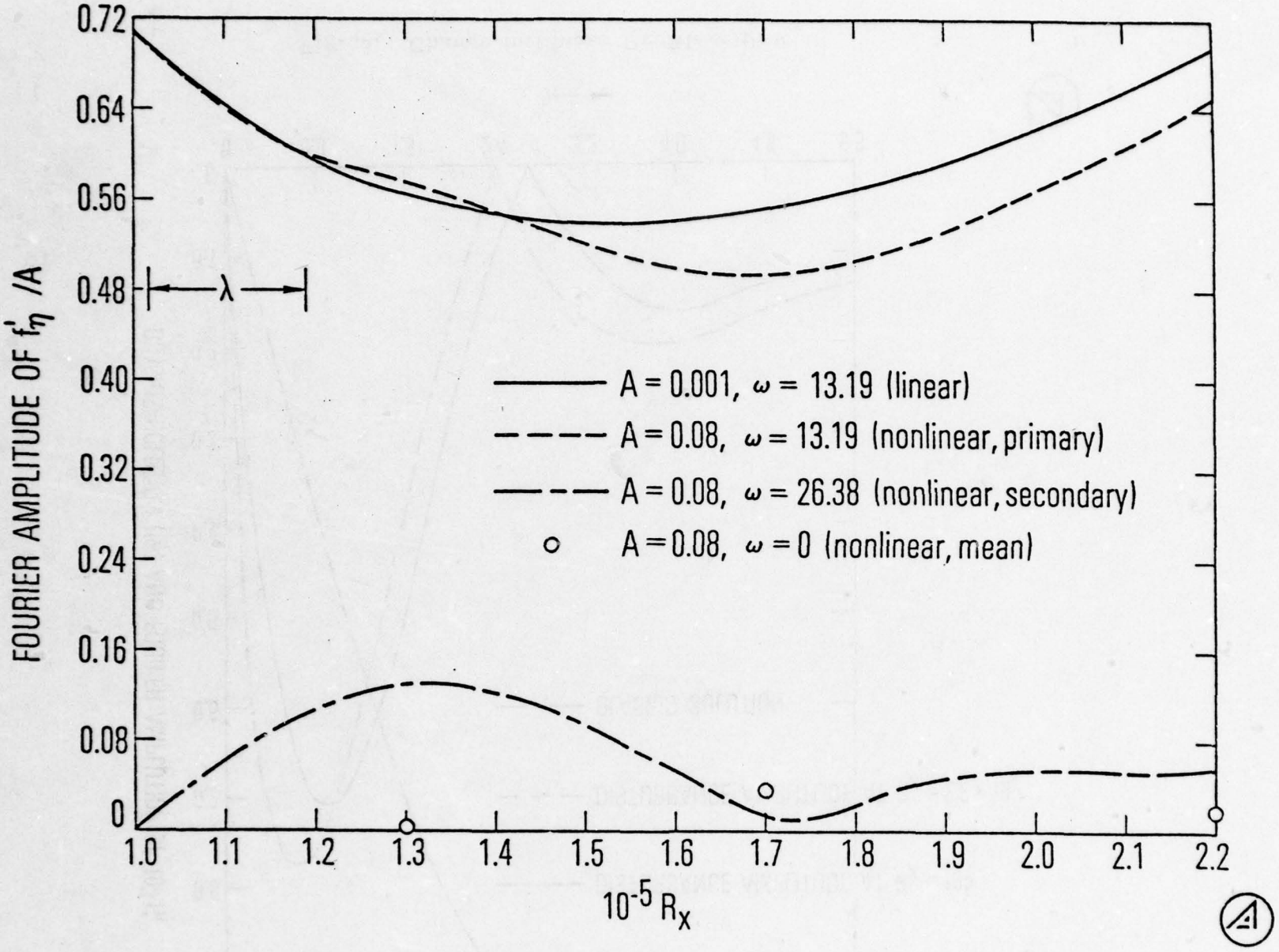

Fig. 4. Fourier Transformed Velocity at $\eta = 1.0$

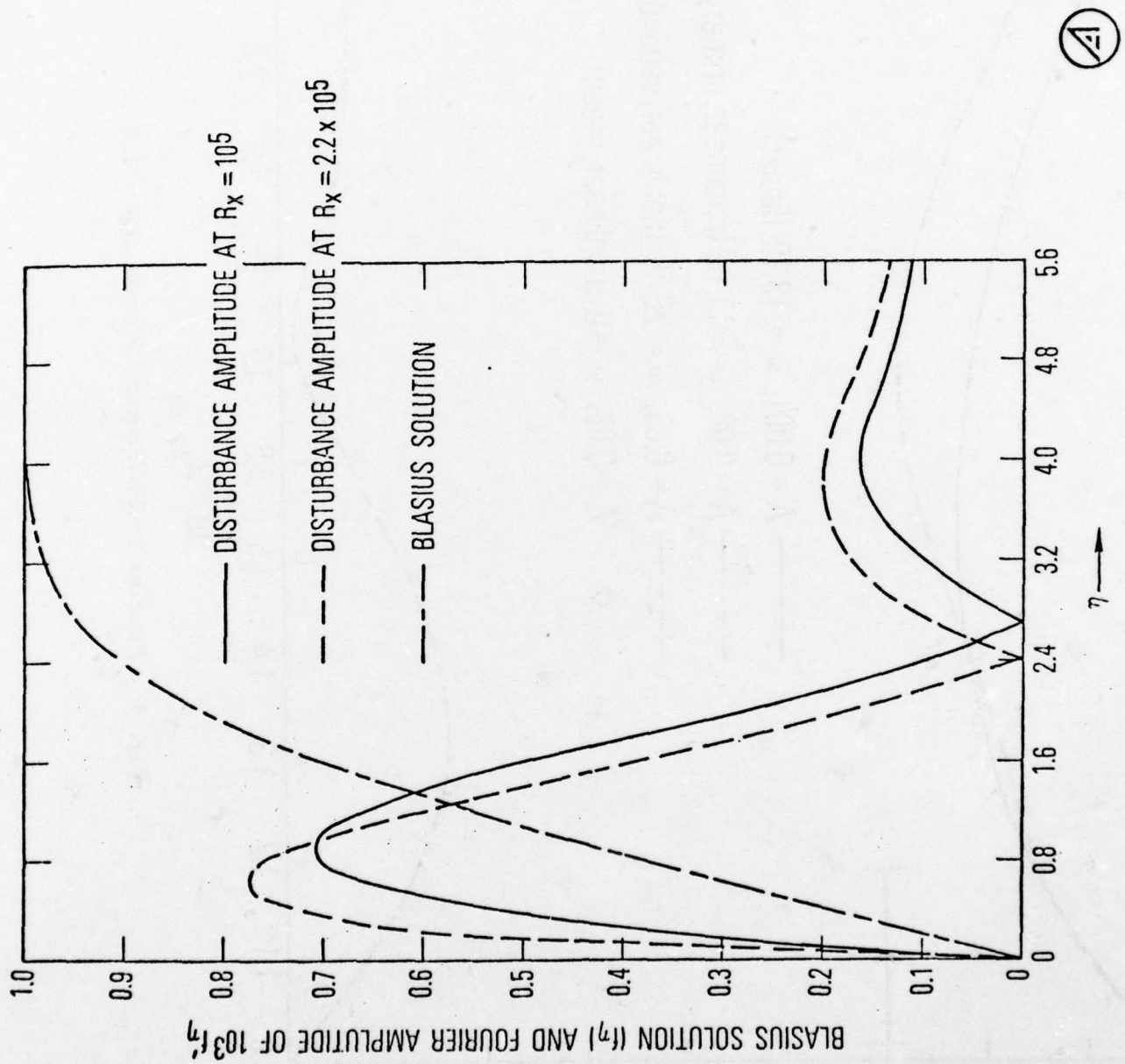

Fig. 5. Change in Linear Profile with R_x

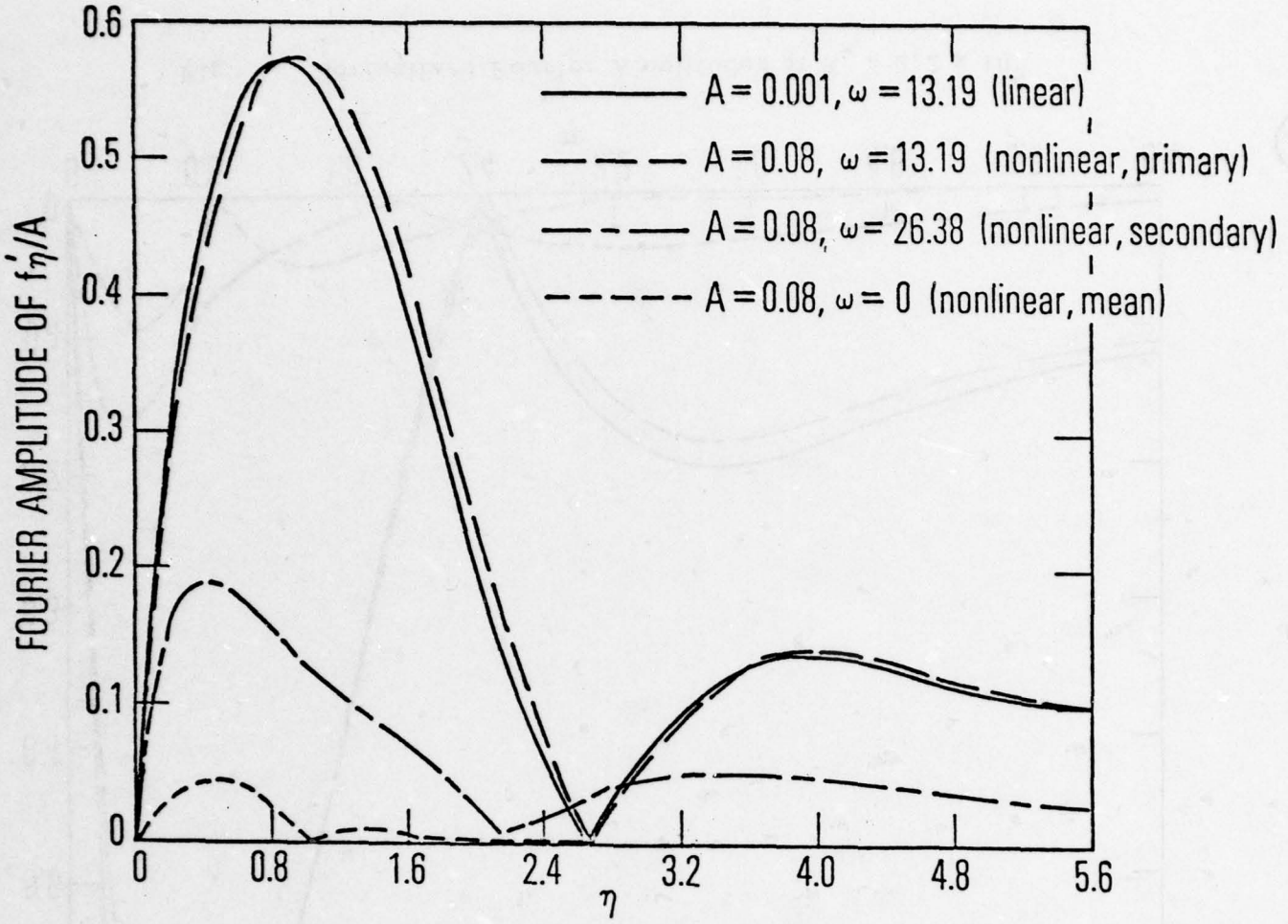

Fig. 6. Normalized Fourier Amplitudes at $R_x = 1.3 \times 10^5$

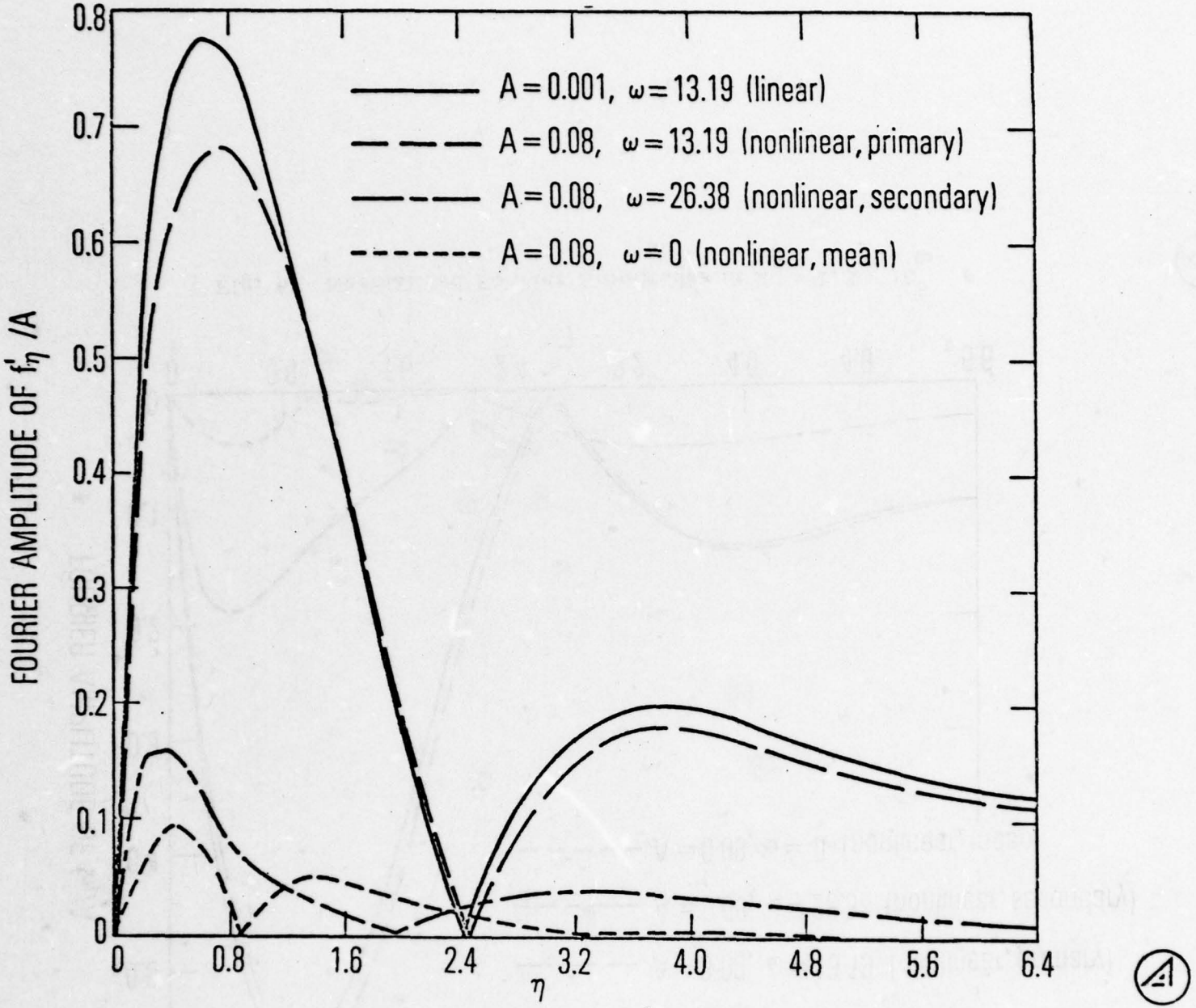

Fig. 7. Normalized Fourier Amplitudes at $R_x = 2.2 \times 10^5$

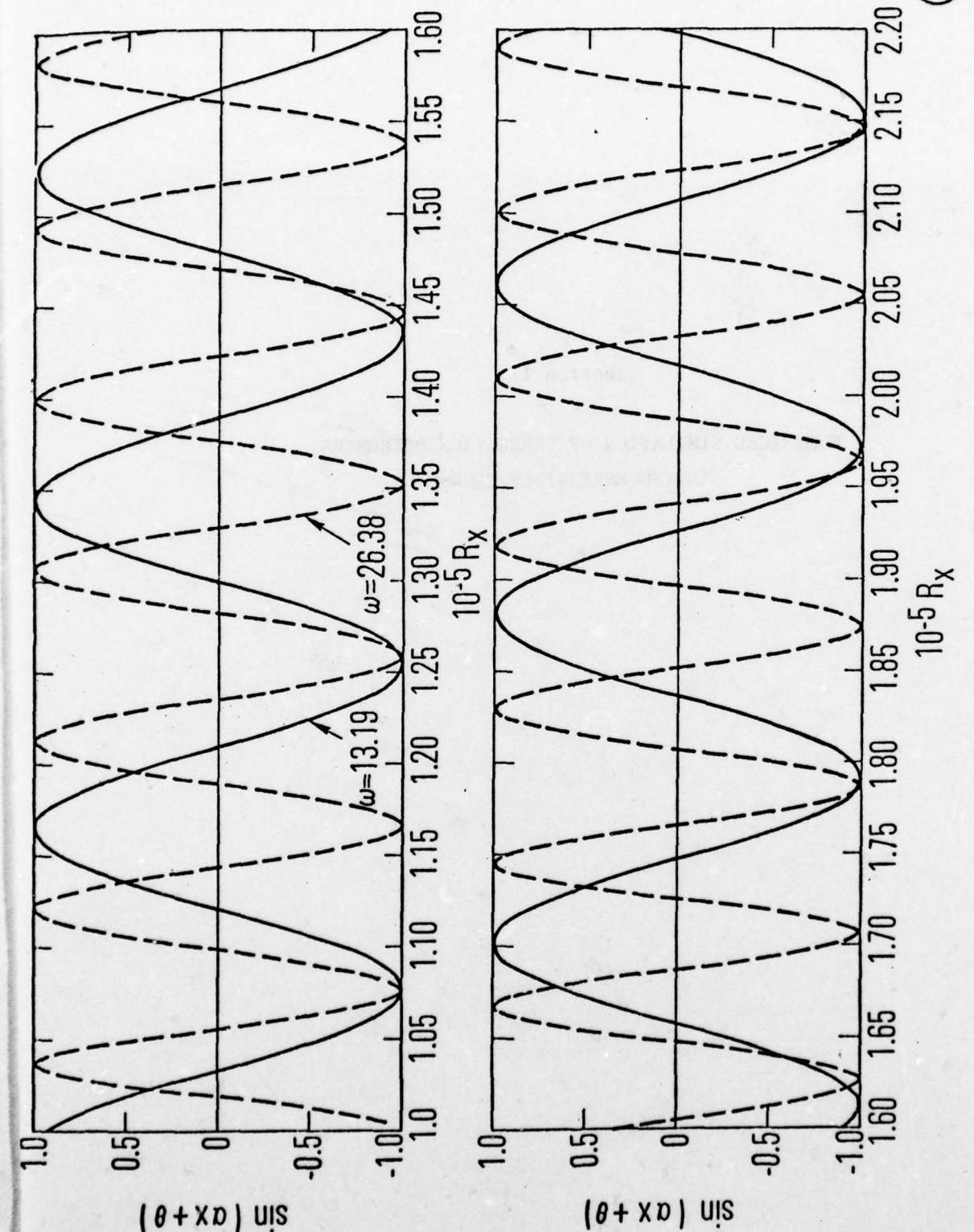

Fig. 8. Sine of the Phase Angle of the Primary and Secondary Wave at $\eta = 0.2$

Section I

NUMERICAL SIMULATION OF TRANSITION PHENOMENA IN INCOMPRESSIBLE FLOWS

I-2 NUMERICAL SIMULATION OF TRANSITION PHENOMENA IN INCOMPRESSIBLE FLOWS

H. Fasel
Institut A für Mechanik
Universität Stuttgart
Stuttgart, Germany

For the investigation of stability and phenomena of initial transition in incompressible, two-dimensional flows an implicit finite difference method for the solution of the complete Navier-Stokes equations was developed (1). The applicability of the numerical method for such investigations was demonstrated by simulations of Tollmien-Schlichting waves in boundary layer flows on a flat plate. In the numerical model these waves were produced by introducing periodic disturbances at the upstream boundary A-D of a rectangular integration domain (Figure 1). The reaction of the flow to such disturbances was then directly determined by solving the Navier-Stokes equations within the rectangular domain using appropriate boundary conditions.

For perturbations of very small amplitudes (maximum disturbance amplitude of stream-wise velocity component 0.05 percent of free stream velocity) extensive comparative calculations showed good agreement with linear stability theory and experimental measurements (2,3). Amplification of the disturbances occurred approximately in the same region of Reynolds number and disturbance frequency as in the experiments and in linear stability theory, particularly when non-parallel flow effects were taken into account in the linear stability theory analysis (4). A comparison of the numerically determined amplification rates and amplitude distributions of the disturbances with linear stability theory and experimental measurements was equally satisfactory.

The usefulness of the numerical model for stability and transition studies has been further tested by applying it to another type of flow, i.e. the plane Poiseuille flow between two parallel plates. It was possible to demonstrate that for small sinusoidal disturbances, which were introduced at a fixed downstream location, space-wise (in downstream direction) amplification of the disturbances can occur within a certain Reynolds number - frequency region. In Figure 2, for example, amplification curves for two typical test cases are shown, one for a stable and the other for an unstable disturbance. This evidence of spatially growing disturbances in plane Poiseuille flow was also verified experimentally by Nishioka et al. (5).

In the development of the numerical method it was possible to avoid any restrictions with regard to amplitude or form of the perturbations. Thus, the numerical model lends itself for the investigation of a number of other aspects of stability and transition for which treatment with other theoretical models becomes extremely difficult. One of the main points of interest in this field is focused on the investigation of later stages of the transition process which follow the amplification of unstable Tollmien-Schlichting waves.

For an investigation of the two-dimensional non-linear development in the transition process, numerical experiments are performed in which the boundary layer flow is disturbed at the upstream boundary A-D of the rectangular integration domain (Figure 1) with periodic perturbations of larger amplitudes. In these experiments, disturbance amplitudes of the stream-wise velocity component are increased up to 5 percent of the free stream velocity. In Figure 3 typical results are shown for calculations with a Reynolds number (based on displacement thickness) of 635 and a frequency parameter ($F = \beta\nu/U_\infty^2$) of $1.32 \cdot 10^{-4}$. In these calculations the loca-

tion of the upstream boundary corresponds to a point on the lower branch of the neutral curve of linear stability theory. The amplification curves for different disturbance amplitudes which are plotted in Figure 3 clearly indicate a dependency of the amplification rate on the amplitude of the disturbances. As expected, the influence of the magnitude of the disturbance amplitude for amplitudes below one percent is practically negligible. However, for larger amplitudes an increase in disturbance amplitude has considerable influence on the amplification rate of the disturbances.

In these investigations strong emphasis is also placed on a thorough study of the role of other harmonic disturbance wave components in the transition process. The numerical results indicate the existence of other harmonic wave components superimposed on the primary disturbance wave. The influence of these wave components seems to become more and more dominant when disturbance amplitudes are increased.

Another effort involves a detailed study of the influence of a single roughness element on the transition process in a flat plate boundary layer flow, corresponding to the experimental work of Klebanoff and Tidstrom (6). Because of the simpler geometry, however, a backward facing step was chosen as roughness element, as shown in Figure 4. In this study the step heights are ranging from one half to two displacement thicknesses. By means of comparative calculations with identical flow conditions for a flat plate with the step and without the step the effects of the roughness element on the transition processes can be clearly observed. For example, when random disturbances are introduced at a fixed downstream station, a certain selection process takes place for both cases where disturbances, that are, according to linear stability theory, most unstable for the particular Reynolds numbers, are singled out. However, the selection process is much more pronounced when the roughness element is present.

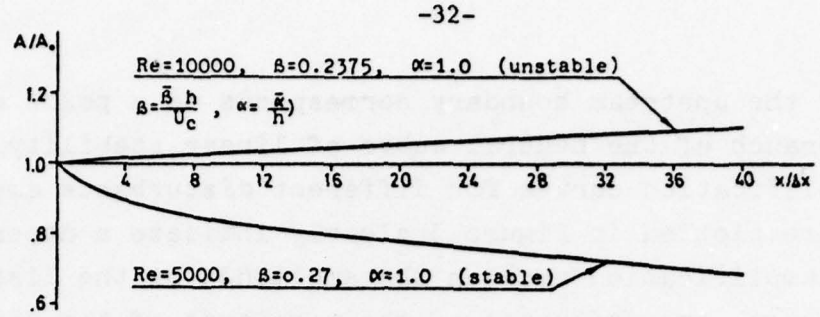

Figure 2. Amplification curves for spatially growing disturbances in plane Poiseuille flow (Disturbance amplitude for maximum of stream-wise velocity component 0.05% of center-line velocity U_c).

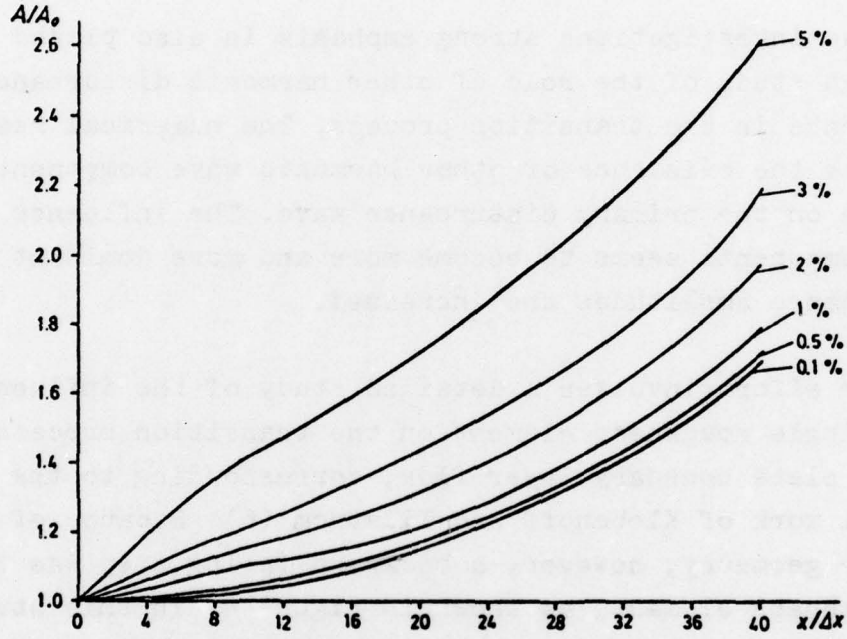

Figure 3. Amplification curves for different disturbance amplitudes (maximum of stream-wise velocity component in relation to free stream velocity).

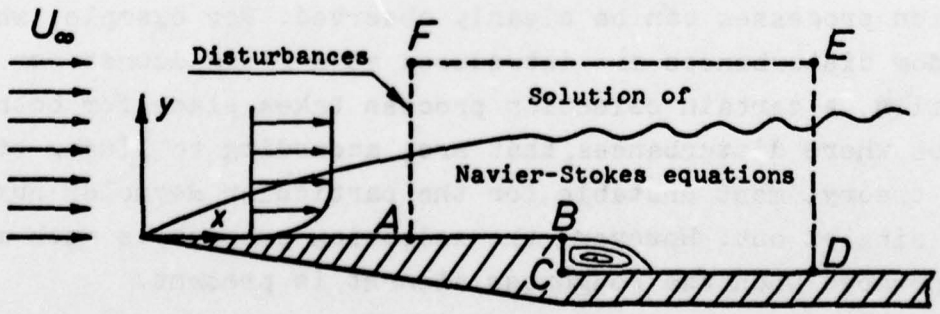

Figure 4. Integration domain for flow over a backward facing step (single roughness element).

References:

1 H. Fasel, Investigation of the stability of boundary layers by a finite difference model of the Navier-Stokes equations. To be published in J. Fluid Mech.

2 G.B. Schubauer & H.K. Skramstad, Laminar boundary-layer oscillations and transition on a flat plate. NACA Report No. 909 (1948).

3 J.A. Ross, F.H. Barnes, J.G. Burns & M.A.S. Ross, The flat plate boundary layer. Part 3. J. Fluid Mech. 43, 819-832 (1970).

4 M. Gaster, On the effects of boundary-layer growth on flow stability. J. Fluid Mech. 66, 465-480 (1974).

5 M. Nishioka, S. Iida & Y. Ichikawa, An experimental investigation of the stability of plane Poiseuille flow. J. Fluid Mech. 72, 731-751 (1975).

6 P.S. Klebanoff & K.D. Tidstrom, Mechanism by which a two-dimensional roughness element induces boundary-layer transition. Phys. Fluids 15, 1173-1188 (1972).

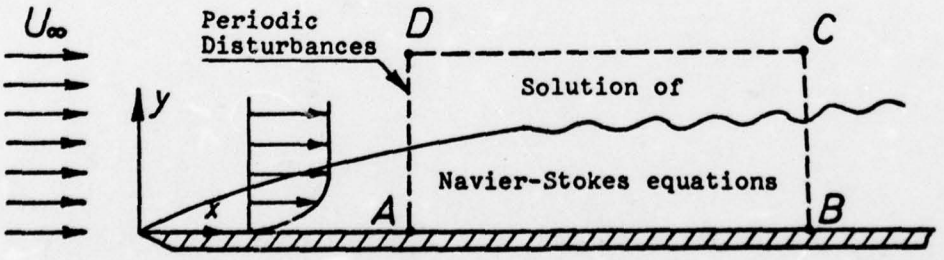

Figure 1. Integration domain for flat plate calculations

Section I

FUNDAMENTAL DYNAMICAL ASPECTS OF INDETERMINACY AND INCOMPLETENESS OF THE NAVIER-STOKES EQUATIONS BEARING ON TRANSITION

I-3 FUNDAMENTAL DYNAMICAL ASPECTS OF INDETERMINACY AND INCOMPLETENESS OF THE NAVIER-STOKES EQUATIONS BEARING ON TRANSITION

by

Paul Lieber, K. S. Wen and J. S. Marks

The application of the Navier-Stokes equations to the calculation of actual flows and in particular transition, by analytical and numerical procedures, is predicated on the supposition that they are in fact complete in specifying the dynamical constraints necessary for so obtaining this information. We demonstrate on the basis of the first principles of mechanics which circumscribe and thus limit the dynamical information content of the Navier-Stokes equations, that this basic presupposition must be fundamentally questioned. This is done by demonstrating the primacy and autonomy of force relative to the principles of mechanics and that this important fact carries over into the Navier-Stokes theory as well and accounts for the most fundamental dynamical aspect of indeterminacy and incompleteness of this theory. This fundamental aspect of indeterminacy which is predicated on the primacy of the forces, allows and calls for the specifications of additional dynamical contraints which augment and complete the Navier-Stokes theory for the purpose of calculating actual realizable flows. We present in outline analytical and numerical results obtained by the application of hydronamical variational principles that were conceived and designed for this purpose.

Certain experimental results which bear both directly and indirectly on transition and which experimentally display other significant aspects of incompleteness and indeterminacy of the Navier-Stokes equations are described as well as the experimental arrangements that produced them. The theoretical considerations that led to the conception of these unconventional hydrodynamical experiments and to the expectations that led to the identification of the results obtained are outlined.

Section II

NUMERICAL SIMULATION OF TRANSITION

II-1 Numerical Simulation of Transition

Steven A. Orszag
Department of Mathematics
M.I.T.
Cambridge, Mass. 02139

In this paper we shall summarize and compare results obtained from two distinct theoretical approaches to the transition problem. In the first, the three-dimensional time-dependent Navier-Stokes equations are solved in a plane channel with appropriate boundary conditions. The evolution of three-dimensional disturbances is studied with regard to cross-stream wavelength selection, spanwise and boundary-layer-wise flow variations, etc. The effects of surface curvature will also be discussed. In the second study, a highly simplified set of Galerkin equations was used to predict transition. Comparisons with the direct numerical simulations will be reported.

Section II

THE EFFECTS OF ACCELERATION ON THE GROWTH RATE OF SMALL DISTURBANCES IN A LAMINAR BOUNDARY LAYER

II-2 THE EFFECTS OF ACCELERATION ON THE GROWTH RATE OF SMALL DISTURBANCES IN A LAMINAR BOUNDARY LAYER

by

C. von Kerczek
David W. Taylor Naval Ship Research and Development Center

The effect of small acceleration on the amplification of disturbances in a laminar boundary layer, as might occur in the latter stages of the flight of a buoyancy propelled body, is considered.

Consider, for example, a circular cylinder whose radius is 15 feet and terminal velocity is 40 knots (i.e., Reynolds number = 67×10^6). We suppose that it accelerates according to the following law $U_\infty(\tau) = (1 - e^{-0.1\tau})$ where $U_\infty(\tau)$ is the dimensionless velocity of the cylinder at an instant of dimensionless time τ. The velocity scale used is the terminal velocity 40 knots and the time scale is the radius of the body divided by the terminal velocity. The above acceleration is a guess of what might be required in order to be near the terminal velocity after a distance of about 1000 feet.

The instantaneous inviscid velocity distribution on the surface of the cylinder is then $U(x,\tau) = 2(1 - e^{-0.1\tau}) \sin x$ where x is the arclength along the circumference of the cylinder measured from the front stagnation point. If one considers the temporal growth of small disturbances in the boundary layer, the analysis of [1] justifies the use of quasi-steady stability theory to determine growth rates. We assume that validity of the quasi-steady assumption to compute temporal growth rates allows the same approximation for computation of spatial growth rates. Thus, we assume that the amplitude A of a disturbance in this accelerating boundary layer is given by

$$\ln \frac{A}{A_0} = \int_{x_h}^{x} \frac{-\alpha_i R_{L_i}}{R_{\delta^*_i}} U \, dx \qquad (1)$$

where $-\alpha_i$ is the instantaneous growth rate, R_{L_i} is the instantaneous length Reynolds number, $R_{\delta^*_i}$ is the instantaneous displacement thickness Reynolds number and x_h is the instantaneous point of neutral stability. The amplification (1) must be calculated following the disturbance with its group velocity, see [2]. However, this second requirement may be relaxed in this case because the group velocity scales on U (e.g., calculations typically show group velocity near

0.2 U) and hence, the disturbances traverse the girth of the cylinder before the boundary layer changes appreciably.

As a sample calculation, Figure 1 shows the results of the unsteady boundary layer calculation (by the time-dependent Pohlhausen momentum integral method) on a sector ahead of but near the top (x = 0.5) of the cylinder. The quantity Λ is the Pohlhausen parameter defined in unsteady flow as $\Lambda = \left(\frac{1}{U}\frac{\partial U}{\partial \tau} + \frac{\partial U}{\partial x}\right)\frac{\delta^2}{\nu}$ where δ is a boundary layer thickness and ν is the kinematic viscosity. The various curves give Λ at different instants of time. The amplification (1) was computed at the instant τ = 12 which is when the body has reached about 70 percent of its terminal velocity. At this instant the disturbance with nondimensional frequency 0.7×10^{-6} traverses the arc (moving with its group velocity) from x = 0.4 to 0.5 in $\Delta\tau < 0.5$. In this increment of time, the boundary layer has little perceptible change as can be inferred from Figure 1. This gives an a posteriori justification of the quasi-steady assumption. Figure 2 shows $\ln A/A_o$ as a function of x at τ = 12. The curve marked (a) is what is obtained in a steady flow having the terminal velocity. The curve marked (b) is what is obtained when the flow is steady at 70 percent of terminal velocity (i.e., effect of acceleration of the flow on Λ is neglected). The curve marked (c) is what is obtained when boundary layer acceleration is taken into account. The conclusion is that the acceleration mainly affects boundary layer profile shape (i.e., Λ). Even though this effect on Λ is fairly small, it can have a large effect on the amplification in the region of the body where Λ would be near zero in a steady flow (i.e., near x = 0.5).

References:

[1] Hall, P. and Parker, K.H., "Stability of the Decaying Flow in a Suddenly Blocked Channel," J. Fluid Mechs., Vol. 75, Part 2, pp. 305-314 (1976).

[2] Loehrke, R.I., Morkovin, M.V. and Fejer, A.A., "Transition in Nonreversing Oscillating Boundary Layers," Trans. ASME, J. Fluids Eng., Series J, Vol. 97, pp. 534-549 (1975).

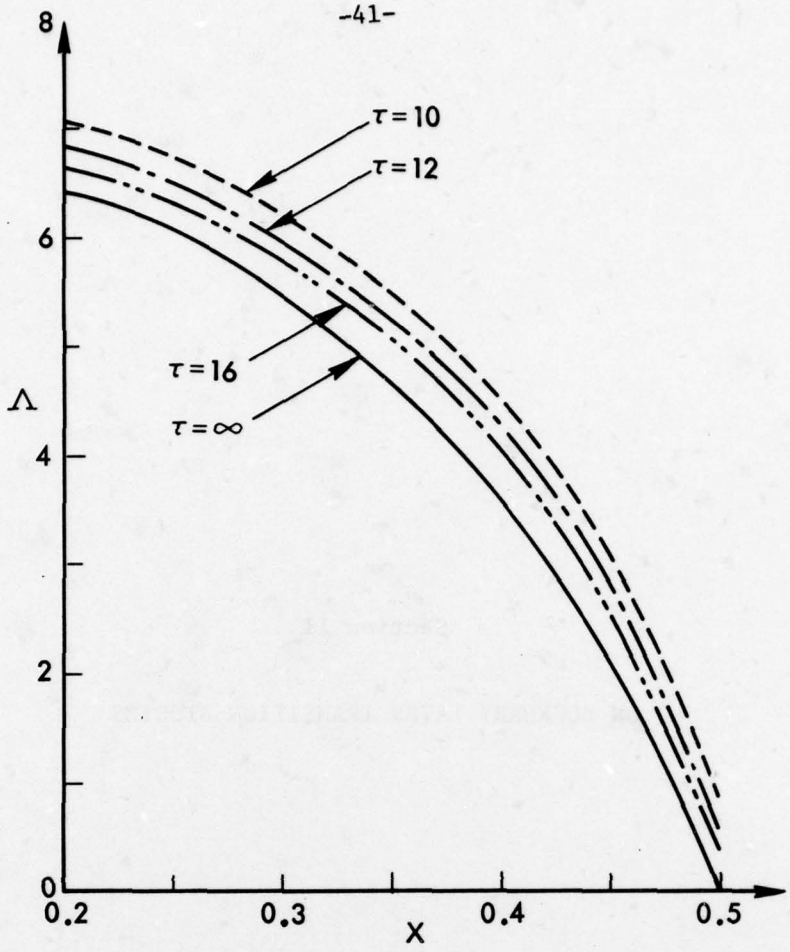
8
6
4
2
0
Λ
τ = 10
τ = 12
τ = 16
τ = ∞
0.2
0.3
0.4
0.5
X

Fig. 1

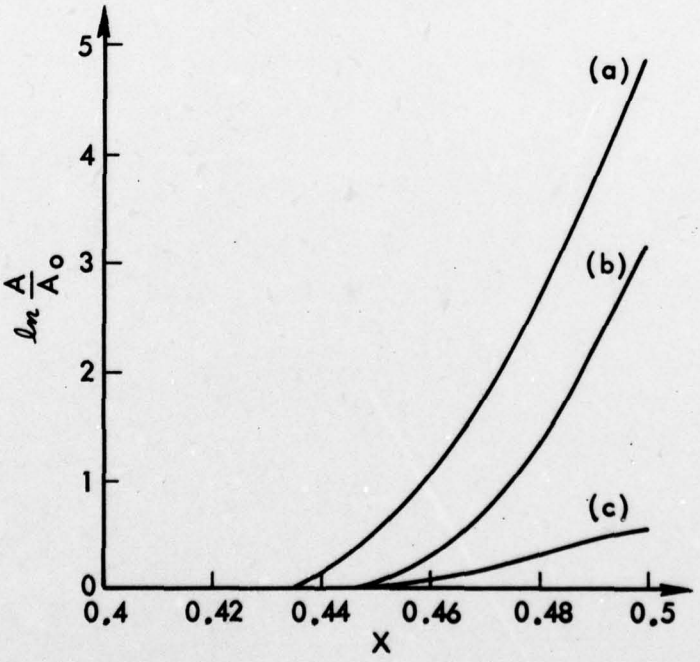
5
4
3
2
1
0
ln A/A₀
(a)
(b)
(c)
0.4
0.42
0.44
0.46
0.48
0.5
X

Fig. 2

Section II

ON BOUNDARY LAYER TRANSITION STUDIES

II-3 ON BOUNDARY LAYER TRANSITION STUDIES

Sin-I Cheng

Princeton University

The development of turbulent spots in the late stages of transition is as important as spot generation in transition studies. Laminar instability is important but not all encompassing even in the early stages of burst formation.

A turbulent boundary layer is visualized as an aggregate of distinct and overlapping turbulent spots convecting downstream in their asymptotic states. The turbulent front of each asymptotic spot develops in its local laminar environment independently of its neighbors until overlaps occur, where upon nonadditive union of spots and annihilation of fronts result. Incipient transition is reached when sufficient number of bursts and turbulent spots are present so that the sum of the transit times of all these spots under asymptotic development will exceed unity (intermittency factor = 1) somewhere downstream. The resulting outgoing turbulent front (mean) will eventually reach its equilibrium position about half way toward the outer edge of the turbulent boundary layer under the large convective effects there. The ingoing front propagates into the thin wall layer where it is promptly dissipated. A fully turbulent boundary layer then results. As such, the mean turbulent properties within a developing spot are those in the fully turbulent boundary layer further downstream.

Kinematics, dynamic and energy considerations of the asymptotic development of a spot and its interaction with the "mean flow" permit an estimate of the asymptotic states and of the transit time of a spot. Such estimates are in substantial agreement with observations. A criterion of incipient transition is then formulated in terms of the transit times of all the asymptotic spots resulting from the population of bursts and spots at a given station. A burst is presumed to be generated when the disturbance amplitude exceeds what is needed to extract sufficient energy from the mean flow for establishing a self-sustaining turbulent front of an asymptotic spot. This cut off amplitude increases with the scale and frequency of the disturbance to enhance such selectivity in burst formation.

If external disturbances are sufficiently large and numerous, the proposed transition criterion provides specific functional relations between transition Reynolds number and the external disturbances that describe adequately the observational data. If insufficient, transition will require additional spots from growing laminar disturbances with sufficiently large amplification rate. The many faces of transition can then be put in proper perspective to further better understanding and the construction of some practically useful transition criterion.

Section II

TRANSITION, PRESSURE GRADIENT, SUCTION, SEPARATION AND STABILITY THEORY

II-4

TRANSITION, PRESSURE GRADIENT, SUCTION, SEPARATION AND STABILITY THEORY.

J.L. van Ingen

Department of Aerospace Engineering, Delft University of Technology, Kluyverweg 1, Delft, The Netherlands.

SUMMARY.

A semi-empirical method is presented for the prediction of transition in two-dimensional incompressible flows with pressure gradient and suction. Included is the case of the laminar separation bubble, where transition is preceded by laminar separation.

The method employs linear stability theory to calculate the amplification factor σ for unstable disturbances in the laminar boundary layer. (σ is defined as the natural logarithm of the ratio between the amplitude of a disturbance at a given instant or position to the amplitude at neutral stability). It is found that at the experimentally determined transition position the calculated amplification factor for the critical disturbances attains nearly the same value (about 10) in many different cases for flows with low free stream turbulence levels. An attempt is made to include the effects of higher free stream turbulence levels by allowing the critical amplification factor to decrease with increasing free stream turbulence.

NOTATION.

The symbols used are the conventional ones for boundary layer and stability theory. To avoid confusion a few of them are mentioned specifically below.

c reference length

$$m = -\frac{\theta^2}{\nu}\frac{dU}{dx}$$

$$R_c = \frac{U_\infty c}{\nu}$$

$$R_\theta = \frac{U\theta}{\nu}$$

U velocity at edge of boundary layer

U_∞ reference velocity

$\bar{U} = U/U_\infty$

x or s distance along contour of body

x_c distance along chord

$\bar{x}$ $\frac{x}{c}$

$\bar{s}$ s/c

subscript sep refers to conditions at separation.

LINEAR STABILITY THEORY.

In linear stability theory a given two-dimensional laminar main flow is subjected to sinusoidal disturbances with a disturbance stream function:

$$\psi = \phi(y)\, e^{i(\alpha x - \omega t)} \tag{1}$$

For the spatial mode ω is real and α is complex $\alpha = \alpha_r + i\,\alpha_i$. This leads to a factor $e^{-\alpha_i x}$ in the disturbance amplitude and σ follows from:

$$\sigma = \int_{x_o}^{x} -\alpha_i dx = \frac{U_\infty c}{\nu}\, 10^{-6} \int_{\bar{x}_o}^{\bar{x}} T.\bar{U}\, d\bar{x} \tag{2}$$

where x_o is the streamwise position where the disturbance with frequency ω is neutrally stable.

T is defined as:

$$T = \frac{-\alpha_i\, \theta}{R_\theta}\, 10^6 \tag{3}$$

In the temporal mode the same expression (2) for σ is found with a different definition for T.

It is clear that σ is a function of x and ω for a given boundary layer; σ can be calculated as soon as stability diagrams are available for the velocity profiles for successive streamwise positions x.

For a long time Pretsch' stability diagrams for the temporal stability of the Hartree similar velocity profiles, have been the only source of detailed stability data for flows with non-zero pressure gradient [6]. Results for the spatial stability of the Hartree flows have been given by Wazzan, Okamura and Smith [7] and Kümmerer [8], stability diagrams for the reversed flow solutions of the Falkner-Skan equation have been obtained by Taghavi and Wazzan [11].

STABILITY AND TRANSITION OF THE FLAT PLATE BOUNDARY LAYER.

Fig. 1a shows σ for the flat plate according to Pretsch for different non-dimensional frequencies $\frac{\omega\nu}{U^2}$. The envelope of these curves gives the maximum value of σ for each streamwise position. In what follows we will in general mean this maximum value when we mention σ. The curve labelled 3 in fig. 1b is the envelope according to [7] and [8]; the curve labelled 2 will be discussed later. A well known result for the experimentally determined transition region is due to Schubauer and Skramstad [12]. They find for low free stream turbulence levels Reynoldsnumbers at beginning and end of transition equal to 2.8×10^6 and 3.9×10^6 respectively. To these Reynolds numbers correspond certain values σ_1 and σ_2 for σ which are indicated in table 1.

FIRST VERSION OF THE PREDICTION METHOD (1956).

The present author used Pretsch charts in [1] to calculate amplification factors for an airfoil section (EC 1440) at different values of angle of attack and Reynolds number.
It was shown that σ_1=7.6 and σ_2=9.7 gave a reasonably accurate prediction of the transition region. Smith and Gamberoni [3], defining a transition point rather than a transition region found that σ=9 would correlate different transition experiments reasonably well.
Although it is clear that a transition criterion should be based on the actual amplitude of the disturbance, rather than on an amplification ratio, the method has been used extensively. Its success may have been due to the fact that the initial disturbances - due to free stream turbulence for instance - have been about the same for the cases investigated.
Another way to explain the success of the method may be that σ is a suitable factor in which different factors, known to influence transition, may be correlated.

SECOND VERSION, ALSO APPLICABLE TO FLOWS WITH SUCTION.

In 1965 the present author extended the method to the case of two-dimensional incompressible boundary layers with suction [2].
Since at that time the Pretsch charts were still the only source of detailed information on amplification rates, some drastic

simplifying assumptions had to be made. First it was assumed that all possible stability diagrams, including those for suction boundary layers, formed a one-parameter family with the critical Reynolds number as parameter. Furthermore, it was assumed that the critical Reynolds number could be determined from an approximation formula due to Lin. The suction boundary layer was calculated using a two-parameter method of integral relations. This necessitated a new "calibration" of the transition prediction method against the flat plate without suction, leading to curve 2 in fig. 1b with σ_1=9.2 and σ_2=11.2.

To facilitate the amplification calculations using a computer Pretsch' charts have been brought in a tabular form. Fig. 2 shows an application to the EC 1440 airfoil; some results for an airfoil with suction through a porous surface are shown in figs 3 and 4. In view of the many simplifying assumptions which had to be made the correspondence between theory and experiment may be considered to be good.

Since 1965 this version of the method has been included in a computer program for the analysis and design of airfoil sections [13]. The streamwise position for the end of the transition region (determined by σ_2) has been used as the starting point for the turbulent boundary layer calculation.

It has been found that an improved transition prediction could be made by allowing the value for σ_2 to vary from 11.2 for favourable and zero pressure gradient to about 20 for boundary layers near separation. (In the last version σ_2 is again more nearly constant). In general the position of transition was predicted within a few percent of the chord. An example of application of this airfoil analysis program taken from [14] is shown in fig. 5 . The airfoil investigated is that of the horizontal tailplane of the Italian sailplane M300 "Aliante". The airfoil was designed by cambering the NACA 63_3-018 section. The tailplane is produced through an extrusion process which caused appreciable surface waviness. An actual specimen of this tailplane was tested as a two-dimensional model in the low speed wind tunnel of the Department of Aerospace Engineering at Delft. It was found that the surface waves caused early transition in a certain angle of attack range; this could be remedied by smoothing

the forward part of the surface. The calculation, starting from the airfoil coordinates for both conditions, predicted this change quite well.

It should be stressed again that the present method may be considered as a method to correlate different transition experiments. The calculated amplification factors need not have a precise physical meaning. It is however a definite advantage of the method that linear stability theory is used which has proved to be a valuable tool to describe the early phases of the transition process. It should also be observed that inaccuracies in one of the elements of the method (viz. boundary layer calculation; calculation of the critical Reynolds number using Lin's formula; the stability diagrams used) may have been neutralized by inaccuracies in another element. Hence if any element is changed, a new calibration is necessary.

An important imperfection in the second version of the method was that the stability characteristics in laminar separation bubbles were obtained by extrapolation from the attached flow. This may have been the cause of the high values of σ_2 required to predict accurately the end of the transition region in boundary layers near to or after separation.

A SHORT CUT METHOD TO PREDICT TRANSITION IN SEPARATION BUBBLES.

In [5] the present author published a short-cut method to predict transition in separated flow. The method is based on the stability diagrams for reversed flows due to Taghavi and Wazzan [11] and some additional calculations by the present author for the limiting stability characteristics when $R_\theta \to \infty$, using the inviscid stability equation (Rayleigh equation). The following assumptions are made

1) U, θ and R_θ in the separation bubble are independent of x and equal to their values at separation. Then a constant value of ω also means a constant value of $\frac{\omega\theta}{U}$.
2) The separation streamline is straight, and leaves the wall at an angle γ determined by:

$$tg(\gamma) = \frac{B}{\left(\frac{U\theta}{\nu}\right)_{sep}} \qquad (4)$$

where B is a constant equal to 17.5.

3) The Reynolds number is so high with respect to the (very low) critical Reynolds number that the stability characteristics are given with sufficient accuracy by the limiting values determined from the inviscid stability equation.
Then $-\alpha_i\theta$ only depends on the value of $\frac{\omega\theta}{U}$ and the velocity profile shape parameter.

Finally we introduce the shape parameter $z=g \times m_{sep}$, where g is the height of the separation streamline above the wall devided by θ and $m_{sep} = -\frac{\theta^2}{\nu}\frac{dU}{dx}$ at separation. Then the integration w.r.t. x in (2) can be replaced by an integration w.r.t. to z leading to:

$$\sigma = \frac{(R_\theta)_{sep}}{B.m_{sep}} \int (-\alpha_i\theta)dz \qquad (5)$$

(a similar result may be obtained for a small region upstream of separation when integration w.r.t. $\ell = \frac{\tau_o\theta}{\mu U}$ is used).

The inviscid instability for different values of the Hartree parameter β is shown in figs 6 and 7. Values of $10^4 \int (-\alpha_i\theta)dz$ are shown in fig. 8 for different values of $\frac{\omega\theta}{U}$ together with the envelope giving the maximum value I of the integral as a function of Z. (See also table 2). Hence in the separation bubble we have:

$$\sigma = \frac{10^{-4}\ (R_\theta)_{sep}\ I}{B.m_{sep}} \qquad (6)$$

Using this short-cut method it was found in [5] that σ_2 for separation bubbles on an airfoil in a small "noisy" tunnel was about 12.5 (fig. 9). For separation bubbles on a circular cylinder with a tapered tail in the large low turbulence wind tunnel, values of σ_2 between 13.2 and 15.7 were found, depending on the wind speed. Using the same short-cut method Van der Meulen [15] obtained σ_2=7 for a body of revolution in a small high speed water tunnel.

PRESENT STATUS OF THE TRANSITION PREDICTION METHOD.

All stability data obtained from [7,8,11] and the inviscid stability calculations mentioned in the preceding section, have been reduced to a table containing about 300 numbers.
Using this table, the amplification rate T can easily be obtained for any velocity profile, as soon as the critical Reynolds number is known.

The present author employs a boundary layer calculation method [5] which for attached flow is similar to Thwaites' method. It contains an extra parameter however, which makes the prediction of the separation position as accurate as for Stratford's two-layer method. In separated flows an integral method is used in which the shape of the separation streamline is prescribed. Both for attached and separated flow the primary profile shape parameter is m/m_{sep}. The critical Reynolds number is a function of m/m_{sep}; this function is assumed to be equal to that obtained for the Falkner-Skan solutions. From calculations with the full method it has been found that the short-cut method, described in the preceding section, gives a very good approximation in separation bubbles. Furthermore it has been found that the values of σ_1 and σ_2, when transition occurs near separation are much nearer to the flat plate values than for the second version. It can now be expected that σ_1 and σ_2 will be more or less constant for flows with the same initial disturbances. However, σ_1 and σ_2 may have to vary with the level of initial disturbances due to free stream turbulence and noise.
From curve 3 in fig. 1 and table 1 it follows that $\sigma_1 = 8.3$ and $\sigma_2 = 10.4$ if Schubauer and Skramstad's transition results for the flat plate are used. From Spangler and Wells' experiment on a flat plate in a tunnel with reduced background noise [16,17] and from the authors own experiments somewhat larger values for σ_1 (12) and σ_2 (14.5) would be obtained. Jaffe, Okamura and Smith [9] applied their solution technique for the Orr-Sommerfeld equation to velocity profiles that had been obtained numerically for two-dimensional and axi-symmetric flows. They find σ_1=8.3 for the Schubauer and Skramstad results and σ_1=11.8 for Well's results; for a large number of flows with pressure gradient σ_1 values ranging from 6.8 to 12.1 were obtained. A good overall correlation of transition position was obtained using σ_1=10.

RELATION BETWEEN σ_1, σ_2 AND FREE STREAM TURBULENCE.

Although it is clear that the initial disturbances cannot be sufficiently characterised by the r.m.s. value of free stream turbulence alone, it will be attempted in the present section to find a relation between σ_1, σ_2 and the r.m.s. free stream turbulence Tu (in %).

In many different papers relations between Tu, R_θ or R_x at transition have been given for the flat plate. The measured transition positions may be converted to σ-values using curve 3 from fig. 1b. Then σ will decrease when Tu increases; fig. 10 shows a collection of these data; for Tu > 0.1% the relation used by Mack in fig. 3 of [18] can be approximated by:

$$\sigma_1 = 2.13 - 6.18^{10} \log Tu \qquad (7)$$

while for σ_2 a reasonable approximation is:

$$\sigma_2 = 5 - 6.18^{10} \log Tu \qquad (8)$$

For values of Tu < 0.1% there is much more scatter because in this region sound disturbances may become the factor controlling transition rather than turbulence. We may also use the relations (7) and (8) for Tu < 0.1%; but then we should define an "effective" value for Tu. Of course this does not solve the problem because we can only define an "effective Tu" for a wind tunnel after transition experiments have been made in that same tunnel.

At the time of writing this abstract some additional measurements in the low speed low turbulence wind tunnel of the Department of Aerospace Engineering are being evaluated. Some preliminary results show that the "effective Tu" even may increase at the lower windspeeds where Tu decreases. It is thought that this is due to the fact that the critical frequencies in the boundary layer may better be matched to the wind tunnel noise spectrum at lower speeds.

For the time being it is suggested to use (7) and (8), assuming an effective Tu equal to 0.1% for modern wind tunnels, resulting in $\sigma_1 = 8.3$ and $\sigma_2 = 11.2$.

ACKNOWLEDGEMENT.

The author is indebted to professor A.R. Wazzan for making available some tabular material concerning the stability of reversed flows. Ir. J.J.H. Blom should be thanked for his active participation in the preparation of this paper.

REFERENCES.

1. Ingen, J.L. van: A suggested semi-empirical method for the calculation of the boundary layer transition region. Report VTH-74, Dept. of Aeron. Eng., University of Technology Delft, 1956.
2. Ingen, J.L. van: Theoretical and experimental investigations of incompressible laminar boundary layers with and without suction. Report VTH-124, Dept. of Aeron. Eng. , University of Technology Delft, 1965.
3. Smith, A.M.O. and Gamberoni, N.: Transition, pressure gradient and stability theory. Report ES 26388, Douglas Aircraft Co., 1956.
4. Dobbinga, E., Ingen, J.L. van, Kooi, J.W.: Some research on two-dimensional laminar separation bubbles. AGARD CP-102, paper nr. 2, Lisbon 1972.
5. Ingen, J.L. van: On the calculation of laminar separation bubbles in two-dimensional incompressible flow. In AGARD CP-168: "Flow Separation", Göttingen, 1975.
6. Pretsch, J.: Die Stabilität einer ebenen Laminarströmung bei Druckgefälle und Druckanstieg. Jahrbuch 1941 der deutschen Luftfahrtforschung, I 58.
7. Wazzan, A.R., Okamura, T.T. and Smith, A.M.O.: Spatial and temporal stability charts for the Falkner-Skan boundary layer profiles. DAC 67086, sept. 1968 McDonnell Douglas Corp.
8. Kümmerer, H.: Numerische Untersuchungen zur Stabilität ebener laminarer Grenzschichtströmungen. Dissertation Technische Hochschule, Stuttgart, 1973.
9. Jaffe, N.A., Okamura, T.T. and Smith, A.M.O.: Determination of spatial amplification factors and their application to predicting transition. AIAA Journal, Vol 8, no 2, February 1970, p 301-308.
10. Stratford, B.S.: Flow in the laminar boundary layer near separation. R and M 3002, 1957.
11. Taghavi, H. and Wazzan, A.R.: Spatial stability of some Falkner-Skan profiles with reversed flow. Physics of Fluids, Vol 17, no 12, Dec. 1974, p 2181-2183.
12. Schubauer, G.B. and Skramstad, H.K.: Laminar boundary layer oscillations and transition on a flat plate. NACA Rept 909, 1948.
13. Ingen, J.L. van: Advanced computer technology in aerodynamics; a program for airfoil section design utilizing computer graphics. VKI lecture series 16 on High Reynolds number subsonic aerodynamics, April 21-25, 1969.

14. Boermans, L.M.M. and Blom, J.J.H.: Low-speed aerodynamic characteristics of an 18-percent-thick airfoil section designed for the all-flying tailplane of the M300 sailplane. Report LR-226, Department of Aerospace Eng., Delft University of Technology, 1976.
15. Van der Meulen, J.H.J.: A holographic study of cavitation on axi-symmetric bodies and the influence of polymer additives. Doctoral Thesis, University of Technology Twenthe, 1976.
16. Wells, C.S.: Effects of free stream turbulence on boundary layer transition. AIAA Journal, Vol 5, No 1, January 1967, p 172-174.
17. Spangler, J.G. and Wells, C.S.: Effects of free stream disturbances on boundary-layer transition. AIAA Journal, Vol 6, No 3, March 1968, p 543-545.
18. Mack, L.M.: A numerical method for the prediction of high-speed boundary-layer transition using linear theory. Paper nr. 4 in Aerodynamic analysis requiring advanced computers; NASA SP-347, 1975.
19. Hall, D.J. and Gibbings, J.C.: Influence of stream turbulence and pressure gradient upon boundary layer transition. Journal Mechanical Engineering Science, Vol 14, no 2, 1972, p 134-146.

curve no in fig. 1b	σ_1	σ_2	stability diagram used
1	7.6	9.7	Pretsch, flat plate (β=0); version 1.
2	9.2	11.2	Pretsch, stability diagram for $^{10}\log(\frac{U\theta}{\nu})_{crit}$=2.345 which according to Lin's formula would apply to the flat plate velocity profile in version 2.
3	8.3	10.4	from [7] and [8]

Table 1: Critical values for σ at beginning (σ_1) and end of the transition region (σ_2) on a flat plate according to different stability calculations. Transition Reynolds numbers 2.8 and 3.9 x 10^6 according to [12].

β	$z=g\bar{x}m_{sep}$	I
-.198838	0	127
-.198	.042	145
-.197	.061	154
-.195	.088	167
-.190	.134	190
-.180	.199	225
-.160	.307	285
-.150	.360	315
-.140	.420	348
-.120	.556	422
-.100	.682	483
-.075	1.107	659
-.050	1.864	883
-.025	4.249	1331

Table 2: z and I as a function of the Hartree shape parameter β for reversed flows.

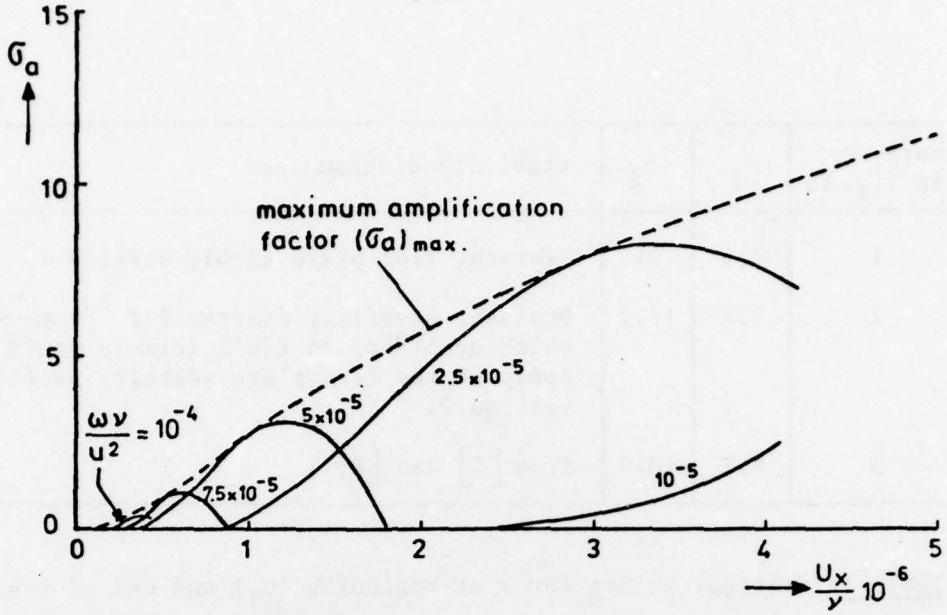

Fig. 1a: Amplification factor for the flat plate according to Pretsch [6].

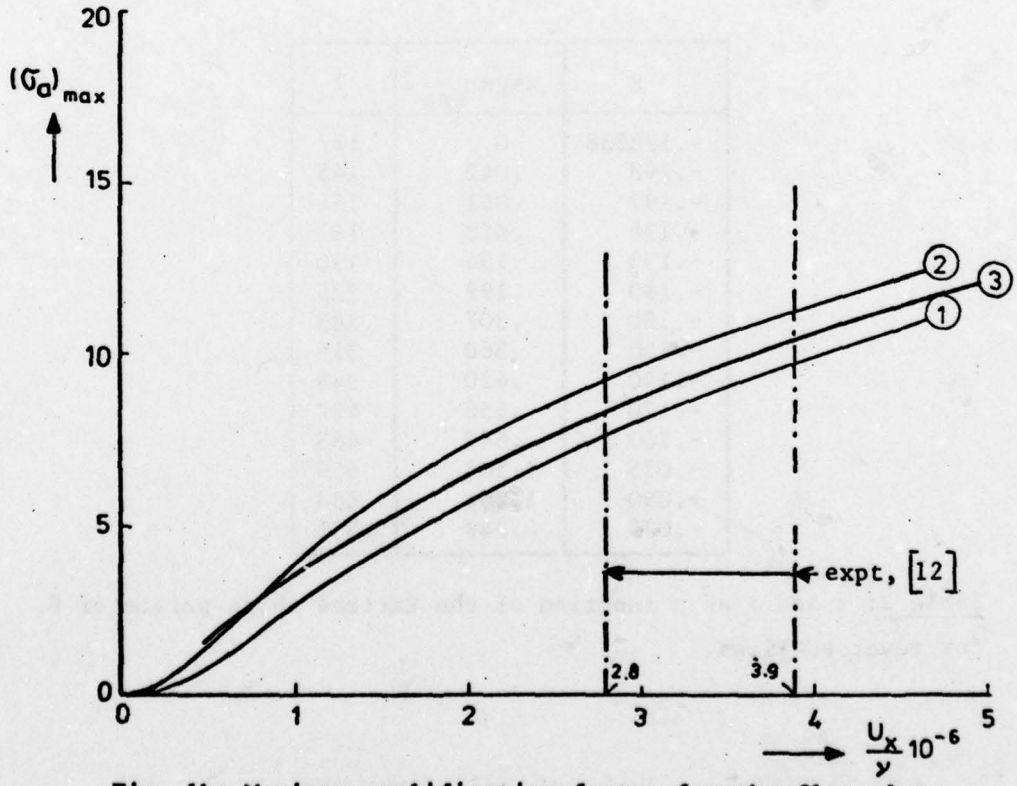

Fig. 1b: Maximum amplification factor for the flat plate according to different stability calculations (see also table 1).

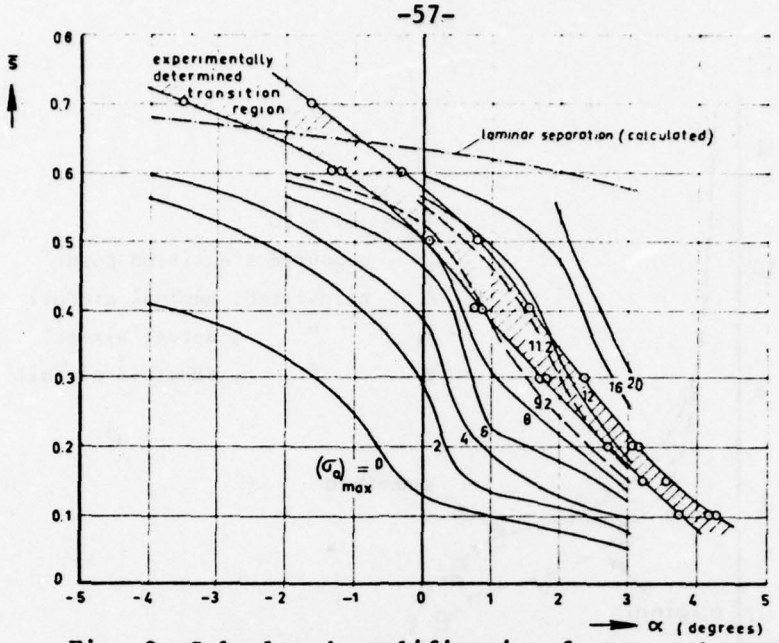

Fig. 2: Calculated amplification factor and measured transition region for the EC 1440 airfoil section.

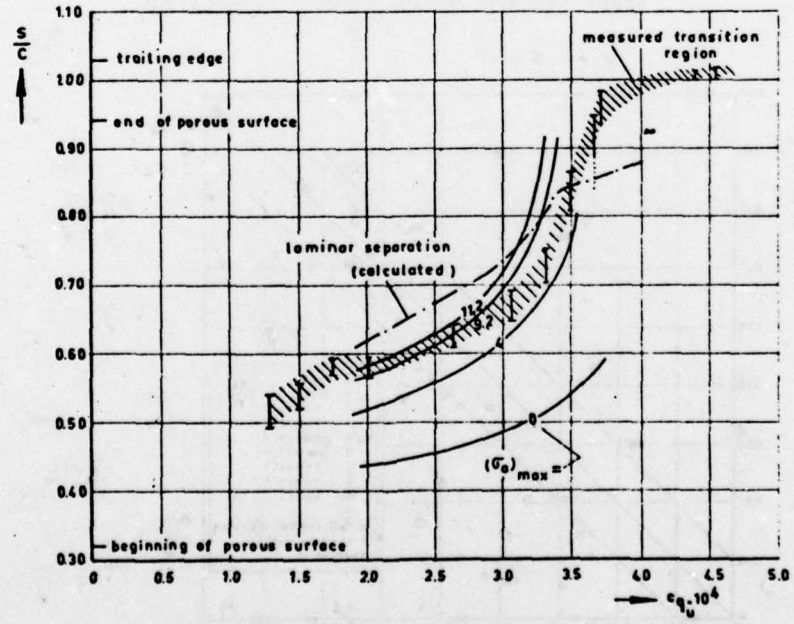

Fig. 3: Measured transition and calculated amplification factor for the upper surface of the suction model, $\alpha=0^o$, $R_c=3.37 \times 10^6$. (c_{q_u} is the suction flow coefficient for the upper surface; $c_q = \frac{Q}{U_\infty c}$; Q is volume flow of sucked air per unit span).

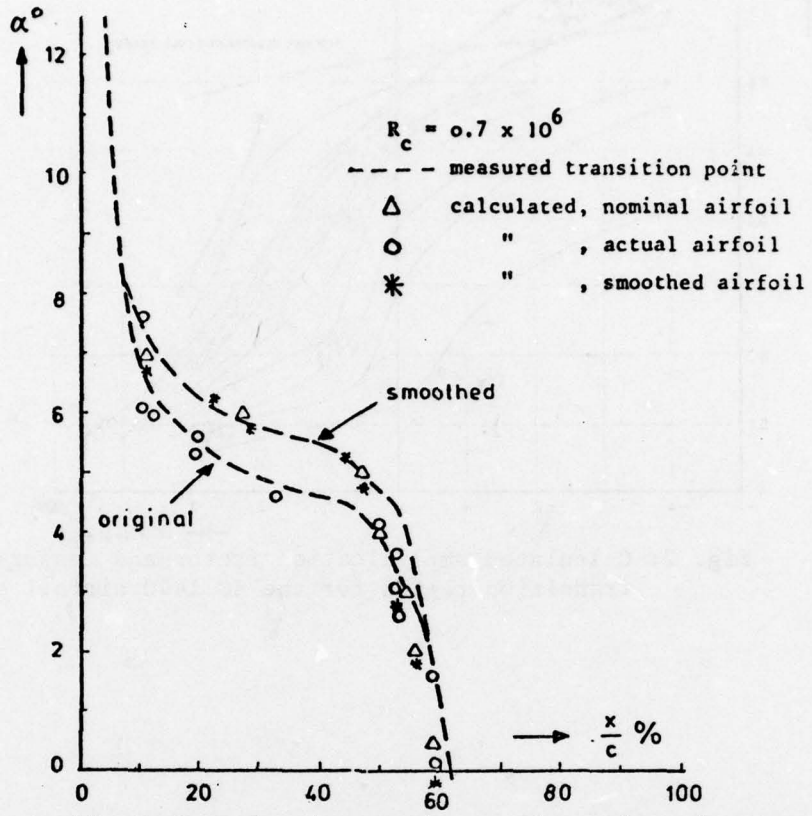

Fig. 5: Comparison between theory and experiment for the upper surface of the M-300 airfoil [14].

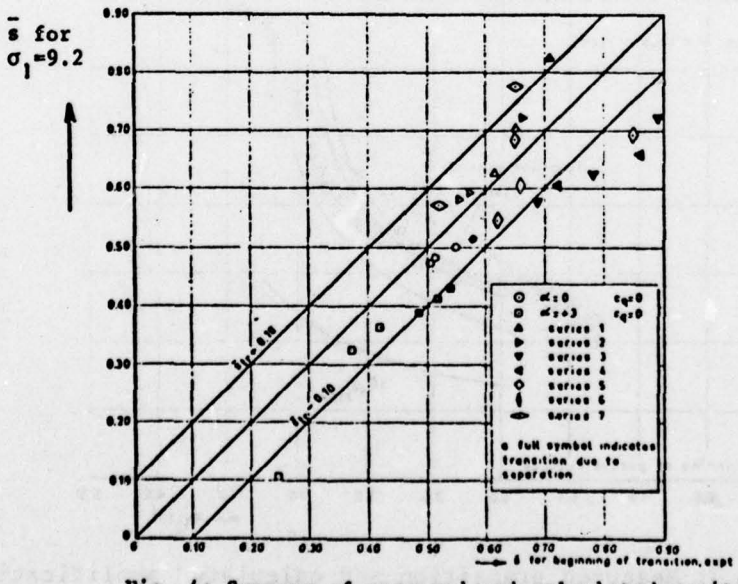

Fig. 4: Summary of measured and calculated positions of the beginning of transition for the airfoil with suction [2].

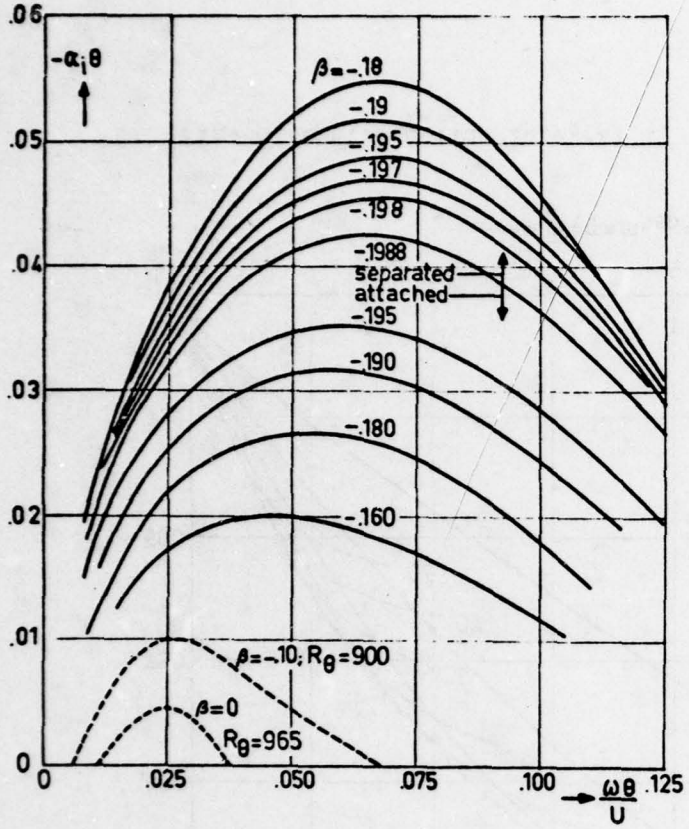

Fig. 6: Attached and separated flow.

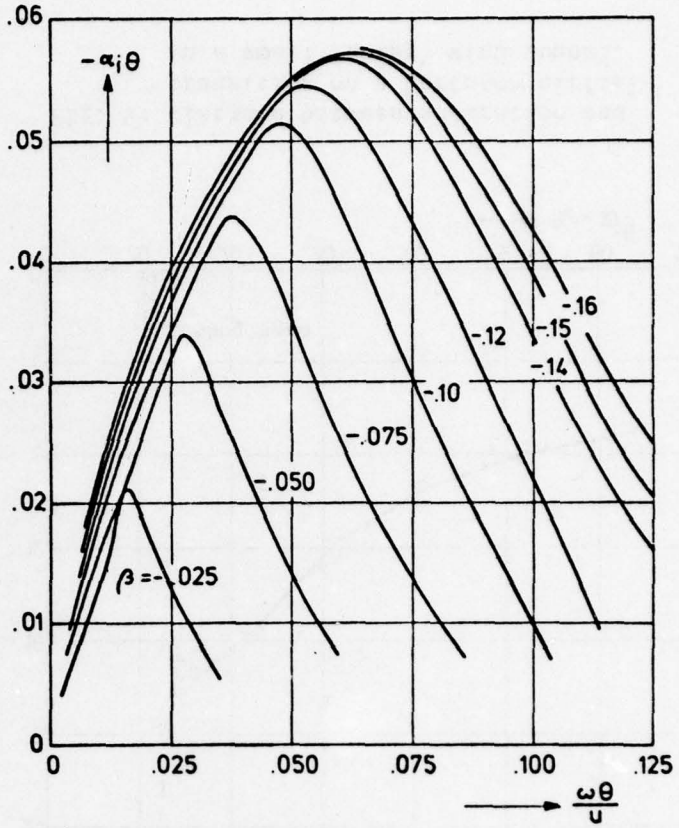

Fig. 7: Separated flow.

Figs 6 and 7: Inviscid instability for Hartree's and Stewartson's velocity profiles. For attached flow $-\alpha_i\theta \to 0$ for $\beta \to 0$, for comparison the viscid instability is shown for $\beta = 0$ and $-.10$ when R_θ is about 1000.

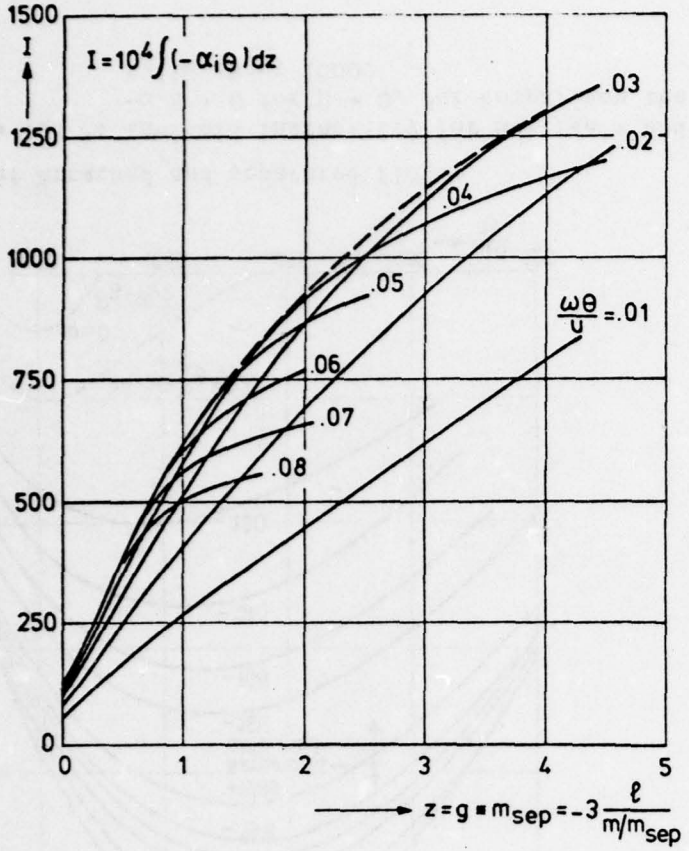

Fig. 8: Amplification integral I

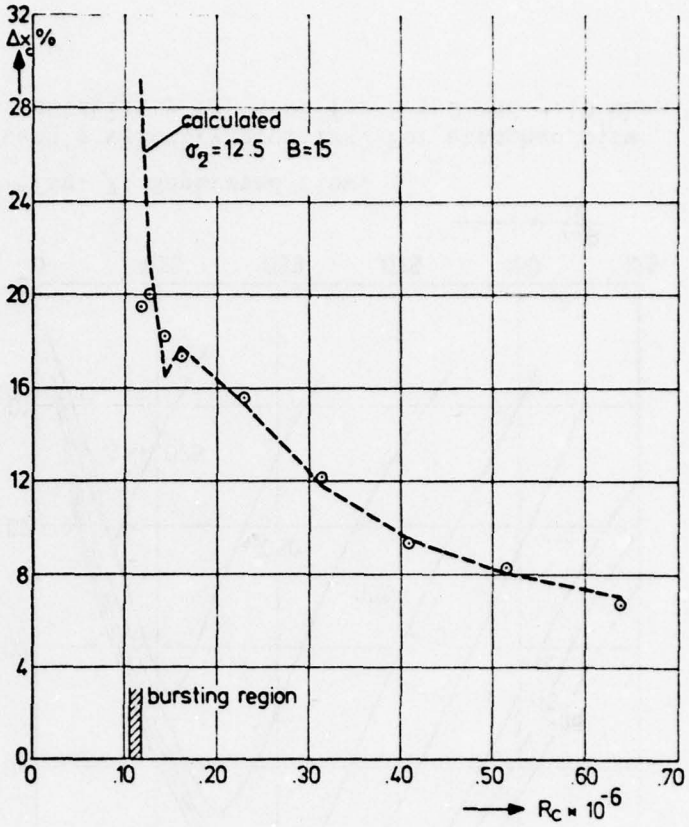

Fig. 9: Distance between separation and transition on a Wortmann airfoil in a small "noisy" wind tunnel.

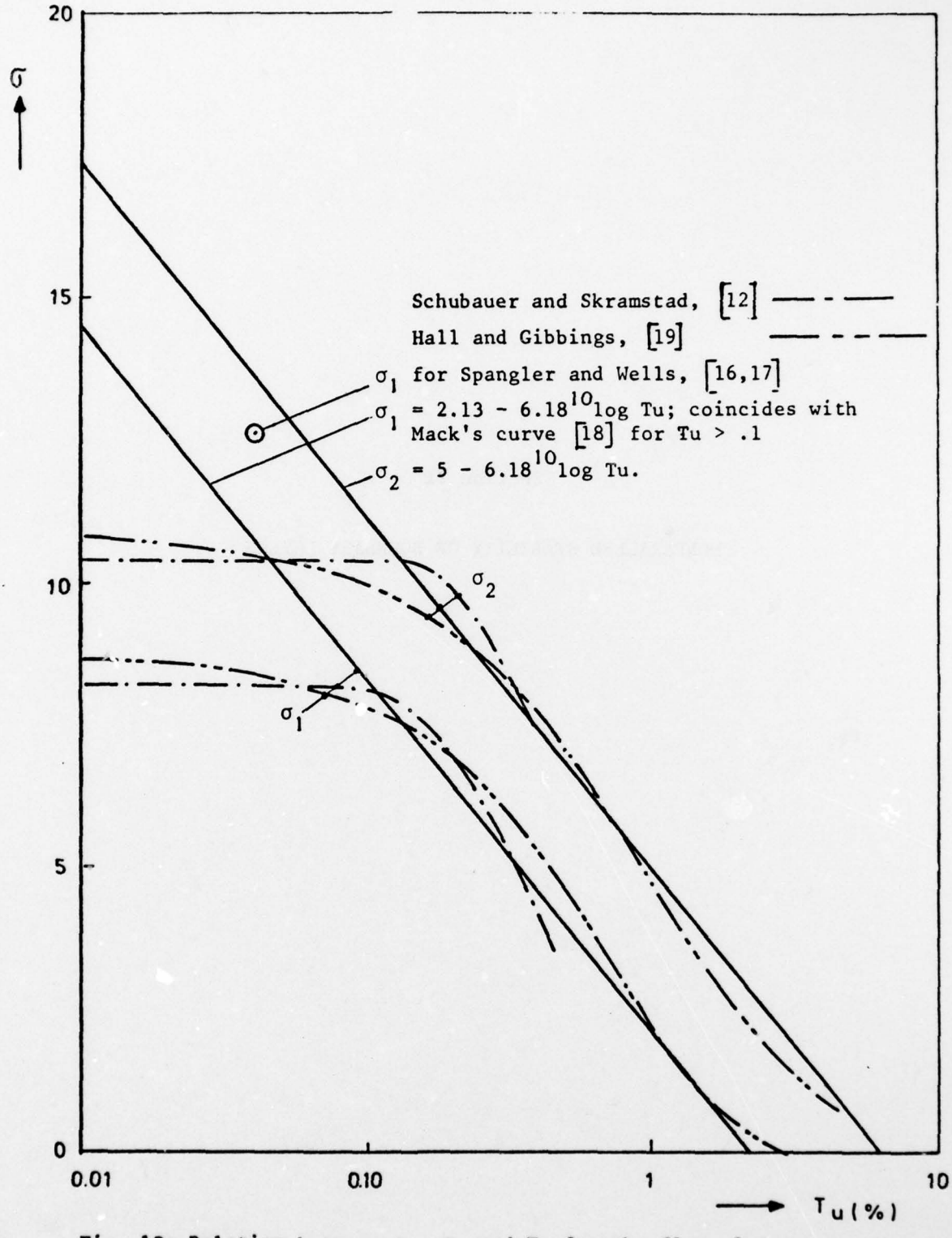

Fig. 10: Relation between σ_1, σ_2 and Tu for the flat plate.

Section II

NONPARALLEL STABILITY OF BOUNDARY LAYERS

II-5 Nonparallel Stability of Boundary Layers

William S. Saric and Ali Hasan Nayfeh
Department of Engineering Science and Mechanics
Virginia Polytechnic Institute and State University
Blacksburg, Virginia 24061 U.S.A

This paper investigates the stability of flows that are not parallel. That is to say, the mean-flow velocity is a function of two dimensions and thus, it has a streamwise as well as a transverse component. In this work, we confine our attention to the following class of flows: boundary layers with variable pressure gradients and blowing or suction. A common feature of these flows is that they are weakly nonparallel and thus many previous stability analyses have assumed the primary flow to be parallel that is, the flow is one-dimensional and identical at every streamwise location.

Recently, considerable attention has been given to linear stability theories of shear flows that account for nonparallel flow effects (Bouthier 1973, Nayfeh, Saric & Mook 1974, Gaster 1975, Saric & Nayfeh 1975) because classical linear stability theories which treat the primary flows as quasi-parallel flows have not produced satisfactory results. For a flow past a flat plate (Blasius flow), the critical Reynolds number predicted by parallel stability theories is about 30% above the experimental results of Schubauer & Skramstad (1947), Ross, Barnes, Burns, & Ross (1970), Wortman (1955), and Strazisar, Prahl, & Reshotko (1975), as shown in figure 1. A survey of stability analyses and their application to transition is given by Reshotko (1976).

For a parallel mean flow, the spatially varying disturbance stream-

function can be expressed as

$$\Psi = \zeta(y)\exp\{i(k_0 x - \omega t)\} \tag{1}$$

where ζ is the mode shape, ω is the disturbance frequency, and k_0 is a complex constant. Since the mode shape ζ is assumed to be independent of x, the streamwise behavior of any disturbance quantity, such as the velocity, the pressure, and the kinetic energy, is governed by the exponent k_0. In particular, the amplification and attenuation rates of any disturbance are given uniquely by the imaginary part of k_0. On the other hand, for a near parallel flow, the disturbance stream function has the form

$$\Psi = A_0\zeta(y;x_1)\exp\{i\int(k_0 + \varepsilon k_1)dx - i\omega t\} \tag{2}$$

Thus, the effects of nonparallelism are to make k_0 be a function of the long scale $x_1 = \varepsilon x$, where ε is a small parameter characterizing the nonparallelism of the mean flow, to produce a correction $\varepsilon k_1(x_1)$ to k_0, and to make the mode shape ζ vary in the streamwise direction. Hence, the streamwise variation of each flow quantity depends on its distance from the wall. Moreover, at each distance from the wall, the different flow quantities vary differently in the streamwise direction. Thus, unless these factors are taken into account, meaningful comparisons cannot be made between theoretical and experimental results. Figure 1 shows good agreement between the nonparallel neutral stability curve calculated by Saric & Nayfeh (1975) and the results of various experiments.

Recent experiments by Strazisar, Prahl & Reshotko (1975) in a water tunnel and by Kachanov, Kozlov & Levchenko (1975) in a wind tunnel have provided additional data which can be used for comparison. Figure 2 shows a comparison of the maximum amplification rates calculated by using parallel

and nonparallel theories and those determined experimentally by Strazisar, Prahl & Reshotko. We note that the maximum amplification rates calculated by using the nonparallel theory is approximately 1½ times those calculated by using the parallel theory for low Reynolds numbers. Figures 3 and 4 show good agreement between the amplitude histories calculated by using the nonparallel theory and those determined experimentally by Kachanov, Koslov & Levchenko. Thus the theory is in good agreement with available experiments for neutral stability, amplification rate, and amplitude history. Comparison between other nonparallel theories are made in the paper.

Our nonparallel stability model has been extended to include the effects of pressure gradients, suction or blowing, and higher-order boundary-layer terms.

ACKNOWLEDGMENT

Work supported by NASA - Langley Research Center

REFERENCES

BOUTHIER, M. 1973 J. de Mécanique 12, 75.

GASTER, M. 1974 J. Fluid Mech. 66, 465.

KACHANOV, YOU. S., KOZLOV, V. V. & LEVCHENKO, V. YA. 1975 Ycheniye Zapiski Ts. A. G. I. VI, 137.

NAYFEH, A. H., SARIC, W. S. & MOOK, D. T. 1974 Arch. of Mech. 26, 401.

RESHOTKO, E. 1976 Ann. Rev. Fluid Mech. 8, 311.

ROSS, J. A., BARNES, F. H., BURNS, J. G. & ROSS, M. A. S. 1970 J. Fluid Mech. 43, 819.

SARIC, W. S. & NAYFEH, A. H. 1975 Phys. Fluids 18, 945.

SCHUBAUER, G. B. & SKRAMSTAD, H. K. 1947 J. Res. Nat. Bur. Stand. 38, 251.

STRAZISAR, A. J., PRAHL, J. M. & RESHOTKO, E. 1975 Case Western Reserve Univ. Dep. Fluid, Thermal, Aerospace Sci. FTAS/TR-75-113.

WORTMAN, F. X. 1955 In Fifty years of Boundary Layer Research, Braunschweig, 6.

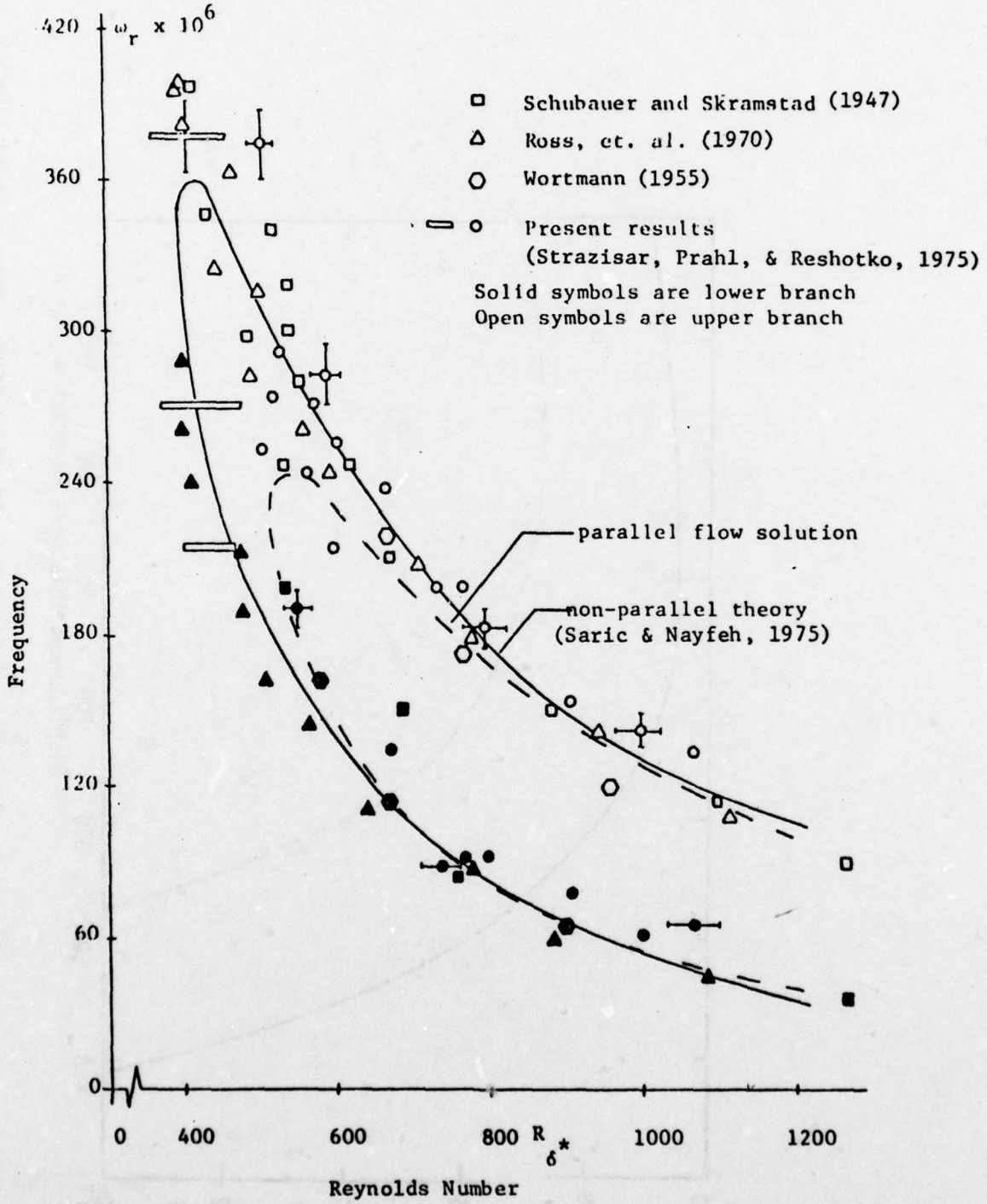

Figure 1. Comparison of experimental results and nonparallel theory for Blasius boundary layer. From Strazisar, Prahl, & Reshotko, 1975.

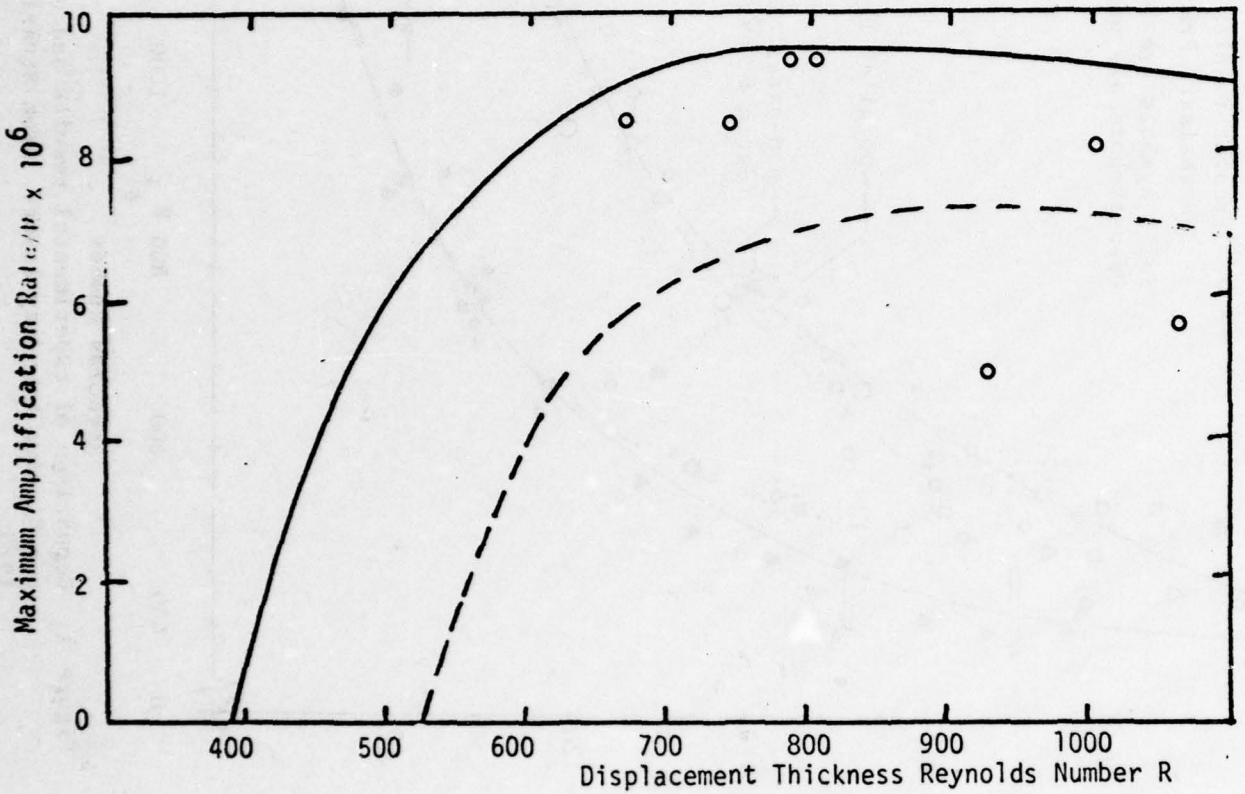

Figure 2. Maximum amplification rate vs Reynolds number. Solid line is nonparallel theory. Dashed line is parallel theory. Open symbols are experiments of Strazisar, Prahl, & Reshotko, 1975.

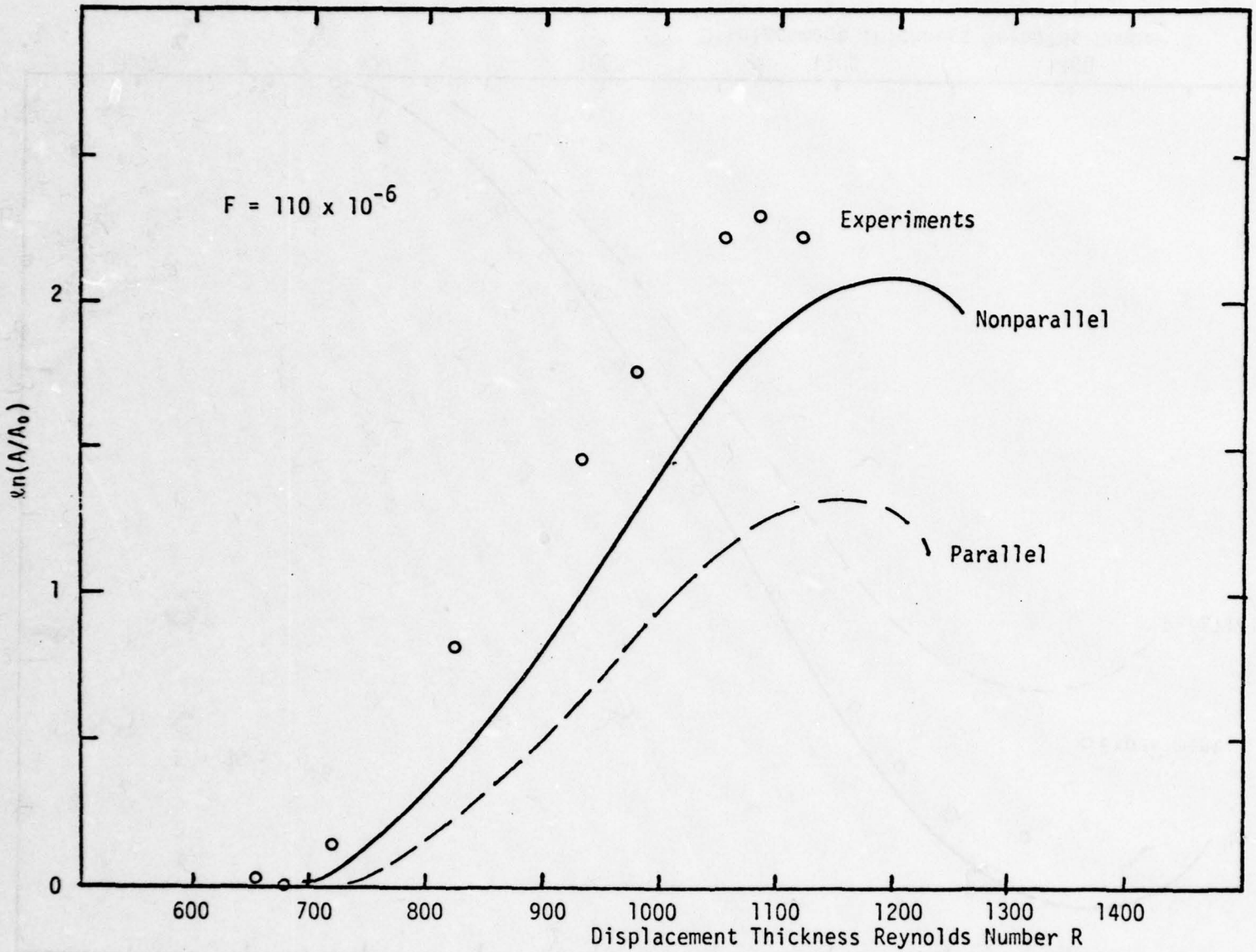

Figure 3. Amplitude vs Reynolds number. Solid line is nonparallel theory. Dashed line is parallel theory. Open symbols are experiments of Kachanov, Kozlov, & Levchenko (1975) at a frequency of $F = 110 \times 10^{-6}$.

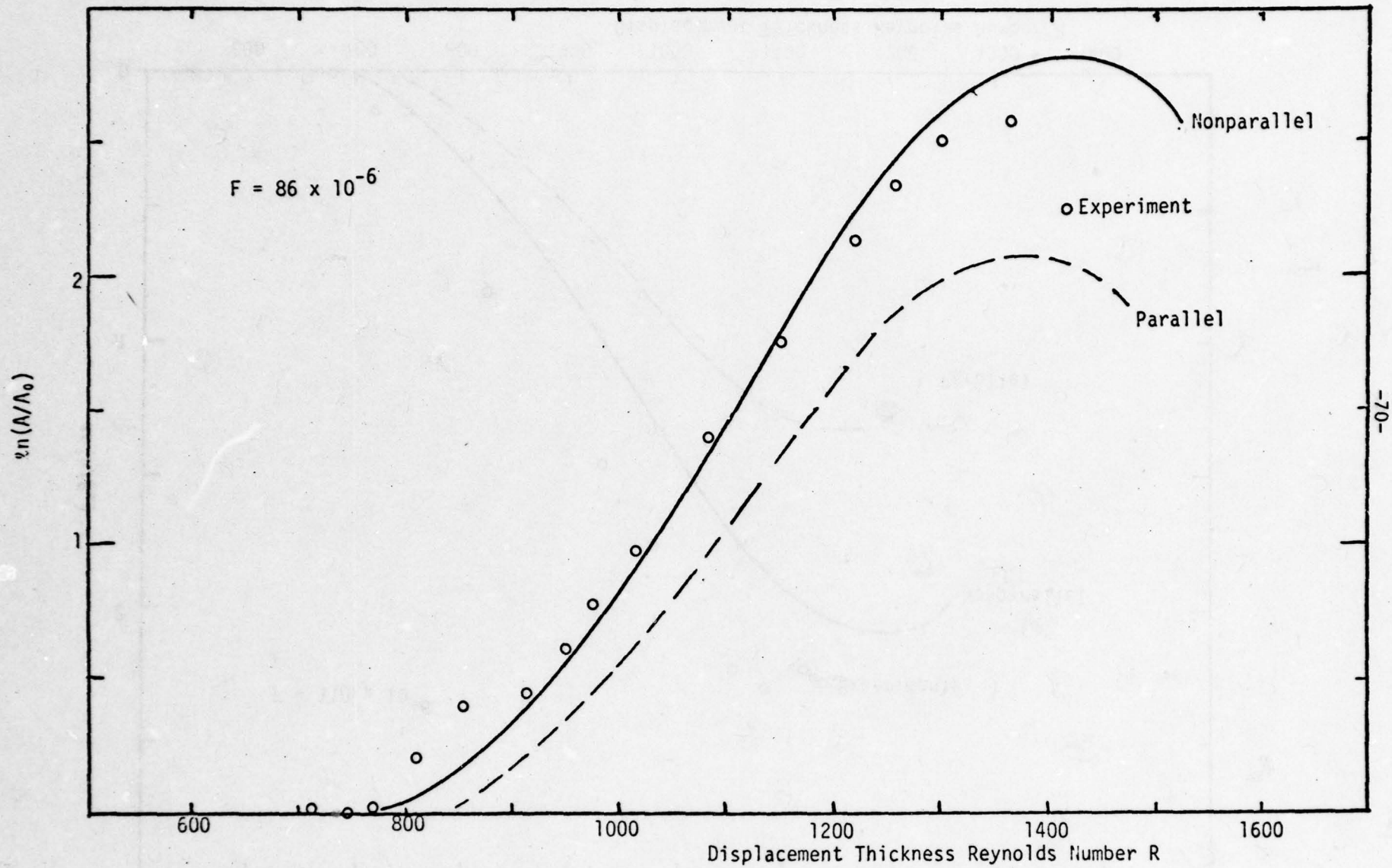

Figure 4. Amplitude vs Reynolds number. Solid line is nonparallel theory. Dashed line is parallel theory. Open symbols are experiments of Kachanov, Kozlov, and Levchenko (1975) at a frequency of F = 86 x 10^{-6}.

Section II

WAVE MECHANICAL ASPECTS OF TRANSITION

II-6 Wave Mechanical Aspects of Transition

M. T. Landahl
Mass. Inst. Technology

Synopsis

The final stage of transition of wall bounded shear flows is usually characterized by a sudden, almost explosive onset of a short-wave secondary instability with a characteristic scale much smaller than that typical of the unstable Tollmien-Schlichting waves. Such onset is found, for example, in turbulent spots (see e.g. picture by Elder, J.F.M. 9, 35), and in the formation of low-speed "spikes," (Klebanoff, et al., J. Fluid M. 12, 1). The propagation of such disturbances, considered as wave packets, can be analyzed by aid of kinematical wave theory applied to propagation in a slowly varying nonhomogeneous medium. This theory may be considered as an asymptotic one to first order in a small parameter measuring the ratio of secondary wave length to the characteristic scale of the primary inhomogeneity. For the case when the large-scale in homogeneity is a travelling wave of permanent shape, a critical condition for strong secondary instability was found to arise (Landahl, J. Fluid M. 56, 775) when the group velocity of the secondary, locally unstable wave is equal to the phase velocity of the large-scale (primary) wave. When this condition is met, space-time focusing of the small-scale disturbance on the large-scale wave will take place. The simple theory was found to give results in good agreement with measurements for the prediction of the location of the first appearing spike, as well as for the frequency of the secondary instability (Landahl, loc. cit.). Some new results are presented from breakdown calculations for a simple stratified shear flow model (Fig. 1). Breakdown can occur for both stable and unstable primary waves. The maximum wave slope attainable for the most unstable pure shear wave (zero Richardson number) before breakdown is found to be about 30°. The simple breakdown condition can be generalized to hold for arbitrary time-dependent three-dimensional primary flows.

Its implication for dispersive and nondispersive systems is discussed and a comparison made with ordinary ray (space-) focusing (Fig. 2).

New developments in kinematical wave theory for general classes nearly conservative fluid-flow systems (W. Chin, M.I.T. Ph.D. Thesis, 1975) show that shock-like transition giving discontinuities on the scale of large-scale flow are possible for systems that are supercritical in the sense of the breakdown condition. The discontinuities arise both in the large-scale flow and in the amplitude of the wave train (Fig. 3). Such a transition could be regarded as a generalization of the classical hydraulic pump or gas dynamic shock wave, and is proposed as a unified mechanism for fluid-flow transition phenomena.

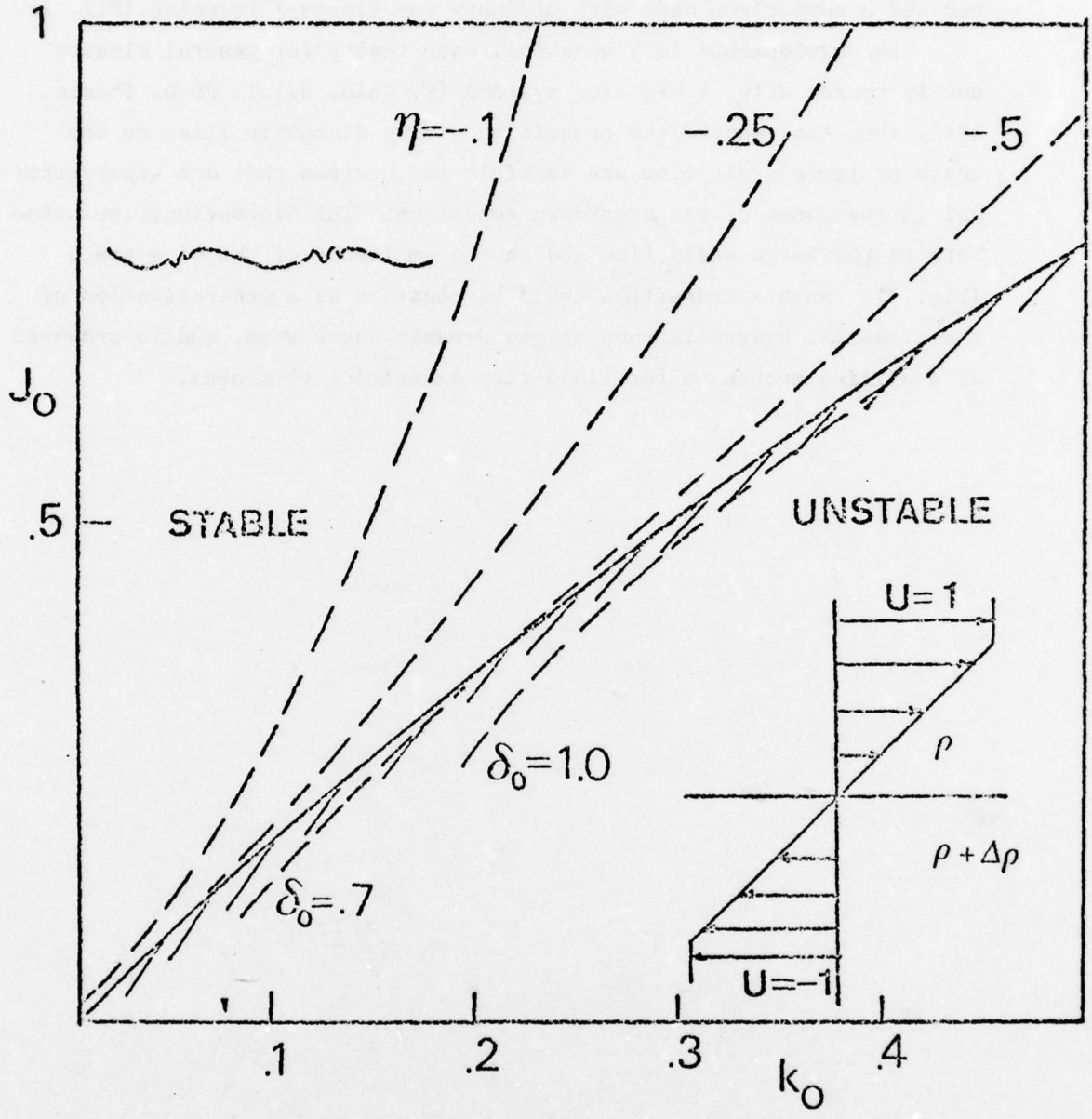

Largest attainable wave slope for most amplified primary wave: (J_o=0, k_o=0.4)

$k_o\delta_o \simeq 0.62 \quad (\sim 30^\circ)$

Fig. 1.

FOCUSSING IN 2-D WAVE PROPAGATION

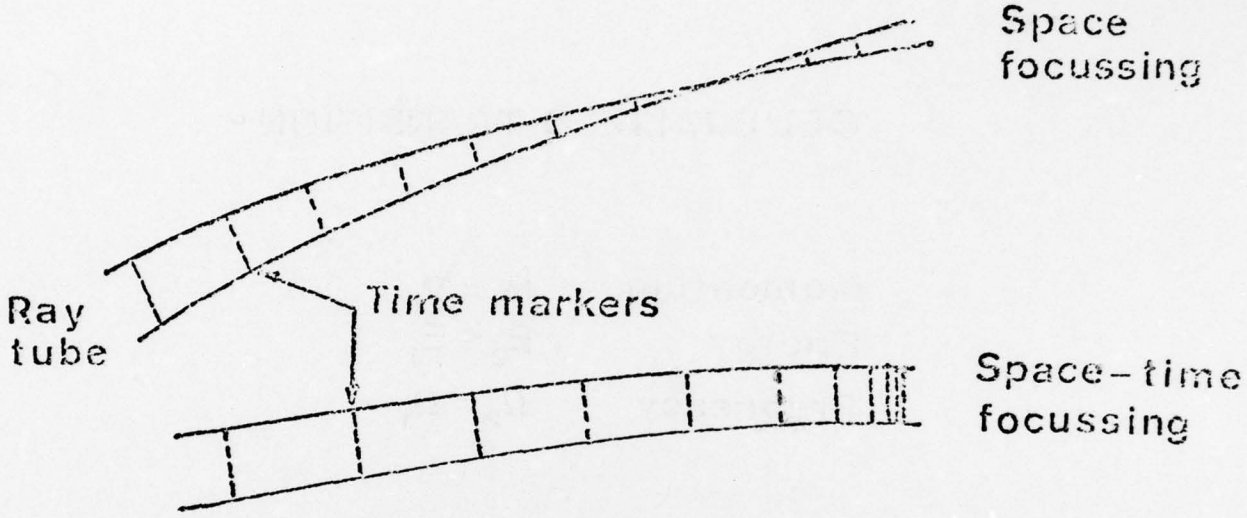

Fig. 2.

GENERALIZED TRANSITION

Momentum	$P_2 = P_1$
Energy	$E_2 \leq E_1$
Frequency	$\Omega_2 = \Omega_1$

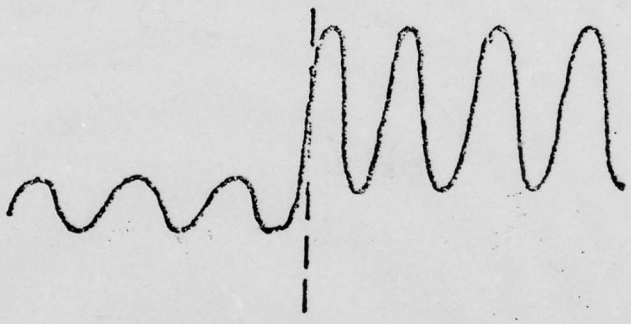

Fig 3.

Section III

THEORETICAL AND EXPERIMENTAL TRANSITION STUDIES AT ONERA / CERT

III-1 THEORETICAL AND EXPERIMENTAL TRANSITION STUDIES AT ONERA / CERT

R. MICHEL

Département d'Aérothermodyanmique, ONERA / CERT, Toulouse, FRANCE

In the beginning, the study has been undertaken essentially with the aim of defining means of calculation less empirical and more coherent than the available criterions, for predicting the onset and development of transition, under the complex influence of the various factors which can appear in practical problems.

For controlling the hypotheses and results of such a calculation method, it was felt necessary to carry out an experimental investigation giving sufficiently detailed informations about the development of mean and fluctuating characteristics of the boundary layer from the laminar to the turbulent regime ; this study led in fact to observations obviously concerned with the fundamentals of the transition process, and involved as a logical consequence, special and we hope, interesting developments.

1 - PREDICTION OF TRANSITION BY MODEL EQUATIONS.

On the theoretical side, the technique makes use of transport equations for different turbulent quantities, like turbulence intensity K, turbulent shear-stress $\overline{u'v'}$, and the dissipation of turbulence ε.

A two equations model (K, ε) was more intensively developed; the modelization is based in a first stage on the structure of established turbulent shear flows ; empirical functions using essentially the properties of the viscous wall region of a turbulent boundary layer, are introduced after that for taking account of the effects of viscosity upon turbulence.

Very encouraging results were obtained by showing at first that the metho is actually able to predict a damping for a given perturbation if it is introduced at a sufficiently low Reynolds number, and after that amplification at a Reynolds number corresponding to the experimental transition Re-number (fig. 1).

Different applications have been made, which led to a good agreement with experiments for the onset of transition as well as for its development up to the turbulent regime for problems like :

- transition as function of external turbulence on a flat plate in incompressible flow (fig. 2),
- combined effects of pressure gradient and external turbulence,
- combined effects of pressure gradient, turbulence and wall heat transfer (calculation of transitional boundary Layers on the upper and lower surfaces of turbine blades, fig. 3).

2 - FUNDAMENTAL EXPERIMENTAL STUDY OF TRANSITION.

On the experimental side, the transition on a cylinder aligned along the axis of an axisymmetric channel has been studied (Velocity : 33 m/s ; zero pressure gradient ; external turbulence : 0,25 %), involving at first a detailed determination of the mean velocity and fluctuations profiles in the transition region.

A good agreement with a calculation by the two equations model was obtained for the velocity profiles and mean flow characteristics of the boundary layer (fig. 4). A general coherence was observed also as concerns the development of turbulence, but the experiments revealed complex phenomena, especially related with a marked intermittency that the present calculation model is obviously unable to represent.

A careful investigation could show in evidence Tollmien-Schlichting waves and their amplification ; a spectral analyzis of the fluctuation led to interesting observations, by showing notably the coherence between the properties of the waves observed and the results of instability theory (fig. 5).

A specially significant aspect of the study is concerned with the formation of turbulent spots and with intermittency. A systematic conditional sampling of the signal delivered by the hot wire (fig. 6) was performed, and led to detailed informations for :

- the distribution of the intermittency factor (fig. 7),
- the passage velocities of successive laminar and turbulent flows,
- the classification of turbulent spots and the establishment of well defined characteristics for the formed spots,
- the determination of a statistical type-picture for the sequence of laminar and turbulent flows which could lead to a modelization of the intermittency phenomenon for future analytical developments.

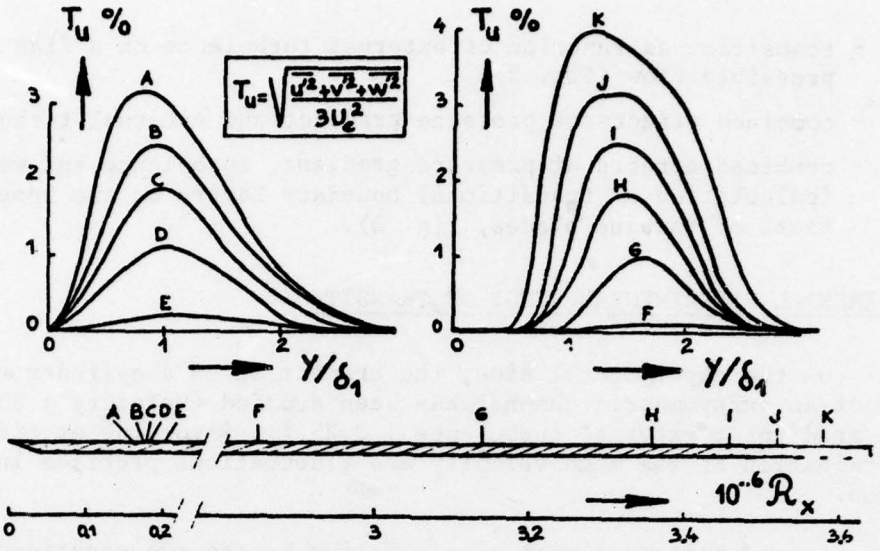

FIG. 1 - Damping and amplification of turbulent kinetic energy in a laminar boundary layer (T_{u_e} = 0,02 %) Calculation by means of the K, ε model method.

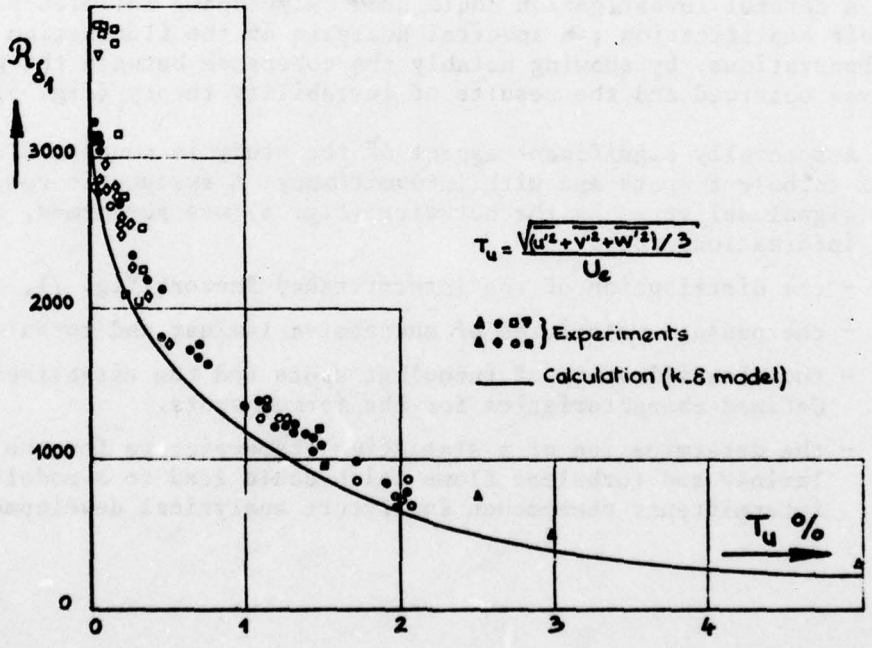

FIG. 2 - Displacement thickness Reynolds Number at beginning of transition (flat plate in incompressible flow).

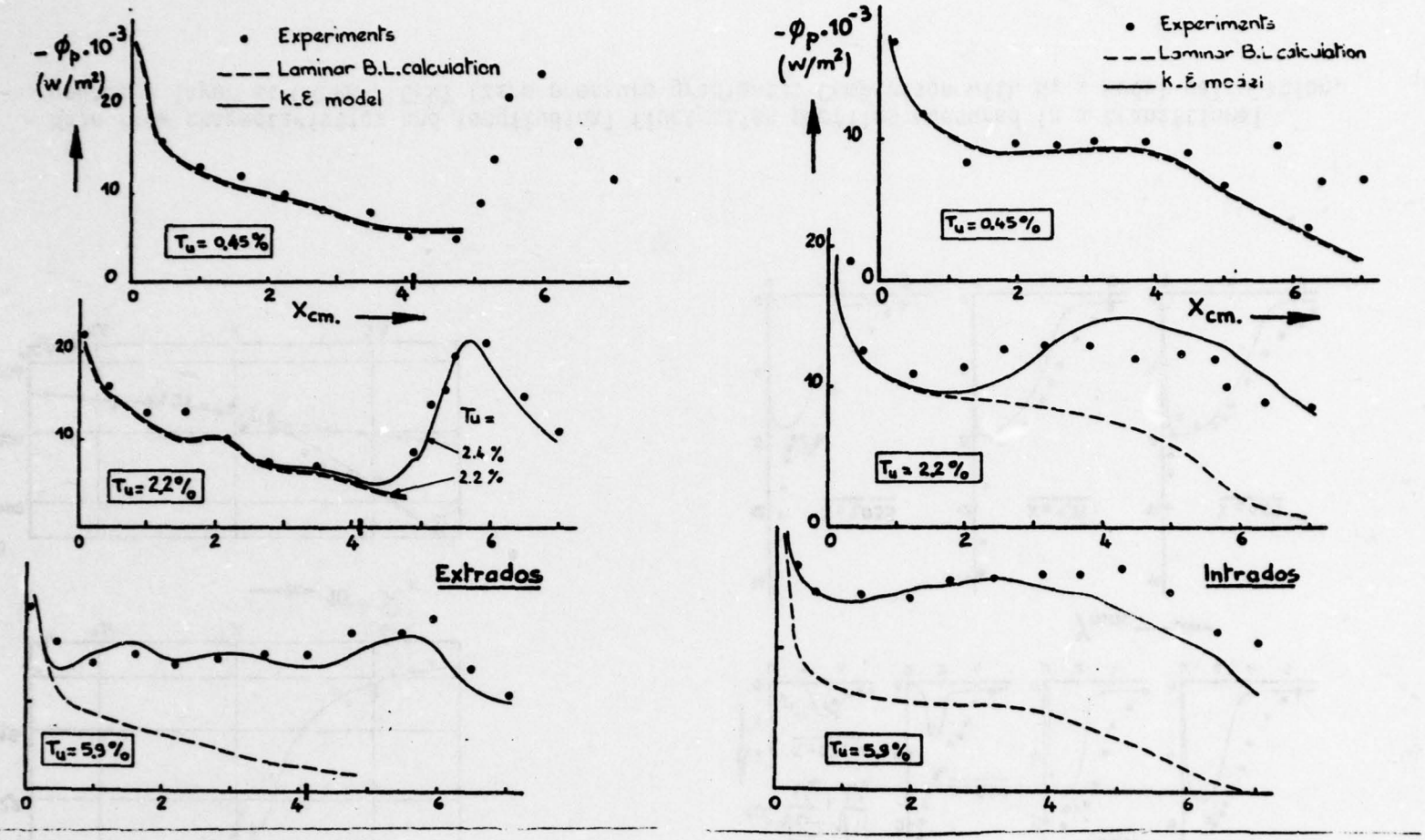

FIG. 3 - Calculation of transitional boundary layers heat transfer on a cooled turbine blade. Comparison with Turner's experiments.

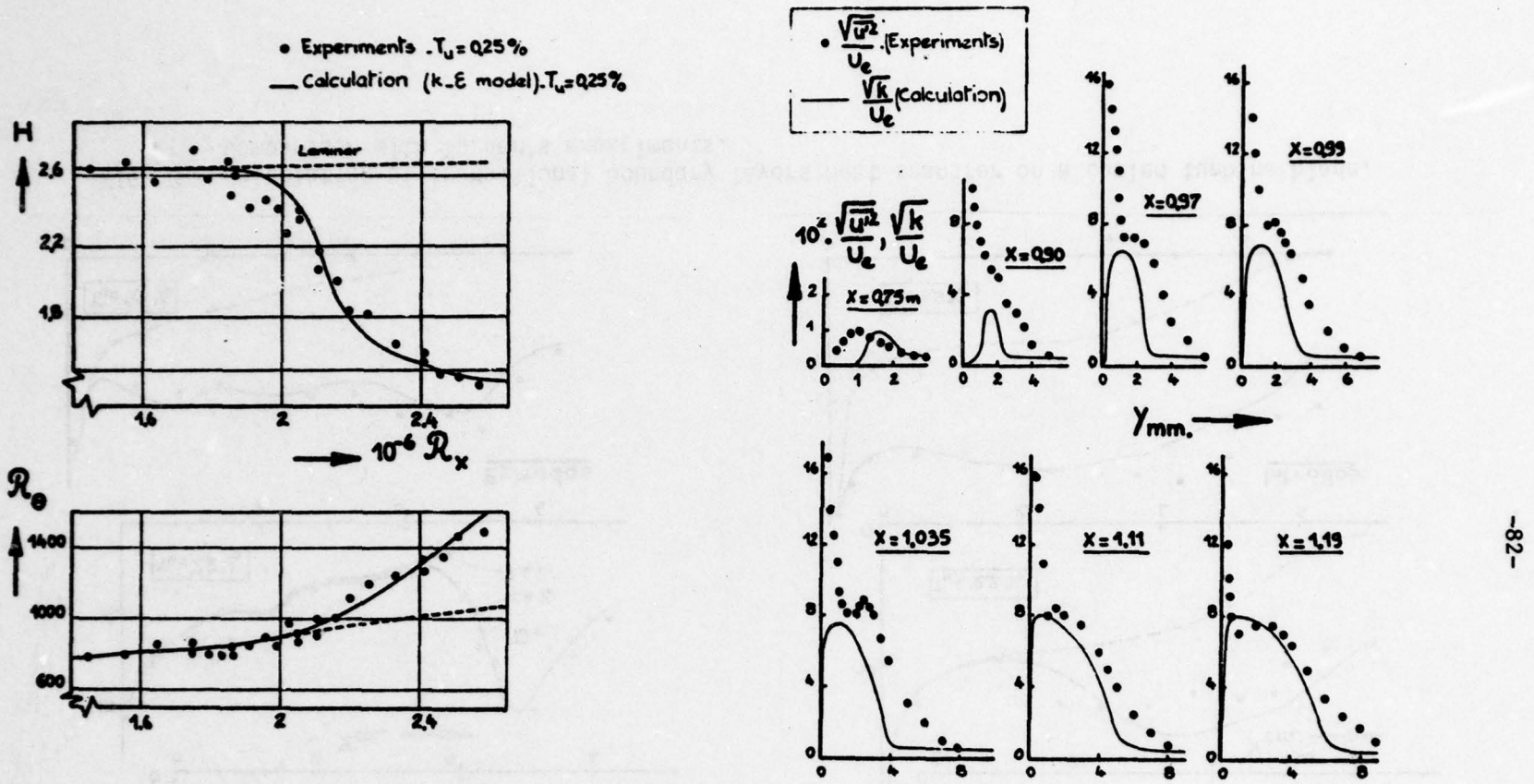

FIG. 4 - Mean flow characteristics and longitudinal fluctuation profiles measured in a transitional boundary layer at ONERA / CERT (zero pressure gradient). Comparison with K, ε model calculation.

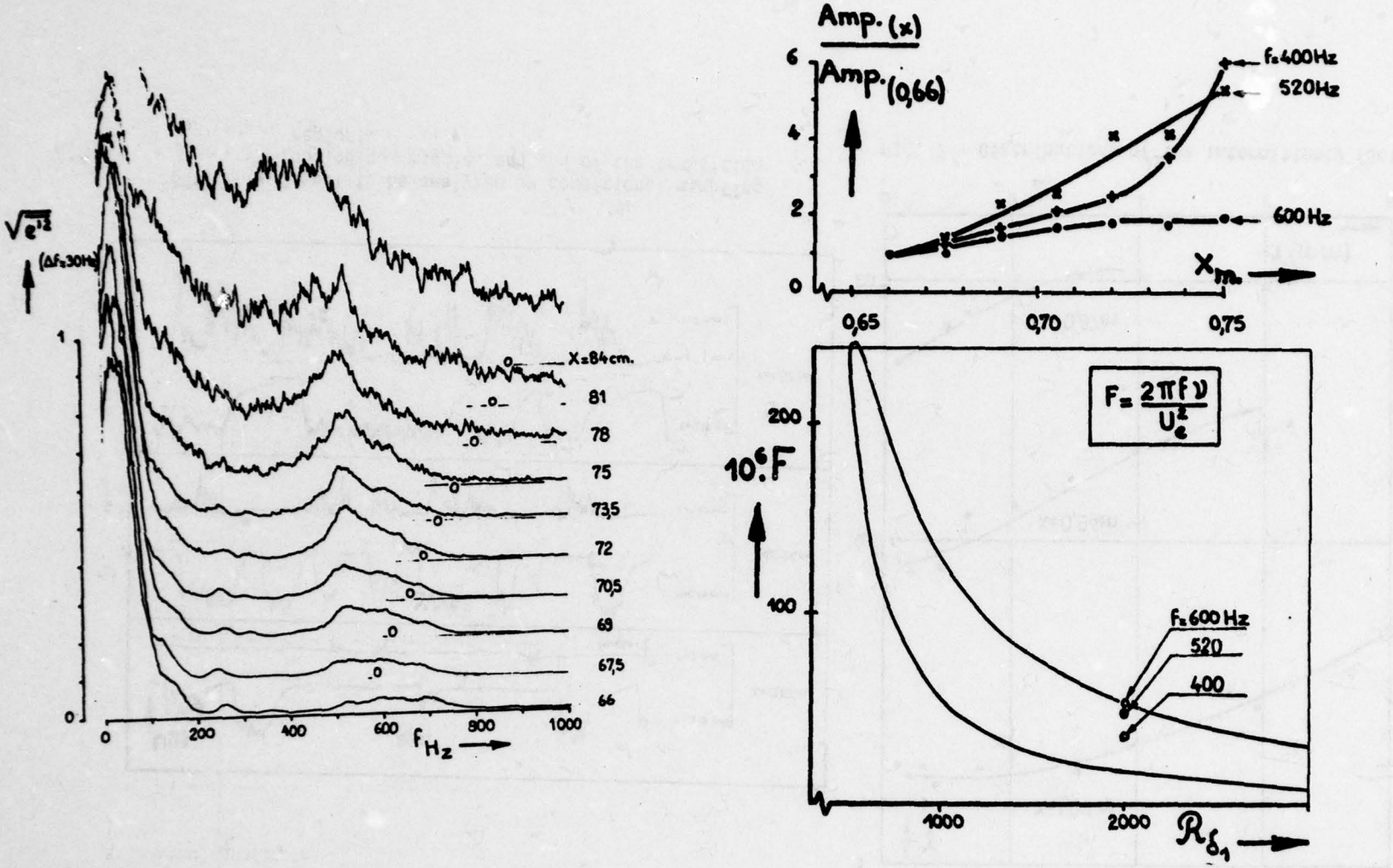

FIG. 5 - Spectral analysis of the longitudinal fluctuation at the beginning of transition ($\frac{y}{\delta}$ = 0,2). Amplification of the Tollmien-Schlichting waves and instability theory.

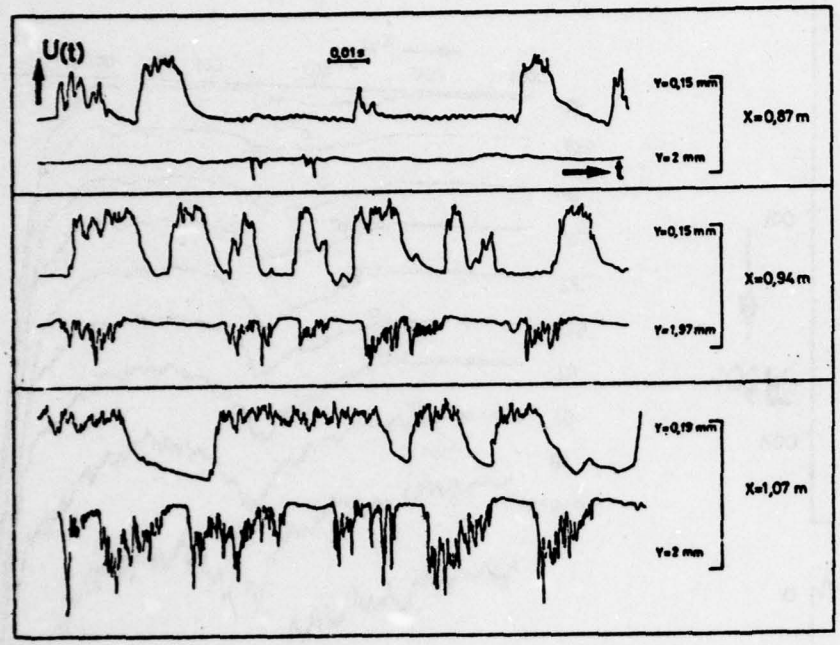

FIG. 6 - Signal to be analyzed by conditional sampling (beginning, middle, and end of the transition region).

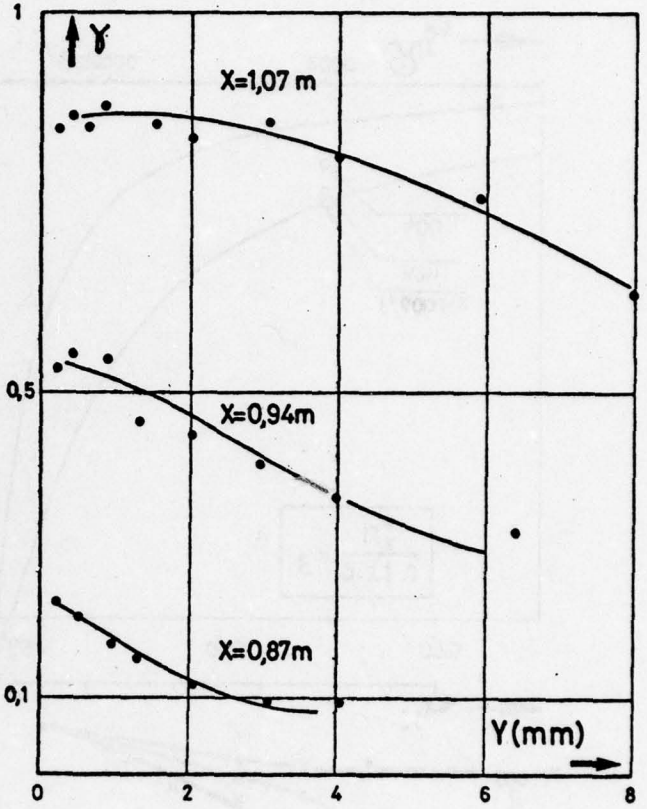

FIG. 7 - Distributions of the intermittency factor.

Section III

TURBULENCE-MODEL PREDICTED EFFECTS OF SURFACE HEAT TRANSFER ON BOUNDARY-LAYER TRANSITION

III-2 TURBULENCE-MODEL PREDICTED EFFECTS OF SURFACE HEAT TRANSFER ON BOUNDARY-LAYER TRANSITION

by

D. C. Wilcox and T. L. Chambers
DCW Industries, Inc.
Sherman Oaks, California

Effects of surface heat transfer on boundary-layer transition have been analyzed using a second-order closure turbulence model. The primary objective of the program has been to use the model to analyze effects of surface heating on hydrodynamic boundary-layer transition. As a secondary objective, the model has been used to study transition sensitivity to suction, surface roughness and freestream turbulence.

With no transition-specific modifications, the turbulence model predicts salient features of incompressible boundary-layer transition including sensitivity to freestream turbulence and surface roughness. As shown in Figures 1 and 2, in addition to accurately predicting effects of freestream turbulence, the model accurately simulates transition width, skin friction overshoot and transitional velocity profiles.

With transition modifications based on linear stability theory, the model accurately predicts transition sensitivity to surface heat transfer, pressure gradient and suction. Figure 3 compares predicted and measured transition Reynolds numbers for surface roughness effects and for the latter three effects on aerodynamic boundary layers. Of particular interest to the main project objective, consistent with measurements, the model predicts that heating destabilizes an aerodynamic boundary layer.

Figure 4 presents results of computations for four hydrodynamic bodies with and without surface heating. Again consistent with

measurements, the model indicates that small heating rates have a strong stabilizing effect on hydrodynamic boundary layers.

In summary, the model accurately simulates the various effects pertinent to hydrodynamic boundary-layer transition. The primary unresolved question is the model's sensitivity to freestream turbulence and the model's inability to directly account for Tollmien-Schlichting waves. These problems are undoubtedly tied to the masking of spectral information attending long-time (Reynolds) averaging. While the method's utility for many engineering applications does not appear to be significantly hindered by these unresolved issues, a hybrid linear-stability/turbulence-model (in contrast to linear-stability/e^9) simulation of transition may provide a more physically sound method than is currently provided either by the model or by linear-stability methods.

FIGURE 1

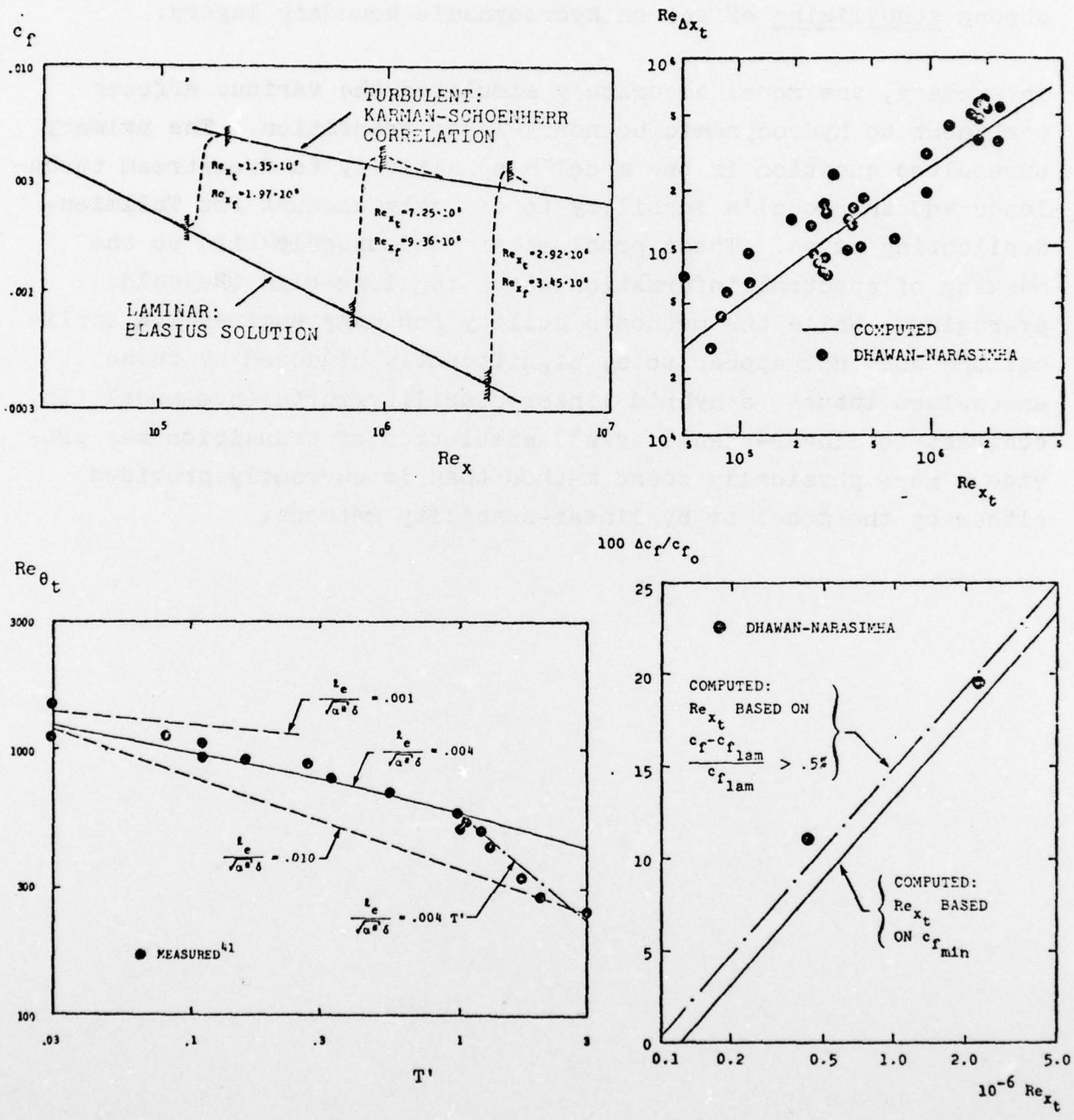

COMPARISON OF COMPUTED AND MEASURED PROPERTIES OF TRANSITIONAL FLAT-PLATE BOUNDARY LAYERS UNDER INCOMPRESSIBLE FLOW CONDITIONS.

FIGURE 2

INCOMPRESSIBLE FLAT-PLATE BOUNDARY LAYERS

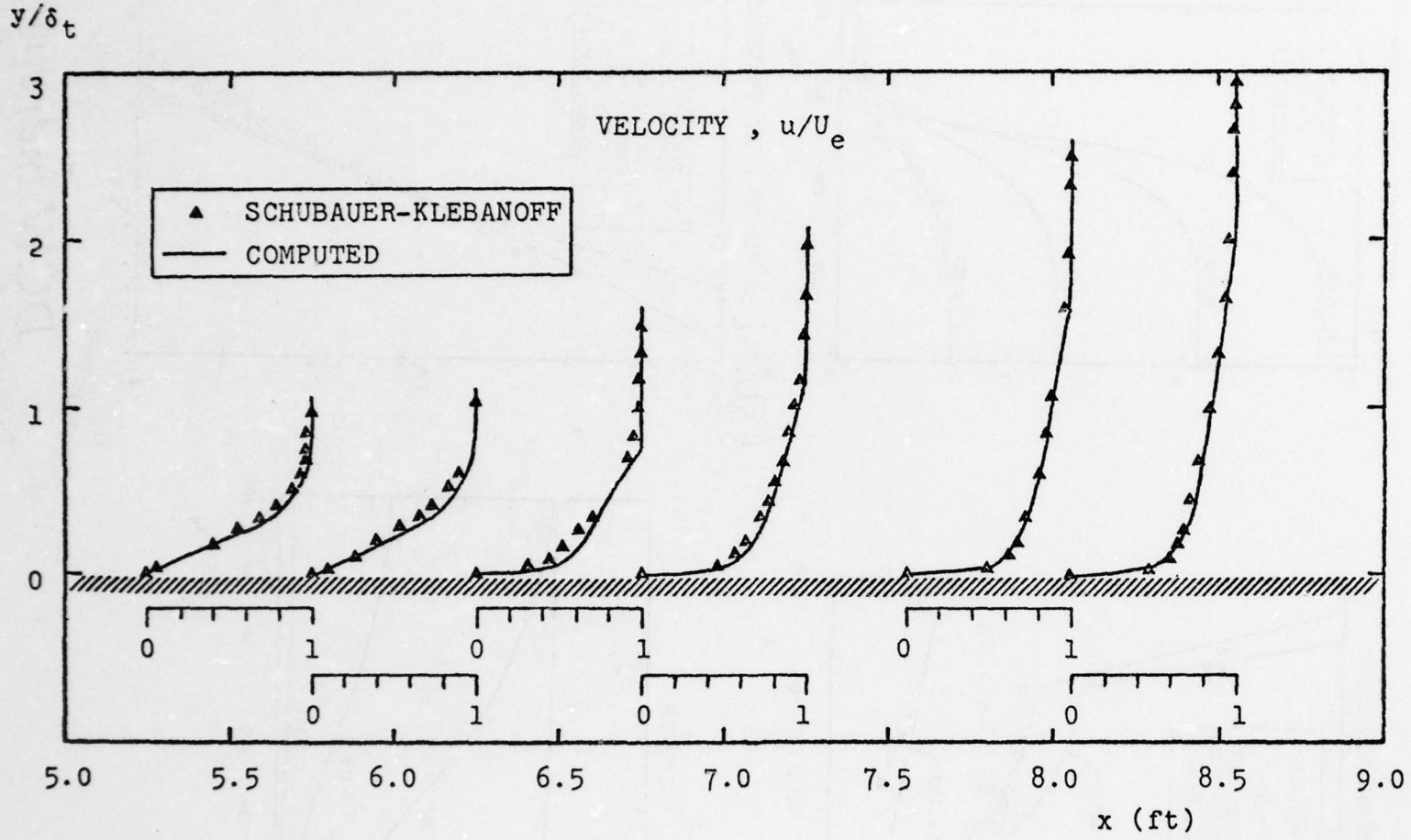

COMPARISON OF COMPUTED AND MEASURED TRANSITIONAL VELOCITY PROFILES FOR AN INCOMPRESSIBLE FLAT-PLATE BOUNDARY LAYER: T' = .03%; $\ell_e/\sqrt{\alpha^*_\infty}$ = .09; $Re_\infty = 5.2 \cdot 10^5$ PER FOOT.

FIGURE 3

TRANSITION SENSITIVITY TO VARIOUS EFFECTS

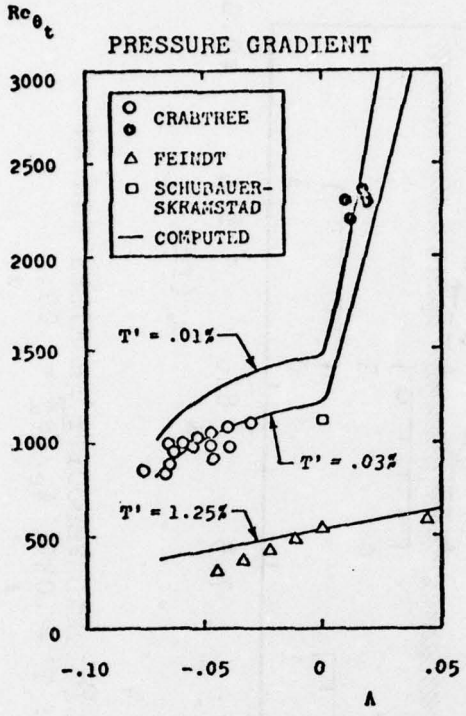

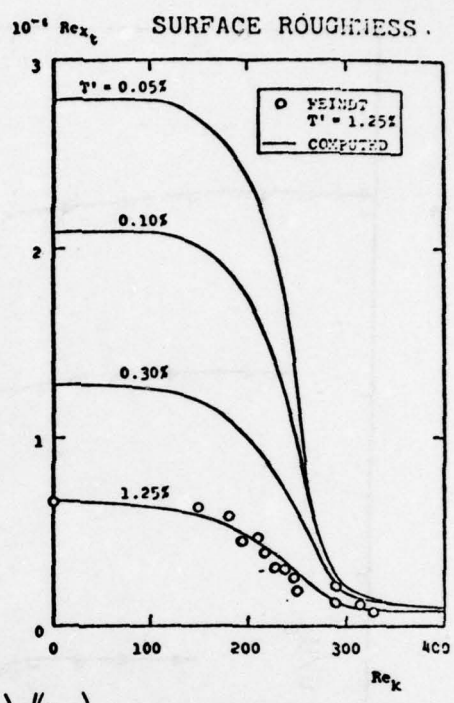

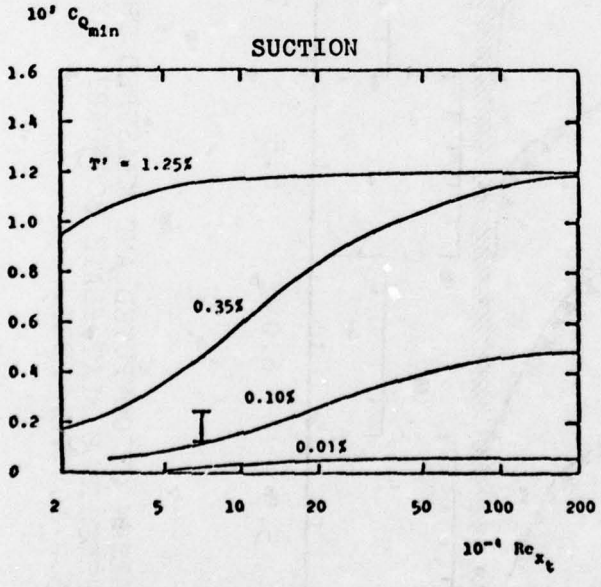

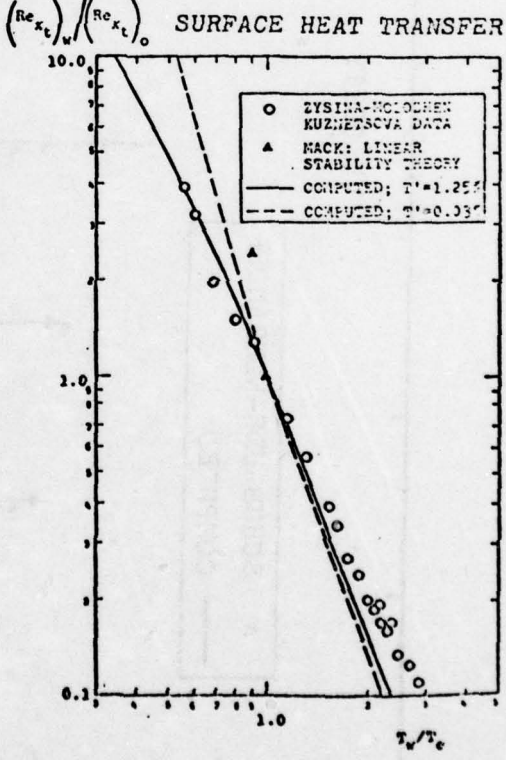

FIGURE 4

TRANSITION PREDICTIONS FOR HYDRODYNAMIC BODIES

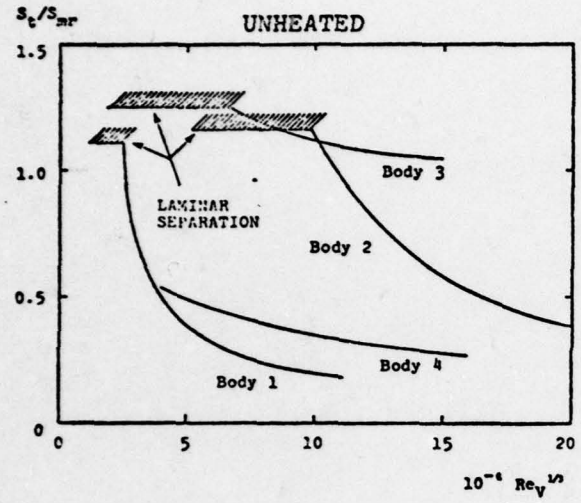

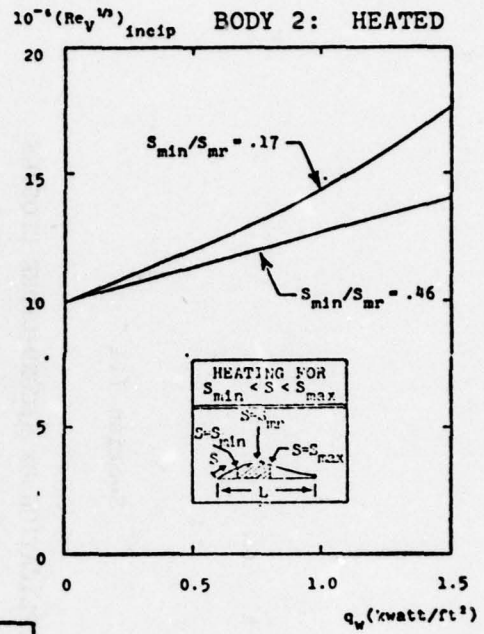

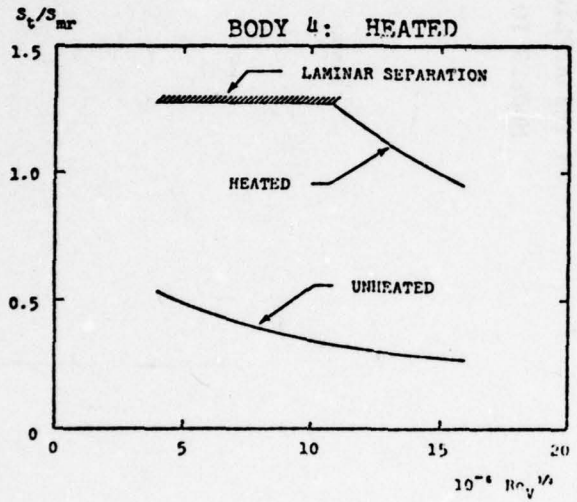

DCW Industries

Section III

ON THE APPLICATION OF SECOND-ORDER CLOSURE MODELS TO BOUNDARY LAYER TRANSITION

III-3 ON THE APPLICATION OF SECOND-ORDER CLOSURE MODELS TO BOUNDARY LAYER TRANSITION

Michael L. Finson

Physical Sciences Inc.
Woburn, MA 01801

Second-order closure models have been applied to a wide variety of turbulent flows in recent years. There are several advantages in applying such methods to transition problems. One obvious advantage is that second-order models are non-linear, and may provide useful results in the later stages of the transition process as the flow becomes fully turbulent. Also, the governing equations can be solved with straightforward numerical techniques, even in rather complicated situations. However, it has yet to be demonstrated that the required closure approximations can be made in a manner that is physically sound for transition regimes. For example, the second-order models cannot be expected to reproduce linear stability theory. It might be anticipated that second-order models would have greatest applicability in "by-pass" situations, where transition is triggered by relatively high levels of initial fluctuations, introduced by free-stream turbulence or surface roughness.

Our studies have utilized a "five equation" model; the dependent fluctuating quantities are the three components of the fluctuating kinetic energy $\overline{u'^2}$, $\overline{v'^2}$, $\overline{w'^2}$, the Reynolds stress $\overline{u'v'}$, and either the dissipation rate Φ or the length scale Λ. A typical equation, for the kinetic energy $q^2 = (\overline{u'^2} + \overline{v'^2} + \overline{w'^2})/2$, is

$$\frac{Dq^2}{Dt} = -\overline{u'v'}\ \frac{\partial U}{\partial y} - \Phi\ \frac{\partial}{\partial y}\left(\nu + c\,\frac{q^2 v^2}{\Phi}\ \frac{\partial q^2}{\partial y}\right) \qquad (1)$$

where the terms represent convection, production, dissipation, and molecular and turbulent diffusion. The required closure approximations for turbulent

flows have been developed from basic laboratory turbulence measurements, wherever possible.

A careful examination of the adequacy of the various closure requirements for the transition regime has been performed. The production terms are treated exactly in our formulation (such is not the case with "2-equation" models), and so are the molecular diffusion terms. Concerning the dissipation, we claim (without proof, here) that adequate treatments can be developed, since exact solutions are known in the limit $Re \to 0$.

The difficult terms are the "redistribution" terms $\left(\overline{u_i' \frac{\partial p'}{\partial x_j}}\right)$ that appear in the equations for the individual components of the Reynolds stress tensor. Turbulent closure approximations have been developed by Rotta[1] and Hanjalic and Launder[2], but these approximations become suspect near solid walls, for length scales that are not small compared to mean flow dimensions, or for non-turbulent spectra. Such terms play an important role in the production of fluctuating energy. With the direct production terms, $\overline{u'^2}$ is produced by $\overline{u'v'} \frac{\partial U}{\partial y}$ and $\overline{u'v'}$ is produced by $\overline{v'^2} \frac{\partial U}{\partial y}$ but (under the boundary layer approximations) there are no terms to produce $\overline{v'^2}$ or $\overline{w'^2}$ directly. The direct production terms will not yield transition since $\overline{v'^2}$ is not produced and the production of $\overline{u'v'}$ will hence be small. However the turbulent closure for the p' terms introduces additional terms of the form $\overline{u_i' u_j'} \frac{\partial U}{\partial y}$. These terms tend to isotropize the production process, and cause an extremely rapid amplification in a transition calculation. In reality, the pressure-strain terms must be considerably smaller in the transition regime.

Several potential modifications to the pressure-strain terms have been investigated. First there are wall effects, which are important in a transitional boundary layer or in the viscous sublayer. If Λ/y is not small, the normal fluctuations v' are reduced by the presence of the wall. To obtain the proper behavior as $y \to 0$, the turbulent closure terms for

pressure-strain should be reduced by $(1 + \Lambda^2/y^2)^{-1}$. Second, the pressure-strain terms are generally the first terms in a series expansion in Λ/δ. Additional terms such as

$$\frac{\partial \overline{u_i' u_j'}}{\partial y} \quad \frac{\partial^2 U}{\partial y^2} \quad \Lambda^2$$

become important in transitional situations where Λ/δ is not necessarily small. Note that this term introduces a dependence on $\frac{\partial^2 U}{\partial y^2}$. The net result of these modifications is a more reasonable production cycle in the transition regime. However, it should be emphasized that the present treatment is rather tentative and cannot yet be considered adequate.

Figure 1 compares the results of the present model for the effect of free-stream turbulence on flat plate transition with the data of various investigators. In the calculations the level of the free-stream turbulence (assumed isotropic) was specified as a boundary condition at $y \to \infty$, and the length scale in the free-stream was taken to be sufficiently large that the turbulence there would not decay over the distances considered. The results implicate a somewhat more rapid transition than observed, but the comparison should be qualified by the uncertain nature of the free-stream turbulence in most tests (probably acoustic rather than vortical). Spangler and Wells[3] observed a smaller transition Reynolds number, for a given rms fluctuation level, when the free-stream turbulence was generated by a grid, consistent with our results.

The effect of distributed surface roughness on transition has also been examined. In so doing, we modeled the manner by which roughness elements introduce disturbances into the flow by assuming that the flow around individual elements is attached. A distributed sink term (for $y \leq k$) is included in the mean momentum equation to account for the drag of the elements, and a distributed source term in the kinetic energy equation describes the introduction of fluctuations downstream of each element. The details

may be found in Ref. 4. Figure 2 shows the resulting computations for transition, compared with Feindt's[5] data on flat plates roughened with sandpaper. At roughness Reynolds numbers below about 250, free-stream turbulence appears to be responsible for transition.

The model described here shows promise for predicting transition, at least for some conditions such as those where there are relatively high levels of initial disturbances. As indicated above, the closure approximations required for the pressure-strain terms are critical in the transition region. Our current treatment can only be considered to be an initial attempt, and further work is required to assure a physically sound closure.

REFERENCES

1. Rotta, J., "Statistische Theorie nichthomogener Turbulenz", Zeitschrift fur Physik., 129, 547-572 (1951), and 131, 51-77 (1951).

2. Hanjalic, K. and Launder, B. E., "A Reynolds Stress Model of Turbulence and its Application to Thin Shear Flows", J. Fluid Mech., 52, 609-638 (1972).

3. Spangler, J. C. and Wells, C. S., Jr., "Effects of Free-stream Disturbances on Boundary-Layer Transition," AIAA J., 6, 543-545 (1968).

4. Finson, M. L., "A Reynolds Stress Model for Boundary Layer Transition with Application to Rough Surfaces," Physical Sciences Inc. TR-34 (1975).

5. Feindt, E. G., "Untersuchungen uber die Abhangigkeit des Umschlages laminar-turbulent von der Oberflachenrauhigkeit und der Druckverteilung", Jahrbuch 1956 der Schiffbautechnischen Gesillschaft 50, 180-203 (1957).

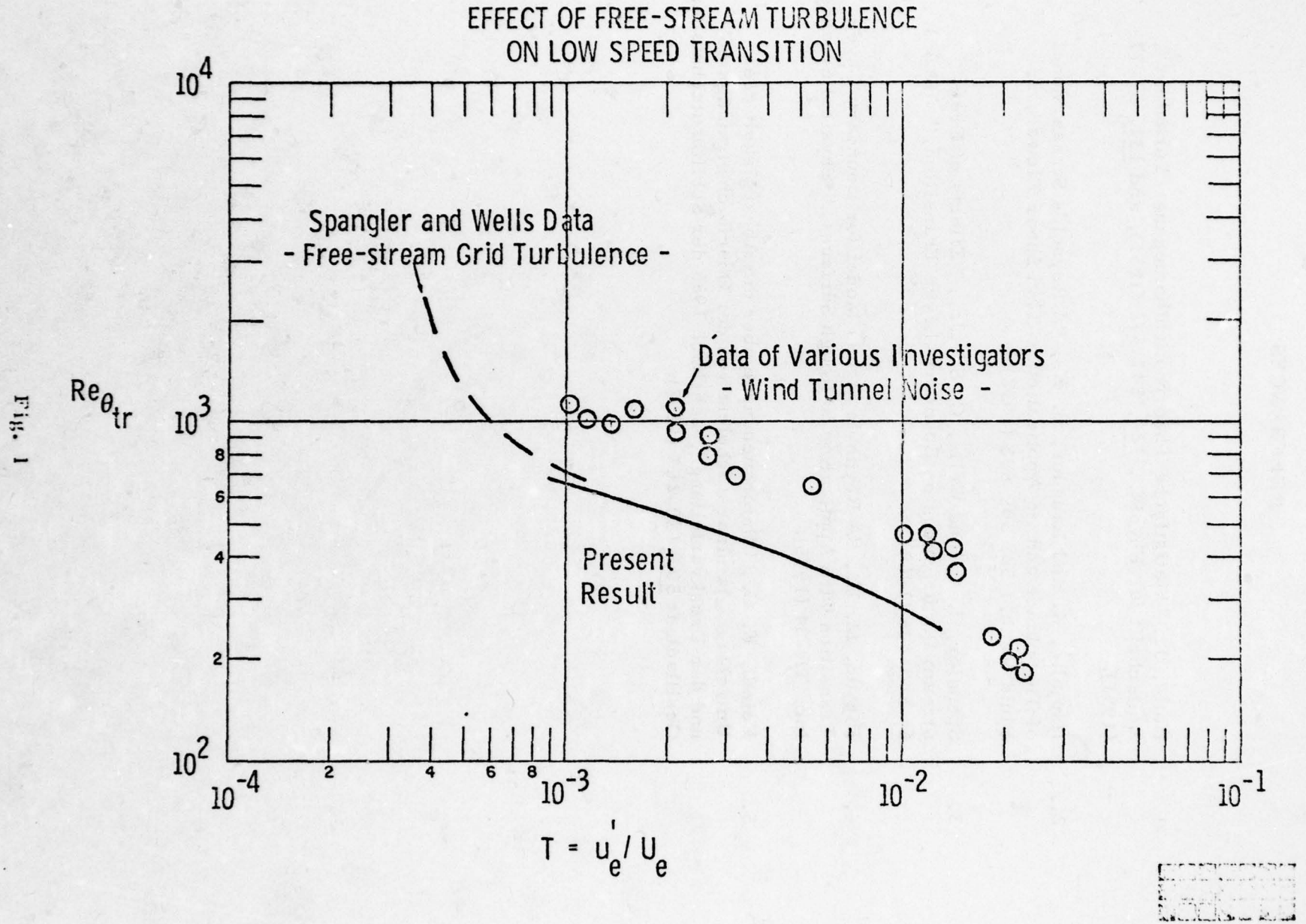
EFFECT OF FREE-STREAM TURBULENCE
ON LOW SPEED TRANSITION
Spangler and Wells Data
- Free-stream Grid Turbulence -
Data of Various Investigators
- Wind Tunnel Noise -
Present
Result
$Re_{\theta_{tr}}$
$T = u_e'/U_e$
10^4
10^3
10^2
8
6
4
2
10^{-4}
10^{-3}
10^{-2}
10^{-1}

Fig. 1

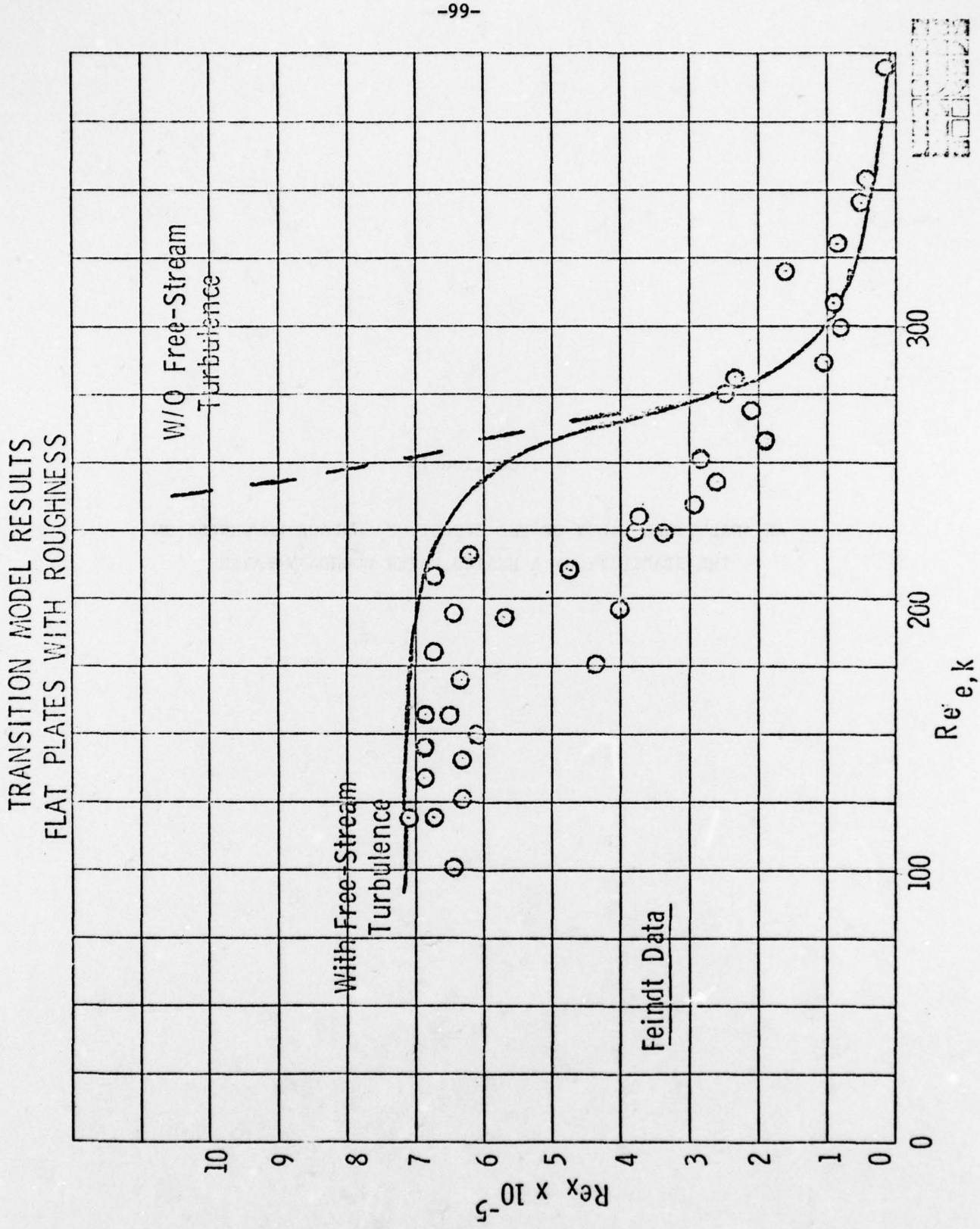
TRANSITION MODEL RESULTS
FLAT PLATES WITH ROUGHNESS
W/O Free-Stream Turbulence
With Free-Stream Turbulence
Feindt Data
$Re_x \times 10^{-5}$
$Re_{e,k}$
0
1
2
3
4
5
6
7
8
9
10
0
100
200
300

Fig. 2

Section IV

AN ANALYTICAL STUDY OF THE EFFECT OF SURFACE ROUGHNESS ON THE STABILITY OF A HEATED WATER BOUNDARY LAYER

IV-1 AN ANALYTICAL STUDY OF THE EFFECT OF SURFACE ROUGHNESS ON THE STABILITY OF A HEATED WATER BOUNDARY LAYER*

By

Denny R. S. Ko and M. Kosecoff

Physical Dynamics, Inc.
Torrance, Calif.

This study analyzes the effects of surface roughness on low speed boundary layer stability and transition in a liquid environment. An analytical model for distributed surface roughness elements, spaced closely compared to the characteristic wavelength of the boundary layer disturbances, is presented. The model postulates an enhanced momentum and heat exchange near the wall induced by the presence of these roughness elements. A "turbulent roughness layer" with a thickness of the order of the mean roughness height is assumed to be imbedded within the ordinary laminar boundary layer. Enhanced momentum and energy exchange within this layer is modeled by an effective eddy diffusity. The presence of the turbulent roughness layer modifies the mean flow (velocity and temperature) profiles which, in turn, alter the stability characteristics. The effect on boundary layer transition is then inferred by adopting a semi-empirical e^n criterion.

To demonstrate the effect of the distributed surface roughness on a heated water boundary layer, the model is incorporated into a set of similarity equations for estimating the mean flow profiles. These profiles are then used in linear stability calculation, which, when coupled with the e^n criteria, gives the transition location. The linearized stability equations use a parallel flow assumption and incorporate the variation of viscosity and conductivity with temperature. These equations are solved using a code developed by Lowell and Reshotko. Amplification rates are calculated as functions of k/θ and ΔT_w for fixed values of Re_θ and dp/dx, where k is the roughness height, θ is the momentum thickness, and ΔT_w is the difference between the wall and ambient temperatures.

* This work is supported by the DARPA under ONR Contract Number N00014-76-C-0967.

For a given dp/dx, it is found that there exists a range of values of k/θ for which the wall may be considered essentially smooth. However, the more favorable the pressure gradient, the narrower this range is. As anticipated, heating and/or a favorable pressure gradient tend to stabilize the boundary layer for small roughness, and these effects are reduced for moderate roughness. However, when k/θ is sufficiently large, heating tends to destabilize the boundary layer. Furthermore, as the pressure gradient becomes more favorable, the criteria for "large k/θ" reduces significantly. Finally, roughness substantially increases the range of frequencies which are unstable at a given Re_θ. A semi-quantitative summary of these results is given in Table 1.

Table 1: Effect of Roughness on Amplification Rates

Falkner-Skan parameter, β	$\frac{k}{\theta}$	$\Delta T = 0^\circ F$	$\Delta T = 30^\circ F$
0	$\leq .25$	negligible	negligible
	.5	small	moderate
	.75	drastic	drastic
-0.05	$\leq .5$	negligible	negligible
	.75	moderate	drastic
	1.0	drastic	drastic
0.2	$\leq .15$	negligible	negligible
	.25	moderate	drastic
	.4	drastic	drastic

Section IV

ON THE EFFECT OF FREESTREAM TURBULENCE ON BOUNDARY-LAYER TRANSITION

IV-2 On the Effect of Freestream Turbulence on Boundary-Layer Transition

Leslie M. Mack

Jet Propulsion Laboratory

The results of several experiments are summarized in figure 1 and show a strong influence of freestream turbulence on the transition of a flat-plate laminar boundary layer. Most of the data in figure 1 are from the Schubauer-Skramstad experiment, where tunnel noise dominated transition below u_1'/U_1 of about 0.1%. (u' and U are the rms and mean x-velocity components; the subscript 1 refers to freestream conditions.) Only the data for $u_1'/U_1 > 0.1\%$ represent the effect of freestream turbulence. Figure 2 interprets these data in terms of linear stability theory to emphasize just how strongly turbulence affects transition. The maximum amplitude ratio of linear stability theory, $\ell n\,(A/A_o)_{max}$, decreases from a value of 8.1 at the transition Reynolds number, $Re_t = U_1 x/\nu$, for $u_1'/U_1 = 0.1\%$, to 2.6 at $u_1'/U_1 = 1\%$. Consequently, if A at transition is a constant, A_o must at the same time increase by a factor of 245. The power-law relation $A_o \sim (u_1'/U_1)^{2.4}$ accounts quite well for this behavior of A_o.

The most straightforward way of using linear stability theory as a means of transition prediction is the so-called e^9 method of Smith-Gamberoni and Van Ingen. A value of $n = \ell n\,(A/A_o)$ is chosen, and transition is considered to occur whenever the maximum of $\ell n\,(A/A_o)$ at some Reynolds number equals n. Obviously a fixed value of n is incompatible with figure 1. The easiest way to incorporate the effect of turbulence into the e^9 method is to let n be a function of u_1'/U_1. The data of figure 1 are fitted closely by

$$n = -8.43 - 2.4\,\ell n\,(u_1'/U_1)\ .$$

As the above relation is based solely on flat-plate data, another method has been developed which is intended to have wider application. This method, which can be referred to as an amplitude method to distinguish it from the amplitude-density e^9 or modified e^9 methods, is based on the following ideas:

a) it uses the actual disturbance amplitude which is made up of harmonic components of all frequencies and orientations:

b) the initial amplitude density $A_o(\omega, \beta)$, where ω is the frequency and β the transverse wave number, is related to the corresponding component of the freestream turbulence by an interaction relation;

c) isotropic turbulence theory is used to characterize the freestream turbulence.

With the individual harmonic components of the boundary-layer disturbance assumed to have random phase relations, the disturbance amplitude is given as a function of Reynolds number by

$$A_d^2(R) = \int_0^\infty d\left(\frac{\omega L}{U_1}\right) \int_{-\infty}^\infty \left[\frac{A}{A_o}\left(\frac{\omega \nu}{U_1^2}, \beta\right)\right]^2 A_o^2\left(\frac{\omega L}{U_1}, \beta\right) d\beta ,$$

where L is an integral length scale of the turbulence. If advantage is taken of the sharp tuning of the boundary-layer response, this expression can be simplified to

$$A_d^2(R) = A_o^2(\omega_{max}, \beta_{max}) \int_0^\infty d\left(\frac{\omega L}{U_1}\right) \int_{-\infty}^\infty \left[\frac{A}{A_o}\left(\frac{\omega L}{U_1^2}, \beta\right)\right]^2 d\beta .$$

Because the function A/A_o always has roughly the same shape, a further simplification can be made to

$$A_d^2(R) = C_1^2 A_o^2(\omega_{max}, \beta_{max}) \left(\frac{U_1 L}{\nu}\right) \times \left[\frac{A}{A_o}\left(\frac{\omega\nu}{U_1^2}, \beta\right)\right]^2_{max} \Delta\left(\frac{\omega\nu}{U_1^2}\right) \Delta\beta \ .$$

The two factors $\Delta(\omega\nu/U_1^2)$ and $\Delta\beta$ are consistently defined response bandwidths, and along with $(A/A_o)_{max}$ and $(\omega\nu/U_1^2)_{max}$ are obtained from stability theory with little more computational effort than is required for the e^9 method. For a two-dimensional incompressible boundary layer, the maximum response is always at $\beta = 0$. Since it has been observed for these same boundary layers that $\Delta\beta$ is only slightly dependent on the Reynolds number, this factor will be absorbed into the constant C_1. The scale Reynolds number $U_1 L/\nu$ is set by the freestream turbulence, and A_o^2 is to be found from an interaction model.

In the absence of compelling theoretical or experimental arguments as to the mechanism by which freestream turbulence produces laminar instability waves, the following arbitrary assumptions are made:

a) instability waves originate near the solid boundary;

b) their amplitude is proportional to the normal viscous velocity of the forced response in the viscous sublayer of the freestream turbulence;

c) the forced response is given by Prandtl's model of the sublayer (boundary-layer equations with $U = 0$).

The result of the analysis for the rms normal viscous velocity v_v' of component ω, β is given by

$$\left[\frac{v_v'(\omega, \beta)}{U_1}\right]^2 = \left(\frac{\omega\nu}{U_1^2}\right) \left[\frac{p'(\omega, \beta)}{\rho U_1^2 \cos^2\psi}\right]^2 ,$$

where ψ is the angle between the wave-number vector in the plane of the surface and the freestream direction. The component rms pressure fluctuation $p'(\omega, \beta)$ is represented by a two-dimensional power-spectrum function $F_2(\omega, \beta)$:

$$\left[\frac{p'(\omega, \beta)}{\rho U_1^2}\right]^2 = \left(\frac{p'}{\rho U_1^2}\right)^2 \left[\frac{U_1 F_2(\omega, \beta)}{L^2}\right] .$$

The wide-band pressure fluctuation p' is taken to be that of isotropic turbulence, and is thus related to the velocity fluctuation by

$$\frac{p'}{\rho U_1^2} \propto \left(\frac{u_1'}{U_1}\right)^2 .$$

With A_o assumed proportional to v_v', the interaction relation is

$$A_o^2(\omega, \beta) = C_2^2 \left(\frac{\omega\nu}{U_1^2}\right) \left(\frac{u_1'}{U_1}\right)^4 \left[\frac{U_1 F_2(\omega, \beta)}{L^2}\right] .$$

The final expression for the disturbance amplitude is, with $\beta = 0$ and $C = C_1 C_2$,

$$A_d^2(R) = C^2\left(\frac{U_1 L}{\nu}\right)\left[\frac{U_1 F_2(\omega)}{L^2}\right]\left(\frac{u_1'}{U_1}\right)^4$$

$$\times \left(\frac{\omega\nu}{U_1^2}\right)_{max}\left[\frac{A}{A_o}\left(\frac{\omega\nu}{U_1^2}\right)\right]_{max} \Delta\left(\frac{\omega\nu}{U_1^2}\right) .$$

The only remaining task is to develop an expression for the spectrum function $F_2(\omega)$. The two-dimensional wave number spectrum is given in terms of the three-dimensional spectrum by

$$F_2(k_1,_2) = \int_{-\infty}^{\infty} F_3(k)\, dk_3 ,$$

where $k^2 = k_1^2 + k_2^2 + k_3^2$, and $k_{1,2}^2 = k_1^2 + k_2^2$. The one-dimensional spectrum is

$$F_1(k_1) = 2\pi \int_{k_1}^{\infty} k\, F_3(k)\, dk .$$

Consequently,

$$F_2(k_1,_2) = -\frac{1}{\pi}\int_{k_1,_2}^{\infty} \frac{1}{(k^2 - k_{1,2}^2)^{\frac{1}{2}}} \frac{dF_1}{dk}\, dk .$$

The normalized one-dimensional pressure spectrum which corresponds to the von Karman interpolation formula for the one-dimensional velocity spectrum is

$$F_1(k_1) = 4\left[1 + \left(\frac{5}{6} k_1\right)^2\right]^{-7/6} .$$

Use of this expression leads to the following interpolation formula for $F_2(k_{1,2})$:

$$F_2(k_{1,2}) = 1.78 \left[1 + (0.82\ k_{1,2})^2\right]^{-5/3} .$$

Both F_1 and F_2 are shown in figure 3. For the $\beta = 0$ component, which is the only one used in the present calculations, $k_{1,2}$ can be replaced by $\omega L/U_1$.

Calculations have been made on the basis of the amplitude and modified e^9 methods for Falkner-Skan boundary layers with the pressure-gradient parameter β equal to 0 (flat plate) and 0.1. All of the numerical results were obtained from the newly developed JPL stability and transition computer program BLSTR. This program starts with a single damped eigenvalue, and first locates the unstable region. Then, as it advances downstream, it adds and subtracts frequencies as needed to cover only the unstable region and keep the number of damped frequencies to a minimum. After the eigenvalues have been computed at each Reynolds number, least-squares fits to $\ell n\ (A/A_o)$ are used to evaluate $\ell n\ (A/A_o)_{max}$, the corresponding dimensionless frequency $F_{max} = (\omega\nu/U_1^2)_{max}$, and the bandwidth ΔF defined as the difference in F in the direction of decreasing F such that $\ell n\ (A/A_o)_{max} - \ell n\ (A/A_o) = 1$. The interaction relation is evaluated for F_{max} and the disturbance amplitude computed. If the transition criterion of $A_d = 0.04$ is not satisfied, the program advances to the next Reynolds number. Typical execution times on the medium-speed UNIVAC 1108 computer are about 1½ sec for each eigenvalue, and also a total of 1½ sec to do all of the transition-prediction calculations (neutral points, A/A_o, $(A/A_o)_{max}$, A_o, A_d) for a dozen Reynolds numbers.

The numerical results from stability theory for the two boundary layers are given in figure 4. It is to be noted how close to a straight line are the two envelope curves $\ell n\ (A/A_o)_{max}$ for the larger amplifications. Figure 5 shows the disturbance amplitude A_d for the flat-plate boundary layer as a function of $Re^{\frac{1}{2}}$ for several turbulence levels and $U_1 L/\nu = 4 \times 10^4$. The constant C in the relation for A_d was evaluated once and for all by requiring that $A_d = 0.04$ at $Re = 2.8 \times 10^6$ with $u_1'/U_1 = 0.001$. Finally, figure 6 gives Re_t as a function of u_1'/U_1 for $\beta = 0$ and 0.1 according to the two prediction methods. For the amplitude method, $U_1 L/\nu = 4 \times 10^4$ as in figure 5. Further comparisons with experiment are needed to evaluate the worth of the two methods.

This paper presents the results of one phase of research carried out at the Jet Propulsion Laboratory, California Institute of Technology, under Contract No. NAS7-100, sponsored by the National Aeronautics and Space Administration.

Jet Propulsion Laboratory
Pasadena, California 91103

September 10, 1976

EFFECT OF FREESTREAM TURBULENCE ON FLAT-PLATE TRANSITION (EXPERIMENTAL)

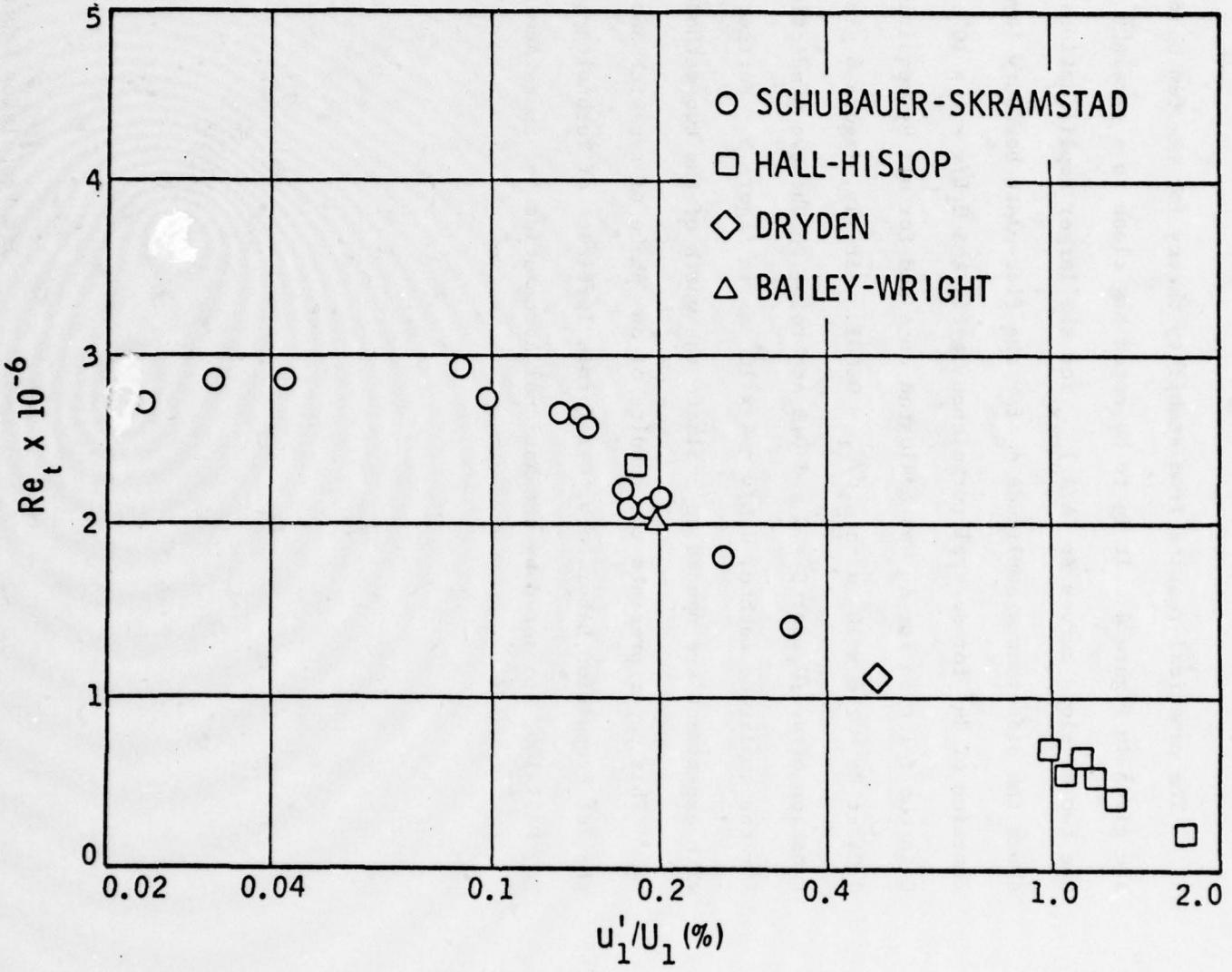

FIG. 1

FIG. 2

STABILITY THEORY AND FLAT-PLATE TRANSITION EXPERIMENTS

u_1'/U_1	$Re_t \times 10^{-6}$	$\ell n\ (A/A_o)_{max}$	$A_o/A_o(0.001)$
0.001	2.8	8.1	1.0
0.002	2.1	6.4	5.5
0.004	1.4	4.8	27
0.010	0.7	2.6	245

FIG. 3

PRESSURE FLUCTUATION INTERPOLATION SPECTRA

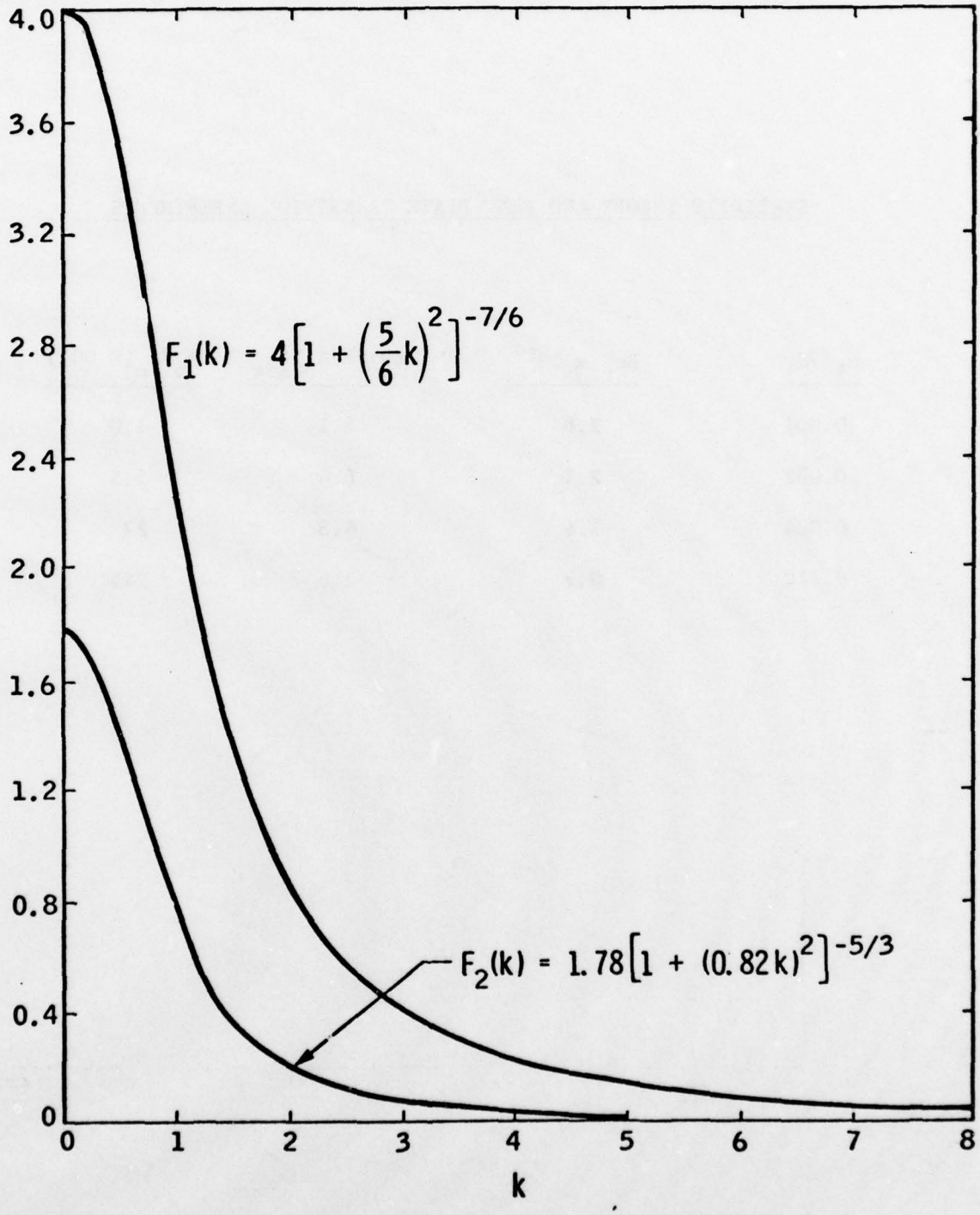

STABILITY CHARACTERISTICS OF TWO FALKNER-SKAN BOUNDARY LAYERS

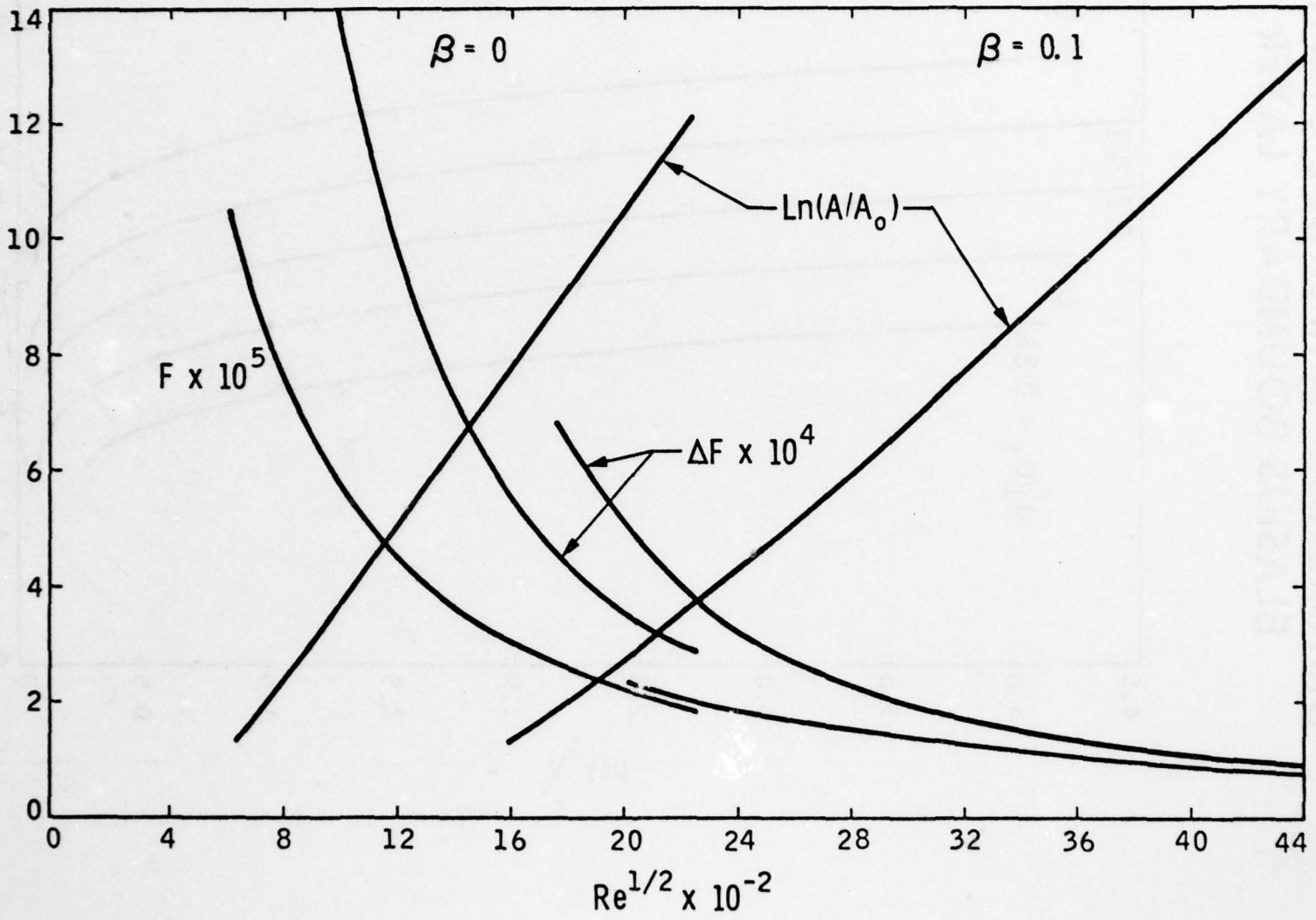

FIG. 4

FIG. 5

DISTURBANCE AMPLITUDE GROWTH BLASIUS BOUNDARY LAYER

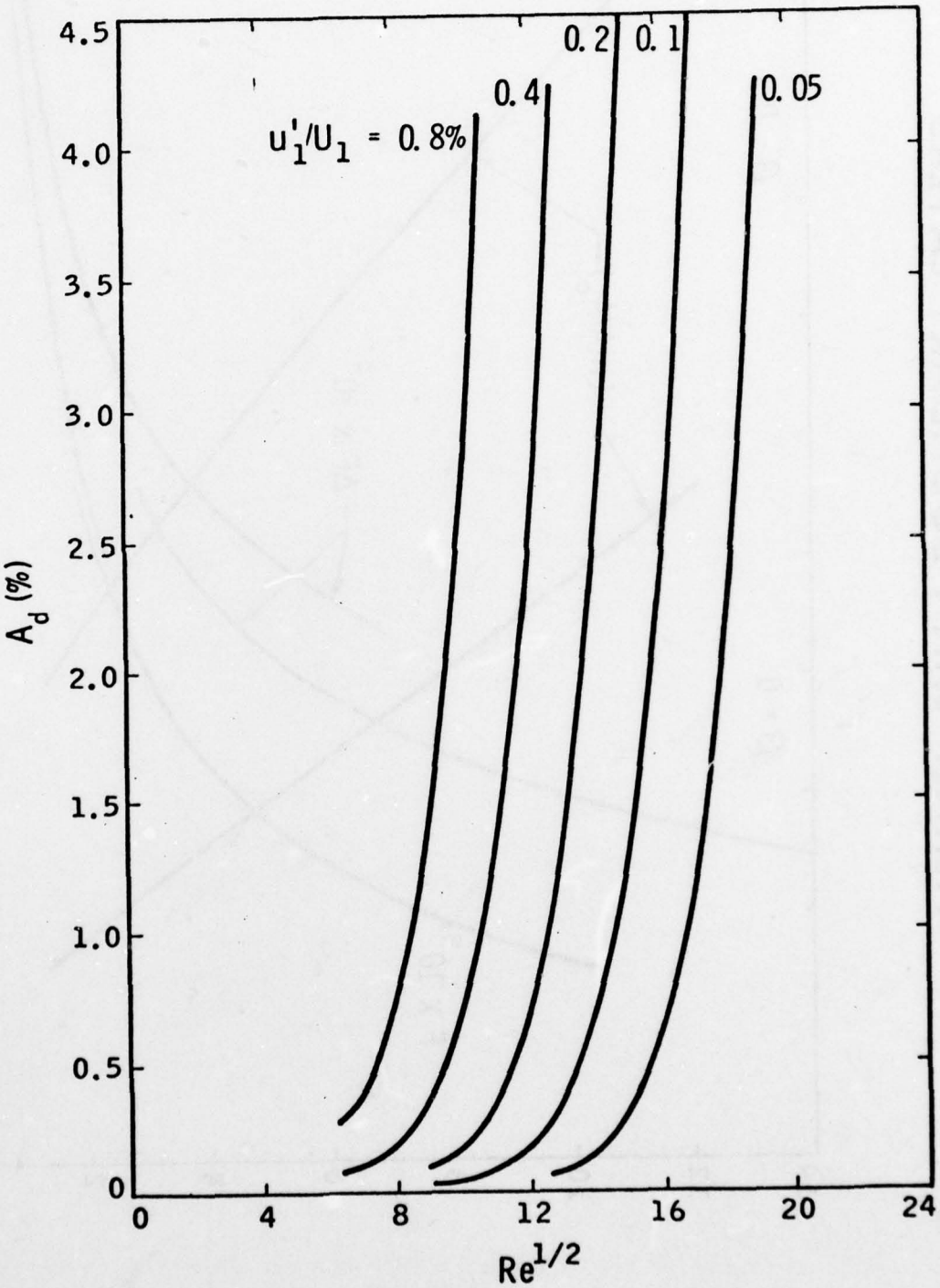

FIG. 6

EFFECT OF FREESTREAM TURBULENCE ON TRANSITION-THEORY AND EXPERIMENT

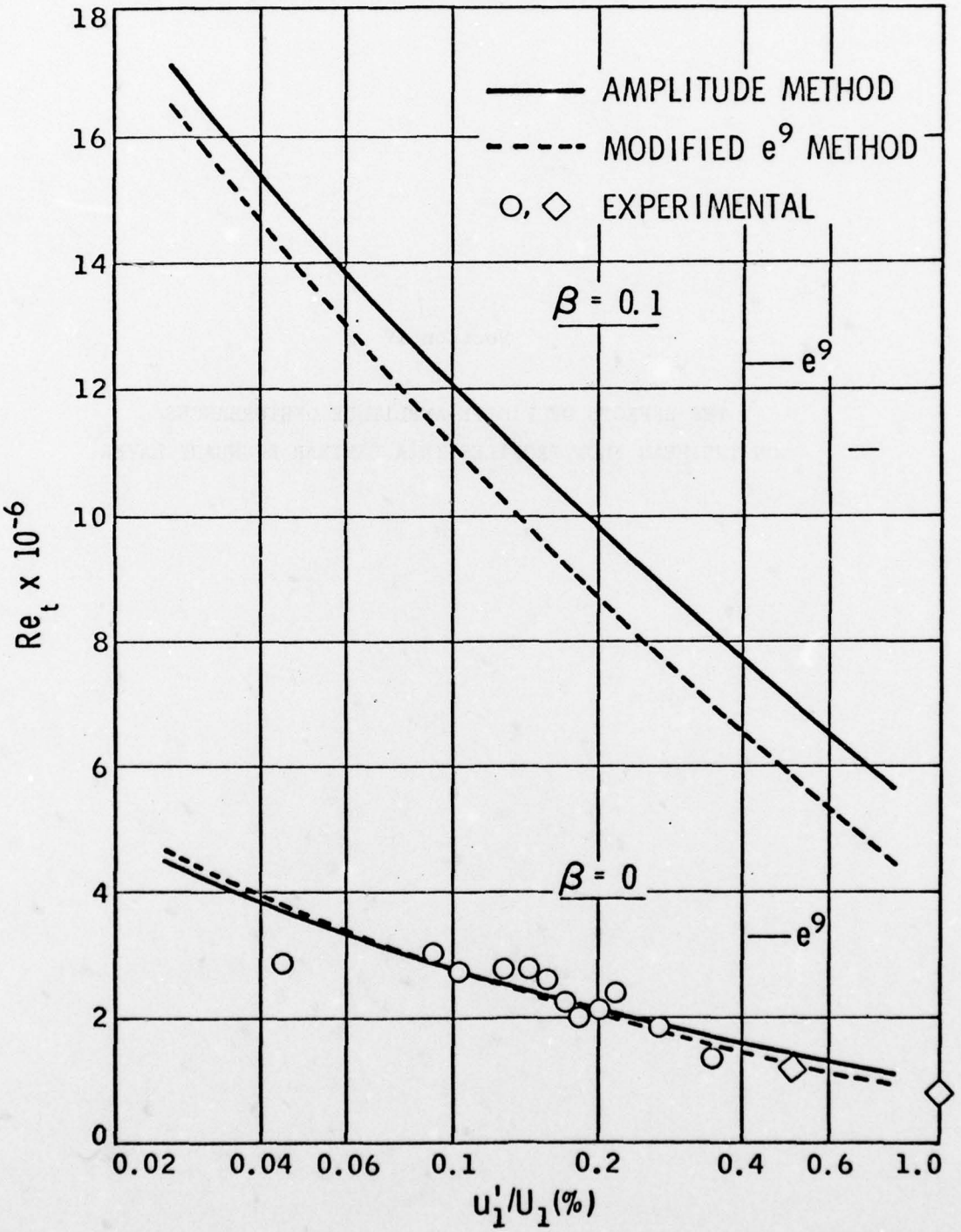

Section IV

THE EFFECTS OF FINITE-AMPLITUDE DISTURBANCES ON THE MEAN FLOW PROFILES IN A LAMINAR BOUNDARY LAYER

PDT-76-86P-B

IV-3 The Effects of Finite-Amplitude Disturbances on the Mean Flow Profiles in a Laminar Boundary Layer

BY

C. L. Merkle

D. R. S. Ko

and

T. Kubota

The use of the linear stability characteristics of boundary layers to indicate the location of transition from laminar to turbulent flow has proven to be one of the best available methods for predicting transition on bodies of general engineering interest. The underlying reason for this success is almost certainly related to the superior theoretical foundation of the stability approach as compared to that of other existing methods. Despite the relative success of the method, the actual relationship between stability and transition is poorly understood, and is generally incorporated in the predictions in an empirical manner in conjunction with an implicit assumption that the ensuing nonlinear amplification region which follows the linear growth region is very brief and leads quickly to transition. The most stringent limitation on this approach arises because there is no mechanism in the linear theory for deducing when the disturbances become large enough that nonlinear effects begin to be important. The present approach is directed towards including the appropriate additional terms in the stability analysis so that the effects of the disturbances and their growth can be deduced directly from the stability analysis itself without recourse to additional considerations. Since only the leading-order finite-amplitude effects are included, the analysis still requires an empirical calibration to relate the finite-amplitude effects to the observed location of transition. The present approach also requires a knowledge of the characteristics of the initial disturbance levels inside the boundary layer, but their origin and character are not addressed in the current study.

The extension of stability theory to include finite-amplitude disturbances starts from a formal perturbation expansion which includes the complete nonlinear stability characteristics of the boundary layer. This expansion procedure demonstrates that, for a single-frequency disturbance, the leading-order effects of a finite-amplitude wave result in a distortion

of the mean flow profile. In particular, the distortion of the mean flow profile is a phenomenon which is of second order, $O(A^2)$, in the disturbance amplitude, whereas, the nonlinear disturbance-disturbance interaction is of third order, $O(A^3)$. These observations suggest that the distortion of the mean flow profile can be accurately computed while still retaining a linear equation system for the disturbances. Extension of the analysis to more realistic multi-frequency and three-dimensional disturbance environments shows that although the nonlinear disturbance-disturbance interactions now become of the same order as the mean flow distortion (namely, order A^2), the second-order accurate description of the mean flow can still be obtained from a first-order accurate (linear) representation of the disturbances (i.e., second-order changes in the disturbance growth rate cause third-order changes in the mean flow profiles). Such a simplification to a linear wave system is, of course, fundamental to the analysis from the viewpoint of computational economy. Further, the concept that the mean flow profile distortions can be accurately computed from a linear disturbance analysis is in general agreement with experimental evidence which has indicated that the generation of harmonic disturbances is of only minor significance in the transition process.

In contrast to these results for boundary layers, the analogous deductions for the more intensively-studied Poiseuille-flow case appear to be considerably different. Although an identical expansion scheme has been used for most nonlinear stability studies in Poiseuille flows, the attention in this latter family of flows has been almost unanimously focused on predicting the changes in the growth rate, and has required a knowledge of both the mean flow distortion and the wave-wave interaction. Specifically, these analyses have been carried to third order, $O(A^3)$, accuracy. The differences in the emphasis of the nonlinear approach in these two situations comes not from the theory itself, but from the comparison of the theory with experiment. In boundary layers, the predicted region in which disturbances are amplified is in very good agree-

ment with extensive experimental evidence. For Poiseuille flow, transition to turbulence occurs below the critical Reynolds number at which disturbances first begin to be amplified, implying that amplification can take place in this low Reynolds number regime. As a result of this discrepancy, the major impetus of nonlinear stability studies in Poiseuille flows has been towards modifying the qualitative results of linear stability theory and using the nonlinear terms to show that regions which are stable to infintesimal linear waves are unstable to finite-amplitude waves. Such a qualitative change in the stability properties of boundary layers is not needed, and would disagree with experiment if found.

Some initial numerical results which are based on single two-dimensional disturbances in boundary layers are presented to demonstrate the types of mean flow distortions which can be generated by finite-amplitude disturbances. The curvatures of the velocity profiles have been used as particularly sensitive indices of the cumulative effects of the interaction between the disturbance and the mean flow. In the presence of finite-amplitude disturbances, the curvature near the wall decreases while that farther from the wall increases, eventually leading to a point of inflection. Comparisons of zero-pressure-gradient boundary layers with favorable and unfavorable pressure gradient cases indicates that significant distortion begins at lower values of the disturbance amplitude when the pressure gradient is favorable as compared to when it is unfavorable; however, at all times, substantial interaction occurs while the disturbance is very small (typically $u'v'$ less than 10^{-5} times the free-stream velocity squared). The current results suggest that either the velocity profile curvature or the ratio of the disturbance-generated Reynolds stresses to the local shear stress could serve as effective practical indicators of transition. Finally, we note that the use of a transition indicator which is based on the distortion of the mean profiles by the disturbances in the laminar boundary layer seems particularly attractive for applications such as advanced laminar flow

vehicles where extrapolation of the current transition data base to higher Reynolds numbers, through the use of pressure gradient, heating and suction is required. The reduced degree of reliance on the empirical information in the transition analysis should increase the reliability of this extrapolation.

Section IV

FLUCTUATIONS IN A BOUNDARY LAYER INTRODUCED BY TRAVELING-WAVE IRROTATIONAL FREESTREAM DISTURBANCES

IV-4 FLUCTUATIONS IN A BOUNDARY LAYER INTRODUCED BY TRAVELING-WAVE IRROTATIONAL FREESTREAM DISTURBANCES*

Harold L. Rogler
Department of Mechanical and Aerospace Engineering
Case Western Reserve University; Cleveland, Ohio 44106

INTRODUCTION TO IRROTATIONAL DISTURBANCES

If you wave your hand above your desk, the fluctuations which are generated arise from the bound circulation associated with any lift produced by your hand (which might be represented as a sheet of vorticity or a potential vortex), from the thickness of your hand (which might be represented as a distribution of sources and sinks), and from the trailing wake of vorticity shed behind your hand as you unsteadily wave and alter that lift (which might be modeled as a vortex sheet of varying strength or a set of free vortices). The disturbances introduced by the thickness and bound circulation effects are everywhere irrotational, while those introduced by the trailing vorticity are effectively irrotational at some distance away from the patches or layers of vorticity.

Irrotational fluctuations are also generated by a rotor blade translating past a stator blade in a jet engine, by wavy walls, or by the small amplitude waves at the surface of the ocean. A fish swimming through rapids is subjected to irrotational fluctuations as it swims through water which is: (1) flowing around rocks, (2) influenced by standing vortices or eddies behind those rocks, or (3) influenced by eddies which are being convected downstream. Of course it is possible that the fish swim (or airplanes fly) through a patch of vorticity, but we are not concerned in this study with the special effects arising from rotational disturbances.

In all these cases, the disturbances are induced by some surface or body in the flow, by some arrangement of sources, sinks, doublets, monopoles, etc., by interfaces between stratified fluids, by bound circulations, and by patches, sheets, rings, or layers of vorticity. If a plate is inserted into a flow with freestream vorticity fluctuations and if these vorticity

---

*This work was supported by the Air Force Office of Scientific Research under Grants AFOSR-74-2577A&B. The support and encouragement by Dr. E. Reshotko are gratefully acknowledged. The author thanks Dr. J. Paul for the use of his streamline plotting program.

fluctuations are sufficiently far away from the plate such that the vorticity does not convect into or diffuse into the boundary layer, then as far as the boundary layer is concerned, these disturbances are irrotational.

HOW FAST DO IRROTATIONAL DISTURBANCES PROPAGATE?

The phase speeds of irrotational fluctuations are intimately connected to the propagation speed of the source. If that source is the traveling, wavy-wall of a wind tunnel, then the fluctuation propagates at that speed also. In turbomachinery, the relative motion between blades would be important as well as the convection of vortex sheets downstream. If the source is a set of low-intensity vortices being convected with the mean flow, then the propagation speed is the local mean velocity at the vortex centers. If the source is a vortex street downstream of a bluff body, then the nonlinear interactions between the vortices cause the vortices to propagate at a speed either slower or faster than the freestream, depending on the case considered. It is possible that the disturbances propagate upstream as well as downstream, or they can be standing waves and not propagate at all. The response in the boundary layer is very sensitive to the phase speed, at least for some wave-numbers and Reynolds numbers.

INVISCID INTERACTION OF AN IRROTATIONAL DISTURBANCE WITH A SEMI-INFINITE PLATE

If the freestream disturbance has the normal velocity

$$v^{(a)}(x,y,t;k,c) = \hat{v}(k,c)e^{ky}e^{ik(x-ct)} \qquad (1)$$

with (real and positive) wavenumber k and phase speed c, and a semi-infinite plate is inserted into the flow along the x-axis with leading edge at the origin, then by conformal mapping the inviscid, irrotational solution for all amplitudes can be found which satisfies impermeability along the plate. The streamline pattern for this flowfield is shown in Figure 1. This pattern reflects only the disturbance flow; the uniform mean flow from left to right is not included.

Two features are important here. First note that the fluctuations vanish beneath the plate. As far as the boundary layer developing on the bottom side of the plate is concerned, any influence of the irrotational fluctuation generated above the plate of the form $e^{ky+ik(x-ct)}$ very probably arises near the leading edge. Far-downstream of the leading edge on the

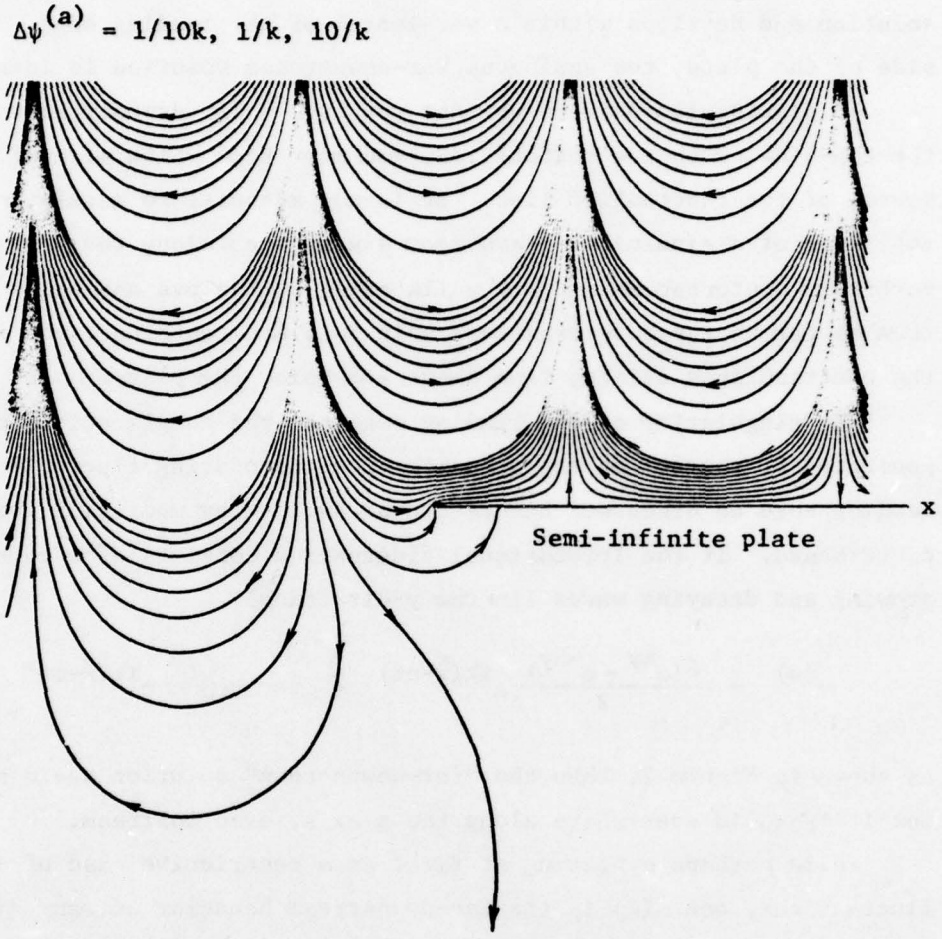

Figure 1. Disturbance streamlines of an irrotational free-stream disturbance generated by some source far-above the plate which propagates along and interacts with a semi-infinite plate. The source might be a vortex sheet or a wavy wall.

bottom side, there is no fluctuation. At the leading edge, a singularity arises with infinite speeds. Secondly, note on the top side of the plate that a pattern rapidly develops which subsequently propagates along without further significant change. This solution is called the "far-downstream" solution and develops within a wavelength of the leading edge. On the bottom side of the plate, the analogous far-downstream solution is identically zero.

To distinguish between whether you have a far-downstream solution as on the top-side or on the bottom-side, you must know which side of the plate the source of the fluctuation lies. It is not adequate to merely know the amplitude of a sinusoidal freestream disturbance along the x-axis. If vorticity disturbances or wavy walls exist <u>both</u> above and below the plate, then as far as the far-downstream solutions are concerned, you must sort out the contributions arising from above and below the plate.

The singularity at the leading edge and the complications of disturbances generated by sources on the opposite side introducing fluctuations near the leading edge as discussed before can be avoided by modifying the freestream disturbance. If the irrotational fluctuation consists of a combination of growing and decaying waves (in the y-direction)

$$v^{(a)} = \frac{\hat{v}(e^{ky} - e^{-ky})}{2} e^{ik(x-ct)} = \hat{v} \sinh(ky)\, e^{ik(x-ct)} \qquad (2)$$

as shown in Figure 2, then the "far-downstream" solution again appears except now it is valid everywhere along the x-axis, even upstream.

While perhaps appearing at first as a restrictive case of irrotational fluctuations, eqn. (2) is the far-downstream behavior of many disturbances of scientific and engineering significance. It is the irrotational freestream disturbance which will be used to introduce fluctuations in the boundary layer.

FORMULATION FOR THE RESPONSE IN A BOUNDARY LAYER TO IRROTATIONAL FLUCTUATIONS

If the velocities and pressure are separated into mean and disturbance components in the Navier-Stokes and continuity equations for a 2-D, incompressible flow, and the disturbance velocities and pressure are further separated into the two parts

$$v' = v^{(a)} - v, \quad u' = u^{(a)} - u, \quad \text{and} \quad p' = p^{(a)} - p$$

v, u, p: change to the freestream disturbance caused by the boundary layer and no-slip

$v^{(a)}$, $u^{(a)}$, $p^{(a)}$: freestream disturbance which exists in the <u>absence</u> of the plate

$\Delta\psi^{(a)} = 1/10k,\ 1/k,\ 10/k$

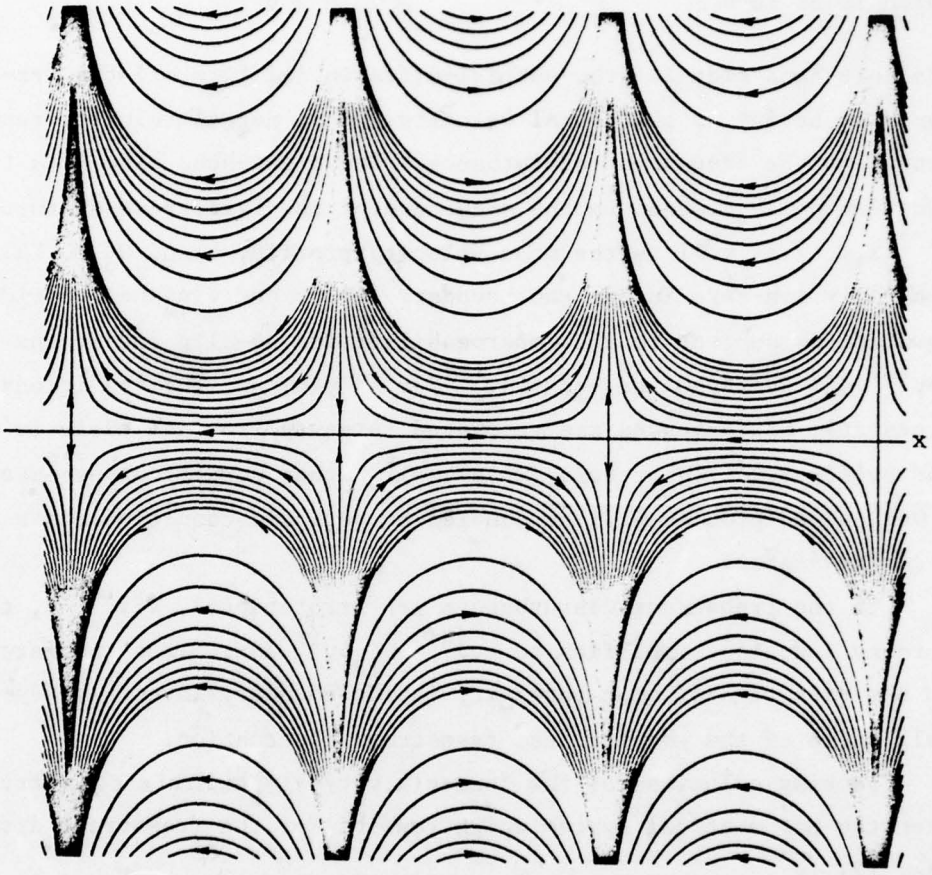

$u^{(a)} = -\cosh(ky)e^{ik(x-ct)}$

$v^{(a)} = \sinh(ky)e^{ik(x-ct)}$

nondimensionalized against the maximum longitudinal velocity along the x-axis

Figure 2. Disturbance streamlines of an irrotational free-stream disturbance generated by sources both above and below the plate. These two sources are out of phase by 180° and a purely longitudinal fluctuation is produced along the x-axis.

the parallel-flow representation of the boundary layer is introduced, and the results are linearized, then the following nonhomogeneous equation results

$$\{\frac{\partial}{\partial t} + \bar{U}(y)\frac{\partial}{\partial x} - \nu\nabla^2\}\nabla^2 v - \bar{U}_{yy}(y)\frac{\partial v}{\partial x} = [\bar{U}(y) - U_\infty]\frac{\partial}{\partial x}\nabla^2 v^{(a)} - \bar{U}_{yy}(y)\frac{\partial v^{(a)}}{\partial x}$$

which is of form $$\mathcal{L} v = \mathcal{F} v^{(a)}$$

The left-hand side is (the partial-differential form of) the Orr-Sommerfeld operator acting on the normal velocity. This normal velocity represents the change to the freestream disturbance. The right-hand side is a forcing function which depends on the structure of the freestream disturbance $v^{(a)}(x,y,t)$ as well as the mean velocity profile, $\bar{U}$ and $\bar{U}_{yy}$. This forcing is generally non-zero inside the boundary layer, but vanishes outside. The equation is subject to the impermeability and no-slip conditions ($v'=0$ or $v=v^{(a)}$ and $\partial v'/\partial y=0$ or $\partial v/\partial y=\partial v^{(a)}/\partial y$ at $y=0$) and the conditions that the freestream disturbances are recovered far-away from the plate ($v'\to v^{(a)}$ or $v\to 0$ and $\partial v'/\partial y\to\partial v^{(a)}/\partial y$ or $\partial v/\partial y\to 0$ as $y\to\infty$). Other conditions necessary to yield a well-posed problem will be handled by periodic conditions in x and t as specified later.

If the freestream disturbances are irrotational, $\nabla^2 v^{(a)}=0$, then the forcing function simplifies to $\mathcal{F} v^{(a)}=-\bar{U}_{yy}\partial v^{(a)}/\partial x$. Thus the forcing depends on the variation of mean vorticity in the boundary layer $\partial\bar{\xi}(y)/\partial y=-\bar{U}_{yy}$ and the wall value of the longitudinal freestream fluctuation.

Seeking solutions of the form $v(x,y,t)=\phi(y)\exp[ik(x-ct)]$ where ϕ is complex, then the mathematical system which results for the freestream disturbance of eqn. (2) is

$$\{[\bar{U}(y) - c](D^2 - k^2) - \bar{U}_{yy}(y) + \frac{i}{kR_{\delta*}}(D^4 - 2k^2D^2 + k^4)\}\phi(y) = -\bar{U}_{yy}(y)\sinh(ky) \tag{4}$$

subject to $\phi=0$, $D\phi=k$ at $y=0$ and $\phi\to 0$, $D\phi\to 0$ as $y\to\infty$.

where $D\equiv d/dy$, $R_{\delta*}=\bar{U}_\infty\delta*/\nu$, and $\bar{U}(y)$ is the mean velocity nondimensionalized with respect to U_∞. The dimensionless wavenumber is related to the dimensional wavelength and displacement thickness by $k=2\pi\delta*/\lambda$. The phase speed is also nondimensionalized against U_∞.

In general, a numerical solution must be obtained because the coefficients $\bar{U}(y)$ and $\bar{U}_{yy}(y)$ are variable and are available only as data. However, two analytical solutions have been obtained for simple velocity profiles.

EXPLICIT SOLUTION WHEN $\bar{U}=1$ EVERYWHERE

If the mean flow is uniform, as would arise if the top surface of the plate were composed of a belt which moved along at the freestream speed, then the equation reduces to $\{(1-c)(D^2-k^2)+\frac{i}{kR_{\delta*}}(D^2-2k^2D^2+k^4)\}\phi=0$. An explicit solution for ϕ can be found and $v'=\{\sinh(ky)-\phi(y)\}e^{ik(x-ct)}$ formed as

$$v' = \mathrm{Real}\left(\left[\sinh(ky)+\frac{e^{-ky}-e^{-\left(1+iR_{\delta*}(1-c)/k\right)^{\frac{1}{2}}ky}}{1-\left(1+iR_{\delta*}(1-c)/k\right)^{\frac{1}{2}}}\right]e^{ik(x-ct)}\right) \quad \text{for } c\neq 1$$

$\delta*$ is a dummy parameter kept only so that this result can be compared with solutions where a boundary layer is present. When c=1, a modified form of this solution results. The streamlines plotted in Figure 3 show that the no-slip condition is satisfied through the creation of a vortex near the wall. The importance of viscosity is dictated by the combination of parameters $R_{\delta*}(1-c)/k=R_{\lambda}(1-c)/2\pi\equiv R$. Note the dependence on phase speed even with this simple mean velocity profile. Hence disturbances near the plate traveling at speeds near the freestream, c=1, are highly viscous and have relatively thick viscous layers.

PARTLY ANALYTICAL, PARTLY NUMERICAL SOLUTION WHEN $\bar{U}$=CONSTANT AND U_{yy}=ANOTHER CONSTANT

If the mean boundary layer is modeled by

$$\bar{U}(y) = U_o \quad \text{and} \quad \bar{U}_{yy}(y) = U_2 \quad \text{for } y \le \delta \text{ (inside the layer)}$$

$$\text{and} \quad \bar{U} = 1 \quad \text{and} \quad \bar{U}_{yy} = 0 \quad \text{for } y > \delta \text{ (exterior to the layer)}$$

where U_o and U_2 are constants, then another explicit solution of eqn. (4) is possible in the form

$$v' = \mathrm{Real}\left(\left(\sum_{j=1}^{4} A_j e^{\alpha_j y}\right) e^{ik(x-ct)}\right)$$

$$\text{where} \quad \alpha_j \equiv \pm\left(\alpha^2+\frac{i\alpha R_{\delta*}(U_o-c)}{2}\pm\frac{i\alpha R_{\delta*}(U_o-c)}{2}\left[1+\frac{4iU_2}{\alpha R_{\delta*}(U_o-c)^2}\right]^{\frac{1}{2}}\right)^{\frac{1}{2}} \quad \text{when } c\neq U_o$$

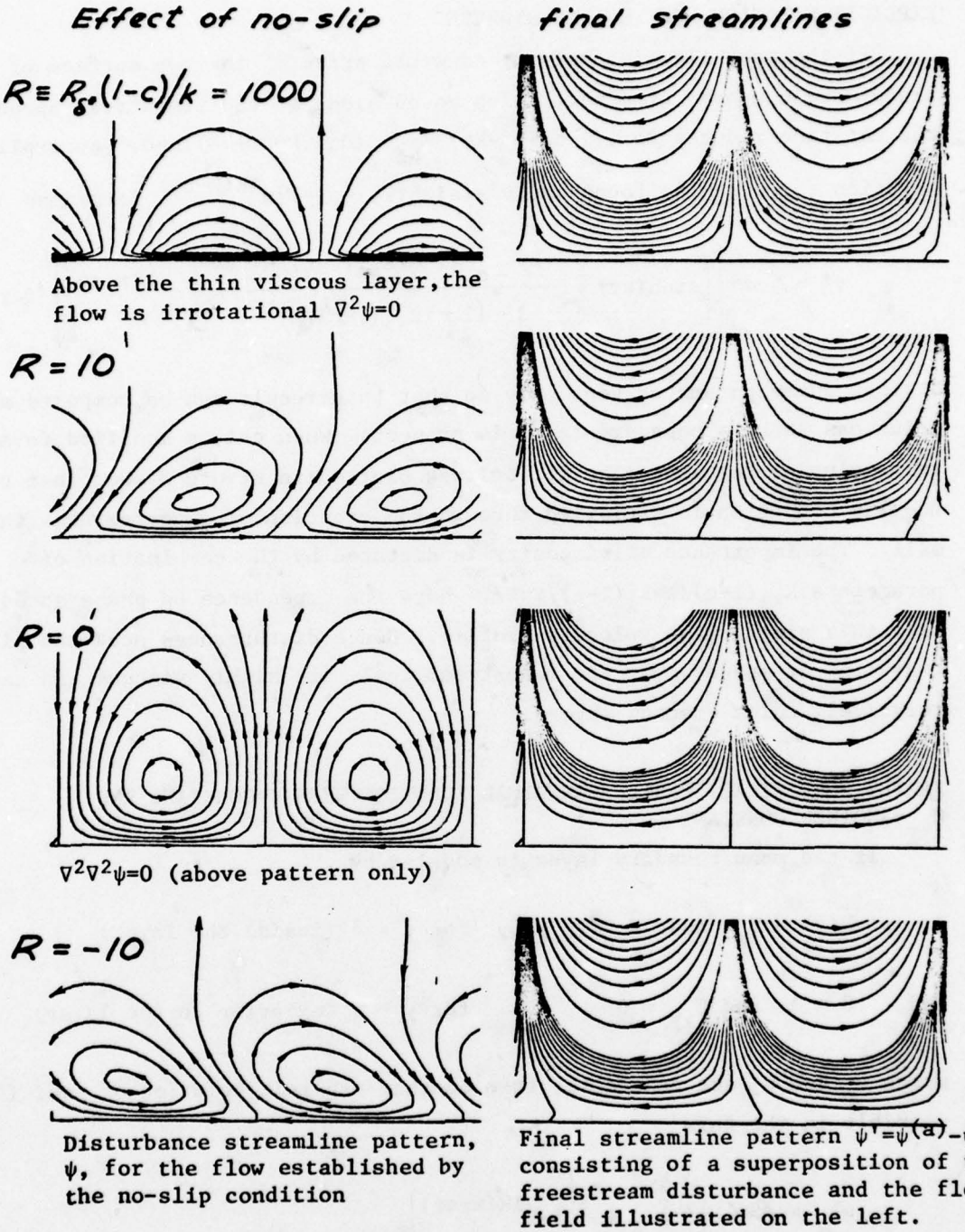

Figure 3. Disturbance streamline patterns for the flow near the wall when the mean velocity is uniform everywhere, $\bar{U} = 1$, for several values of the parameter $R \equiv R_{\delta^*}(1-c)/k = R_{\lambda}(1-c)/2\pi$.

where the four constants A_j and the two constants C_1 and C_2 from the exterior solution are evaluated numerically from a 6x6 matrix. The system holds great promise for economically revealing many features.

NUMERICAL SOLUTIONS WITH A BLASIUS MEAN BOUNDARY LAYER

With $\overline{U}(y)$ and $\overline{U}_{yy}(y)$ represented as data for a Blasius layer, eqn. (4) has the complexities and numerical instabilities of the eigenvalue problem for the stability of a boundary layer. Here, a numerical solution is obtained by an expansion in Chebyshev polynomials

$$\phi(\eta) = \sum_{m=0}^{N-1} a_m T_m(\eta)$$

where $T_m(\eta)$ is the mth Chebyshev polynomial, a_m is the (unknown) mth coefficient, $\eta \equiv \frac{2y}{y_e} - 1$ is the transformed y-coordinate with the range $-1 \le \eta \le 1$ representing $0 \le y \le y_e$, and y_e is the "edge" of the boundary layer. A matrix (often 45x46) is set up representing the expansions of the differential equation and conditions. Solutions are obtained efficiently for u', v', $-\overline{u'v'}$, $-\overline{u'v'}\, d\overline{U}/dy$, dissipation, vorticity, kinetic energy, and pressure. Streamlines, equi-vorticity contours, and pressure isobars are also drawn.

TYPICAL NUMERICAL RESULTS

The streamline patterns for several phase speeds are shown in Figure 4 on the right-hand side. A better view of what's going on follows, however, if only the alteration to the freestream disturbance caused by the boundary layer and no-slip condition are plotted (the impermeability condition is satisfied by the freestream disturbance itself). This alteration is plotted on the left-hand side. For the case of c=0.35, a double pair of rotating vortices are formed, but when c=0.95 the structure has changed to a single pair of vortices. When the freestream disturbances convect at the freestream speed, c=1, the third row of streamlines result. Note the change in patterns when the phase speed is increased from 0.95 to 1.05.

The amplitude of the longitudinal disturbance velocity is plotted in Figure 5 for various phase speeds. Again note the sensitivity to phase speed near c=1. When $c \approx 1$, the amplitudes inside the boundary layer are small. The Reynolds stress is plotted in Figure 6 which shows that a fairly constant stress is produced. This constant stress continues far into the freestream,

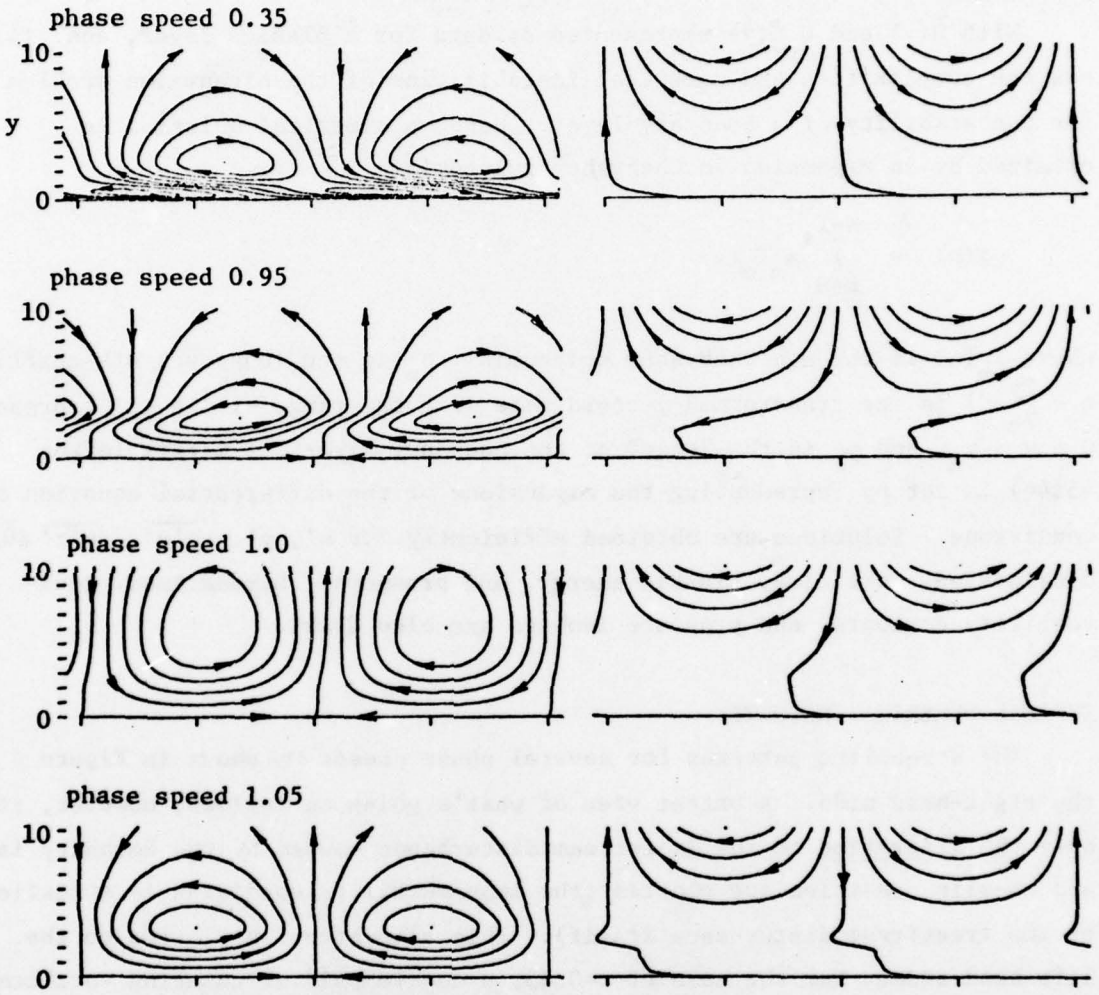

The streamlines for the flowfield representing the alteration of the freestream disturbance by the no-slip condition and the mean boundary layer.

The superposition of the freestream disturbance of Fig. 2 and the flowfield illustrated on the left yields the final disturbance flowfield with streamlines as shown above.

Figure 4. Disturbance streamlines with a Blasius mean boundary layer for various phase speeds and for k=0.2 and R_{δ^*}=1000.

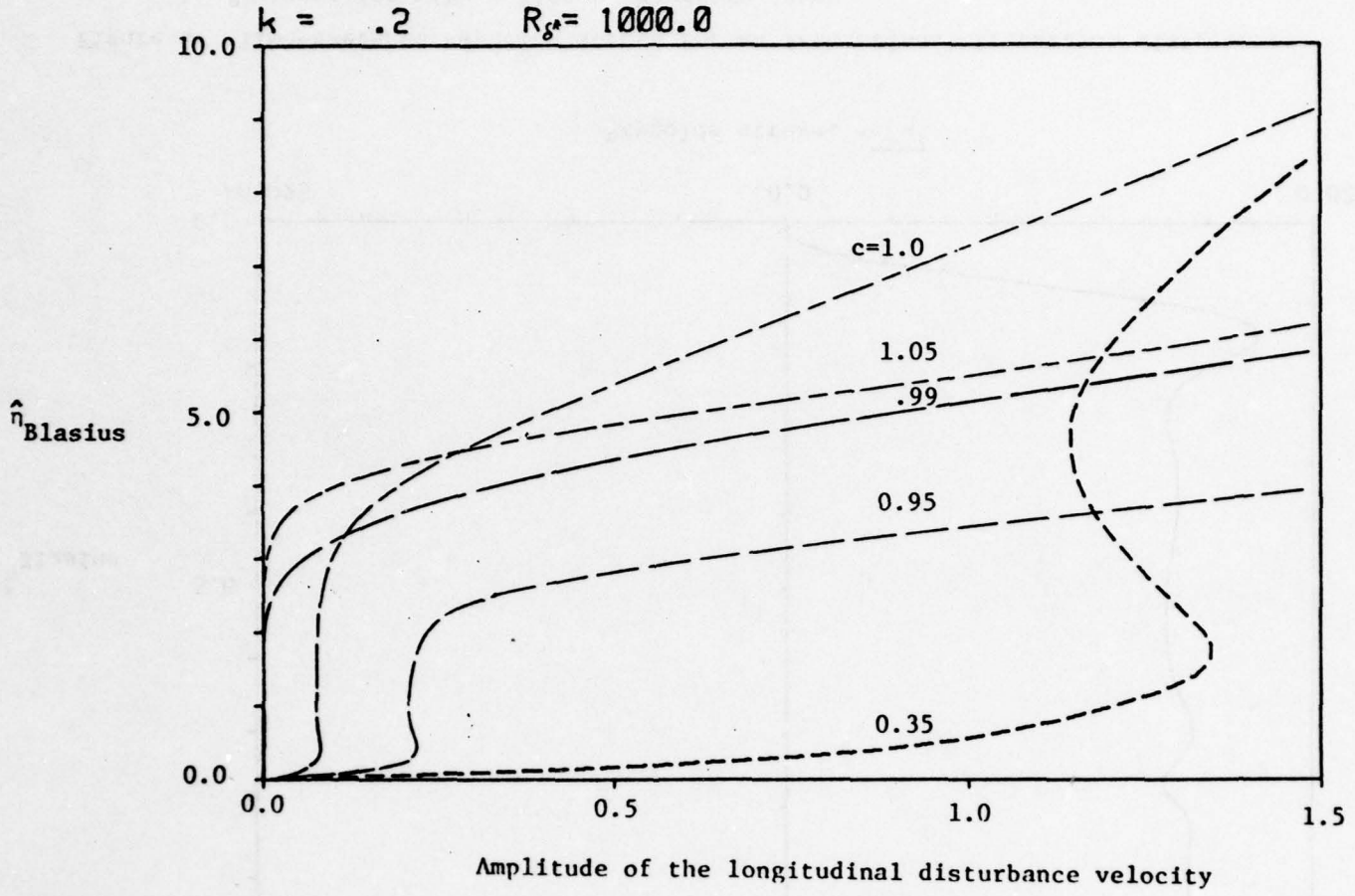

Figure 5. Amplitude of the longitudinal velocity for several phase speeds for an irrotational freestream disturbance interacting with a Blasius boundary layer.

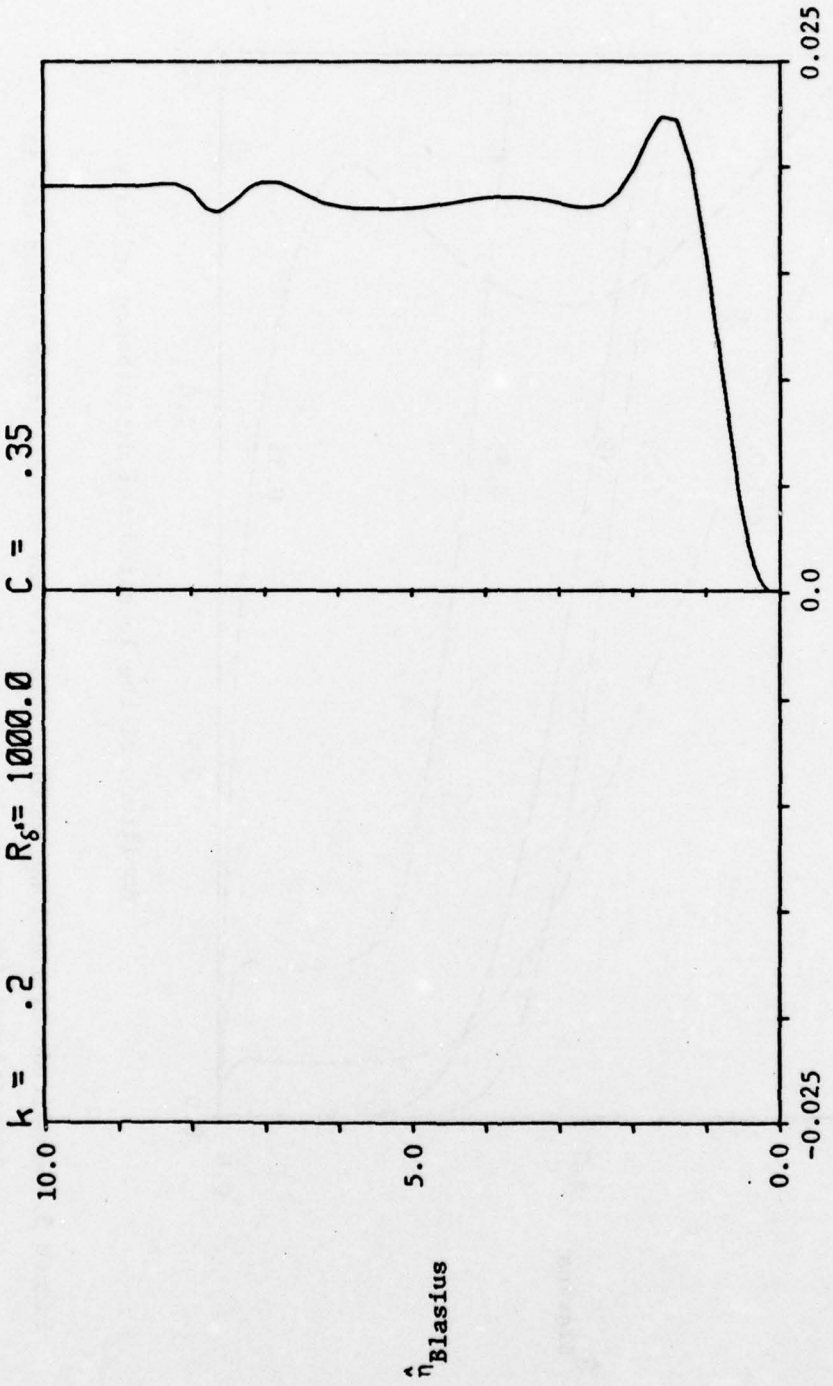

Figure 6. Time-averaged Reynolds stress for an irrotational freestream disturbance interacting with a Blasius boundary layer.

where presumably it vanishes across another viscous layer. The energy production and dissipation are plotted in Figure 7. The production for this set of parameters (c=0.35, R_δ=1000.0 and k=0.2) has a maximum at $\eta \tilde{\sim} 1.5$, while the dissipation is largest in the viscous region near the wall.

REFERENCES

1. H.L. Rogler and E. Reshotko, "Disturbances in a wall boundary layer introduced by an array of low-intensity vortices", FTAS/TR-74-95, Fluid, Thermal and Aerospace Sciences Dept., Case Western Reserve University, (January 1974).
2. H.L. Rogler and E. Reshotko, "Disturbances in a boundary layer introduced by a low intensity array of vortices", SIAM J. Appl. Math., Vol. 28, No. 2, (March 1975).
3. H.L. Rogler, "Galloping, wavy and porous wall tunnels which introduce traveling-wave, unsteady flows", FTAS/TR-76-119, Case Western Reserve University, (June 1976).

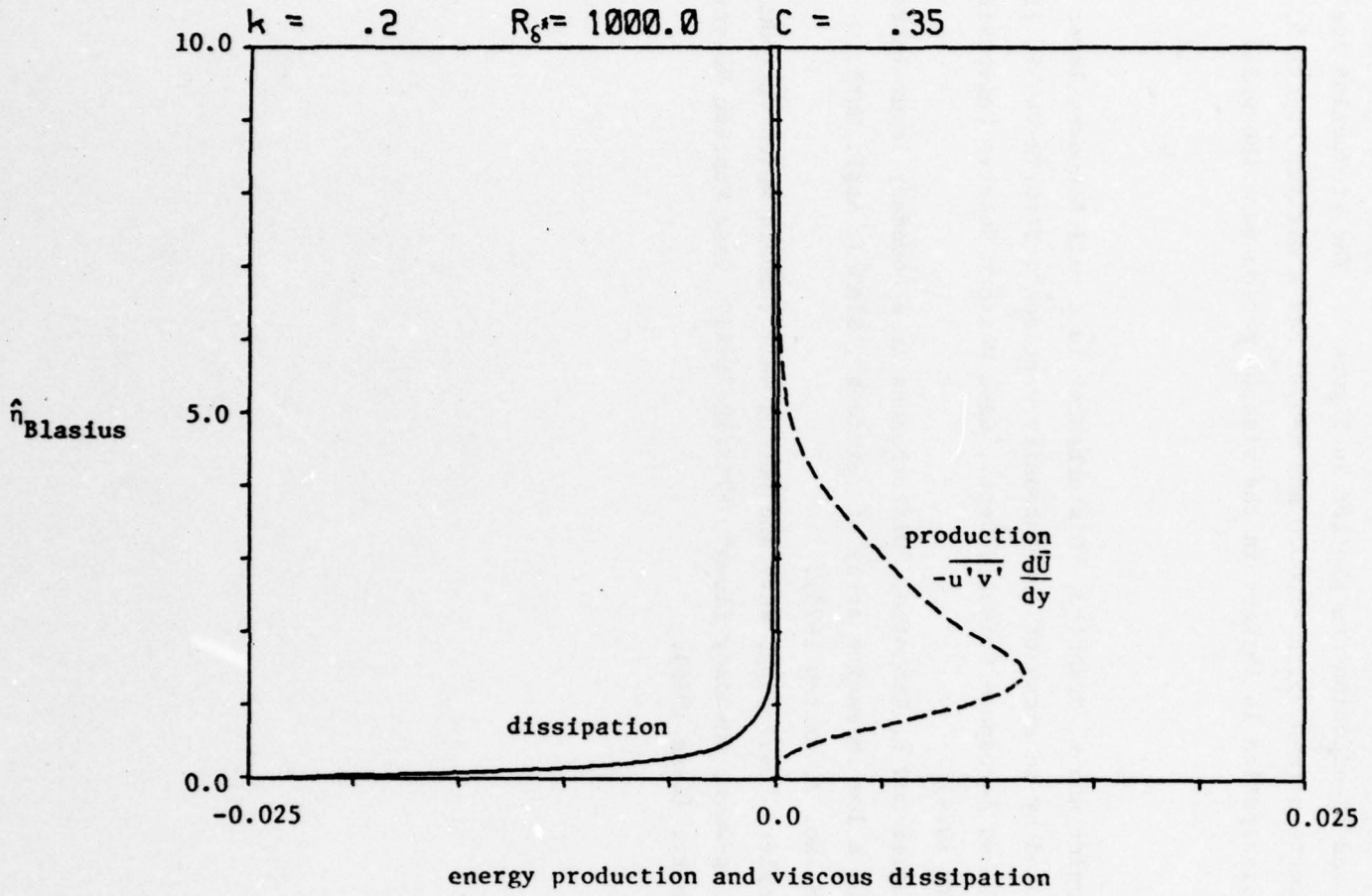

Figure 7. The production and dissipation of disturbance energy of an irrotational freestream disturbance interacting with a Blasius boundary layer.

Section V

STABILITY OF A HEATED WATER BOUNDARY LAYER FOR NON-UNIFORM WALL TEMPERATURE DISTRIBUTIONS

V-1 STABILITY OF A HEATED WATER BOUNDARY LAYER FOR NON-UNIFORM WALL TEMPERATURE DISTRIBUTIONS

A. Strazisar and E. Reshotko

Department of Mechanical and Aerospace Engineering
Case Western Reserve University
Cleveland, Ohio

ABSTRACT

The effect of non-uniform wall temperature distributions on the stability of a heated flat plate laminar boundary layer in water is studied experimentally. The experiment is performed in a closed circuit low turbulence water tunnel with free stream turbulence intensities of 0.1-0.2%. Temperature-compensated hot film anemometry is used to measure the mean flow field as well as the spatial growth characteristics of sinusoidal velocity disturbances introduced into the boundary layer using a vibrating ribbon.

Two types of non-uniform wall temperature distributions are studied: step changes in wall temperature of the form $T_w - T_\infty = 0$ for $x < x_s$, $T_w - T_\infty = \Delta T$ for $x \geq x_s$; and power law wall temperature distributions of the form $T_w(x) - T_\infty = Ax^n$. In order to isolate the effects of the parameters n and x_s on the boundary layer stability, the local wall temperature at a reference location, $T_w(x_{ref}) - T_\infty$, is held constant as n and x_s are varied. In the present work $x_{ref} = 5.5$ inches, which is the center of the region in which stability characteristics are measured. The non-dimensional location of a step change in wall temperature is specified by

the parameter $S = x_s/x_{ref}$.

A similarity solution of the boundary layer momentum and energy equations for power law wall temperature distributions, valid for fluid property variations, is obtained using a modified Howarth-Dorodnitsyn transformation. The resulting ordinary differential equations are integrated numerically. An approximate solution of the boundary layer equations for step changes in wall temperature, valid for constant fluid properties, is obtained by assuming that the thermal boundary layer thickness is small compared to the velocity boundary layer thickness. A closed form solution of the resulting equations is obtained in terms of incomplete gamma functions.

Mean temperature profiles measured with the hot film anemometer operating as a resistance thermometer are compared to predicted profiles for various values of n and S in Figures 1 and 2, where $H = (T-T_\infty)/(T_w-T_\infty)$ and $\eta = y\sqrt{U_e/\nu x}$. The case S = 0 corresponds to uniform wall heating beginning at the leading edge, while S = 1 corresponds to a step change in temperature at $x_{ref} = 5.5$ inches. The case n = -.5 corresponds to input of a finite amount of heat at the leading edge followed by an adiabatic wall. For free stream velocity distributions of the form $U_e = C x^m$, this case occurs whenever $n = -(m+1)/2$. For values of $n < -(m+1)/2$ the direction of heat transfer changes sign, as shown in Figure 1 for n = -0.6.

Both analytic and experimental results indicate that the mean velocity profile is virtually independent of variations in n and S over the range of wall temperatures used in the present work. For values

of n in the range $-0.5 < n < 1.0$, the wall shear stress and profile form factor vary by less than 1.5% at a fixed wall temperature level.

Growth rate characteristics of ribbon-generated disturbances in the boundary layer are determined in the following manner. The Reynolds number $R_{\delta*} = U_e \delta*/\nu$ is first determined using the displacement thickness, $\delta*$, of the mean velocity profile measured at x_{ref}. At a fixed Reynolds number and ribbon frequency the disturbance amplitude is then measured at five stations between x = 5 in. and x = 6 in. The amplitude recorded at each station is the peak amplitude, defined as $A(x) = [u'(\eta,x)/U_e]_{max}$, found by searching through the boundary layer in the y-direction. The spatial disturbance growth rate, $-\alpha_i = (\frac{1}{A}\frac{dA}{dx})_{ref} \frac{\delta*}{R_{\delta*}}$, is then calculated using the slope of a polynomial curve fit of the A(x) data. By repeating the above process for several different frequencies the disturbance growth rate vs. frequency characteristics are determined for a fixed Reynolds number and temperature distribution.

Disturbance growth rate characteristics for uniform wall temperature distributions, n = 0, at $R_{\delta*} = 800$ are shown in Figure 3. The solid lines are smooth curves drawn through the measured points, ω_r is defined as $\omega_r = 2\pi f\nu/U_e^2$, and f is the ribbon frequency. These results provide a measure of the effectiveness of uniform wall heating in the reduction of disturbance growth rates at a fixed Reynolds number.

Stability characteristics for varying values of n, with $R_{\delta*} = 800$, $T_w(x_{ref}) - T_\infty = 5°F$ are shown in Figure 4. Experimental data points are not shown for the sake of clarity, while unheated results have been included as a reference. For $n < 0$ the maximum disturbance growth rates

and the band of frequencies which receive amplification are both reduced relative to the uniform wall temperature case. For n = 1 the maximum disturbance growth rate is greater than that for n = 0, and the band of amplified frequencies has increased relative to the uniform wall temperature case. The results shown here are typical of those obtained at $T_w(x_{ref}) - T_\infty = 3°F$ and 8°F as well. The behavior of the maximum growth rate as a function of n and $T_w(x_{ref}) - T_\infty$ is shown in Figure 5.

The effect of varying S at $R_{\delta*} = 800$, with $T_w(x_{ref}) - T_\infty = 3°F$, is shown in Figure 6. The results shown here are similar to those obtained at $T_w(x_{ref}) - T_\infty = 5°F$ as well. The maximum disturbance growth rate displays a minimum between S = 0 and S = 1 for each temperature level, as shown in Figure 7. This minimum occurs near the minimum critical Reynolds number of the unheated boundary layer. The measured value of $(R_{\delta*})_{\substack{m.c. \\ \Delta T=0}}$ is 400, which corresponds to S = .25, while the predicted parallel-flow value of $(R_{\delta*})_{\substack{m.c. \\ \Delta T=0}} = 520$ corresponds to S = .42.

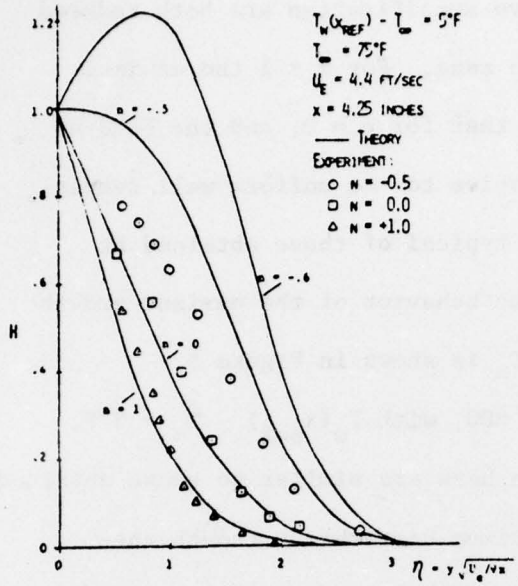

FIG. 1 TEMPERATURE PROFILES FOR POWER LAW VARIATIONS IN WALL TEMPERATURE, $T_w(x) - T_\infty = Ax^N$

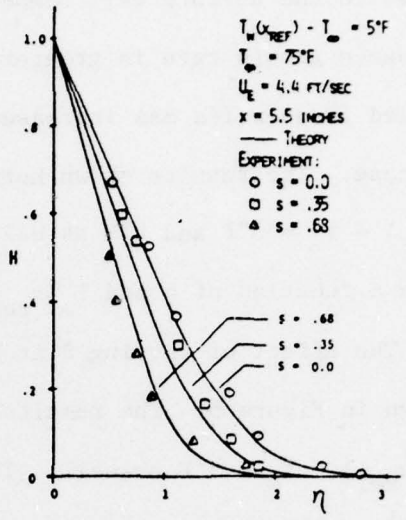

FIG. 2 TEMPERATURE PROFILES FOR STEP CHANGES IN WALL TEMPERATURE

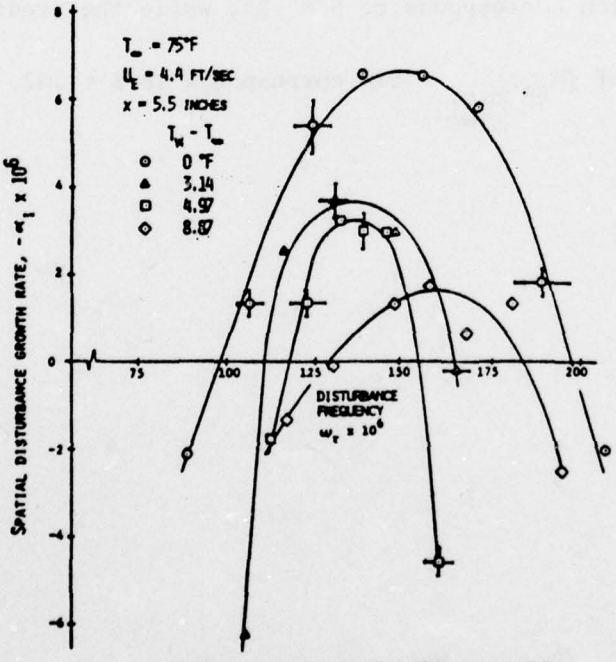

FIG. 3 DISTURBANCE GROWTH CHARACTERISTICS FOR UNIFORM WALL TEMPERATURE DISTRIBUTIONS, $R_{\delta^*} = 800$

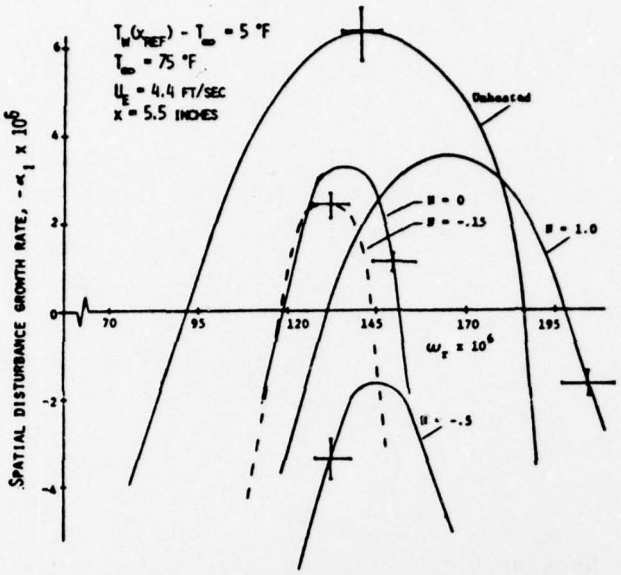

FIG. 4 DISTURBANCE GROWTH CHARACTERISTICS FOR POWER LAW VARIATIONS IN WALL TEMPERATURE, R_{δ^*} = 800

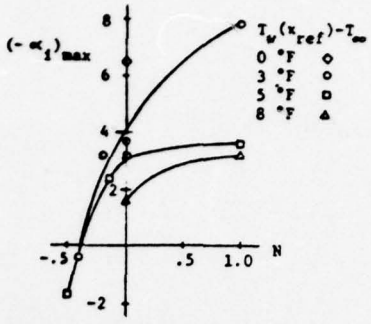

FIG. 5 MAXIMUM DISTURBANCE GROWTH RATE AT R_{δ^*} = 800, T_∞ = 75 °F

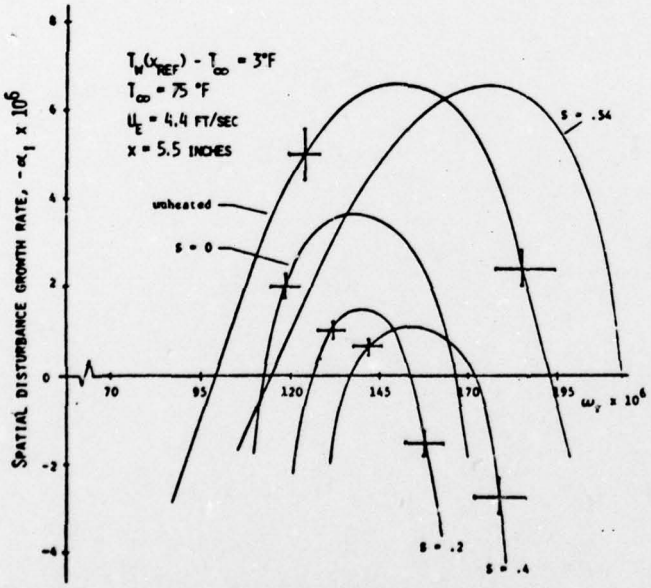

FIG. 6 DISTURBANCE GROWTH CHARACTERISITCS FOR STEP CHANGES IN WALL TEMPERATURE, R_{δ^*} = 800

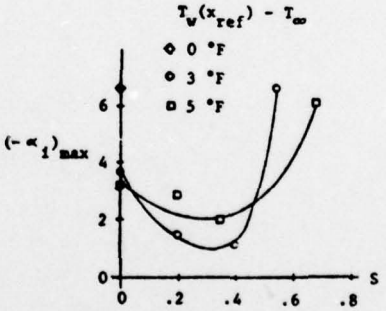

FIG. 7 MAXIMUM DISTURBANCE GROWTH RATE AT R_{δ^*} = 800, T_∞ = 75 °F

Section V

TRANSITION IN AN AXISYMMETRIC BOUNDARY LAYER WITH WALL HEATING

V-2 TRANSITION IN AN AXISYMMETRIC BOUNDARY LAYER WITH WALL HEATING

by

Steven J. Barker
POSEIDON RESEARCH
and
THE UNIVERSITY OF CALIFORNIA AT LOS ANGELES

An extended abstract submitted to the

Low-Speed Boundary Layer Transition Workshop

Rand Corporation - Santa Monica

September 13 - 15, 1976

TRANSITION IN AN AXISYMMETRIC BOUNDARY LAYER WITH WALL HEATING

Recent numerical calculations of boundary layer stability have suggested the possibility of obtaining transition at very high Reynolds numbers in water by using wall heating. The flow-tube experiment is intended to check these predictions, and to determine the feasibility of using heat combined with favorable pressure gradient to delay transition on submerged bodies.

The flow tube is basically an inside-out analog of the boundary layer over a submerged body of circular cross-section moving through the water. A free-stream flow with very low disturbance levels is provided through a 24-inch diameter, 12-foot long settling chamber (see figure 1). This flow then passes through a 34.5 to 1 smooth contraction into a 4-inch diameter circular tube. The boundary layer in the 4-inch tube remains thin relative to the tube diameter throughout the length of the tube ($\delta^* \leq 0.05$ D).

Heat is applied to the inside wall of the flow tube by means of electric strip heaters wrapped around the outside. These heaters are servo-controlled using thermocouples near the inside wall of the tube. Thus the inside wall temperature is maintained at pre-selected values. The length of the tube is divided into 20 sections whose wall temperatures are controlled independently. Thermocouples are also located on the outside wall of the tube at about thirty locations along its length. The temperature difference between the inside and outside wall at a given location provides a measurement of the heat flux into the boundary layer. Since this heat flux will increase by a factor of about ten at the region of transition, it is easy to locate transition with temperature measurement. There is no instrumentation penetrating the inside wall of the tube which could trip the boundary layer. The wall roughness is less than four micro-inches and the waviness is less than one mil per inch.

Three different flow tube test sections are being used. The first is 20 feet in length and uniform in diameter. This tube will simulate a nearly zero pressure gradient boundary layer. (Displacement effect yields a very weak favorable gradient.) At the maximum flow velocity of 90 feet per second, the length Reynolds number of this tube is 125 million. The second and third flow tube will be of non-uniform diameter to simulate two axisymmetric shapes of practical interest. The longest of these tubes will be 44 feet in length.

The experiment is located at the Hydro-Mechanics Laboratory of Colorado State University. This site was chosen over several other possibilities for the following reasons. Although the water is not recirculated, the run time is effectively unlimited. The lab draws its water directly from a large reservoir through a 24-inch diameter pipe. The total pressure at the entrance of the settling chamber is about ninety psig. Thus even at a test section velocity of 90 feet per second, the test section pressure is about 35 psig and the possibility of cavitation can be ignored. The longer run time and higher total pressure are the chief advantages of this facility relative to others.

The first series of measurements in the experiment was a careful documentation of the flow in the settling chamber and test section without wall heating. The test section in this case was a 4-foot straight tube with several types of instrumentation. A pitot-rake was located near the downstream end to check the uniformity of the free-stream mean velocity. A cylindrical hot film sensor was used to measure freestream turbulence intensity and to determine the intermittency in the boundary layer. This probe was used to measure the transition Reynolds number in the absence of heat, which will be discussed below. Two flush-mount wall pressure transducers were also used to locate transition in the tube. An accelerometer was mounted on the outside wall to measure the vibration spectrum.

A hot film probe was also used to survey the flow in the settling

chamber one foot upstream of the contraction. Mean velocity profiles, turbulence levels, and turbulence spectra were measured for various configurations of turbulence management devices. The devices used include 1/8 inch cell aluminum honeycomb, 10 pores per inch porous foam, and wire screen of 34 and 60 mesh per inch. For each turbulence management configuration, the settling chamber flow was documented at several test section velocities. In addition, the unheated transition Reynolds number was measured in the flow tube at 1 flow velocity. Since this transition Reynolds number has been measured in other facilities, it is a good indication of the quality of the freestream flow. A plot of unheated transition Reynolds number versus settling chamber configuration is shown in figure 2. The "best" configurations are seen to produce transition at Reynolds numbers close to 5 million. This is very close to the highest value achieved in the air flow tube facility of C. S. Wells.

Hot film surveys show that the boundary layer in the settling chamber becomes turbulent at test section velocities above 30 feet per second. Since the boundary layer at the downstream end of the contraction must be thin and disturbance-free, a boundary layer suction section was installed between the settling chamber and the contraction. This section uses a 4-inch length of porous wall to remove the entire turbulent boundary layer. Measurements have shown that even at the maximum test section velocity, the boundary layer at the entrance of the contraction can be made laminar with the appropriate amount of suction.

The turbulence levels in the contraction entrance are considerably lower than the original goal of about 1 per cent. At a test section velocity of 45 feet per second, a turbulence level in the settling chamber of 0.2 per cent is typical for the best configurations. This configuration makes use of 1-inch of porous foam followed by two sections of honeycomb and then three screens. Preliminary results using a 3-inch thickness of porous foam show even lower turbulence levels.

Some tests with wall heating were made on the 4-foot flow tube. The results of these were not strongly positive - only a small increase in transition Reynolds number was seen. However, the heating and temperature measuring system on the tube were very crude. Heat was not applied far enough upstream in the tube and the suction section was not yet available. At the date of this writing, the 20-foot straight flow tube is being installed. Early results with this tube may be available at the time of this meeting.

ACKNOWLEDGMENT

The author gratefully acknowledges support provided by the Marine Systems Group, Autonetics Division, Rockwell International.

FLOW TUBE TURBULENCE MANAGEMENT SYSTEM

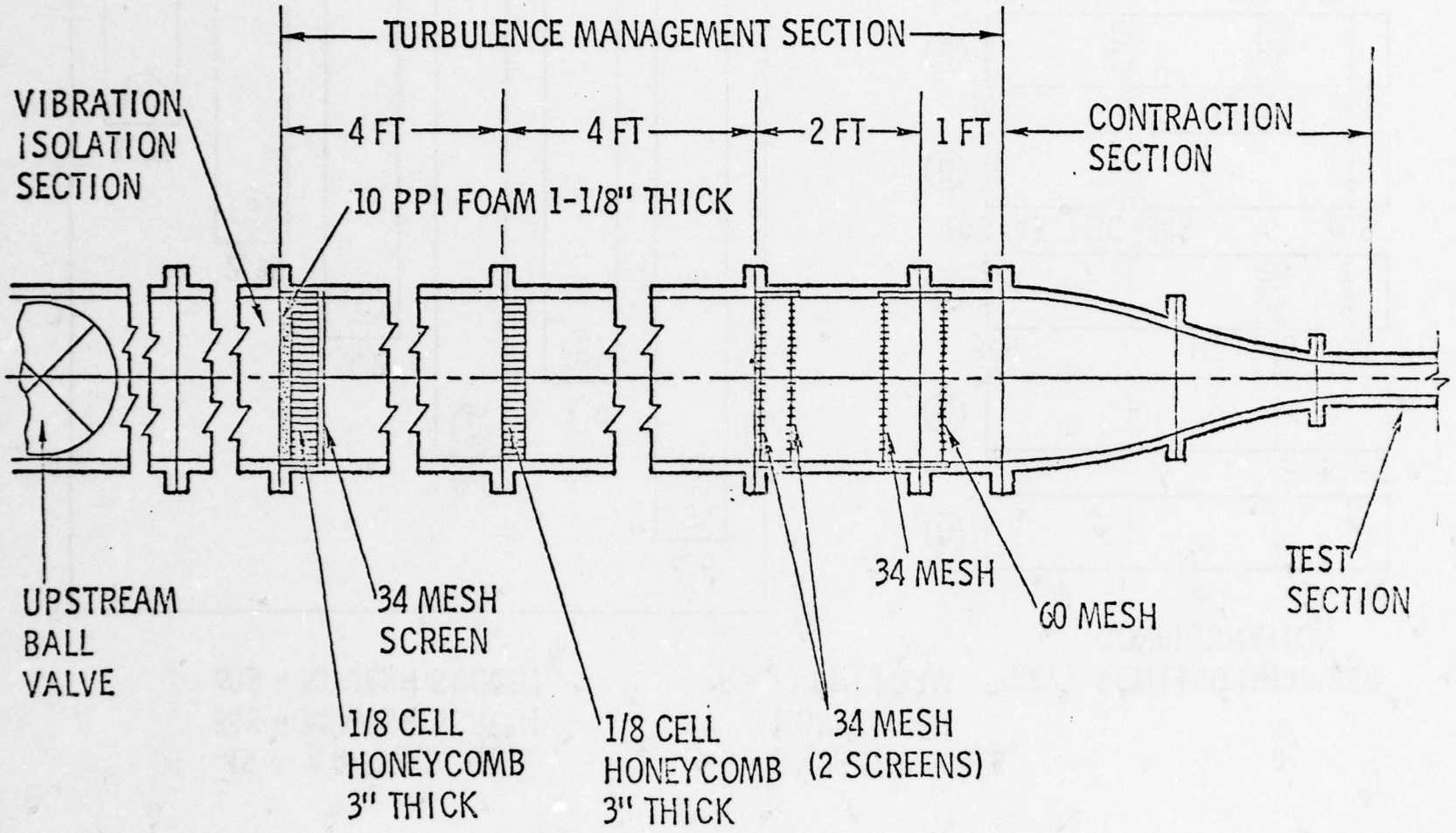

Figure 1

GS6-07142
7-27-76

Rockwell International

TRANSITION REYNOLDS NUMBERS FOR VARIOUS TURBULENCE MANAGEMENT CONFIGURATIONS IN THE SETTLING CHAMBER

4S = 4 MESH SCREEN
34S = 34 MESH SCREEN
60S = 60 MESH SCREEN

HC = 3" OF 1/8" -CELL HONEYCOMB
F = 10 PPI FOAM

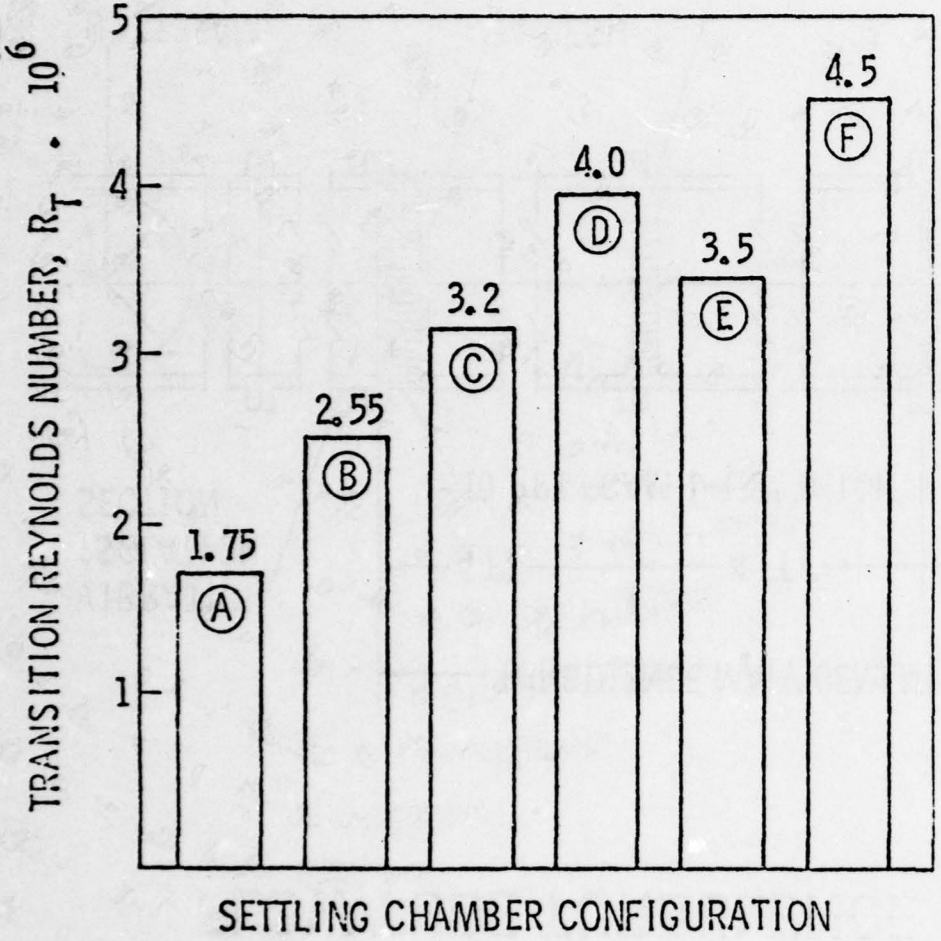

KEY: SETTLING CHAMBER CONFIGURATION

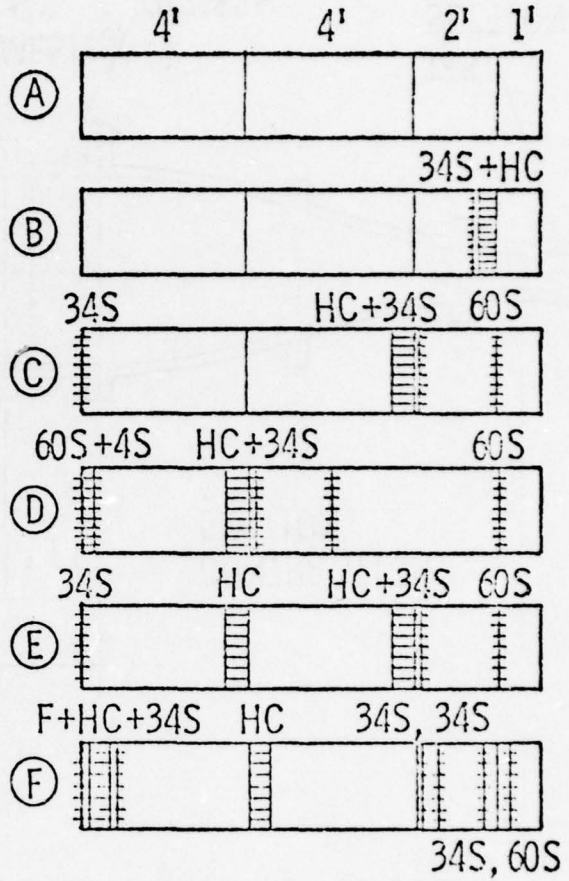

GSG-07141
7-27-76

Figure 2

Rockwell International

Section V

PRESSURE FLUCTUATIONS IN THE TRANSITION REGIONS OF FOREBODIES OF REVOLUTION

V-3 Extended Abstract of Paper for
"LOW-SPEED BOUNDARY-LAYER TRANSITION WORKSHOP: II"
Santa Monica, California
13-15 September 1976

PRESSURE FLUCTUATIONS IN THE TRANSITION REGIONS OF FOREBODIES OF REVOLUTION

by

Thomas T. Huang
David W. Taylor Naval Ship Research and Development Center
Bethesda, Maryland

The transition resulting from the growth of Tollmein-Schlichting disturbances naturally present in a laminar boundary layer is defined as natural. Natural transition should be distinguished from transition triggered by laminar separation. If laminar separation occurs, either as a result of a severe adverse pressure gradient due to body shape or by the use of an artificial turbulence stimulator, transition will usually occur at a very short distance downstream of the flow reattachment.

In the present investigation, the amplitude of the wall-pressure fluctuations during natural transition and following laminar separation due both to adverse pressure gradient and to two-dimensional trip wires was measured by microphones located in the transition regions; these measurements were extended downstream into the fully-established turbulent boundary layer. The fluctuating pressure on the model surface was sensed through an 0.794-mm-diameter pinhole which led to a small cavity enclosed by the protective cap and the microphone diaphragm. The microphone system used had satisfactory response characteristics between 10 Hz and 10 KHz.

The wind tunnel in the Anechoic Flow Facility of the Center has a 2.438 meters x 2.438 meters test section. The free-stream rms turbulence levels in the test section with a model in place were found to be 0.075, 0.090, 0.100, and 0.12-0.15 percent for U_o = 24.4, 30.5, 30.8

and 45.7 meters/sec, respectively. By integrating the measured noise spectrum levels in the test section from 0 to 10,000 Hz to background acoustic noise at 30.5 meters/sec was found to be 93 dB:re 0.0002 dyn/cm^2, which corresponds to an equivalent rms turbulence level of 0.007 percent.

The model, which consisted of the forebody, together with a parallel middle body and a streamlined afterbody, was supported by a single streamlined strut located roughly at the middle of the model. Three small guide struts were used at the tail of the afterbody to increase the rigidity of the model.

Two series of forebodies of revolution were selected for this investigation. One of the series, designated "Forebody T," had a natural transition region, and the other series, designated "Forebody S," had laminar separation which triggered transition. Two-dimensional roughnesses (trip wires), located at various positions upstream of natural transition and laminar separation, were also investigated. Figure 1 shows the geometries of the forebodies used and the computed pressure coefficient. Figure 2 shows typical histogram of microphone output.

The growth of Tollmein-Schlichting disturbances in boundary layers is approximated by the spatial stability charts for the Falkner-Skan boundary layer profile prepared by Wazzan, Okamura, and Smith. Smith's spatial amplification ratio was chosen as a simple yardstick to correlate the instability characteristics of the boundary layer with various measured stages of transition. Whereas the amplification ratio is calculated from linear stability theory, the latter stage of transition is a nonlinear process and is three-dimensional in nature. The calculated spatial amplification ratios A(x) in the natural transition regions of Forebodies T-3, T-6 and T-8 correlated with the flow regimes measured by flush-mounted hot-films are shown in Figures 8, 10 and 11 in the paper by Power*. The measured flow regimes of T-8 do not agree with calculated amplification ratios. The transition characteristics measured in the present wind tunnel do agree well with towing tank results.

Figure 4 shows the correlation between the measured wall-pressure fluctuations and calculated Smith spatial amplification ratios A(x) in the natural transition regions of Forebodies T-3 and T-6. The pressure fluctuations are small for $A < e^9$ to the position of e^{13} where the flow has just become fully turbulent according to the outputs of hot-film probes. The measured wall-pressure fluctuations approach those of a fully-established turbulent boundary layer at approximately e^{18}. However, no large wall-pressure fluctuations in the transition regions of Forebodies T-8 was measured.

*Power, J.L., "A Comparison Between Measured and Computed Locations of Transition on Nine Forebodies of Revolution," paper presented at Rand's Workshop II, 1976

The characteristic lengths ξ and λ, which is the dead-air bubble length, are shown in Figure 5. The data of Gaster and Arakeri for λ are also included in Figure 5. As shown in Figure 6, enormous pressure fluctuations were measured in the regions of flow reattachment following laminar separation on Forebodies S-2, S-1, and S-7. If the distance is measured from the separation point, $S-S_s$, and is nondimensionalized by a characteristic length ξ, the distance between the point of maximum wall-pressure fluctuation and the separation point, then the measured value of $\sqrt{\overline{p'^2}}/(\rho U_o^2/2)$ possess a similar form with respect to the quantity $(S-S_s)/\xi$. The velocity fluctuations in the shear layer right above the end of the dead-air region were found by Gaster to be extremely high ($\sqrt{\overline{u'^2}}/U_o$ is about 0.16). Consequently, the pressure fluctuations are expected to be extremely high there, although direct measurements have not been made.

The turbulent stimulators used were single circular wires of four different diameters: -0.05, 0.127, 0.254, and 0.508 mm - located at different axial positions on the Forebodies T-3 and S-2. Figure 7 shows the locations of inception of intermittent disturbances measured by hot-film probes and maximum wall pressure fluctuations, respectively ζ/d and ξ/d, for four wires of large R_K, and the apparent amplification factor in terms of $[\Delta \ln A]_K$ for wires having R_K in the range $25 < R_K < 100$. Here, $R_K = u_K K/\nu$ is the wire Reynolds number based on the velocity u_K at the tip of roughness height K. The values of $[\Delta \ln A]_K$ were obtained by correlating the measured wall-pressure fluctuations with and without trip wires. Preston's minimum R_K of 400 to 600 is a satisfactory criterion to determine the range of trip wire R_K's which are effective in causing rapid transition. No trace of high pressure fluctuations due to the trip wire was measured after 200 wire diameter downstream of the wire. The Smith and Clutter criterion of a maximum value of R_K of 25 so as not to prematurely trip transition agrees satisfactorily with the present results. For the R_K range $25 < R_K < 100$, transition will move upstream.

Cavitation inception of naval vehicles will be controlled by the unsteady pressure fluctuations in regions of natural transition or laminar separation, superimposed upon the potential-flow static pressure. The location and magnitude of the high pressure fluctuations in the transition regions have profound implications relative to model/full-scale cavitation-inception scaling, boundary-layer self-noise scaling, and other naval applications related to transition phenomenon.

ACKNOWLEDGEMENTS

This work was funded by the David W. Taylor Naval Ship Research and Development Center (DTNSRDC) under its Independent Research Program, Task ZR023 0101, Work Unit 1-1552-102.

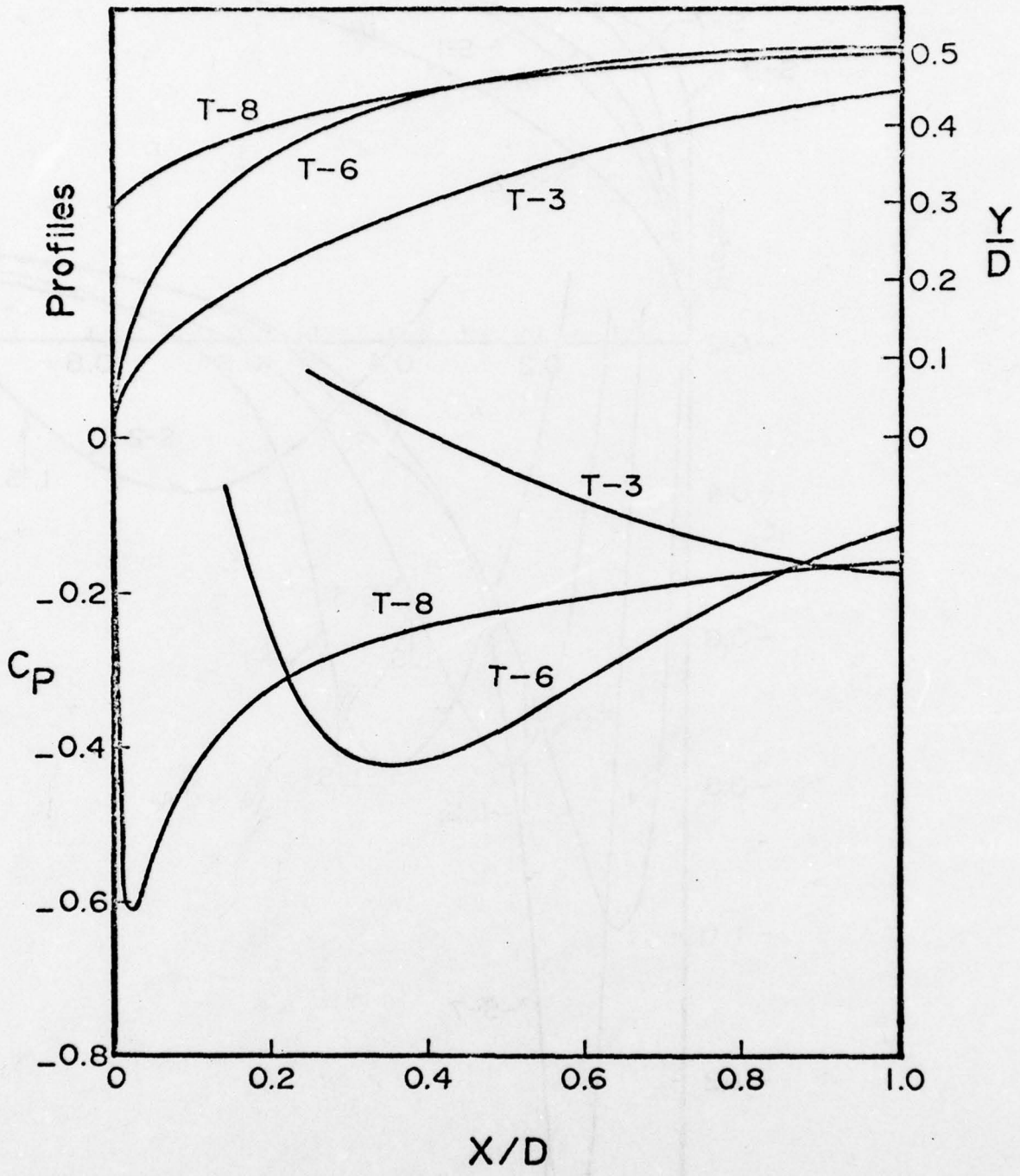

Figure 1-a Surface Profiles and Pressure Coefficients of Three Forebodies with Natural Transition

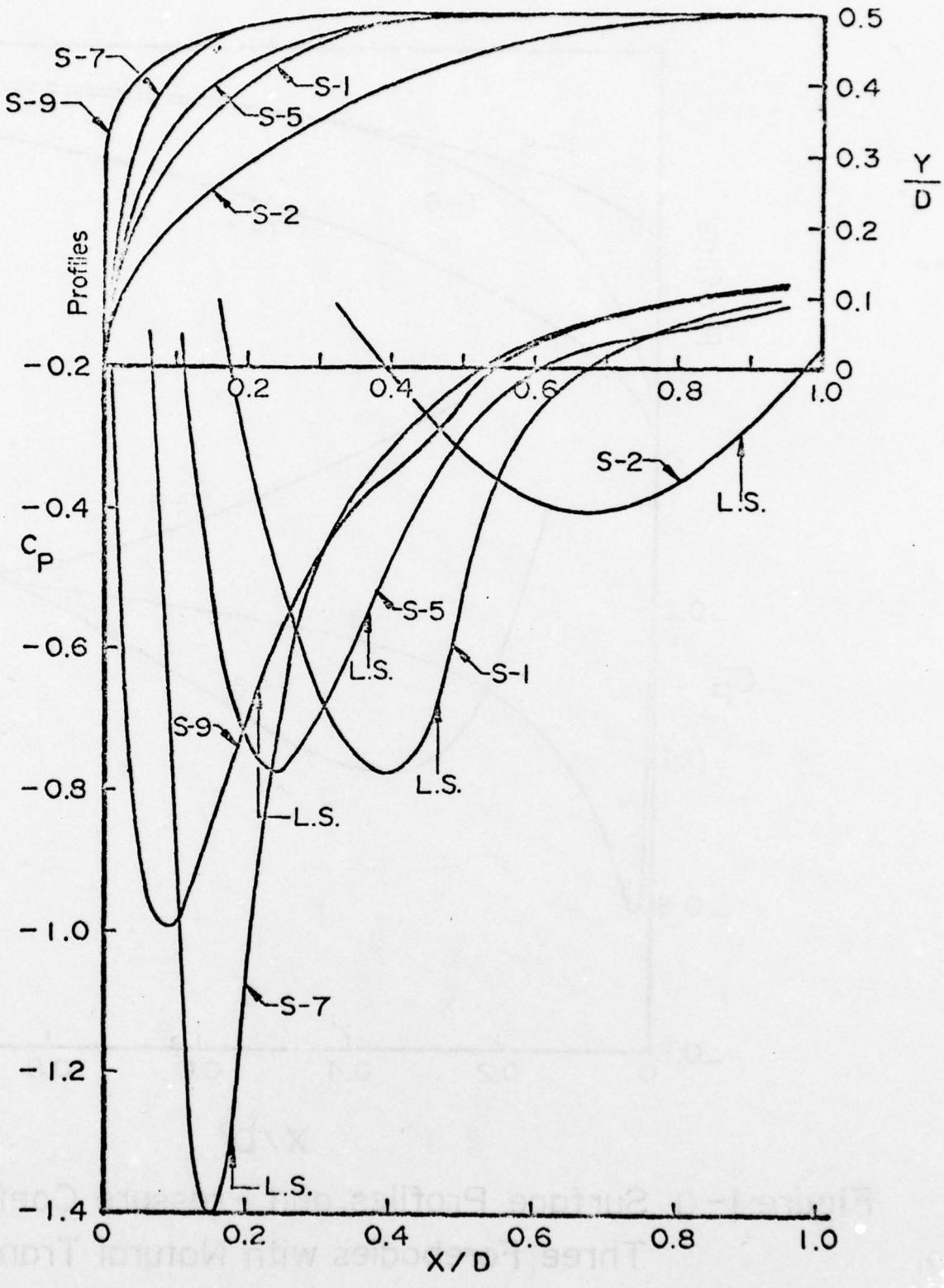

Figure 1-b Surface Profiles and Pressure Coefficients of Five Forebodies with Laminar Separation

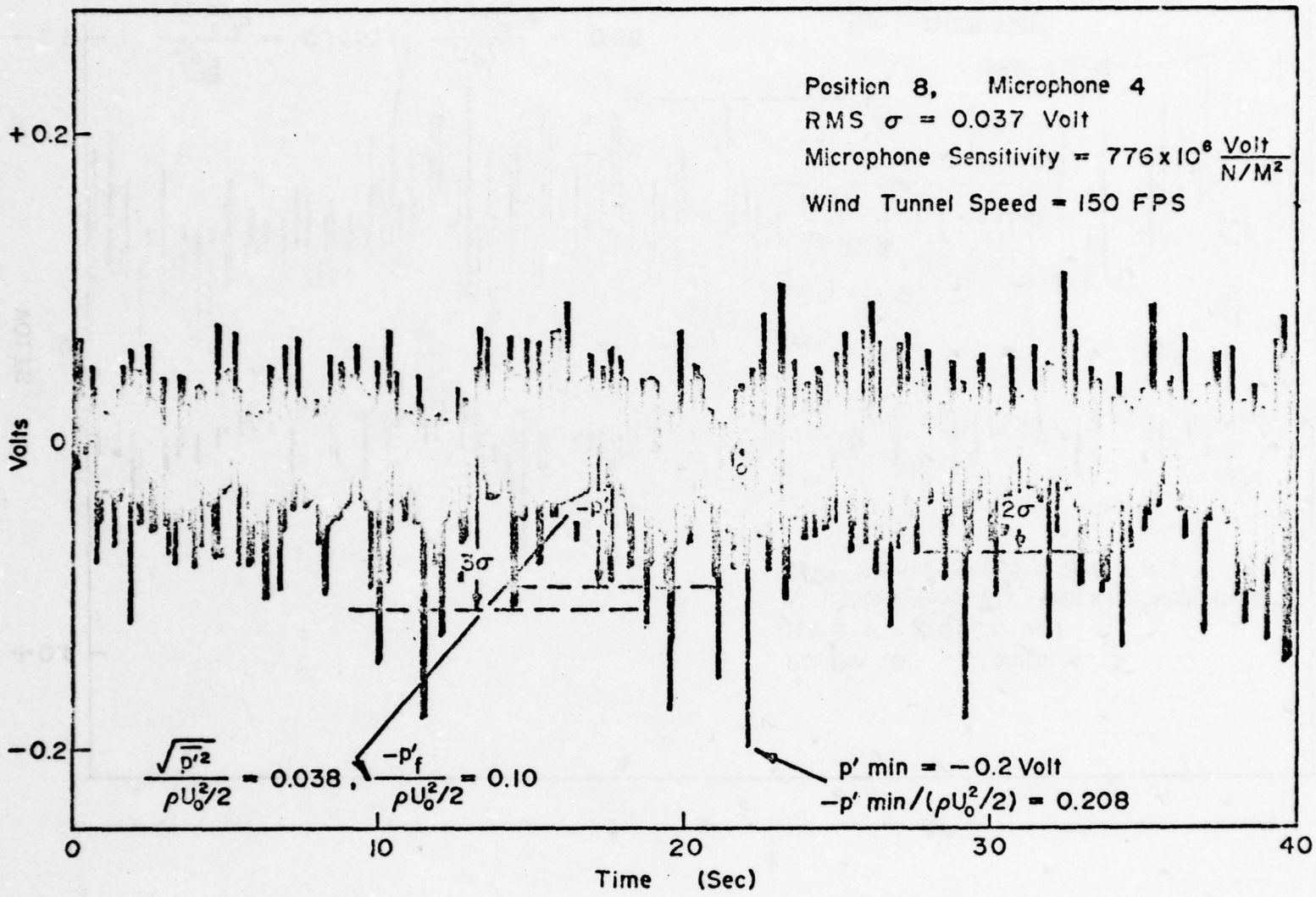

Figure 2a — Typical Histogram of Microphone Output in Natural Transition Region of Body T-3

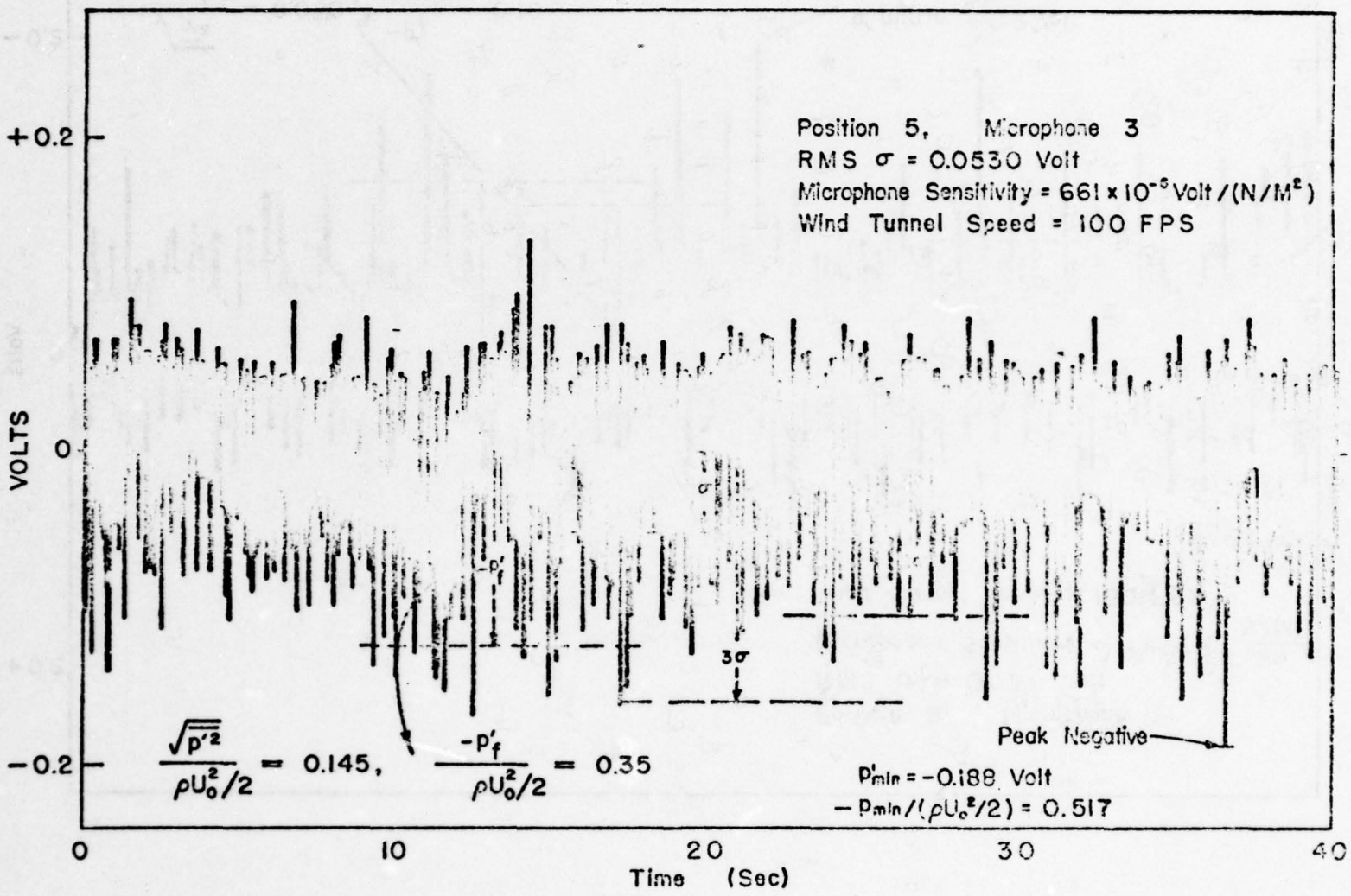

Figure 2b — Typical Histogram of Microphone Output After Laminar Separation on Body S-2

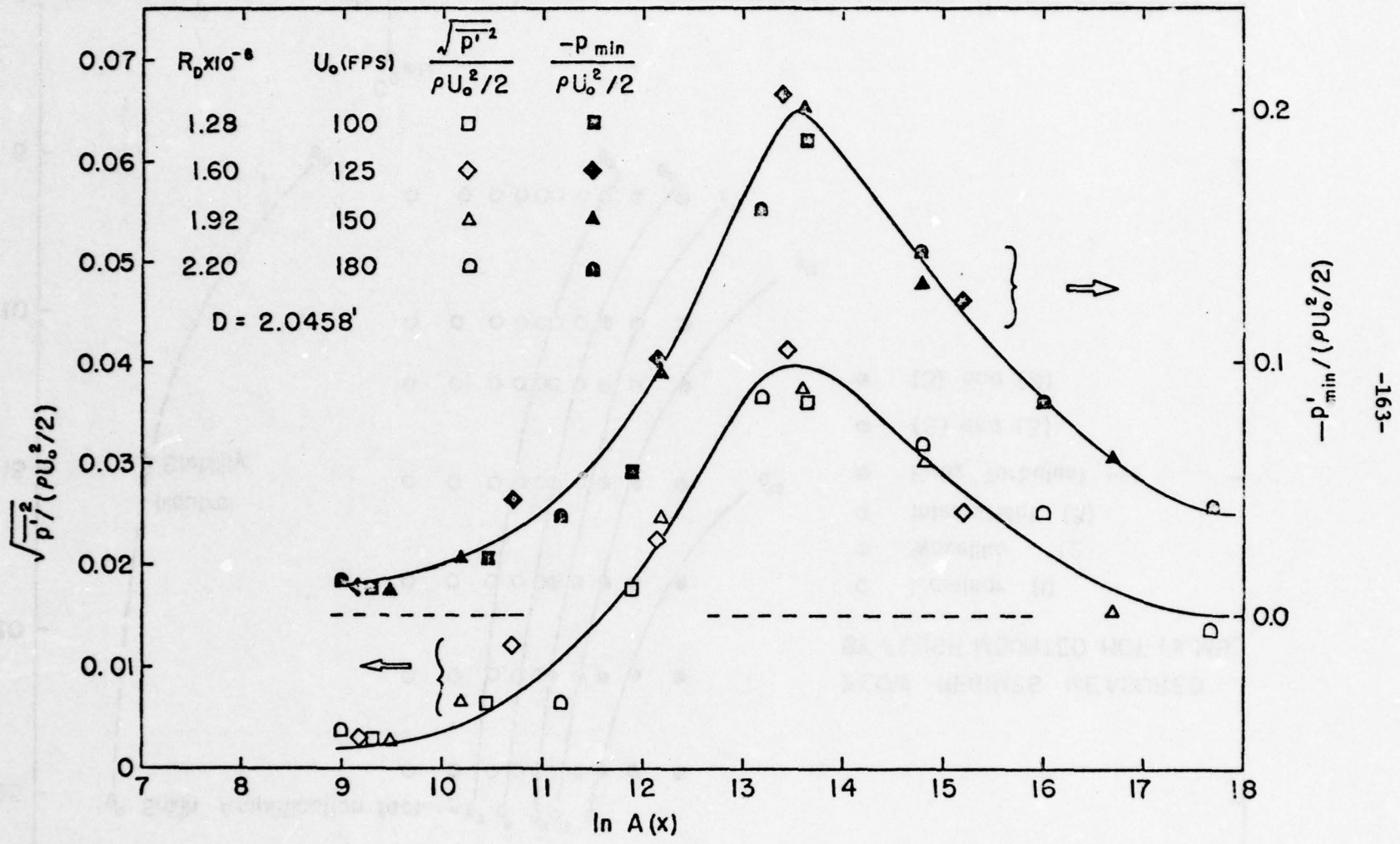

Figure 4a –Root–Mean–Square and Negative Peak, Wall – Pressure Fluctuation In Natural Transition Region of Forebody T – 3

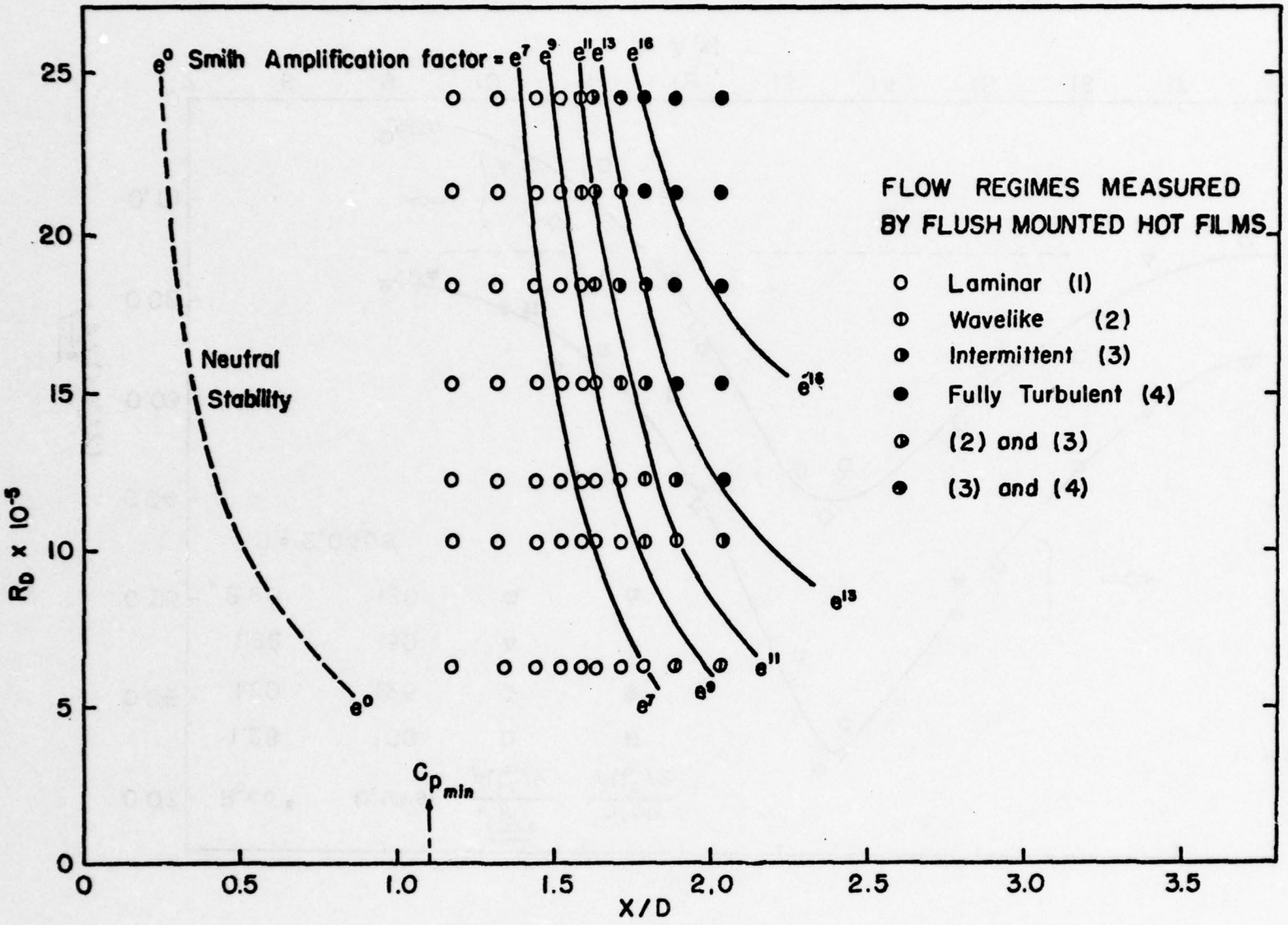

Figure 3a – Measured Flow Regimes On Smooth Forebody T-3 As a Function of Model Reynolds Number R_D

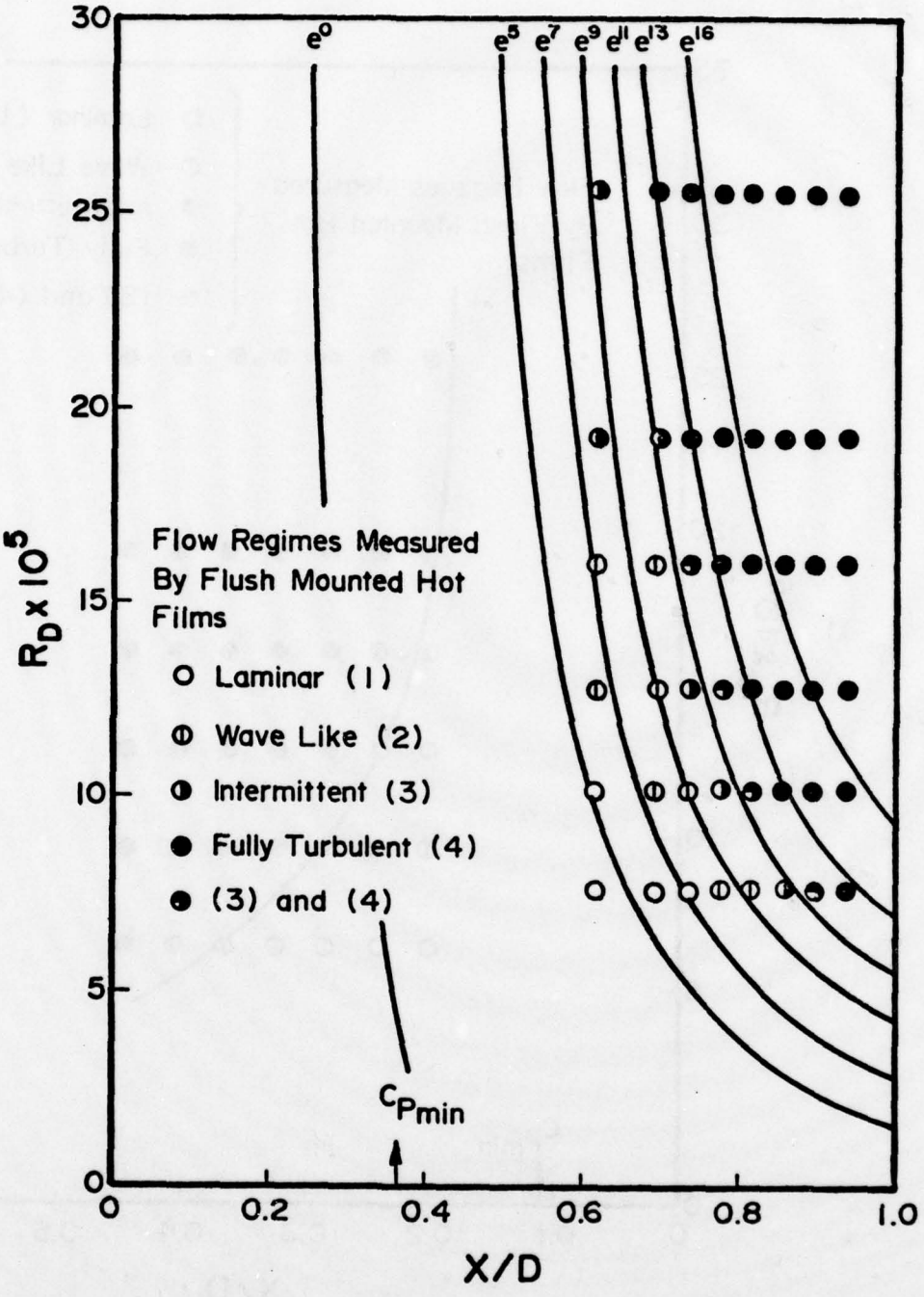

Figure 3-b Measured Flow Regimes on Forebody T-6 as a Function of Reynolds Number R_D

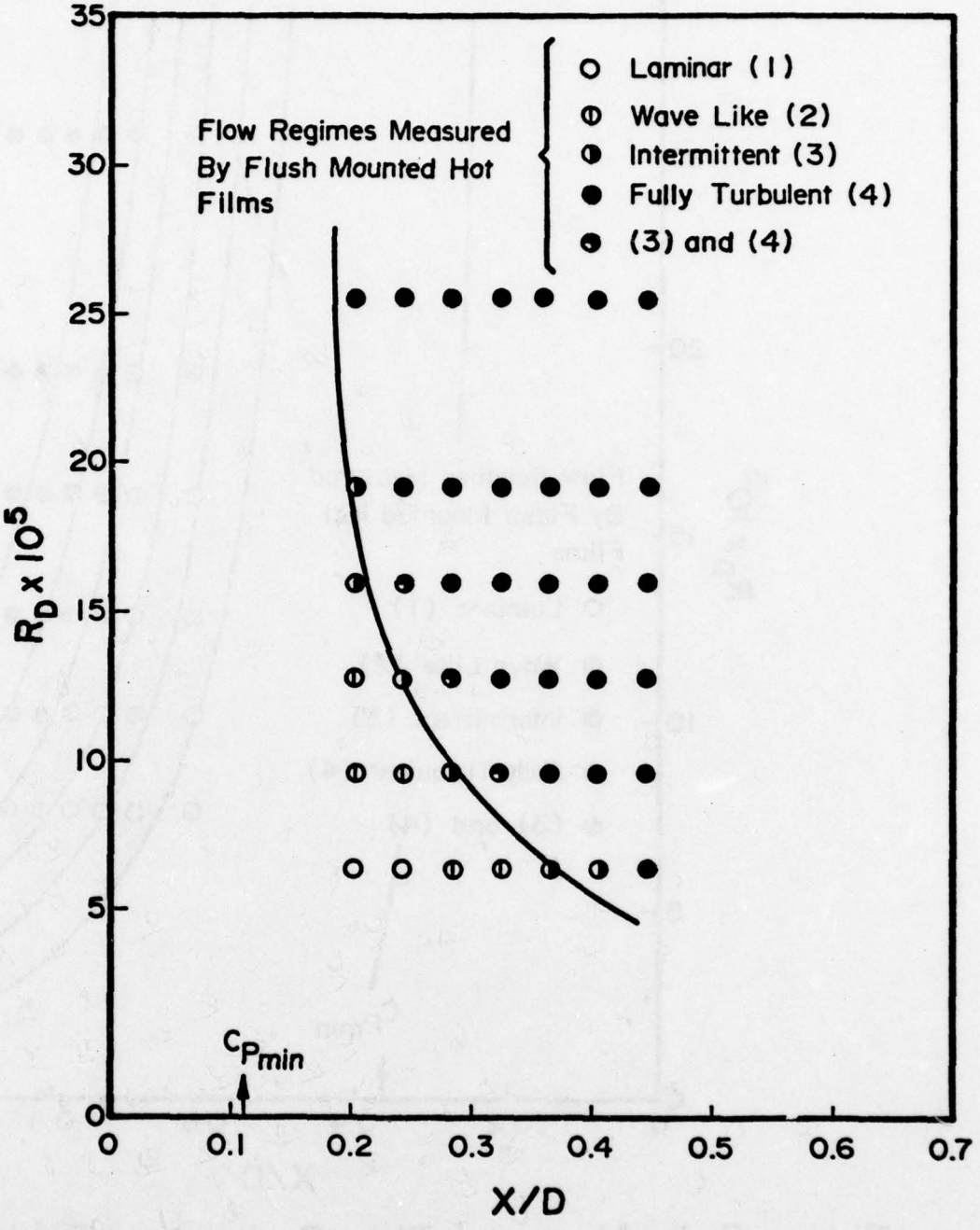

Figure 3-C Measured Flow Regimes on Forebody T-8 as a Function of Reynolds Number R_D

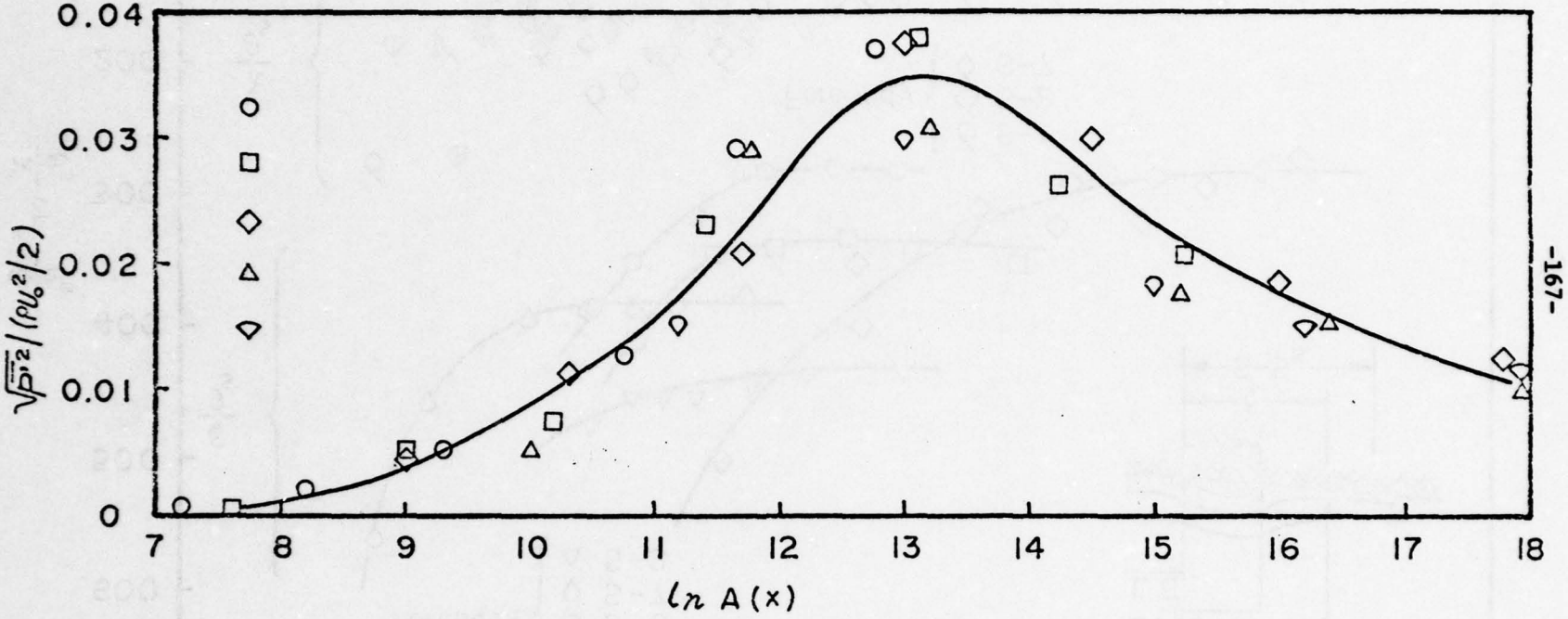

Figure 4-b Root-Mean-Square Wall-Pressure Fluctuation in Natural Transition Region of Forebody T-6

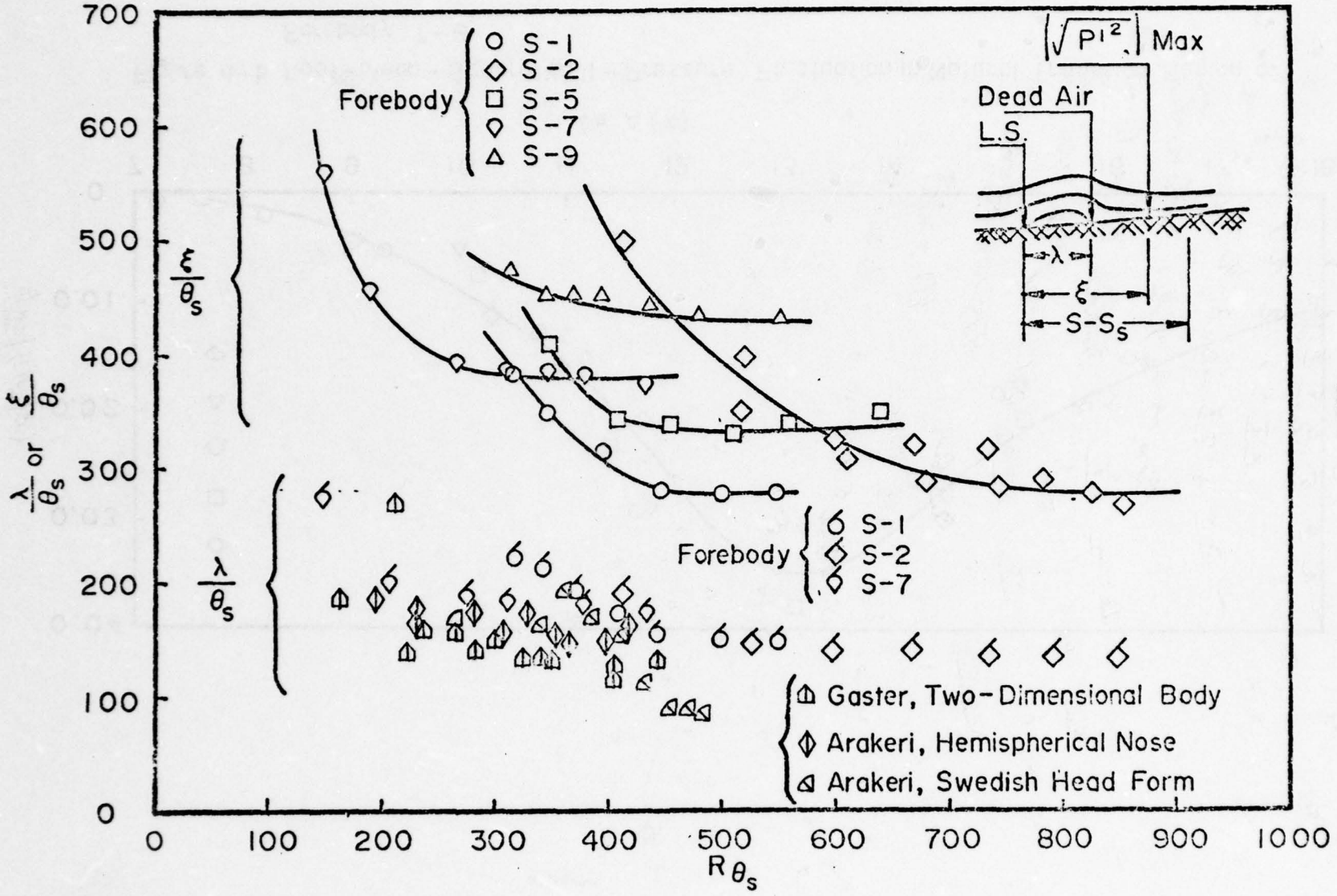

Figure 5 Measured Separation Bubble Lengths Versus Reynolds Number

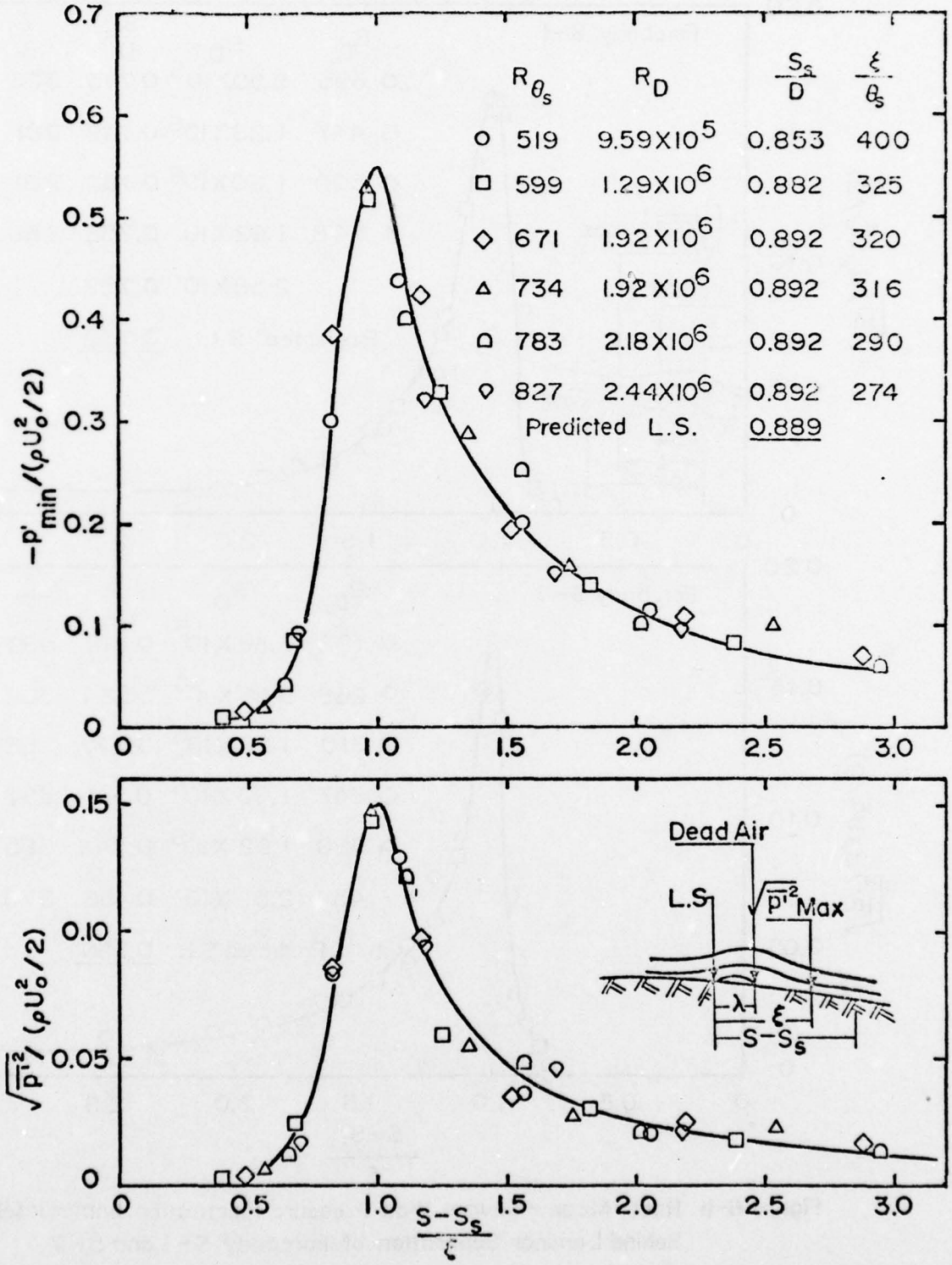

Figure 6a — Root-Mean-Square and Negative Peak, Wall-Pressure Fluctuation Immediately Behind Laminar Separation of Forebody S-2

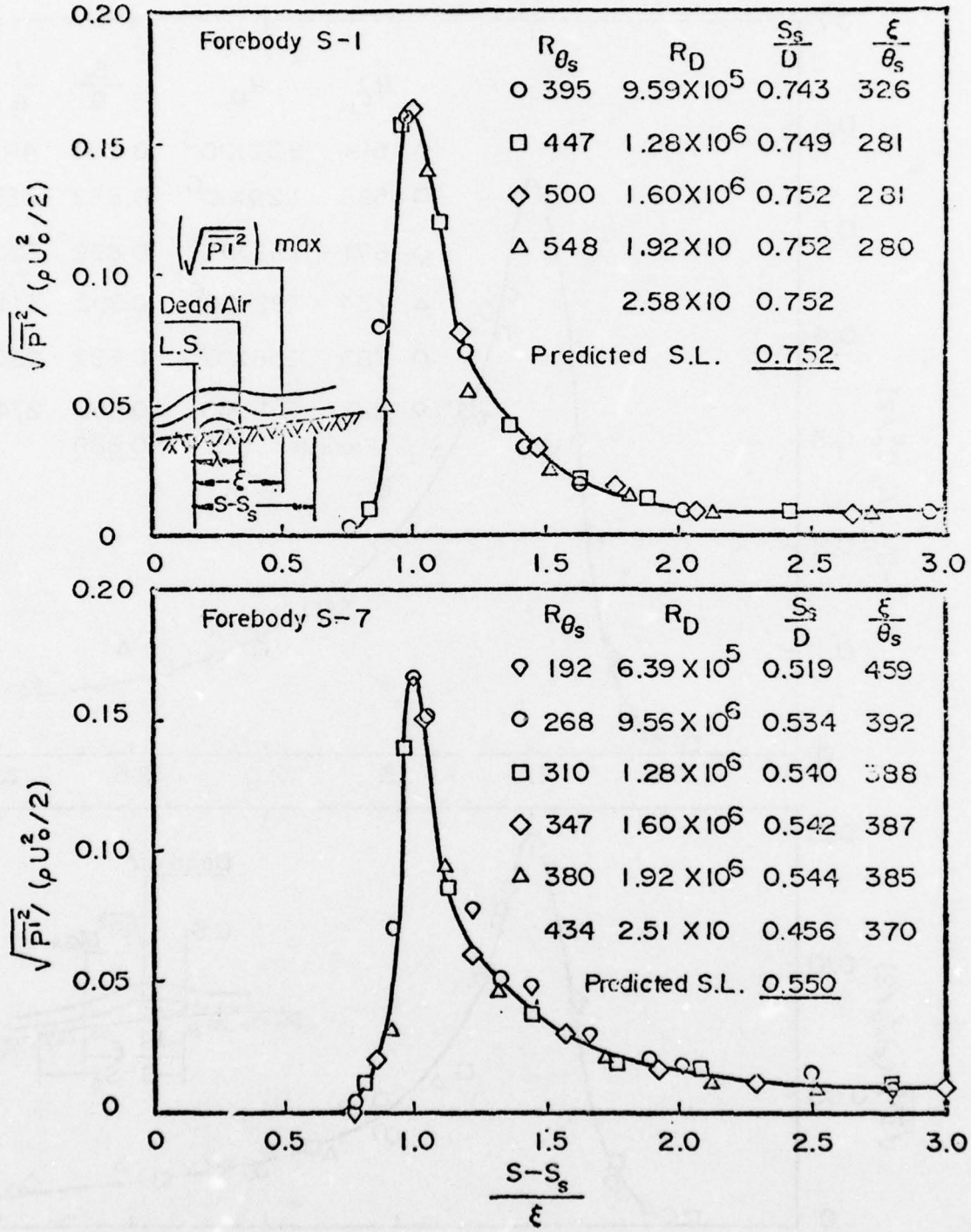

Figure 6-b Root-Mean-Square Wall Pressure Fluctuation Immediately Behind Laminar Separation of Forebody S-1 and 5-7

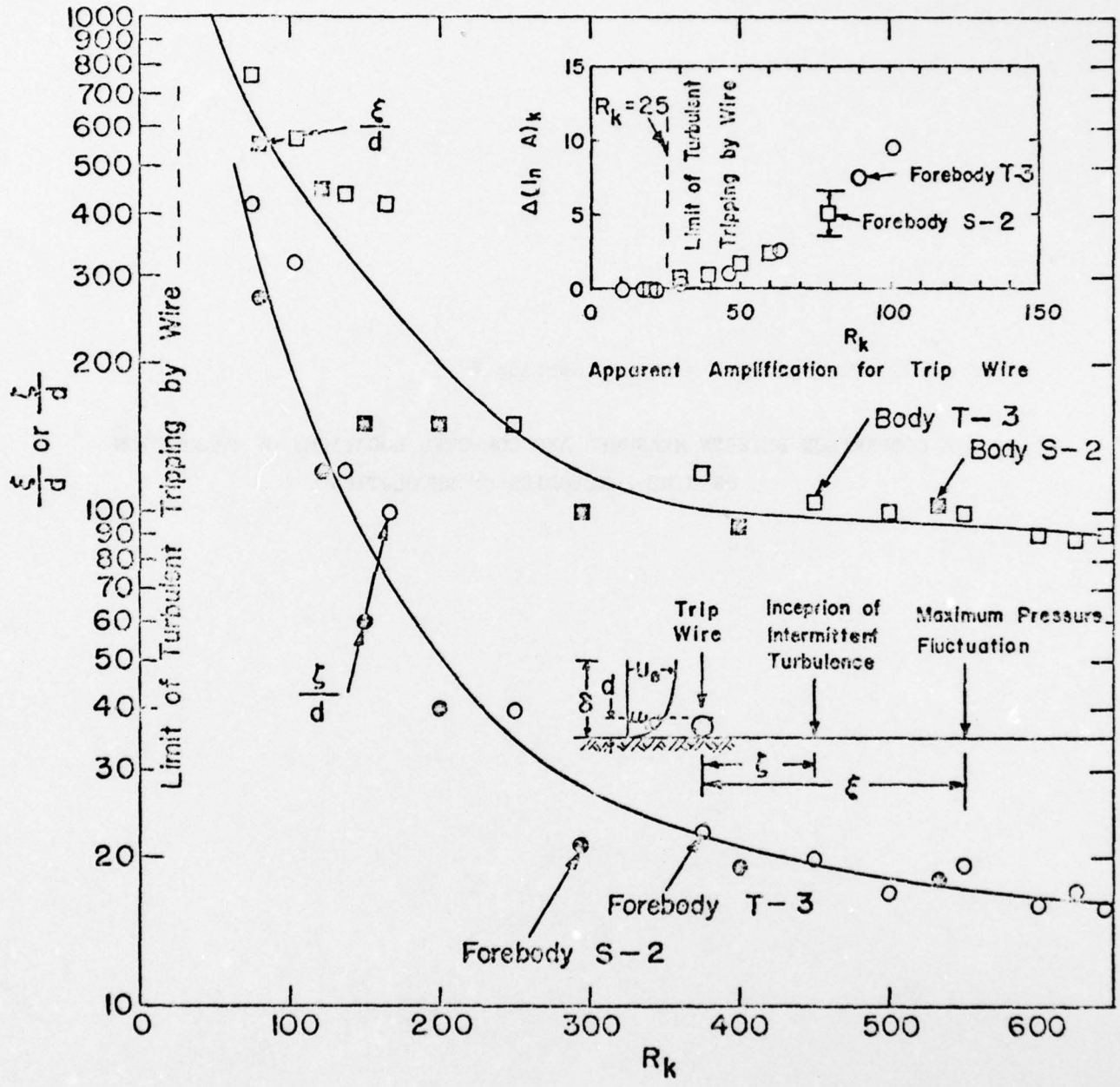

Figure 7 — Locations of Inception of Intermittent Disturbances and Maximum Wall-Pressure Fluctuations Behind Tripwires

Section V

A COMPARISON BETWEEN MEASURED AND COMPUTED LOCATIONS OF TRANSITION ON NINE FOREBODIES OF REVOLUTION

Extended Abstract of Paper for

V-4 "LOW-SPEED BOUNDARY-LAYER TRANSITION WORKSHOP: II"

Santa Monica, California

Sept 13-15, 1976

A COMPARISON BETWEEN MEASURED AND COMPUTED LOCATIONS OF TRANSITION ON NINE FOREBODIES OF REVOLUTION

by

John L. Power

Drag and transition data are given for nine submerged axisymmetric bodies. The bodies have vastly different forebody geometries ranging from very fine to very blunt profiles and include two flat-faced forebodies. The experiments were performed in a towing basin at speeds between 0.5 and 5.1 m/s and at a water depth of 2.7 metres. The experimental arrangement is shown in Figure 1. The models were approximately 7 metres long and had a maximum diameter of 0.62 metres. Constant volume was maintained by varing the length of the parallel middle body.

The geometries of the forebodies were altered by changing two parameters, the length/maximum diameter ratio and the prismatic coefficient. The profiles of four of the nine forebodies are shown in Figure 2. These forebodies have length-diameter ratios of 0.5, 1.00, 1.82 and 3.00 with a constant prismatic coefficient of 0.667. The computed pressure distributions on these forebodies are shown in Figure 3.

The contours of a second set of five forebodies are shown in Figure 4. These shapes are much blunter than those shown in Figure 2 and include two flat-faced bows. The increased bluntness was obtained by increasing the value of the prismatic coefficient. The computed pressure distributions on these bodies are shown in Figure 5.

The extents of the laminar, transitional and turbulent flow regimes were determined by qualitative analysis of the signals from several constant-temperature hot films flush mounted on each forebody. Selection of the hot film locations was assisted by using transition calculations, computer pressure distributions and the Curle-Skan laminar separation criterion. The active elements of the hot films were approximately 1.6 millimeters long. They were mounted on the end of small cylinders which were glued into pre-drilled holes in the models.

As shown in Figure 6 analysis of the hot film probe outputs revealed four types of boundary layer flow: (1) laminar flow, where the hot-film signals were of steady amplitude; (2) a smooth wave-like disturbance; (3) an intermittent turbulent bursting flow; and (4) a fully-turbulent flow of random nature.

Figure 7 gives a summary of the forebody properties and locations of transition or laminar separation for the nine models. The locations given for laminar separation are those computed using the Curle-Skan modified Thwaites criterion. The transition locations were determined from the analysis of the hot film records.

Laminar separation was predicted for five of the nine models. Hot film probes were placed immediately before and after these predicted locations. In all cases, the probe before the separation location predicted laminar flow (Type 1) and the probe after the separation location indicated turbulent flow (Type 4). It was concluded that laminar-separation initiated turbulence and the location of the laminar separation is closely predicted by the modified Thwaites criterion.

The flow regimes for the four forebodies on which laminar separation did not occur are given in Figures 8, 9, 10, and 11. The experimental data are compared with predicted spatial amplification ratios of disturbances as calculated by the Smith-Gamberoni method. In Figures 8 and 9, three predictions corresponding to spatial amplification ratios of e^9, e^{11}, and e^{13} are compared with the measured values from models 4620-3 and 4. For both models, the inception of intermittent turbulent bursting of transition and the e^{11} curves agree quite well. The e^9 curves appear to coincide with the measured inception of Type 2 wave like disturbances. The e^{13} curves correlate very well with the measured inception of fully-turbulent flows.

In Figure 10 five predictions corresponding to spatial amplification ratios of e^5, e^7, e^9, e^{11}, and e^{13} are compared with the measured results from model 4620-6. For this model the e^9 curve is located close to the inception of intermittent turbulent bursting of transition while the e^{11} curve is located well into the turbulent bursting region. For the lower Reynolds numbers, the e^{13} curve correlates with locations near the end of the turbulent-bursting region and at the higher Reynolds numbers, this curve moves well into the fully turbulent (type 4) region. The e^5 curve correlates well with the inception of type 2 wave like disturbances.

In Figure 11, predictions corresponding to spatial amplification ratios of e^3, e^5, e^7, e^9, e^{11}, and e^{13} are compared with measured results from model 4620-8 (a flat-faced model). The correlation between these predictions and the measured results is radically different from the correlations obtained with the three models previously discussed. Here the e^3 curve correlates with the inception of wave-like disturbances. The e^5 curve is located at the end of the wave-like disturbance region and near the start of the turbulent bursting region. The start of fully turbulent flow occurs between the e^5 and e^7 curves. The e^7 and all higher exponent curves lie well within the fully turbulent region.

Also shown in Figure 11 are transition data obtained by T. Huang[1] in a low-turbulence wind tunnel using Model 4620-8. The wind tunnel data are in substantial agreement with the towing tank data. Huang also measured

the transition flow regimes on Models 4620-3 and 8. These data are not shown but similar agreement between towing tank and wind tunnel results were found for these models.

Figure 12 gives the results obtained from the drag measurements. For each model, the computed residual drag coefficients and EHP ratios are given. Model 4620-3 and 6 show the lowest drags and Model 4620-7 shows the highest drag. There is a difference of approximately 4 percent in EHP required for these two extremes.

Ref. 1: Huang, T.T., "Pressure Fluctuations in the Transition Regions of Forebodies of Revolution." Low-Speed Boundary-Layer Transition Workshop: II, Rand Corp., Santa Monica, California (Sept. 1976).

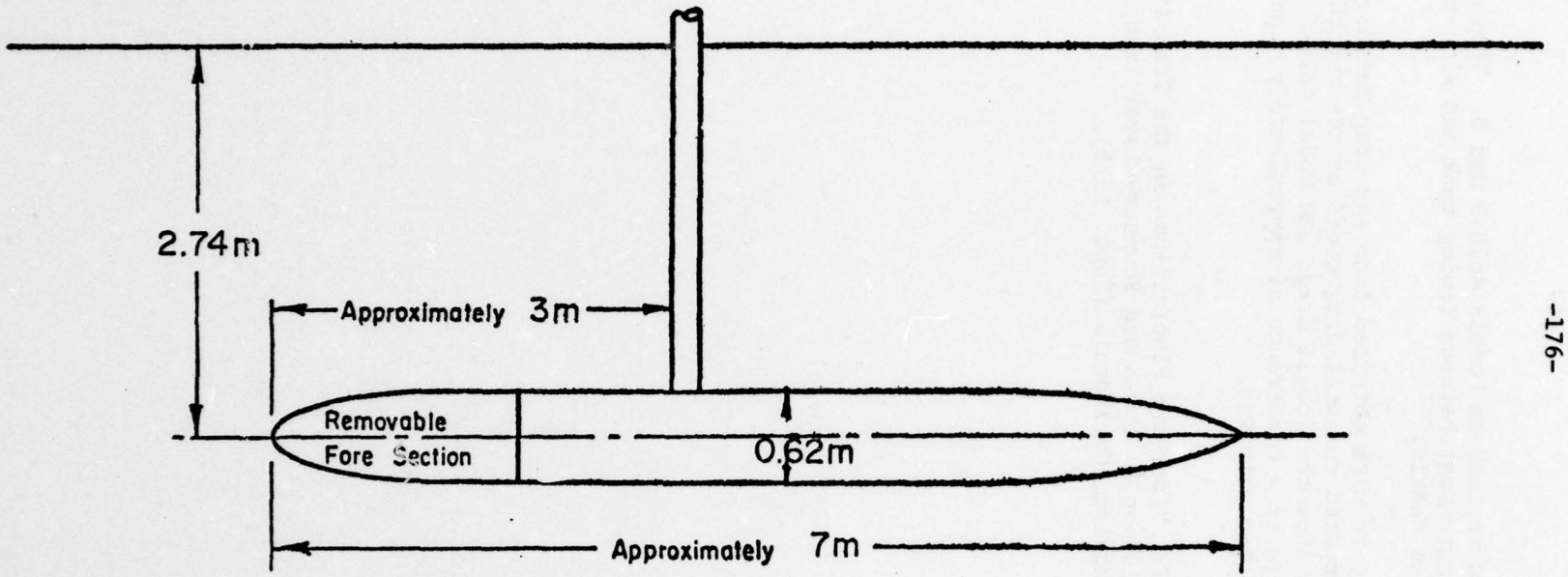

Figure 1—Experimental Arrangement

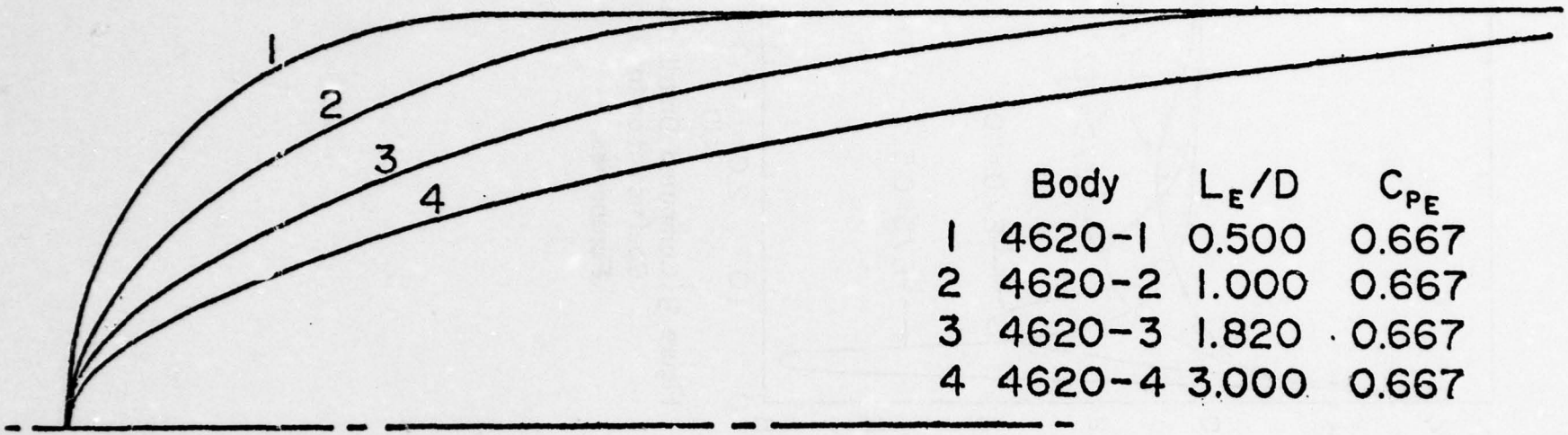

	Body	L_E/D	C_{PE}
1	4620-1	0.500	0.667
2	4620-2	1.000	0.667
3	4620-3	1.820	0.667
4	4620-4	3.000	0.667

Figure 2.—Profiles of Four Forebodies of Series I

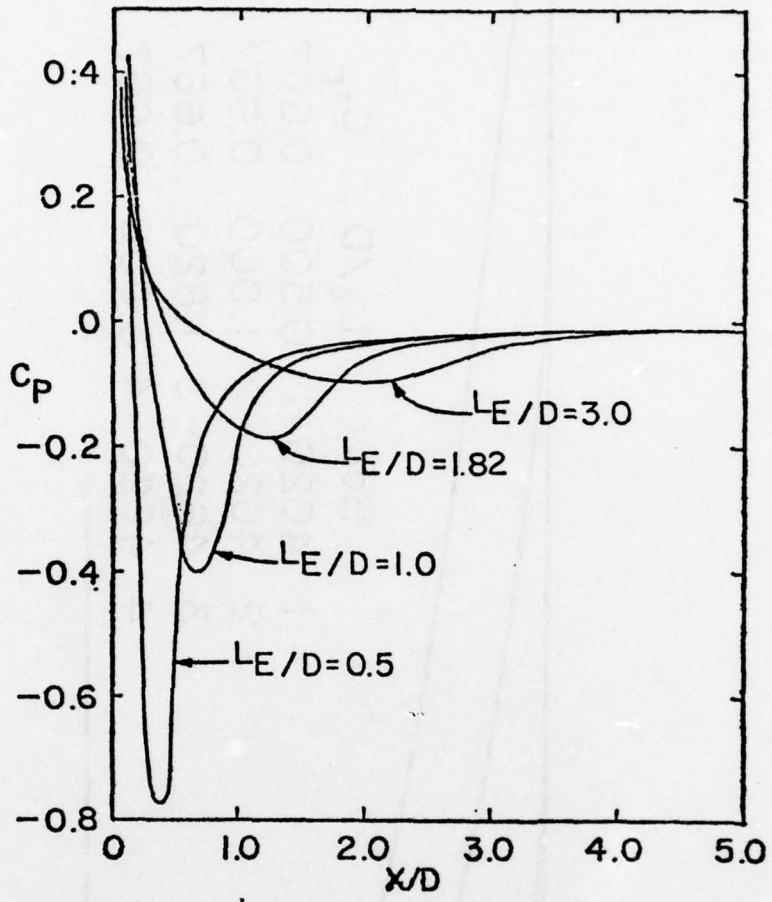

Figure 3 Computed Distributions of Pressure Coefficient on the Axisymmetric Forebodies.

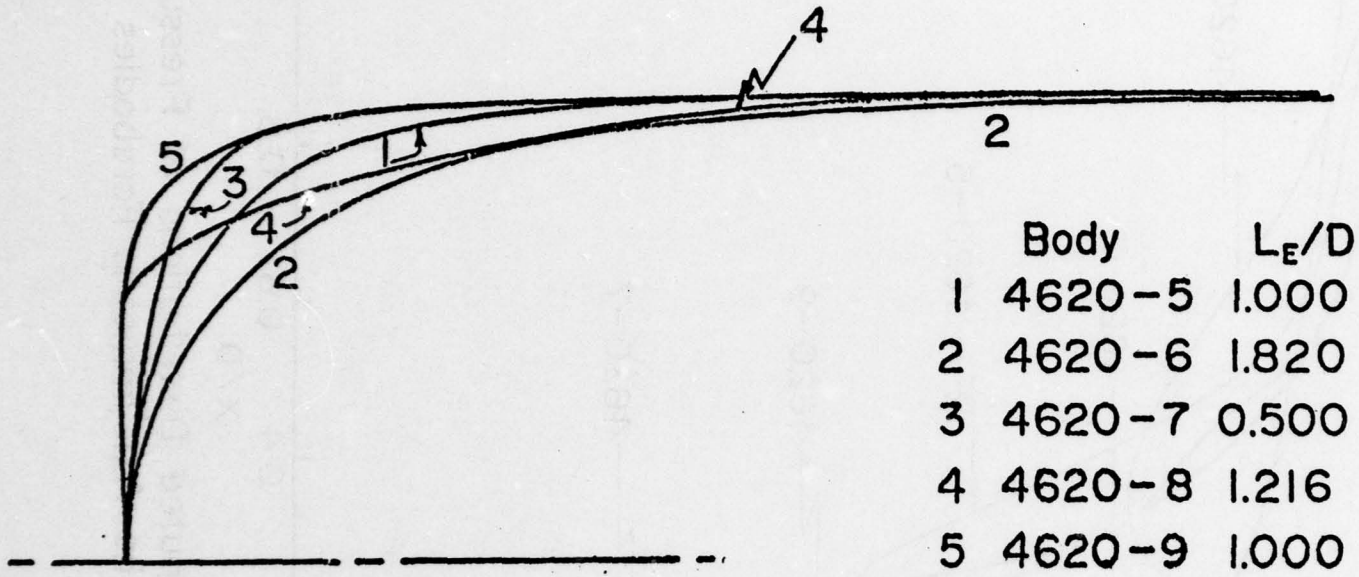

	Body	L_E/D	C_{P_E}	D_F/D
1	4620-5	1.000	0.850	0.0
2	4620-6	1.820	0.850	0.0
3	4620-7	0.500	0.850	0.0
4	4620-8	1.216	0.809	0.540
5	4620-9	1.000	0.933	0.500

Figure 4 – Profiles of Five Forebodies of Series 2

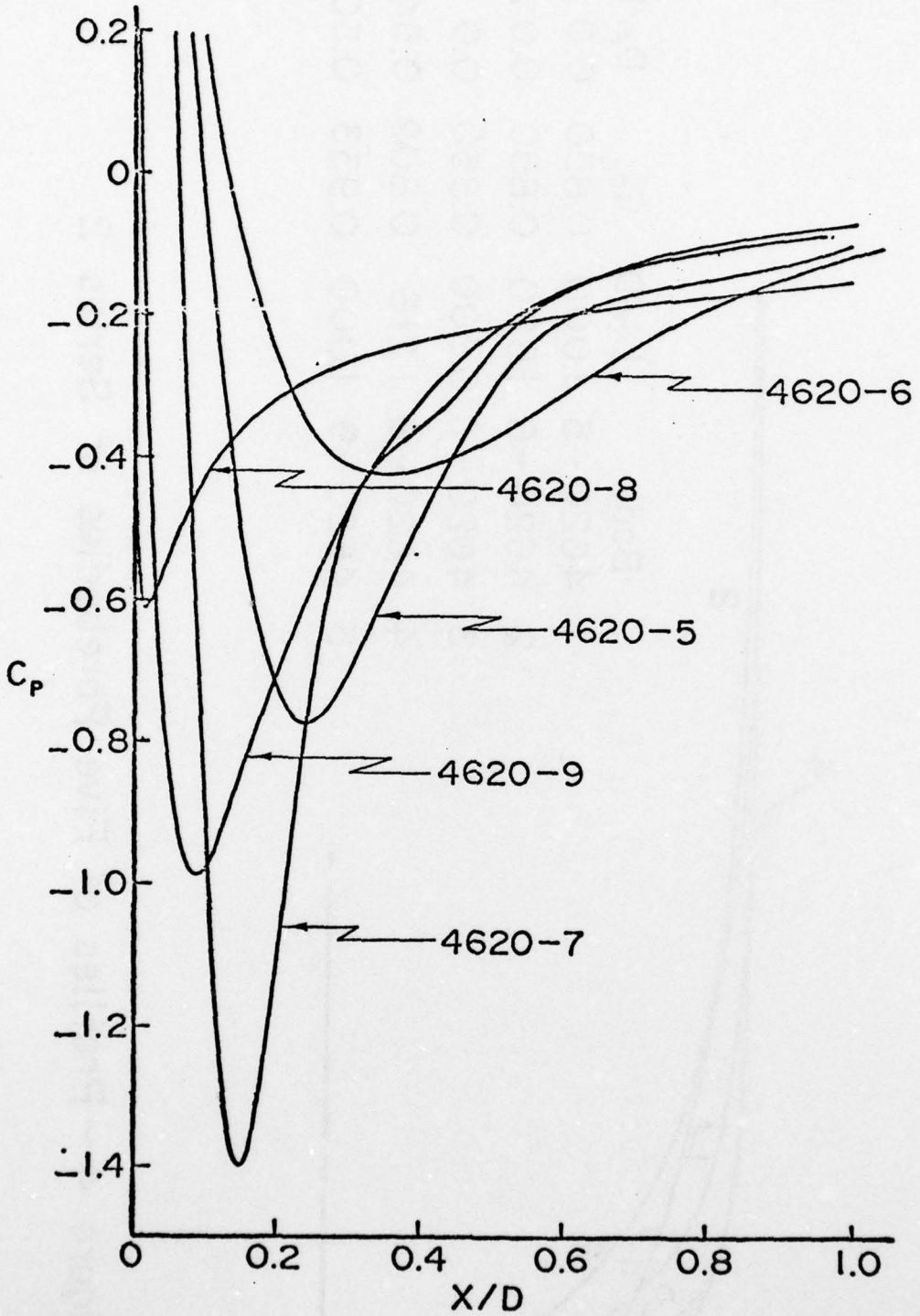

Figure 5 – Computed Distributions of Pressure Coefficient on the Axisymmetric Forebodies of Series 2

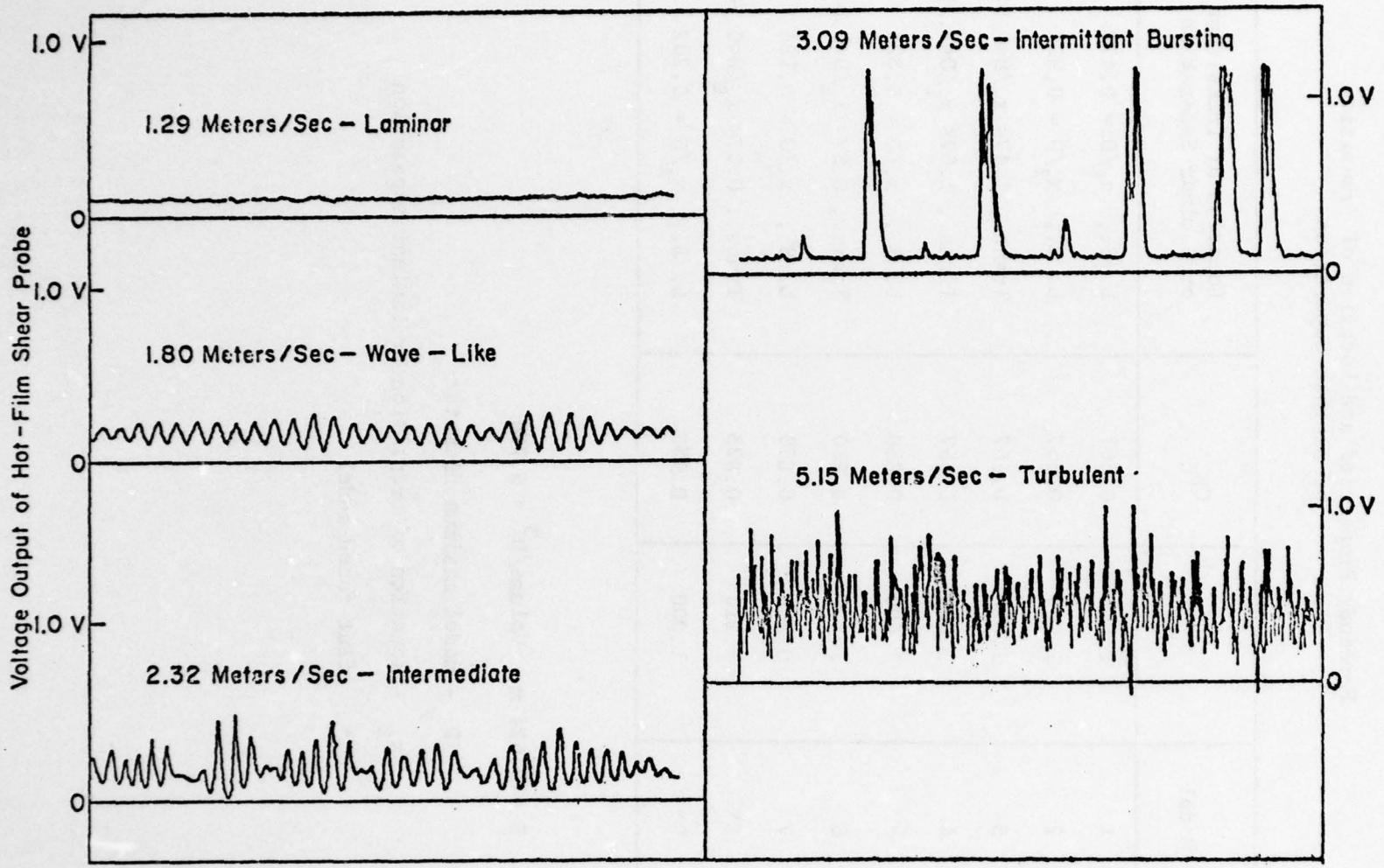

Figure 6 - Representative Hot-Film Signals for Various Flow Regimes (Model 4620-3, Bare Hull)

Figure 7

Forebody Properties and Location of Transition or Laminar Separation

Model	L_E/D	C_{P_E}	Location of Transition or Laminar Separation
1	0.500	0.667	L. S., $x_\ell/D = 0.472$
2	1.000	0.667	L. S., $x_\ell/D = 0.894$
3	1.820	0.667	Trans., $1.47 < x_\ell/D < 1.60$
4	3.000	0.667	Trans., $1.07 < x_\ell/D < 3.30$
5	1.000	0.850	L. S., $x_\ell/D = 0.371$
6	1.820	0.850	Trans., $0.57 < x_\ell/D < 1.04$
7	0.500	0.850	L. S., $x_\ell/D = 0.184$
8*	1.216	0.823	Trnas., $0.07 < x_\ell/D < 0.70$
9*	1.000	0.933	L. S., $x_\ell/D = 0.202$

$D = 0.624$ m, $\text{Volume}/D^3 = 6.786$

D - model maximum diameter

x_ℓ - location of transition or laminar separation

* flat faced model

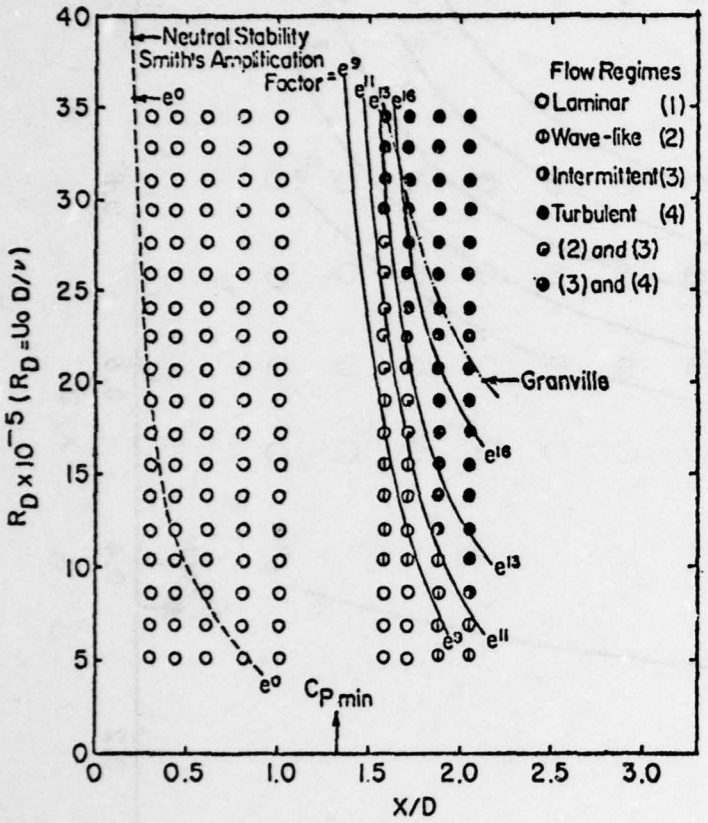

Figure 8 - Measured Flow Regimes on Smooth $L_E/D = 1.82$ Forebody

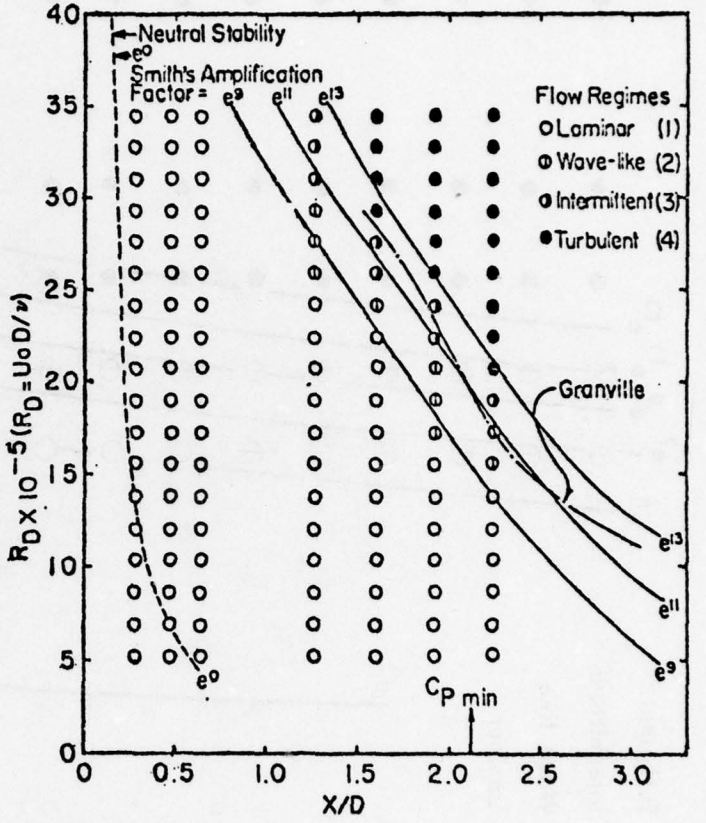

Figure 9 - Measured Flow Regimes on Smooth $L_E/D = 3.0$ Forebody

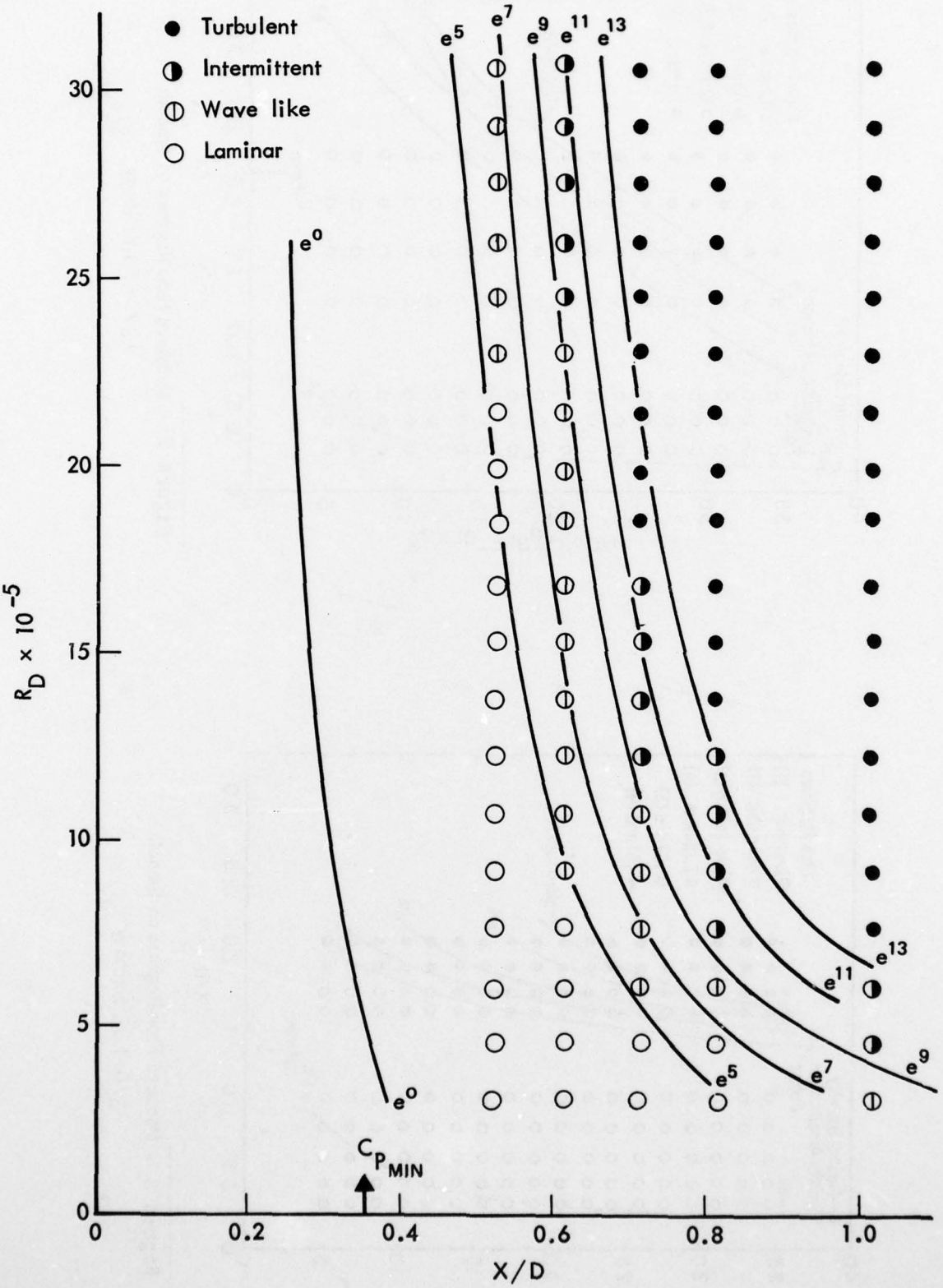

Fig. 10 — Measured flow regimes on Model 4620-6

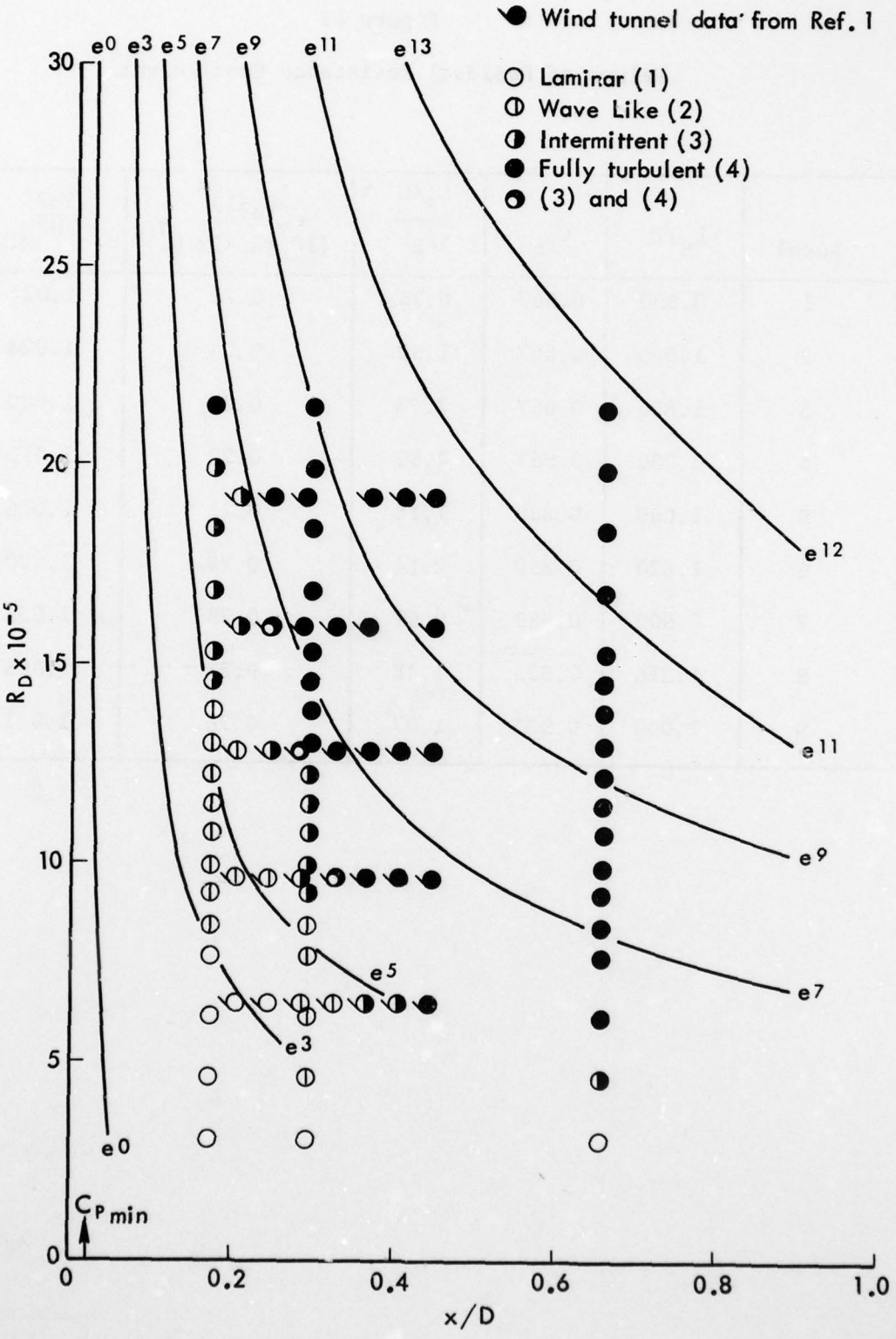

Fig. 11—Measured flow regimes on Model 4620-8

Figure 12

Values of Residual Resistance Coefficient

Model	L_E/D	C_{P_E}	$\frac{L_E/D}{C_{P_E}}$	$C_R \times 10^3$ $(10^7 < R_L < 2 \times 10^7)$	$\frac{EHP}{EHP_{MIN}}$
1	0.500	0.667	0.75	0.25	1.024
2	1.000	0.667	1.50	0.24	1.024
3	1.820	0.667	2.73	0.20	1.000
4	3.000	0.667	4.50	0.20	1.016
5	1.000	0.850	1.18	0.23	1.016
6	1.820	0.850	2.14	0.20	1.000
7	0.500	0.850	0.59	0.28	1.039
8	1.216	0.823	1.48	0.21	1.008
9	1.000	0.933	1.07	0.26	1.031

Section VI

THE COMBINED EFFECTS OF PRESSURE GRADIENT AND HEATING ON BOUNDARY-LAYER STABILITY AND TRANSITION

VI-1 THE COMBINED EFFECTS OF PRESSURE GRADIENT AND HEATING ON BOUNDARY-LAYER STABILITY AND TRANSITION†

by A. R. Wazzan* and Carl Gazley, Jr.

The Rand Corporation
Santa Monica, California

It is well known that major parameters affecting transition from laminar to turbulent flow include pressure gradient and heat transfer. It is also commonly accepted that some insight into the effect of these parameters on transition can be obtained, at least in the case of boundary layer flows, from a study of the effect of these parameters on the stability of boundary layers to small disturbances (Tollmien-Schlichting waves). Previous calculations[1] on the effect of heat transfer on the stability characteristics, and in particular the critical Reynolds number R_{crit}, of laminar water boundary layers show that surface heating stabilizes the flow whereas cooling destabilizes it. In flat plate flow, e.g., with $T_e = 60^{\circ}F$, R_{crit} increases by about thirty fold for a wall temperature of $T_w \cong 135^{\circ}F$. In stagnation flow (Hartree $\beta = 1.0$) complete stabilization is obtained with increasing T_w whereas in flat-plate flow ($\beta = 0$) and separating boundary layers ($\beta = -0.1988$), R_{crit} exhibits a maximum with increasing surface temperature. These results show that heating has a strong effect on stability and that this stabilizing (destabilizing) effect is strongly dependent on the interaction between the pressure gradient and the surface temperature distribution. To ascertain the nature and extent of this interaction, further stability calculations, at other values of Hartree β, are desirable. In addition, such detailed calculations would be useful in assessing the effect of heating on the stability and transition over bodies of practical interest (e.g., bodies of revolution where the local pressure gradient and boundary layer can be approximated by an appropriate wedge flow). For these reasons, we computed the spatial stability (R_{crit}, spatial amplification rates, etc.) for the following two-dimensional wedge flows: $\beta = -0.15, -0.10, -.05, 0, 0.10, 0.20, 0.30$, and 0.40 (at $T_w - T_e = 0, 5, 20$, and $30^{\circ}F$) for $T_e = 67^{\circ}F$.

---

*University of California, Los Angeles; Consultant, the Rand Corporation.

†Paper presented at the Low-Speed Boundary-Layer Transition Workshop II, The Rand Corporation, Santa Monica, Setptember 13-15,1976.

The variation of the following boundary-layer characteristics, $\theta^*/x\sqrt{Re_x}$, $\theta/x\sqrt{Re_x}$, $C_f/2\sqrt{Re_x}$, and $Nu\sqrt{Re_x}\ Pr_e^{1/3}$ with $(T_w - T_e)$ are shown in Fig. 1. $R_{\delta^*_{crit}}$ with $(T_w - T_e)$ is shown in Fig. 2. The effect of surface heating on boundary-layer stability is due primarily to the variation of viscosity with temperature. The results are thus dependent not only on the temperature difference $(T_w - T_e)$ but also on the temperature level, T_e. This is evident in Fig. 2 where previous results for $T_e = 60^oF$ are shown in comparison with the present results for $T_e = 67^oF$. Even this relatively slight change in ambient temperature results in an appreciable difference in the rate of change of viscosity with temperature, and consequently on the predicted stability.

Rayleigh theorems for inviscid instability state that for a boundary-layer flow, the necessary and sufficient condition for amplified and neutral inviscid instability is that U"(y) must vanish somewhere in the boundary layer, i.e., the mean velocity profile must be inflected. In addition, some correlation appears to exist between R_{crit} and the location of the inflexion point.[2] In fact, in adiabatic flows, $T_w \quad T_\infty$, R_{crit} decreases as the location of the inflexion point moves away from the wall. That is, in adiabatic flows, R_{crit} decreases as β becomes more negative. In flows with favorable pressure gradient ($\beta \geq 0$) where the profiles are not inflected, the boundary-layer characteristic of great importance to its stability characteristics is U"(y) and to a lesser extent U"(0).[2] In adiabatic flows it is known that for $\beta \lesssim 0$, where $U''(0) \lesssim 0$, R_{crit} for $\beta < 0$ is smaller than R_{crit} for $\beta > 0$. In fact, when a U"(y) distribution is the result of pressure gradient effects only (adiabatic flows) a strong correlation exists between R_{crit} and β or U"(y) or simply U"(0) or the shape parameter H.[2,3] R_{crit} exhibits a simple variation with U"(0) or with H; R_{crit} increases as H decreases (Fig. 3) or as U"(0) decreases and/or becomes increasingly more negative. This dependence on U" or H, in fact, is to be expected. An inspection of the Orr-Sommerfeld equation shows the boundary-layer characteristics that directly influence the eigen valyes, and hence R_{crit}, are U"(y) and U(y) with U"(y) being the dominant term. Therefore, it may be assumed that the heating of water boundary layers, which produces variation in H similar to those produced

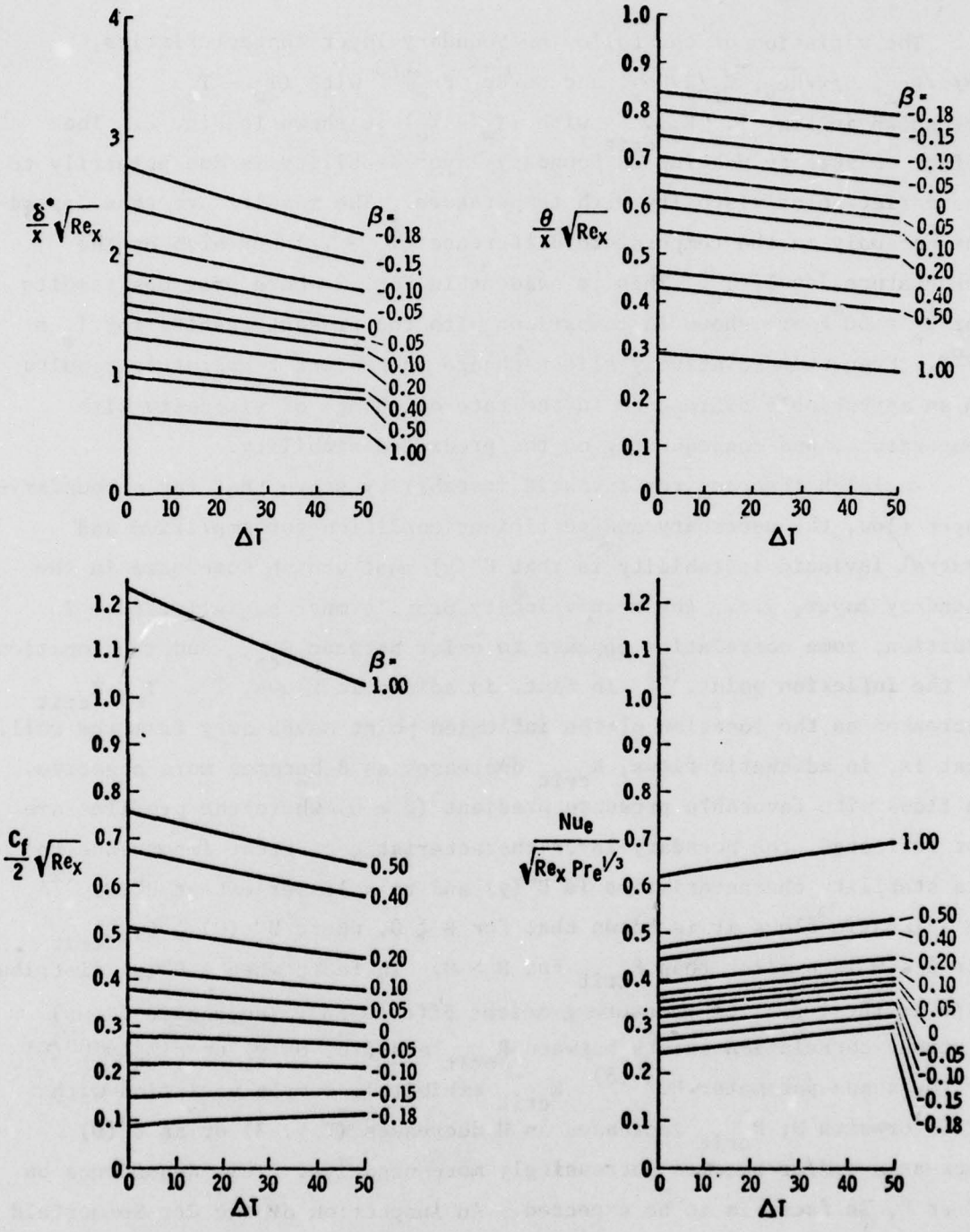

Fig. 1 — Effect of heat transfer on the characteristics of laminar boundary layers in water (T_e = 67°F)

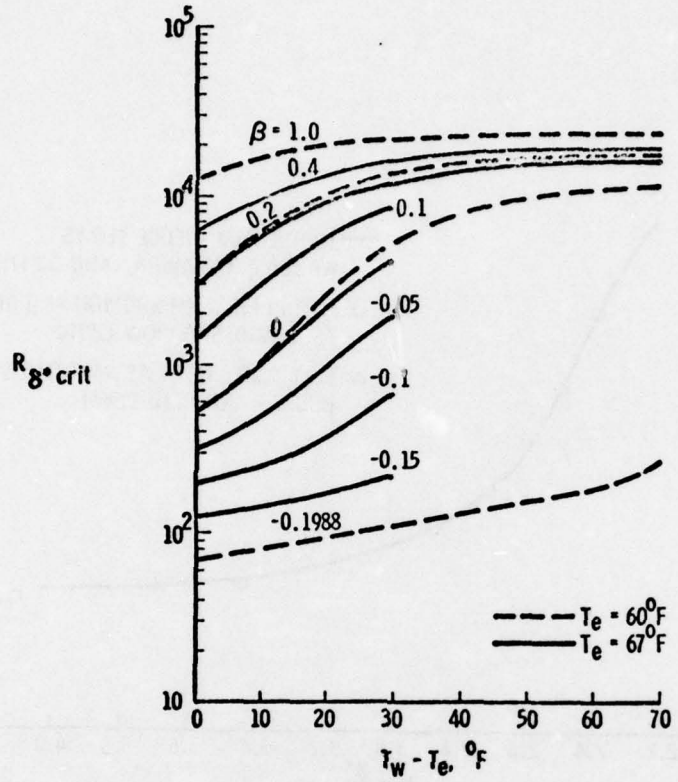

Fig. 2— Stability characteristics of Laminar boundary layers in water

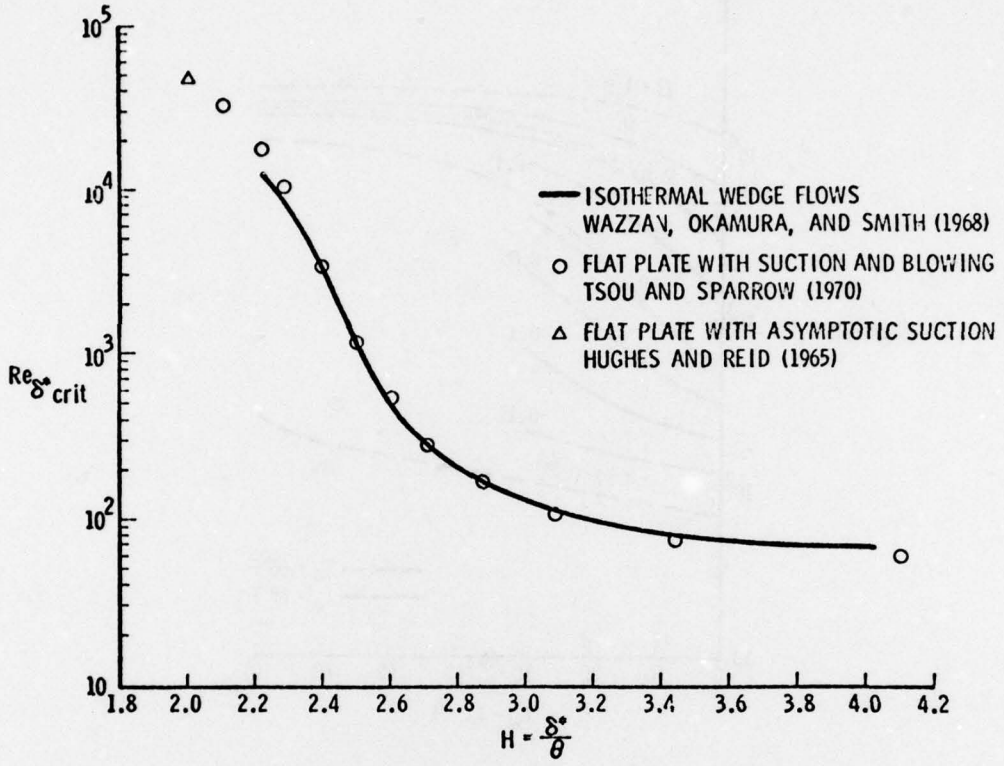

Fig. 3 — Critical Reynolds number as a function of the boundary-layer shape parameter, isothermal wedge flows and flat plate with suction and blowing

through the effect of pressure gradient alone, leads to increased stability and particularly to increasing critical Reynolds number. This assumption, however, is found to be only partially true, Figs. 4 and 5. These figures show that with initial heating H decreases and R_{crit} increases in agreement with the trend observed in Fig. 3. However, Figs. 4 and 5 show that although H decreases monotonically with increasing surface temperature, $R_{\delta^*_{crit}}$ exhibits a maximum (at least for flows with $\beta < 1.0$). The difference in the variation of $R_{\delta^*_{crit}}$ with H, when produced through the effect of pressure gradient alone (adiabatic flows) or through the combined effects of pressure gradient and surface heating, can be qualitatively understood through an examination of the Orr-Sommerfeld equation.

In the adiabatic case, only U" and U appear in the Orr-Sommerfeld equation and hence the monotonic variation of $R_{\delta^*_{crit}}$ with U" or H. In the nonadiabatic case, the small disturbance equation is a modified Orr-Sommerfeld equation that contains not only U" and U but also μ, μ', and μ''. This alters the nature of the problem in two ways. In the adiabatic case the pressure gradient affects $R_{\delta^*_{crit}}$ mainly through the mean velocity or the term U" (which can be represented by some function of H), whereas in the nonadiabatic case heating affects $R_{\delta^*_{crit}}$ not only through the mean velocity or the U" term (which can still be represented by some function of H) but also through the terms μ, μ', and μ'' that appear in the new Orr-Sommerfeld equation. Second, the nature of the eigen function ϕ (and consequently all eigen values and properties depending on the eigen values such as R_{crit}) is different in the two cases. In the adiabatic case, the differential equation for ϕ (the Orr-Sommerfeld equation) includes only the function ϕ and even the derivatives ϕ'' and ϕ'''', whereas in the nonadiabatic case, the differential equation for ϕ (the modified Orr-Sommerfeld equation) includes not only ϕ and the even derivatives ϕ'' and ϕ'''' but also the odd derivatives ϕ' and ϕ'''. Therefore, in the case of heating, although U" or H still characterize the boundary layer, they do not present a complete relationship between the mean flow and the eigen function ϕ, and hence $R_{\delta^*_{crit}}$. Physically, this may be interpreted as follows: with heating, initially H decreases rapidly (indicating a decrease in momentum loss) (Fig. 6) and $R_{\delta^*_{crit}}$ increases. However, with

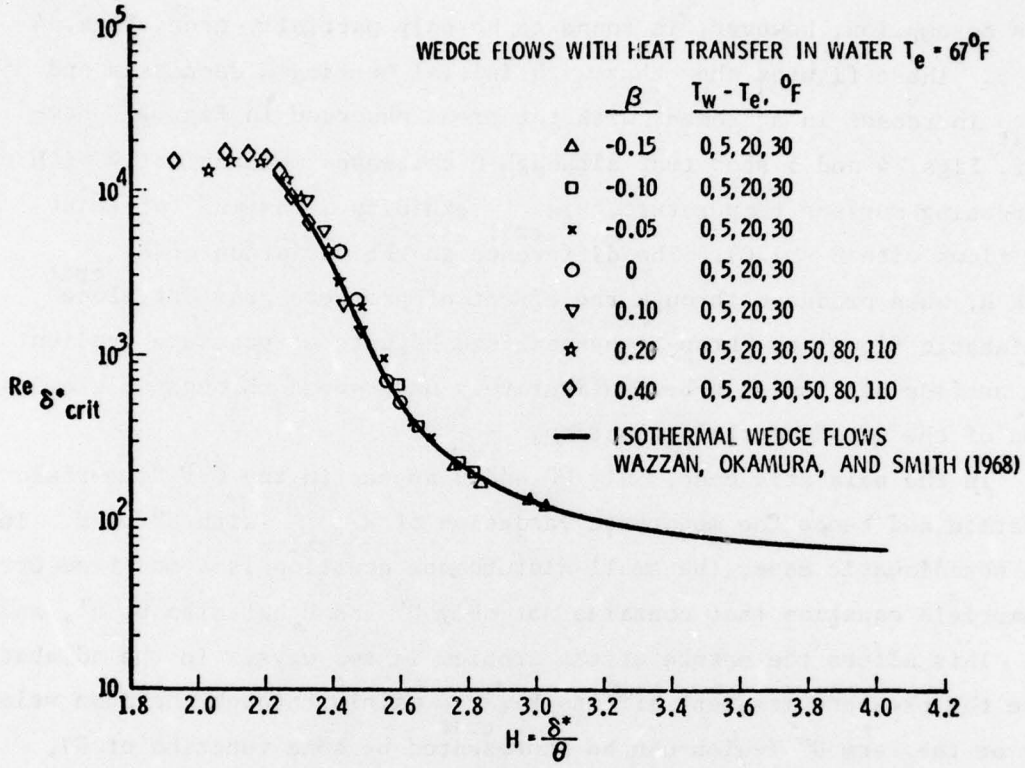

Fig. 4— Critical Reynolds number for heated wedge flows in water

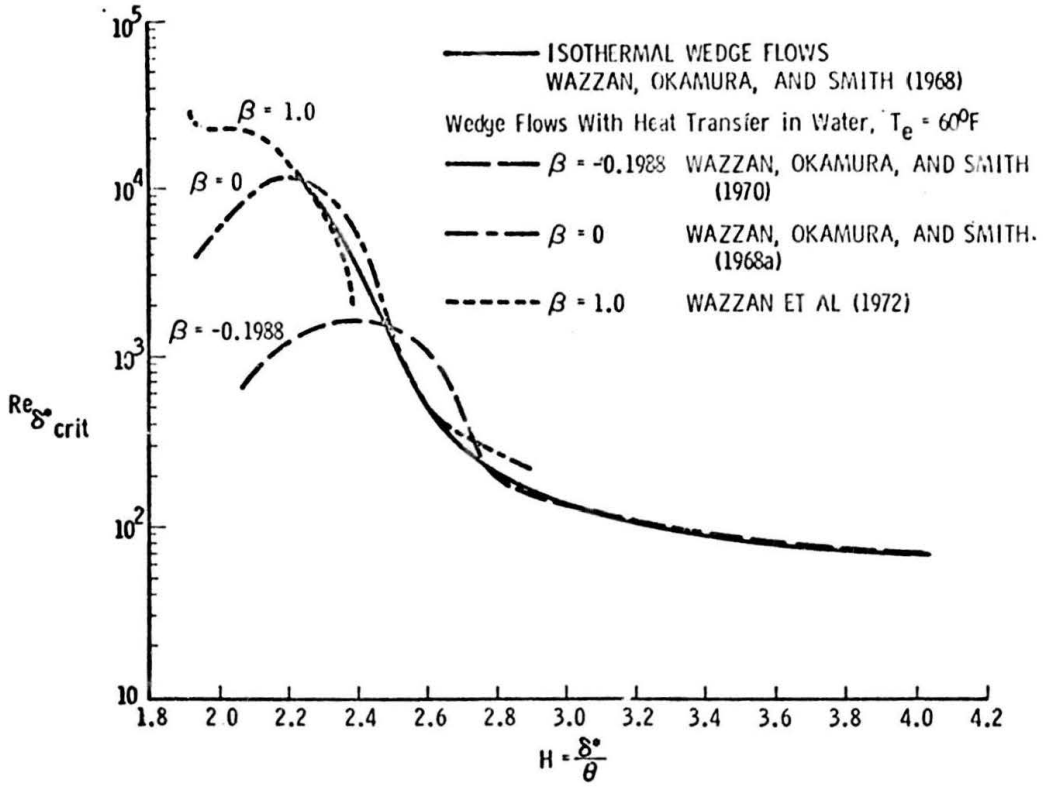

Fig. 5— Previous results for heated wedge flows in water

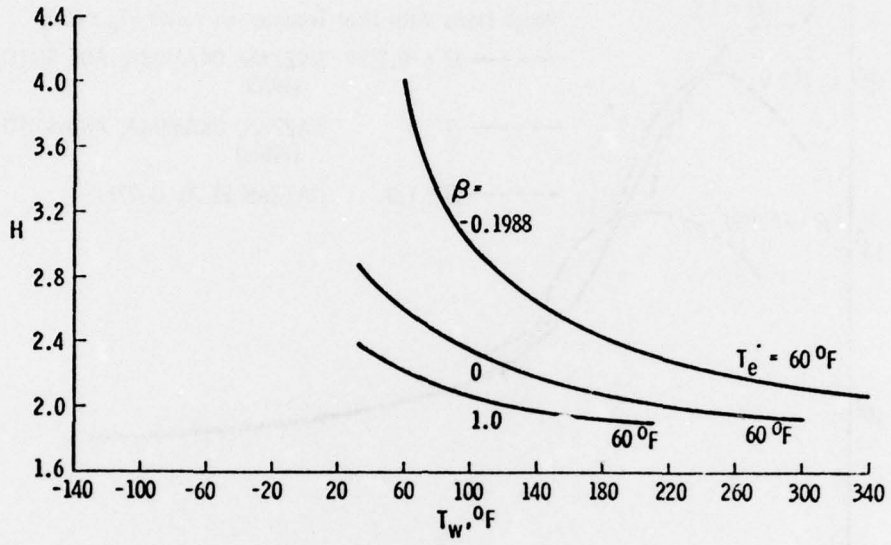

Fig. 6—Variation of the boundary-layer shape parameter H with surface temperature for three wedge flows, $T_e = 60°$ F.

still increased heating, H continues to decrease but at a much slower rate (Fig. 6). In the meantime, μ, μ', and μ'' continue to vary appreciably with increasing T_w. In fact μ, which has a destabilizing effect,[4] continues to decrease monotonically with heating whereas μ' and μ'', and in particular $\mu'(0)$ and $\mu''(0)$, which have a stabilizing effect,[4] reverse their trend in variation with temperature (change from increasing with T_w to decreasing with T_w) near the temperature where R_{crit} exhibits a maximum for wedge flows with $\beta < 1.0$. Therefore, for high heating rates the variation of H with T_w becomes negligible and the variation of μ, μ', μ'' with T_w dominate the effect of heating on R_{crit}. Therefore, at high heating rates it is expected that $R_{\delta^*_{crit}}$ will exhibit a maximum with T_w.

In the case of $\beta = 1.0$, the maximum in $R_{\delta_{crit}}$ with T_w is not observed because the unstable zone (region contained within the neutral curve) is rather limited, and in the initial stages of heating when H is fast decreasing with T_w the unstable zone is fast approaching a point. In fact, just at about the temperature when the variation of H with T_w begins to slow down considerably and μ, μ', and μ'' begins to dominate, the unstable region shrinks to zero and the flow becomes totally stable.

In spite of this entire discussion of the relative importance of H and/or the μ, μ', and μ'' terms on the stability characteristics of a given boundary layer, Figs. 4 and 5 show that over the large range of H values, a decrease in H results in increased stability, e.g., increasing $R_{\delta^*_{crit}}$.

Of more practical importance than the variation of R_{crit} with surface temperature is the effect of heat transfer on transition in boundary-layer flows. Although the transition process is a fairly complex one, and the relation between transition and linear stability theory is at best only qualitatively understood, it appears that in certain instances linear instability theory is capable of providing limits on the transition Reynolds number.[1] These limits must be the critical Reynolds number $R_{x_{crit}}$ as a lower bound, and the Reynolds number where the most dangerous disturbance (or frequency) attains a given amplitude, say A, or when the disturbance with initial amplitude A_o, is amplified by a certain $a \equiv A/A_o$. The relation between transition and this amplification ratio may be

established as follows. A disturbance growing according to linear theory, sooner or later reaches a state where (1) the linear theory ceases to be valid, and nonlinear processes commence; (2) the boundary layer becomes locally turbulent--turbulent spots are formed and grow and increase in number; and (3) these spots spread into the neighboring laminar flow until the mean flow becomes fully turbulent. Therefore, satisfactory assessment of the beginning of transition for approximately two-dimensional boundary layers requires at least three elements:[5] (a) adequate knowledge of the input disturbance and the corresponding boundary-layer receptivity; (b) knowledge of the development of the mean profiles and access to their stability characteristics; (c) information on the length of the nonlinear processes and secondary instability as dependent on pressure gradient, heat transfer, etc. Since the information required in element (a) often is not available in the literature, one usually characterizes a disturbance in terms of of the ratio of its amplitudes (A_{x_2}/A_{x_1}) at two locations, x_1 and x_2.

According to Klebanoff et al.,[6] stage (1) is reached, for a flat plate, when the rms velocity fluctuation u' in the boundary layer reaches $(u'/U)_{max} \simeq .015$, but that the first appearance of turbulence spots is expected at $(u'/U)_{max} \simeq 0.2$. That is, beyond the onset of nonlinearity an amplification factor of 10 to 15 times ($\simeq e^{2.5}$) is required.[5] Liepmann[7] hypothesized that at the breakdown to turbulence the Reynolds stress $\tau = -\rho\overline{uv}$, due to the amplified fluctuations u', becomes comparable in magnitude to the maximum mean laminar shear stress, $\tau_L = \mu\, \partial\bar{u}/\partial y$ in the boundary layer.

$$\tau/\tau_L = \frac{2}{c_{f_L}} \{kb(u'/U_e)^2[a(x)]^2\}_{max} \tag{1}$$

where

$$b = v'/u' \tag{2}$$

and

$$k = \overline{u'v'}/uv \tag{3}$$

where u and v are the velocities in the x and y direction, respectively. For a given frequency ω^* the amplification a is given by

$$a(x,\omega^*) = \exp[-R_L \int_{x_n}^{x} (\alpha_i/R)(U_e/U_\infty)dx] \qquad (4)$$

where R_L = freestream length Reynolds number, $R_L = (U_\infty L/\nu_\infty)$,

α_i = spatial amplification rate,

$x = x^*/L$,

ω^* = nondimensional frequency = $\omega U_e^2/\nu$, and

L - characteristic length.

Smith[8] reduced Liepmann's criterion for transition to an explicit dependence on the local laminar skin friction coefficient, the disturbance input at the neutral point x_n, and the total amplification ratio (A_{x_t}/A_{x_n}) where n refers to the neutral point and t to the transition point. Smith studied available information on transition of attached boundary layers where the freestream turbulence level was low. Assuming linear theory valid up to the transition point, Smith showed that the ratio of the disturbance amplitude at transition A_{x_t} to that at the neutral point A_{x_n} is given by $(A_{x_t}/A_{x_n}) \equiv a(x_t,\omega_t^*) \simeq e^9$. Later, more accurate calculations[9] showed $(A_{x_t}/A_{x_n}) \equiv e^{10}$. In any event, since in the nonlinear zone the amplification to transition is $\simeq e^{2.5}$, we find that for low freestream disturbance levels the linear TS amplification of about $e^{7.5}$ does control to a large extent the major part of the development of the disturbance to the beginning of transition and that element (b), of the transition process, paragraph 1, page 11, appears, at least in this case, to dominate elements (a) and (c).

In spite of the dominant role of element (b), however, the role of element (a) remains extremely important. For example, when Spangler and Wells[10] minimized sound disturbances in their measurements of transition in a low-speed boundary-layer channel, their R_{x_t} exceeded five millions! These results, where a mixture of vorticity and sound disturbances are present, cannot be predicted using any of the present

available forecasting techniques.[11] Hence a knowledge of the receptivity of the boundary layer to vorticity and sound disturbances is needed for further progress, and much attention need be given element (a). In the absence of such information and in view of the fact that the TS mechanism may describe, in the absence of the effects of surface roughness, vibration, and sound, the substantial growth of disturbances up to the emergence of the final three-dimensional turbulent spots and wedges and the beginning of transition, it is not unreasonable to employ, for the present, linear theory as outlined by Smith in bracketing the Reynolds number at the beginning of transition R_{t-B} for two-dimensional and axisymmetric boundary-layer flows (in axisymmetric flows x is replaced by s, the distance measured along the body surface).

Therefore, in certain boundary-layer flows where the linear mechanism dominates the growth of disturbances to transition, the transition Reynolds number can be bound by $R_{x_{crit}}$ on the lower side and by $(R_x)_{e^9}$ on the upper side. Hence, a plot of $R_{x_{crit}}$ and $(R_x)_{e^9}$ for two-dimensional wedge flows with and/or without heating (as shown in Fig. 7) can perhaps be used as a guideline in bracketing $R_{x_{trans}}$ on a body of revolution, for example. This can be accomplished by computing for the body of revolution H vs. Re_x. If this locus of R_x vs. H falls between the two curves labeled $R_{x_{crit}}$ and $(R_x)_{e^9}$ in Fig. 7, then the flow over the body may be considered to be completely laminar. If the locus of R_x vs. H crosses the $(R_x)_{e^9}$ curve, then it is assumed to undergo transition at the R_x of the intersection point. If the locus lies very close to the $R_{x_{crit}}$ curve, then the body is overheated, whereas if the locus lies very close to the $(R_x)_{e^9}$ curve, then more heating would be preferable (to maintain laminar flow). These remarks, of course, may not hold completely since, as stated earlier, in heated flows H alone does not totally control the stability, and hence the transition behavior of the body. Further confidence in this analysis can be gained as some measurements of $R_{x_{trans}}$ vs. H become available and are used to check the validity of the trends indicated in Fig. 7.

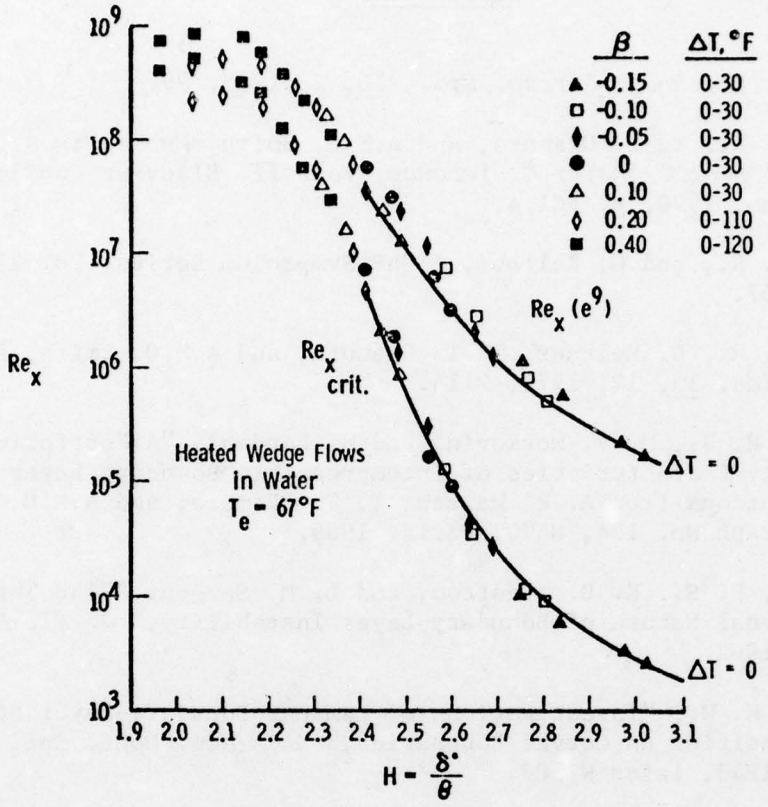

Fig. 7— Critical and predicted transition Reynolds numbers for heated wedge flows in water

REFERENCES

1. Wazzan, A. R., *Prog. Aerosp. Sci.*, 16, 2, 1975, 99.

2. Wazzan, A. R., T. T. Okamura, and A.M.O. Smith, *Proceedings 4th International Heat Transfer Conference, Vol. II*, Elsevier Publishing Co., Amsterdam, 1970, p. FC1.4.

3. Wazzan, A. R., and G. Keltner, AIChE Sympsoium Series, No. 131, 69, 1972, 167.

4. Wazzan, A. R., G. Keltner, T. T. Okamura, and A.M.O. Smith, *Physics and Fluids*, 15, 12, 1972, 2114.

5. Obremski, H. J., M. V. Morkovin, and M. Landahl, "A Portfolio of Stability Characteristics of Incompressible Boundary Layers," with contributions from A. R. Wazzan, T. T. Okamura, and A.M.O. Smith, AGARDograph No. 134, NATO, Paris, 1969.

6. Klebanoff, P. S., K. D. Tidstrom, and L. M. Sargent, "The Three-Dimensional Nature of Boundary-Layer Instability," *J. Fl. Mech.*, 12, 1, 1962.

7. Liepmann, H. W., "Investigations of Laminar Boundary-Layer Stability and Transition on Curved Boundaries," NACA Adv. Conf. Rpt. No. 3H30, August 1943, later W-107.

8. Smith, A.M.O., and H. Gamberoni, "Transition, Pressure Gradient and Stability Theory," Rpt. ES26388, Douglas Aircraft Co., 1956.

9. Jaffe, N., T. T. Okamura, and A.M.O. Smith, "The Determination of Spatial Amplification Factors and Their Application to Predicting Transition," *AIAA J.*, 8, 1970, 301.

10. Spangler, J. G., and C. S. Wells, Jr., "Effects of Free-Stream Disturbances on Boundary-Layer Transition," *AIAA J.*, 6, 1968, 543-545.

11. Granville, P. S., "Comparison of Existing Methods for Predicting Transition from Laminar to Turbulent Flow on Bodies of Revolution," Naval Ship Research and Development Center, TN 111, August 1968.

12. Wazzan, A. R., T. T. Okamura, and A. M. O. Smith, "Spatial and Temporal Stability Charts for the Falkner-Skan Boundary-Layer Profiles," Douglas Aircraft Company, Report No. DAC-67086, September 1, 1968.

13. Hughes, T. H., and W. H. Reid, Jr., *J. Fl. Mech.*, 23, 1965, 715-

14. Tsou, F. K., and E. M. Sparrow, "Hydrodynamic Stability of Boundary Layers with Surface Mass Transfer," *Appl. Sci. Res.*, 22, 1970, 273-286.

Section VI

LAMINARIZATION OF WATER BOUNDARY LAYERS OVER BODIES OF REVOLUTION

VI-2 LAMINARIZATION OF WATER BOUNDARY LAYERS OVER BODIES of REVOLUTION

A.M.O. Smith and A.R. Wazzan
ENERGY AND KINETICS DEPARTMENT
University of California
Los Angeles

I. INTRODUCTION

This paper is in the nature of a progress report and description of the objectives of a contract with the Navy (NOOOO24-76-C-7071). The three main task statements of the contract are:

A. Establish and evaluate design configurations

B. Determine the effect of pressure gradient, body shape, surface heating rates, wall temperature distribution and suction on boundary layer stability and transition characteristics.

C. Calculate and analyze the effects of free stream turbulence, wall roughness, vibration and acoustics disturbances.

Statement B mentions the effect of pressure gradient. The effect is being examined in two ways (1) by the systematic family of bodies to be described and (2) by study of the two dimensional wedge flow family. Some of the results of this study will be reported separately in Wazzan's and Gazley's paper. Concerning Item C, while we are interested in the subject and it is important, the main responsibility for studying the problem has been given to Dr. Leslie Mack under subcontract.

Therefore our attention here will be with a family of bodies that we have developed and are now studying. All the transition studies have used the e^9 method. Hence the value of this study stands or falls with the accuracy of the e^9 method, which is reviewed in the Wazzan-Gazley paper.

Since no shortcut transition method has been found for bodies of revolution, the systematic family of shapes at least offers the chance for interpolation. The study is engineering oriented, trying to show general answers based on the state of the art of the theory rather than trying to advance a special piece of theory - Les Mack's part being an exception. The project started about Feb. 1 and lasts for a year, so it is a bit more than halfway through. Also it might be said that the work is not necessarily new. Many similar studies have been made but results are not available in the public domain. Furthermore, it is hoped that the studies will be more systematic and comprehensive than those of the past. Therefore comprehensiveness and general availability are the justification for this investigation.

II. THE FAMILY OF BODIES

We will first describe the general characteristics of the whole family and then in III describe certain specific attributes found so far. The family of six bodies is shown in Figures 1 through 6. The family is capable of giving some idea of the effect of fineness ratio, pressure gradient and prismatic coefficient upon performance. Except for PR-9 all are derivaties of the Reichardt body, hence the names. Since there was much interest in a 9:1 fineness ratio body, REIK-9, Fig. 1, was chosen as one of the bodies, the 9 being for fineness ratio. Figures 1-6 are complete in a sense. They show the shape, the velocity distribution, the prismatic coefficient, volume, and the basic defining equations. The basic defining equations are not written in terms of x/ℓ but instead use the coordinate system shown on the body. A tail fairing is added to the basic body. The junction point and the length are noted in the drawing. After working out the shapes in these simple coordinates the bodies were then scaled into the x/ℓ system. Since Reichardt's body was defined by one simple equation,

except for the tail, this course was followed for all the others except PR-9. For the bodies with favorable pressure gradient like REIK-4 a considerable number of modification methods were examined but since we do not know exactly what we want as a pressure distribution, the simplest factor, (1 + ax) that gave reasonable shape variations was chosen. REIK-9 and REIK-2 show the effect of thickness ratio. REIK-2, 3, 4, and 5 show the effect of pressure gradient, REIK-4 and 5 show the effect of pressure gradient and thickness.

PR-9 does not fall into the REIK-family. There is so much advantage to high prismatic coefficients that it was decided to see what can be done by heat in overcoming adverse pressure gradients. A cylindrical body always has adverse gradients at the nose, which normally are ruinous to laminar flow. The goal therefore was to take a desirable practical shape and see whether it is possible by judicious use of heat to overcome the injurious effects of the adverse nose gradients. The nose is a modified leminiscate The junction point is noted. The leminiscate matched values and first and second derivatives at the junction point. This body is of 9:1 fineness ratio.

Velocity distribution for all the bodies were calculated by Hess's Higher Order Neumann Method.

III. SPECIFIC BODIES

Because of Navy interest and because of uncertainties about scaling, a basic condition for calculation was $U_\infty/\nu = 6.86 \times 10^6$ per ft. This number corresponds to 75 fps in 67°F fresh water. 67°F fresh water was used because that is representative of a towing tank. Also a specific length was used, 9.5625 ft., giving a length Reynolds number of 65.6×10^6.

A. REIK-9

Figures 7, 8, 9 and 10 are representative results for this body. The object was to stabilize the boundary layer to get laminar flow clear back to separation. Because the velocity distribution is almost perfectly flat, cold transition is about that of a flat plate, i.e., $R_{STr} = 5 \times 10^6$. This number is for $\ell n\ A/A_o = 9$. Now in order to have a margin of safety and to stay in the linear range of Tollmien-Schlichting disturbances, when we are looking for heat requirements we have chosen to try to hold the amplification ratio below e^7. Figures 7 and 8 are two results. Figure 7 is the first try and Fig. 8 the fourth and successful try. What kind of heat distribution to use is an unknown science. Such considerations as the growth of T-S waves cold, where they begin growing, whether they stop growing, shape factor and the like all enter in. The first heat distribution saw the growth of T-S waves begin at about S = 0.35 ft. and the growth exceeded the desired 7.0. Then after two intermediate tries VAR IV, Fig. 8 was tried and the goal of e^7 was successfully met.

It has generally been more convenient and realistic to specify heat input rather than wall temperature. Figure 9 shows results for the two cases just studied. Note that the beginning of heating in VAR IV was slightly further ahead than in VAR I. Examination of the amplification curves indicated more heat was needed forward and less after. Figure 10 shows the wall temperature distribution for the two cases as well as the total heat.

Out of curiosity for what it might show we devised a dimensionless heating coefficient, C_H, (H for heat) defined as follows:

$$C_H = \frac{Q = (\text{energy in to water})}{1/2\rho V^3\ (\text{Vol})^{2/3}}\ (\text{ft - lbs/sec})$$

Values are shown on Fig. 9.

A different kind of result is shown in Fig. 10. Assuming $R_K = U_k k/\nu = 25$ we calculated allowable heights of discrete roughness for REIK-9 moving at $U_\infty/\nu = 6.86 \times 10^6$/ft = 75 fps. The values are very small. Heat, as you see, hurts slightly. However at 1/4 speed, i.e., about 19 fps, roughness can be considerable. The most sensitive part of these bodies is just behind the stagnation point, where there is a minimum. Now it is found that this minimum always seems to be ahead of the point where heat is first applied. Therefore the heat does not affect the minimum and the minimum can be determined by cold calculations alone, see Fig. 10.

B. REIK-2

While calculations have been done, it is a rather uninteresting body again having $\beta = 0$ over most of its length. Therefore it will not be discussed further, except to say that if the flow is laminar to $x/\ell = 0.7$ at $R_\ell = 20 \times 10^6$ separation calculates to be at $x/\ell = 0.96$.

C. REIK-3, 4

Some calculations have been done, but work on these bodies is mostly in the future. REIK-2,3,4,5 form a family having increasingly favorable pressure gradients. For the four respectively, they develop maximum Hartree β's near $x/\ell = .7$ of 0, 0.1[illegible]2 and 0.3 approximately. However, none of these β's are sufficiently high to ge[illegible] real extent of laminar flow at high Reynolds numbers, without the assistance of heat.

D. REIK-5

Because it is doubtful that the full study will be completed because of time and money limitations we have chosen to look at extremes so as to see what the boundaries are. Then later as time and money allow we can fill in with intermediate cases. One might say we are aiming for two-point interpola-

tion and then later as conditions allow, proceed to three-point. Therefore even though not identified with any practical concept we looked next at REIK-5.

Only two heat distribution tries were made. While the favorable pressure gradient alone will not give an extended run of laminar flow, it does indeed help. As a result the first try led to excessive stability and a second try was made. The result is shown in Fig. 11. It is still too stable but the amplification is near enough e^7 that this try has been taken as final, although we know that better can be done. The heating distribution, temperature, and shape factor are shown in Fig. 12. The heat intensity is much less than that found needed for REIK-9. Also the total heat requirement is low although the body has a much larger volume. Notice that the shape factor becomes very low, 2.32. Also that C_H = .0078, or less than 1/4 of that on REIK-9. This body was deliberately made thick, knowing that separation would occur at the tail. The tail would either have to be lengthened or suction would have to be used to prevent separation. At $R_\ell = 20 \times 10^6$ and laminar flow to $x/\ell = 0.70$ separation occurs at $x/\ell = .825$. Some of the boundary layer parameters for the cold case are shown in Fig. 13.

A roughness calculation was done for the cold case to compare with the REIK-9. No surprises were expected but one was found. On REIK-9 the minimum is very far forward and after that the allowable value slowly but definitely grows. (On a flat plate it would grow as $x^{1/4}$). On REIK-5 there is indeed a minimum very near the nose but a large portion of the body has a higher but nearly constant level. The reason is that an expanding body thins the boundary layer. Hence bodies like this should be slightly more sensitive to roughness than a straight Reichardt type.

E. PR-9

This shape has adverse gradients near the nose. Now the name of the game is to see what can be done with heat. Notice on Fig. 15 that β reaches a value of -.135 near the nose. This figure shows the third try. Notice that Q_w = 20 Kw/ft^2 near the nose and that wall temperatures reach nearly 600^{o}R. Figure 16 shows amplification growth, which is a little too much. To try to reduce it slightly the last part of the heat distribution was held constant at 2.5 Kw/ft^2, instead of reducing linearly to zero at 6.5 ft. Compare Figs 15 and 17. This small change led to large changes in the wave growth. The maximum was reduced more than desired from ℓn A/Ao equal to 7.9 in Fig. 16 to 3.9 in Fig. 18. Hence according to our calculation heat is making a poor shape work. But a larger quantity is necessary than for a good shape. For REIK-9, C_H = 0.0334, for PR-9, C_H = 0.0671. That is, for the same fineness ratio body, over twice as much heat was necessary to fix up the poorly shaped body. For REIK-5 which has the most favorable shape C_H = 0.0078. It is easily shown that the following formula applies.

$$\frac{Q \text{ AVAILABLE}}{Q \text{ NEEDED}} = \frac{1 - n_{th}}{n_p \; n_{th}} \cdot \frac{C_{D \; Vol}}{C_H}$$

where Q is the heat rate, n_{th} the thermal efficiency of the engine that runs the device and n_p the propeller efficiency. The ratio of course must be greater than unity.

IV. SURFACE SMOOTHNESS

The last item we present is our work on the subject of allowable surface roughness. First we will discuss Westinghouse's recommended line, see Fig. 19. Westinghouse has assumed that surface smoothness acts the same way as discrete roughness, that is a small roughness develops an unsteady wake behind it. They basically use the number R_k = 25. Then to relate

surface smoothness to this number they estimate that there will be a reasonable number of roughnesses which are 5 times the statistical RMS value. Then they assume that the velocity in the boundary layer at the top of the roughness is 1/5 of the velocity at the edge. Putting all together they get $(U_\infty/\nu \times \text{RMS} < 25$ but actually they use 20. This is their line on Fig. 19.

Now it can be shown that if we follow their basic R_k assumption more carefully we get the $(U_\infty/\nu)^{-3/4}$ line. Let us assume that R_k is to be a constant, say 25, and for simplicity let us look at a flat plate flow. The flow will be as sketched below. A boundary

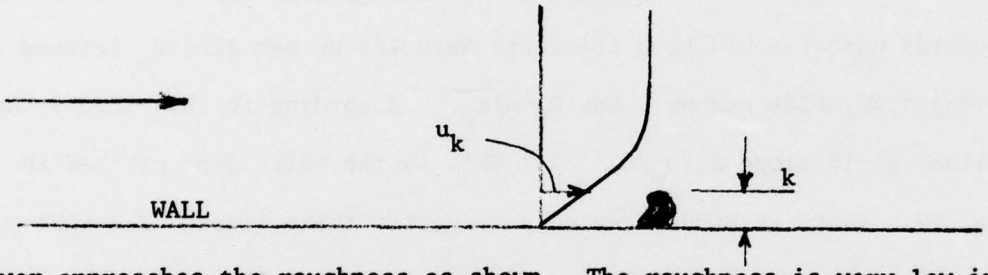

layer approaches the roughness as shown. The roughness is very low in the boundary layer so the profile will be assumed to be straight in this region, an excellent assumption. Then we can write, for a flat plate

$$u_k = k \left(\frac{\partial u}{\partial y}\right)_w = kU\sqrt{\frac{U}{2\nu x}} \quad F''(0) = .332kU\sqrt{\frac{U}{\nu x}}$$

Now using $R_k = \frac{u_k\, k}{\nu} = 25$ we can introduce the above expression for u_k to obtain

$$R_k = \frac{.332\, k^2 U}{\nu} \sqrt{\frac{U}{\nu x}} = 25$$

Now if we solve for k we find

$$k = 8.68\, x^{1/4} \left(\frac{U}{\nu}\right)^{-3/4}$$

The difference from Westinghouse analysis is that we solved for u_k instead of assuming it. The $(U/\nu)^{-3/4}$ line in Fig. 19 was simply put through the same point as Westinghouse at $U/\nu = 10^6$. Hence the authors feel that at higher Reynolds numbers per foot, the Westinghouse criteria is unduly conservative.

However, we are not sure the above is the right approach. The surface may be so smooth that no unsteady wakes are formed. Then a slightly rough surface "tickles" the boundary layer somewhat like small external turbulence does. If that is the case, in view of stability theory the characteristic Reynolds number would be a thickness Reynolds number like R_θ instead of a length Reynolds number. Now $R_\theta \sim \sqrt{R_x}$. According to this theory then, a line should slope as $(U_\infty/\nu)^{-1/2}$. This is the third line plotted in Fig. 19. There is hardly any data to verify these lines. The NACA points are those cited by Westinghouse. At Douglas about 1956 we roughened a surface with several grades of sand paper, measured the roughness with a profilometer and found the effect on transition. The tests were far better designed than those of the NACA. The points are shown. The point at $U_\infty/\nu = 1.1 \times 10^6$ did not affect transition. The other two seem to confirm the $(U_\infty/\nu)^{-1/2}$ slope but there is too little data to be sure. In any case the $(U_\infty/\nu)^{-1}$ curve is not right.

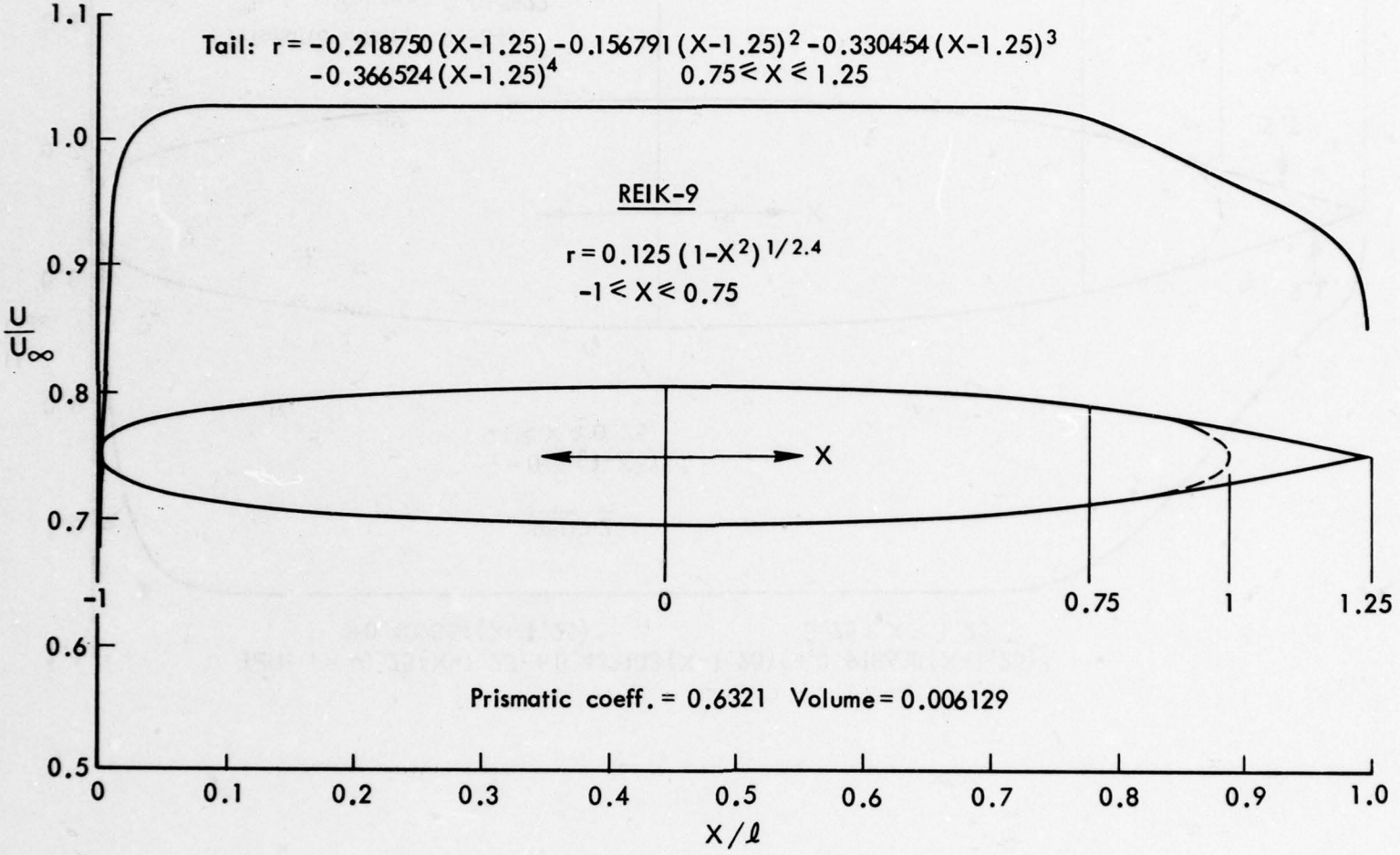
Tail: r = -0.218750 (X-1.25) -0.156791 (X-1.25)² -0.330454 (X-1.25)³
-0.366524 (X-1.25)⁴ 0.75 ≤ X ≤ 1.25
REIK-9
r = 0.125 (1-X²)^1/2.4
-1 ≤ X ≤ 0.75
X
Prismatic coeff. = 0.6321 Volume = 0.006129
U/U∞
X/ℓ
1.1
1.0
0.9
0.8
0.7
0.6
0.5
-1
0
0.75
1
1.25
0
0.1
0.2
0.3
0.4
0.5
0.6
0.7
0.8
0.9
1.0

Fig. 1

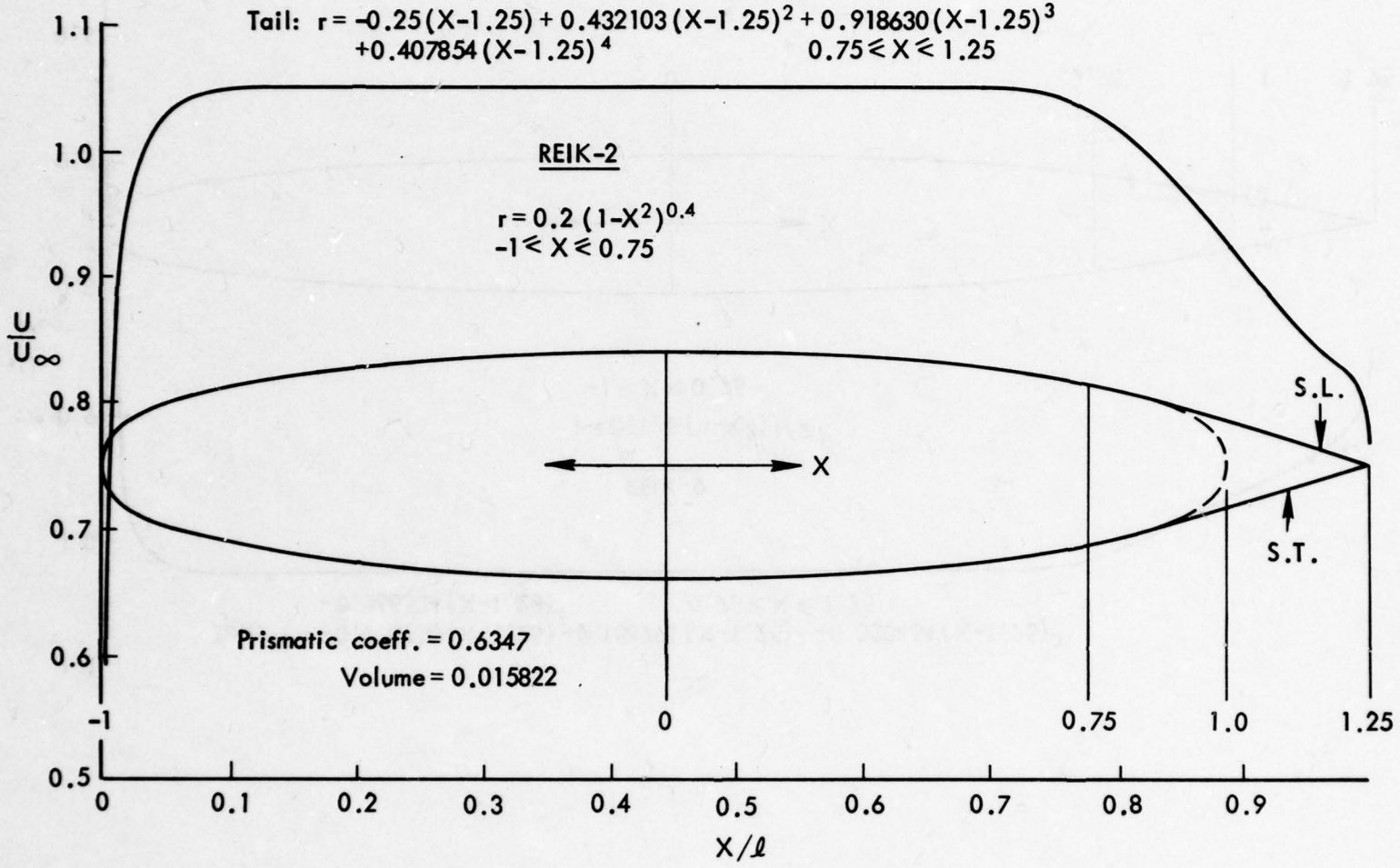
Tail: r = -0.25(X-1.25) + 0.432103(X-1.25)² + 0.918630(X-1.25)³
+0.407854(X-1.25)⁴ 0.75 ≤ X ≤ 1.25
REIK-2
r = 0.2 (1-X²)^0.4
-1 ≤ X ≤ 0.75
S.L.
S.T.
X
Prismatic coeff. = 0.6347
Volume = 0.015822
U/U∞
X/ℓ
1.1
1.0
0.9
0.8
0.7
0.6
0.5
-1
0
0.75
1.0
1.25
0
0.1
0.2
0.3
0.4
0.5
0.6
0.7
0.8
0.9

Fig. 2

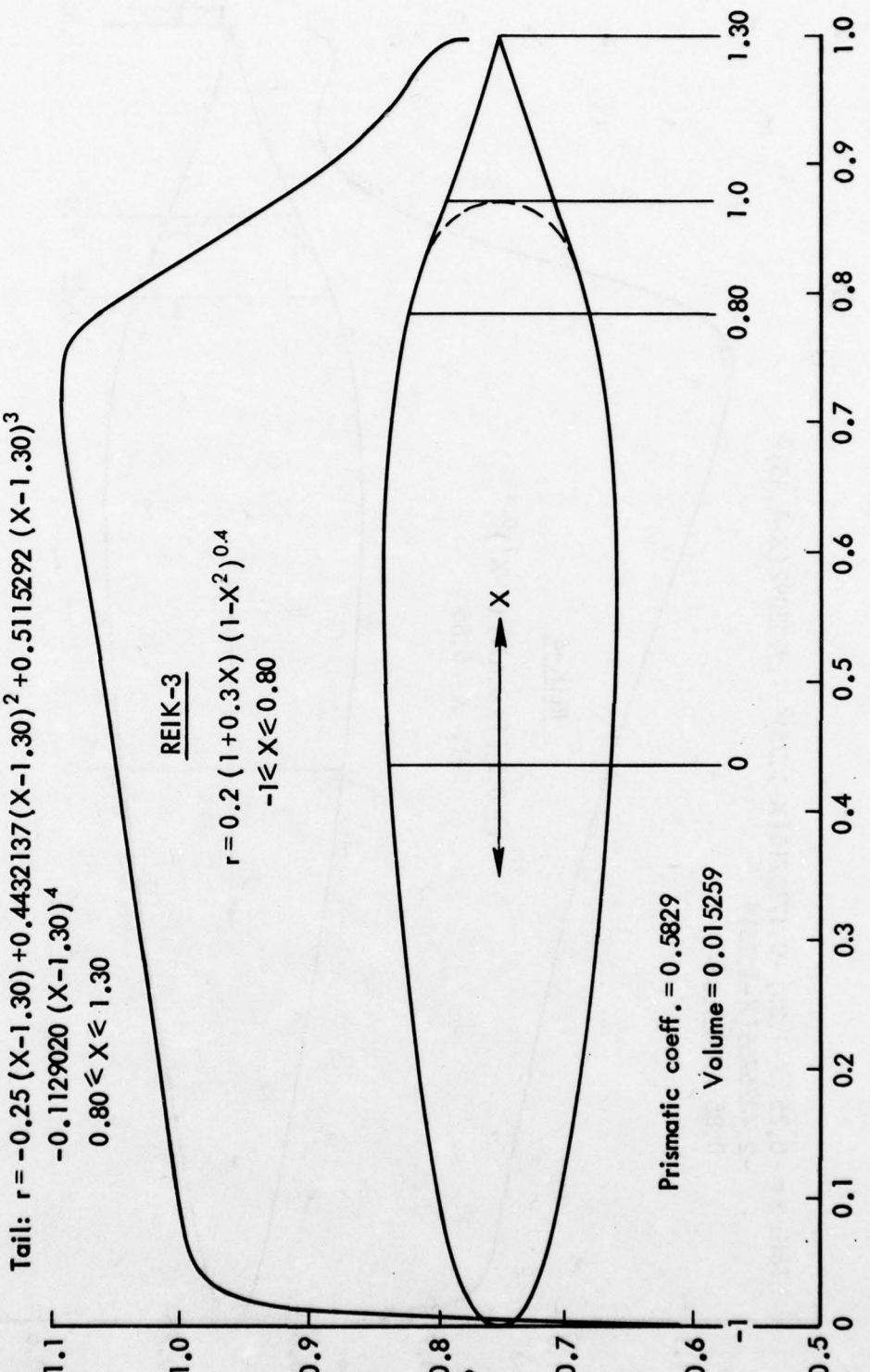
Tail: r = −0.25 (X−1.30) +0.4432137(X−1.30)² +0.5115292 (X−1.30)³
−0.1129020 (X−1.30)⁴
0.80 ≤ X ≤ 1.30
REIK-3
r = 0.2 (1+0.3X) (1−X²)^0.4
−1 ≤ X ≤ 0.80
X
Prismatic coeff. = 0.5829
Volume = 0.015259
U/U∞
S/ℓ
1.1
1.0
0.9
0.8
0.7
0.6
0.5
0
0.1
0.2
0.3
0.4
0.5
0.6
0.7
0.8
0.9
1.0
−1
0
0.80
1.0
1.30

Fig. 3

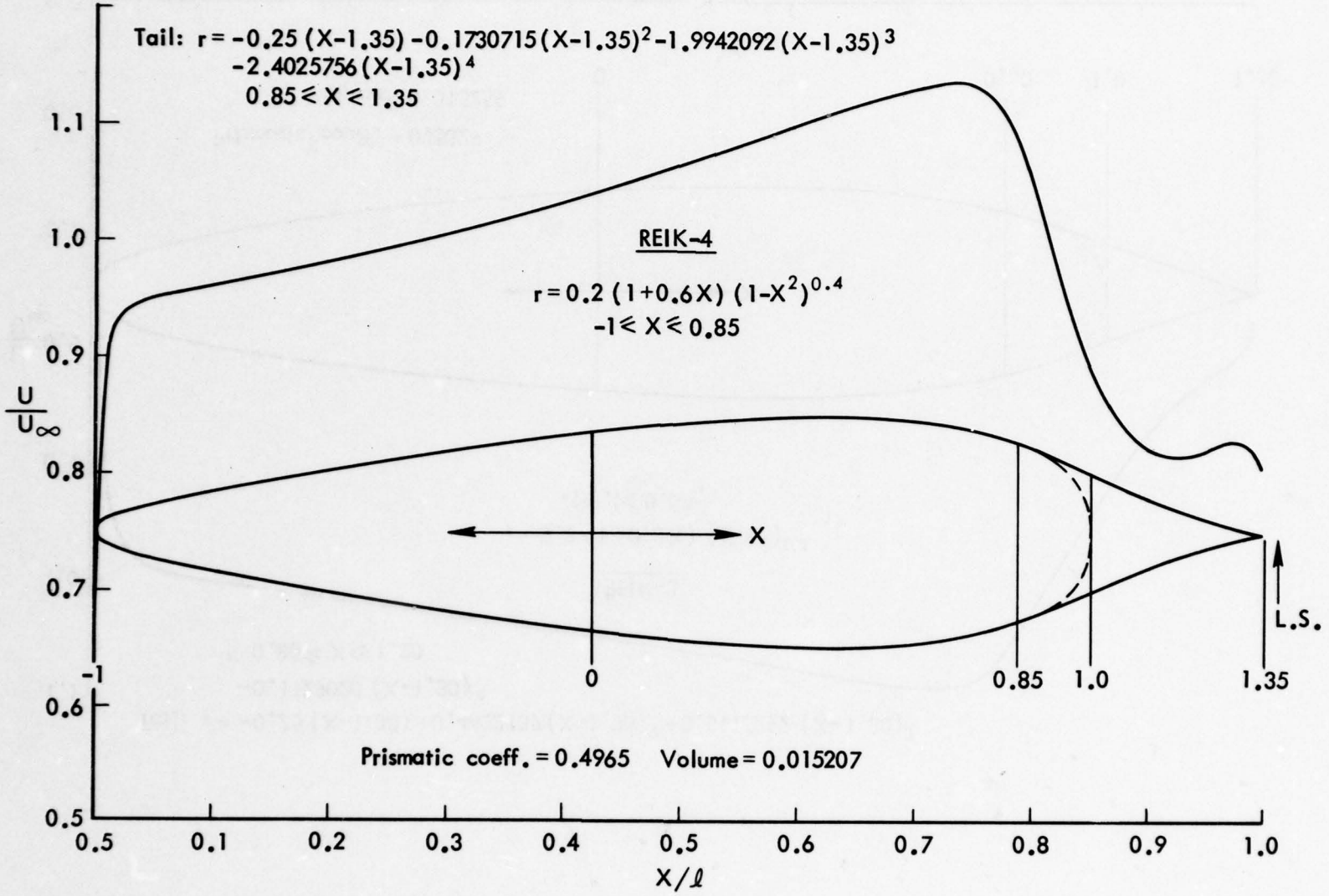
Tail: r = -0.25 (X-1.35) -0.1730715 (X-1.35)² -1.9942092 (X-1.35)³
-2.4025756 (X-1.35)⁴
0.85 ≤ X ≤ 1.35
REIK-4
r = 0.2 (1+0.6X) (1-X²)^0.4
-1 ≤ X ≤ 0.85
U/U∞
X
L.S.
-1
0
0.85
1.0
1.35
Prismatic coeff. = 0.4965 Volume = 0.015207
X/ℓ

Fig. 4

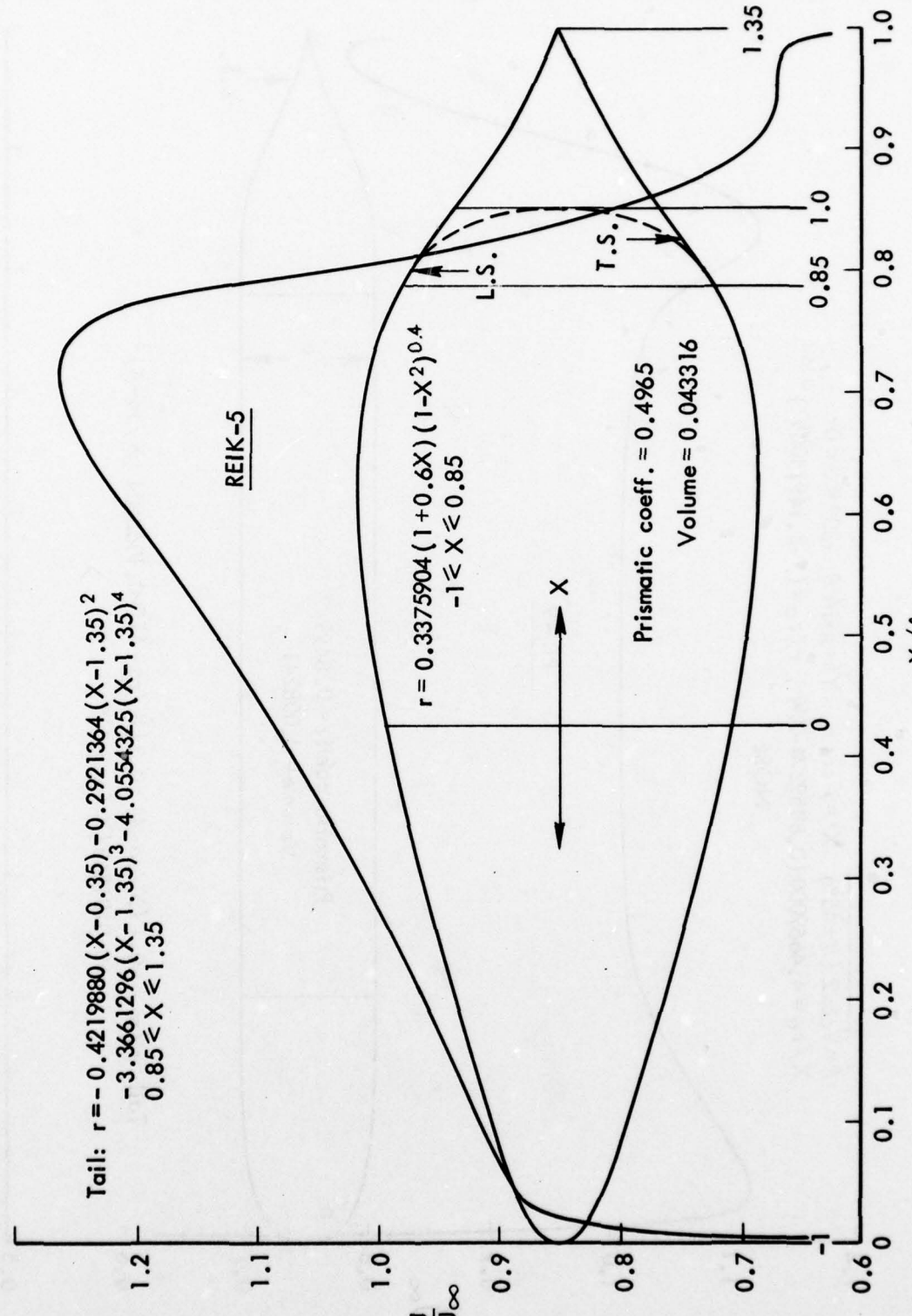
REIK-5
Tail: r = - 0.4219880 (X-0.35) -0.2921364 (X-1.35)²
-3.3661296 (X-1.35)³-4.0554325 (X-1.35)⁴
0.85 ≤ X ≤ 1.35
r = 0.3375904 (1+0.6X) (1-X²)^0.4
-1 ≤ X ≤ 0.85
L.S.
T.S.
X
Prismatic coeff. = 0.4965
Volume = 0.043316
1.35
0.85
1.0
U/U∞
X/ℓ

Fig. 5

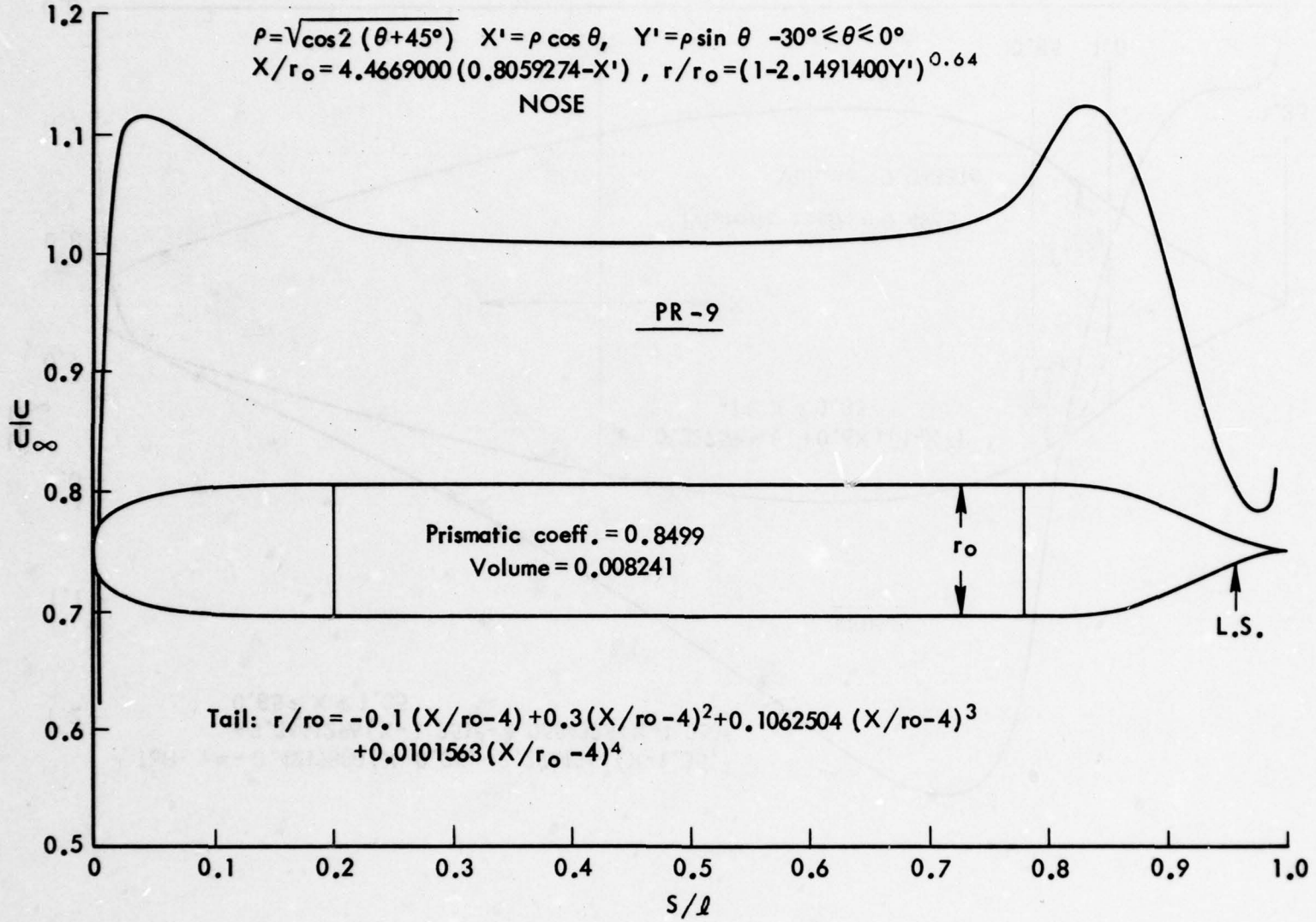
$\rho=\sqrt{\cos 2(\theta+45°)}$ $X'=\rho\cos\theta$, $Y'=\rho\sin\theta$ $-30° \leqslant \theta \leqslant 0°$
$X/r_o = 4.4669000\,(0.8059274-X')$, $r/r_o=(1-2.1491400Y')^{0.64}$
NOSE
PR-9
Prismatic coeff. = 0.8499
Volume = 0.008241
r_o
L.S.
Tail: $r/ro = -0.1\,(X/ro-4)+0.3\,(X/ro-4)^2+0.1062504\,(X/ro-4)^3$
$+0.0101563\,(X/r_o-4)^4$
U/U_∞
S/ℓ
1.2
1.1
1.0
0.9
0.8
0.7
0.6
0.5
0
0.1
0.2
0.3
0.4
0.5
0.6
0.7
0.8
0.9
1.0

Fig. 6

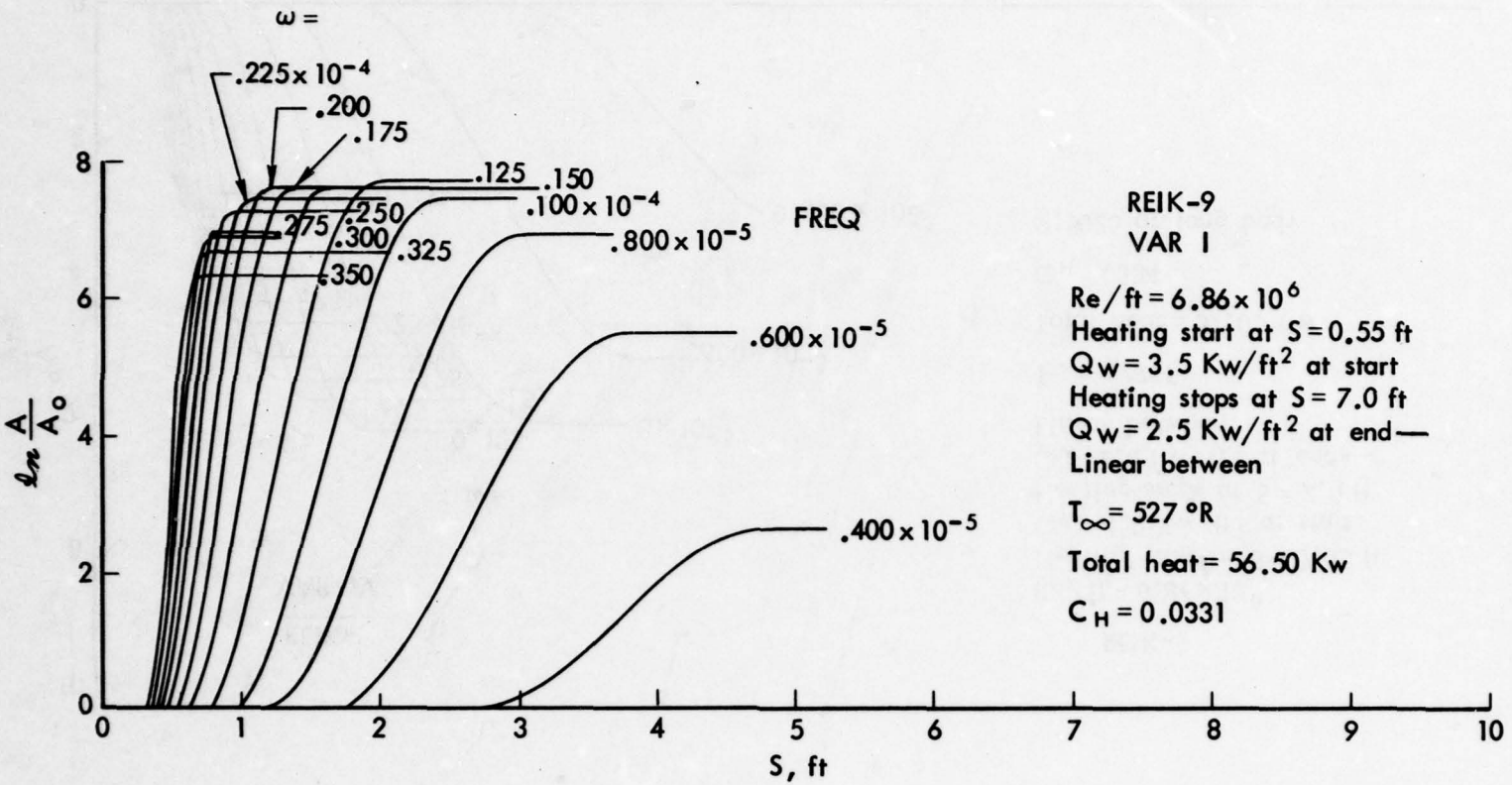
ω =
.225 x 10⁻⁴
.200
.175
.125
.150
.100 x 10⁻⁴
.275
.250
.300
.325
.350
.800 x 10⁻⁵
.600 x 10⁻⁵
.400 x 10⁻⁵
FREQ
REIK-9
VAR I
Re/ft = 6.86 x 10⁶
Heating start at S = 0.55 ft
Qw = 3.5 Kw/ft² at start
Heating stops at S = 7.0 ft
Qw = 2.5 Kw/ft² at end—
Linear between
T∞ = 527 °R
Total heat = 56.50 Kw
CH = 0.0331
ln A/Ao
S, ft
0
1
2
3
4
5
6
7
8
9
10

Fig. 7

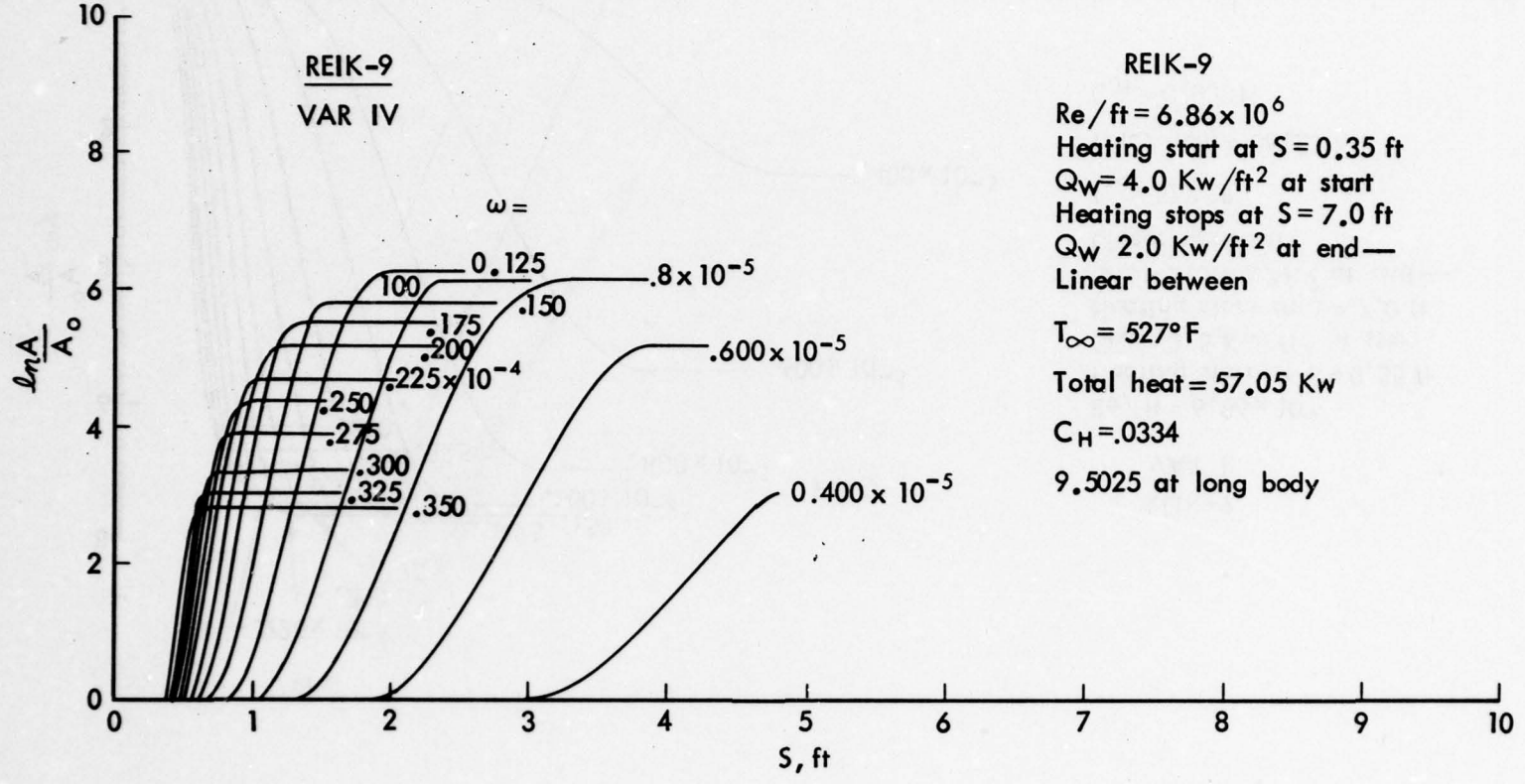

REIK-9

$Re/ft = 6.86 \times 10^6$
Heating start at S = 0.35 ft
Q_W = 4.0 Kw/ft² at start
Heating stops at S = 7.0 ft
Q_W 2.0 Kw/ft² at end —
Linear between

T_∞ = 527° F

Total heat = 57.05 Kw

C_H = .0334

9.5025 at long body

Fig. 8

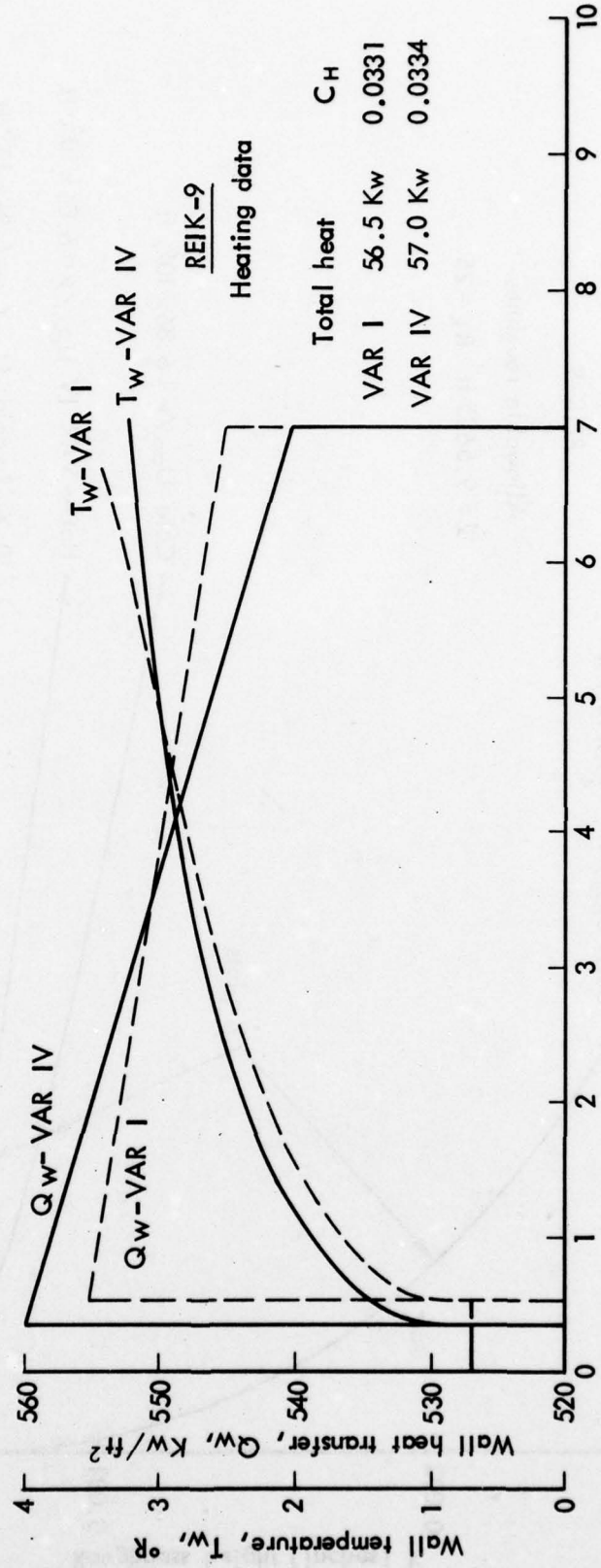
Wall temperature, T_w, °R
Wall heat transfer, Q_w, Kw/ft²
S, ft
Q_w-VAR IV
Q_w-VAR I
T_w-VAR I
T_w-VAR IV
REIK-9
Heating data
Total heat
C_H
VAR I 56.5 Kw 0.0331
VAR IV 57.0 Kw 0.0334

Fig. 9

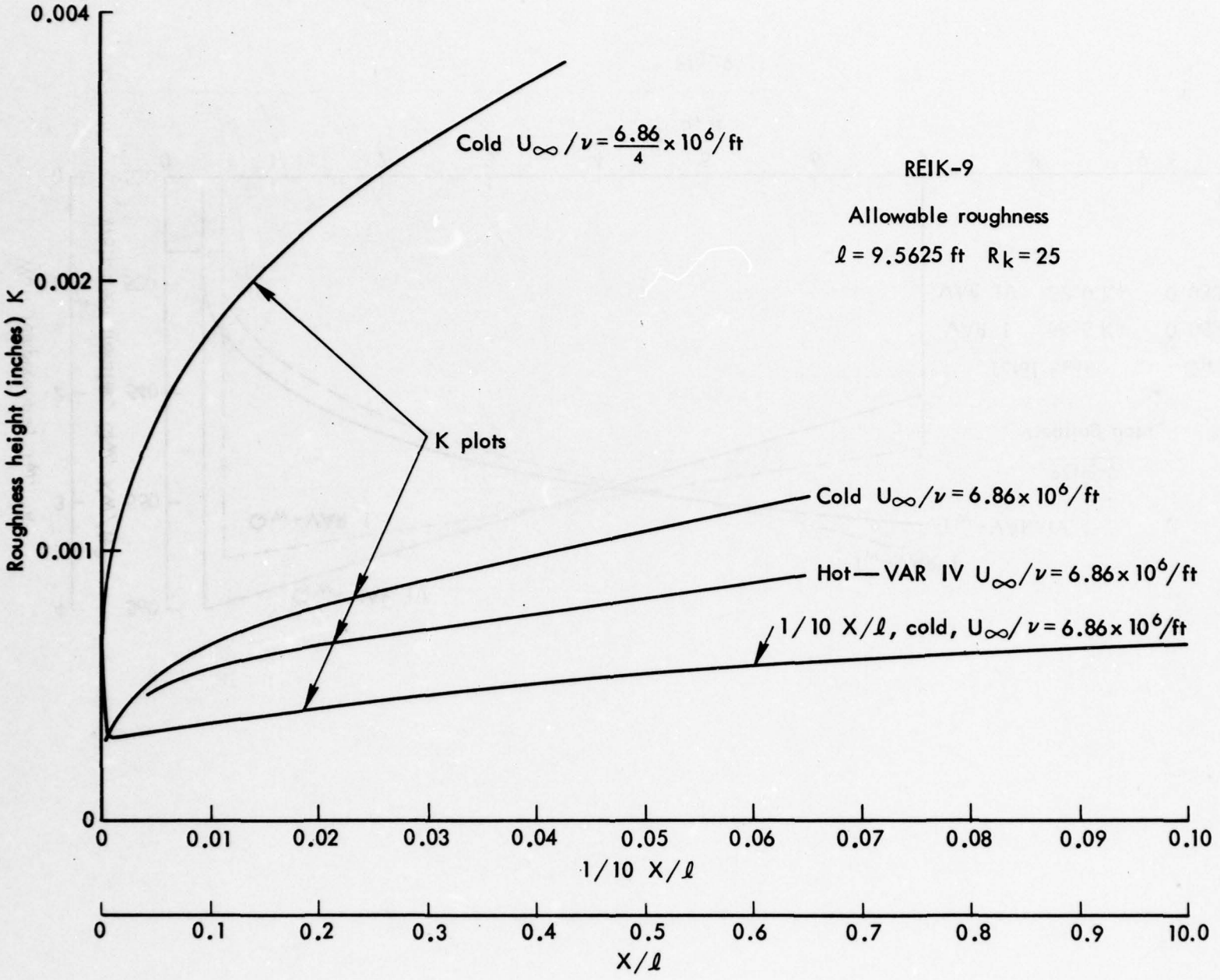
0.004
0.002
0.001
0
Roughness height (inches) K
Cold $U_\infty/\nu = \frac{6.86}{4} \times 10^6/ft$
REIK-9
Allowable roughness
$\ell = 9.5625$ ft $R_k = 25$
K plots
Cold $U_\infty/\nu = 6.86 \times 10^6/ft$
Hot— VAR IV $U_\infty/\nu = 6.86 \times 10^6/ft$
1/10 X/ℓ, cold, $U_\infty/\nu = 6.86 \times 10^6/ft$
0 0.01 0.02 0.03 0.04 0.05 0.06 0.07 0.08 0.09 0.10
1/10 X/ℓ
0 0.1 0.2 0.3 0.4 0.5 0.6 0.7 0.8 0.9 10.0
X/ℓ

Fig. 10

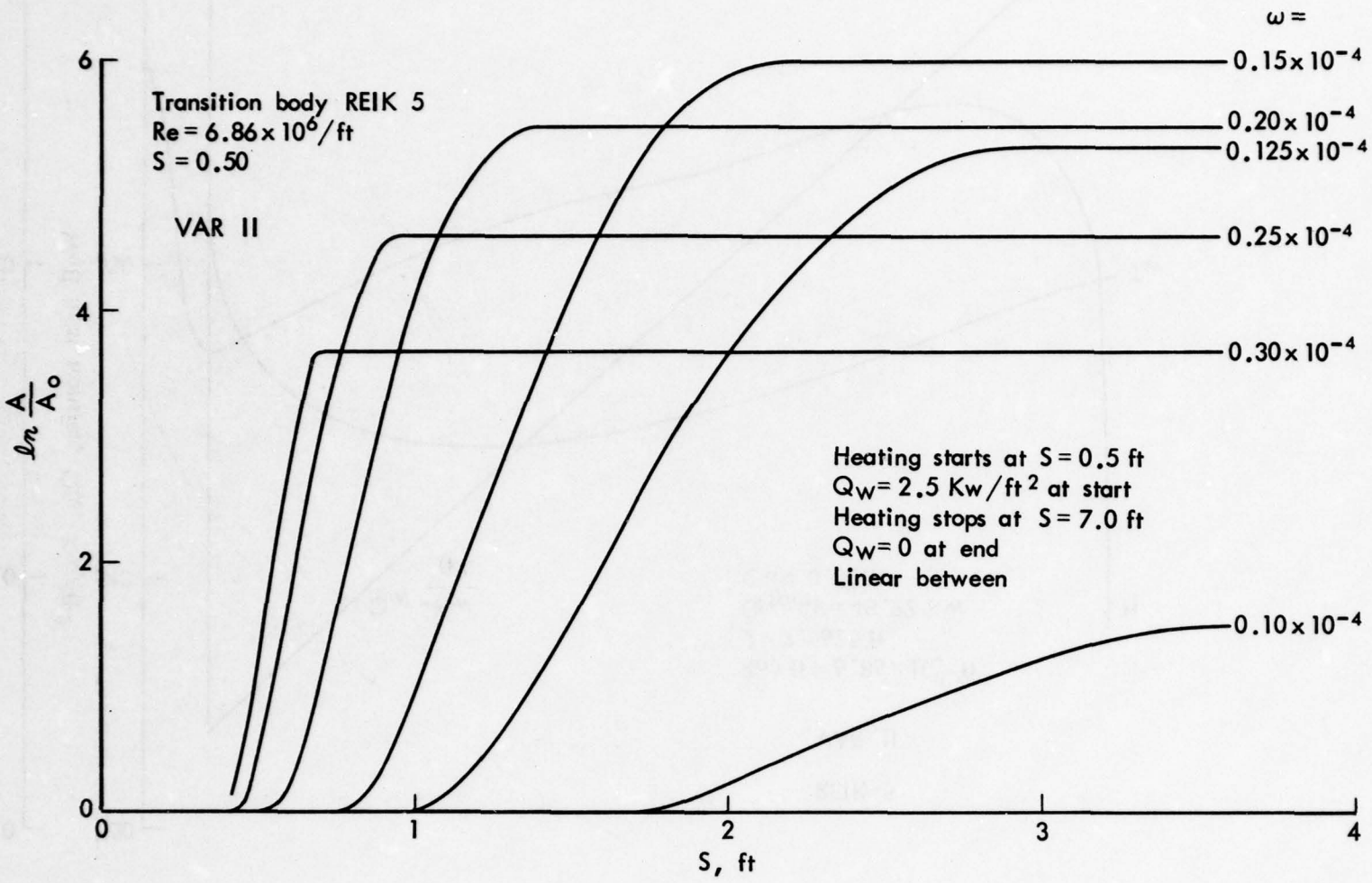
Transition body REIK 5
Re = 6.86 x 10^6/ft
S = 0.50
VAR II
ω =
0.15 x 10^-4
0.20 x 10^-4
0.125 x 10^-4
0.25 x 10^-4
0.30 x 10^-4
0.10 x 10^-4
Heating starts at S = 0.5 ft
Qw = 2.5 Kw/ft^2 at start
Heating stops at S = 7.0 ft
Qw = 0 at end
Linear between
ln A/Ao
S, ft
0
1
2
3
4
6

Fig. 11

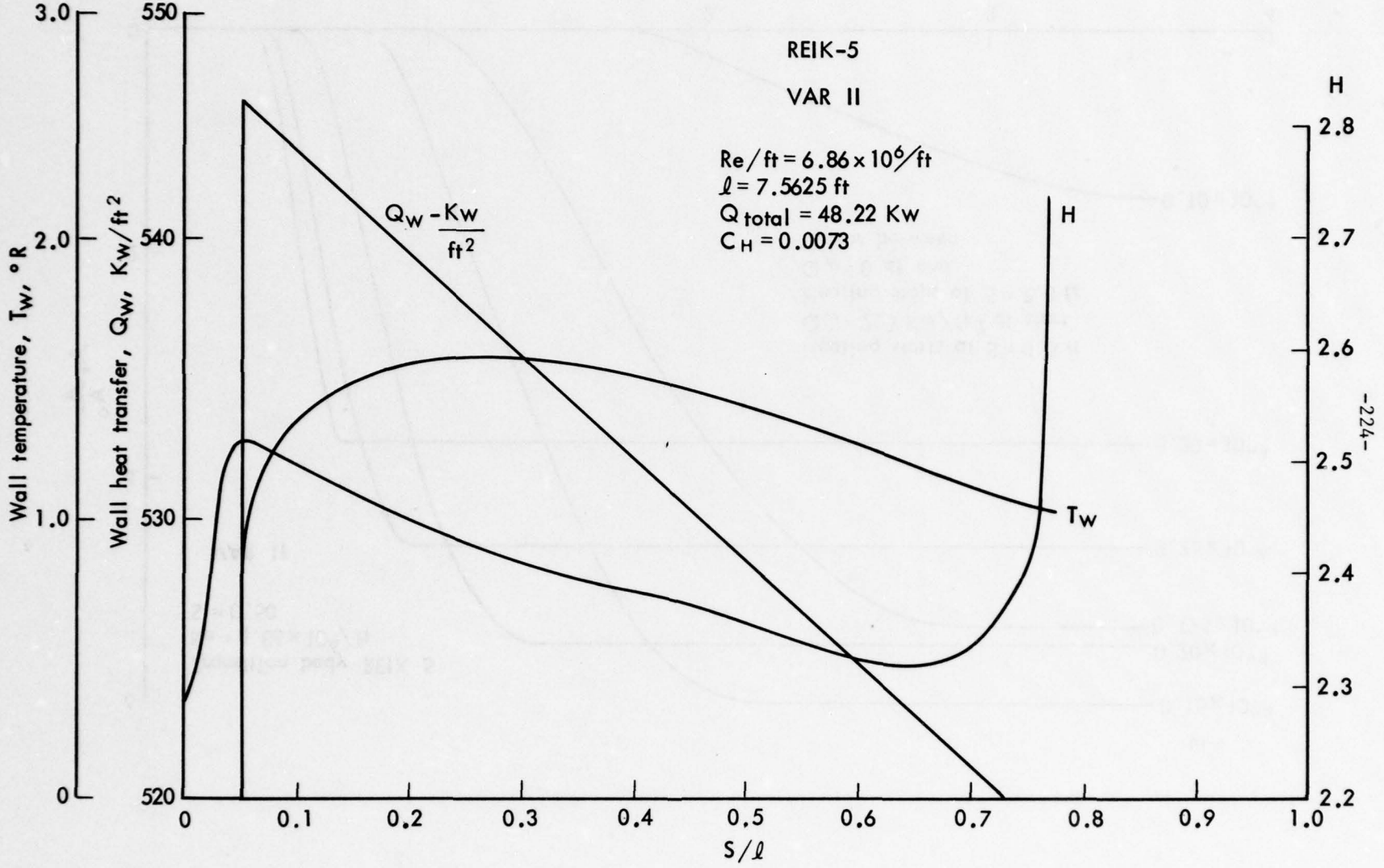
REIK-5
VAR II
Re/ft = 6.86 x 10⁶/ft
ℓ = 7.5625 ft
Q total = 48.22 Kw
C_H = 0.0073
Wall temperature, T_W, °R
Wall heat transfer, Q_W, Kw/ft²
Q_W - Kw/ft²
H
T_W
S/ℓ
3.0
2.0
1.0
0
550
540
530
520
2.8
2.7
2.6
2.5
2.4
2.3
2.2
0
0.1
0.2
0.3
0.4
0.5
0.6
0.7
0.8
0.9
1.0

Fig. 12

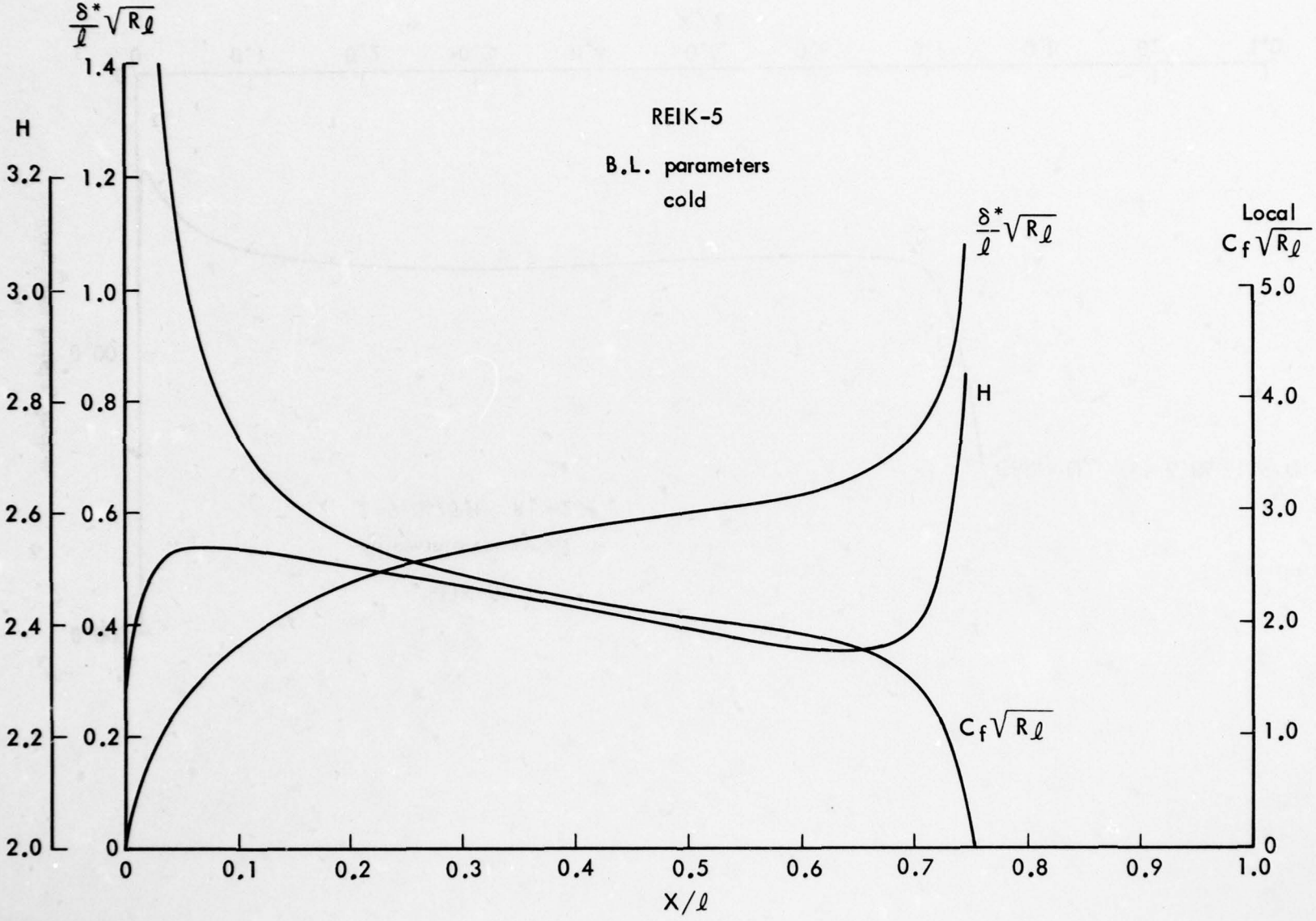
REIK-5
B.L. parameters
cold
$\frac{\delta^*}{\ell}\sqrt{R_\ell}$
H
$C_f\sqrt{R_\ell}$
Local
$C_f\sqrt{R_\ell}$
1.4
1.2
1.0
0.8
0.6
0.4
0.2
0
3.2
3.0
2.8
2.6
2.4
2.2
2.0
5.0
4.0
3.0
2.0
1.0
0
0
0.1
0.2
0.3
0.4
0.5
0.6
0.7
0.8
0.9
1.0
X/ℓ

Fig. 13

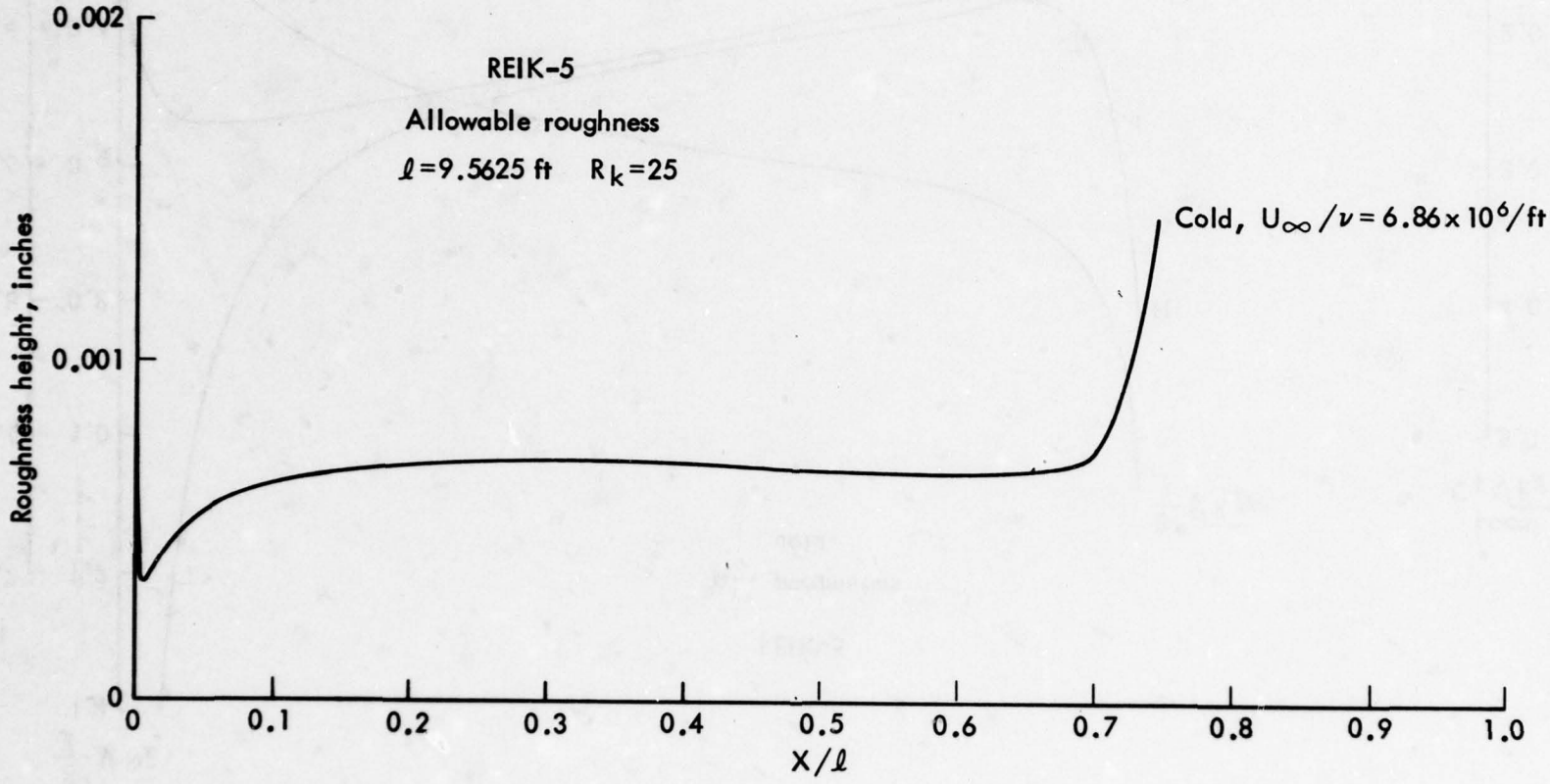
REIK-5
Allowable roughness
ℓ=9.5625 ft R_k=25
Cold, U∞/ν = 6.86 x 10^6/ft
Roughness height, inches
0.002
0.001
0
0 0.1 0.2 0.3 0.4 0.5 0.6 0.7 0.8 0.9 1.0
X/ℓ

Fig. 14

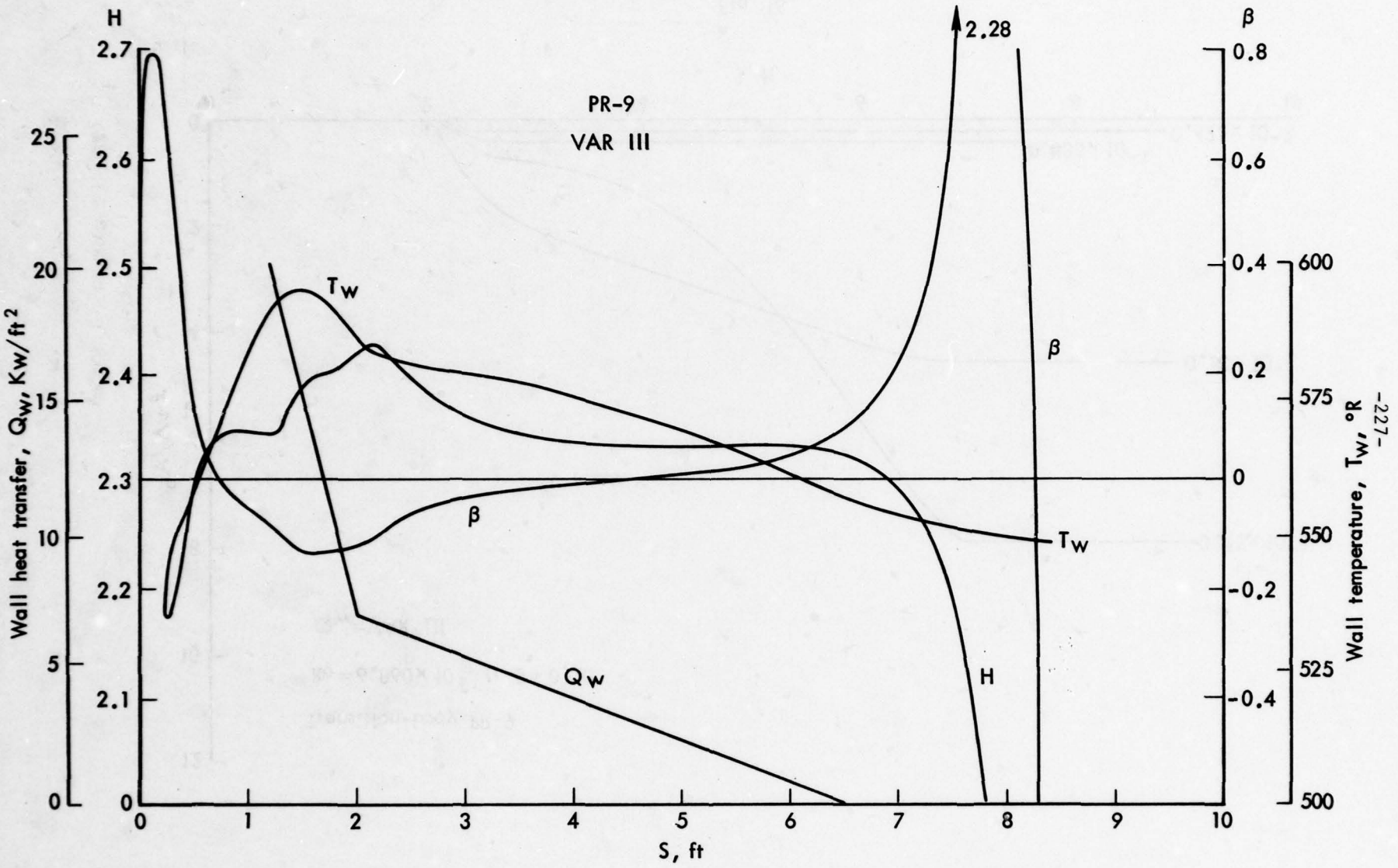
PR-9
VAR III
H
β
2.28
Tw
β
β
Tw
H
Qw
Wall heat transfer, Qw, Kw/ft²
Wall temperature, Tw, °R
S, ft
0
1
2
3
4
5
6
7
8
9
10
2.7
2.6
2.5
2.4
2.3
2.2
2.1
0
25
20
15
10
5
0
0.8
0.6
0.4
0.2
0
-0.2
-0.4
600
575
550
525
500

Fig. 15

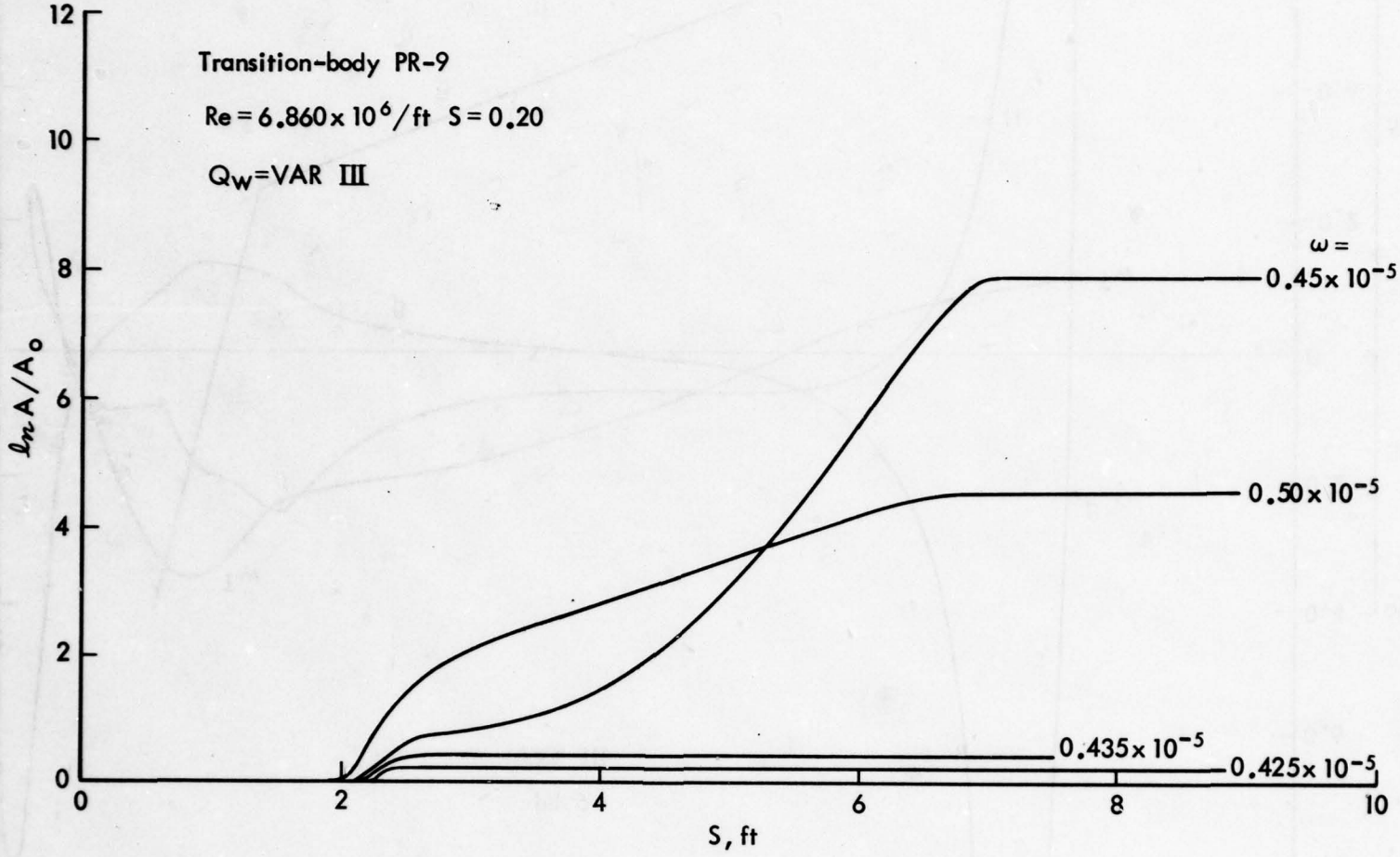
Transition-body PR-9
Re = 6.860 x 10^6/ft S = 0.20
Qw=VAR III
ω =
0.45x 10^-5
0.50x 10^-5
0.435x 10^-5
0.425x 10^-5
ln A/A0
S, ft
0
2
4
6
8
10
12

Fig. 16

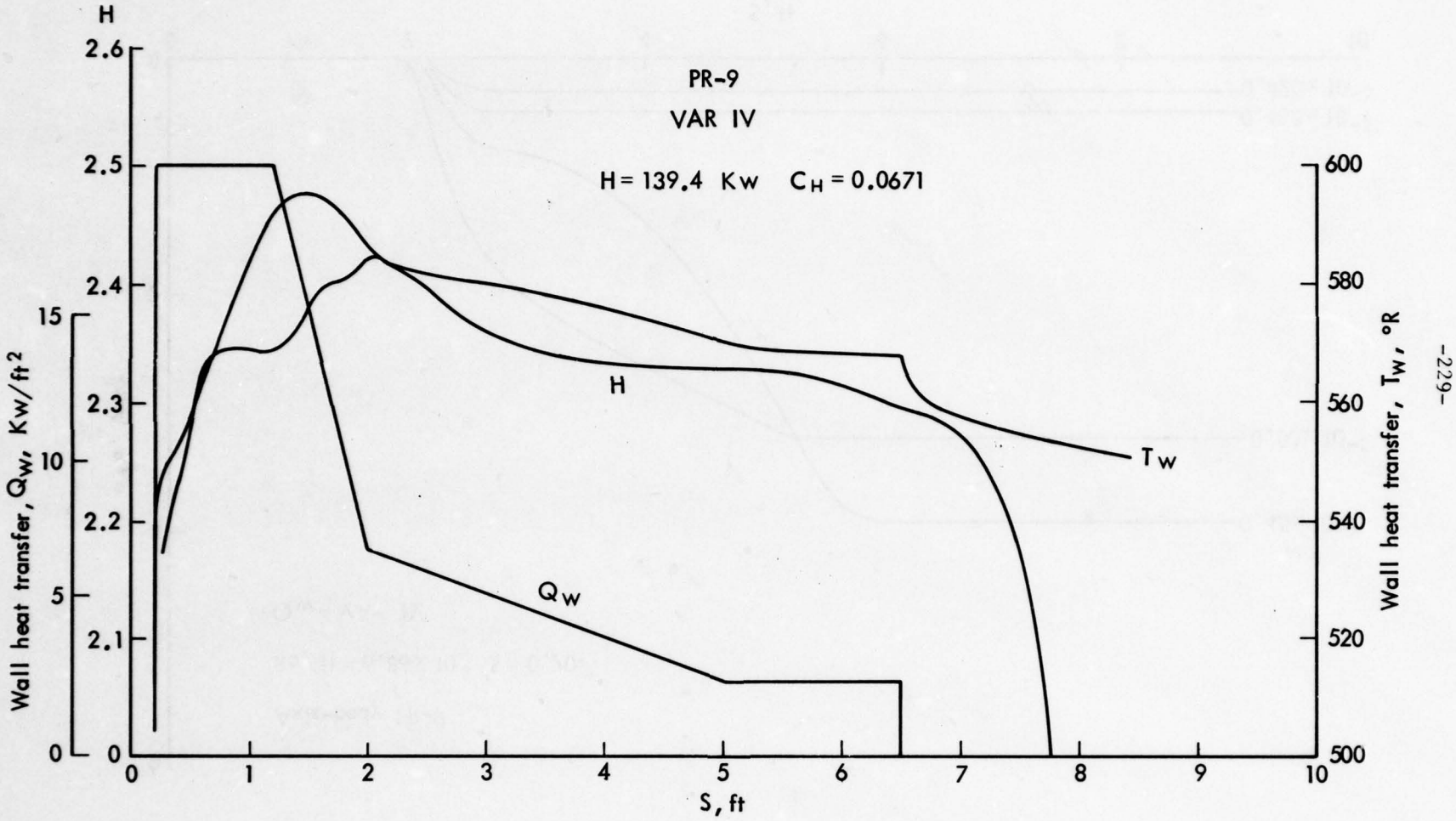
PR-9
VAR IV
H= 139.4 Kw C_H = 0.0671
H
Q_W
T_W
Wall heat transfer, Q_W, Kw/ft²
Wall heat transfer, T_W, °R
S, ft
H
2.6
2.5
2.4
2.3
2.2
2.1
15
10
5
0
600
580
560
540
520
500
0
1
2
3
4
5
6
7
8
9
10

Fig. 17

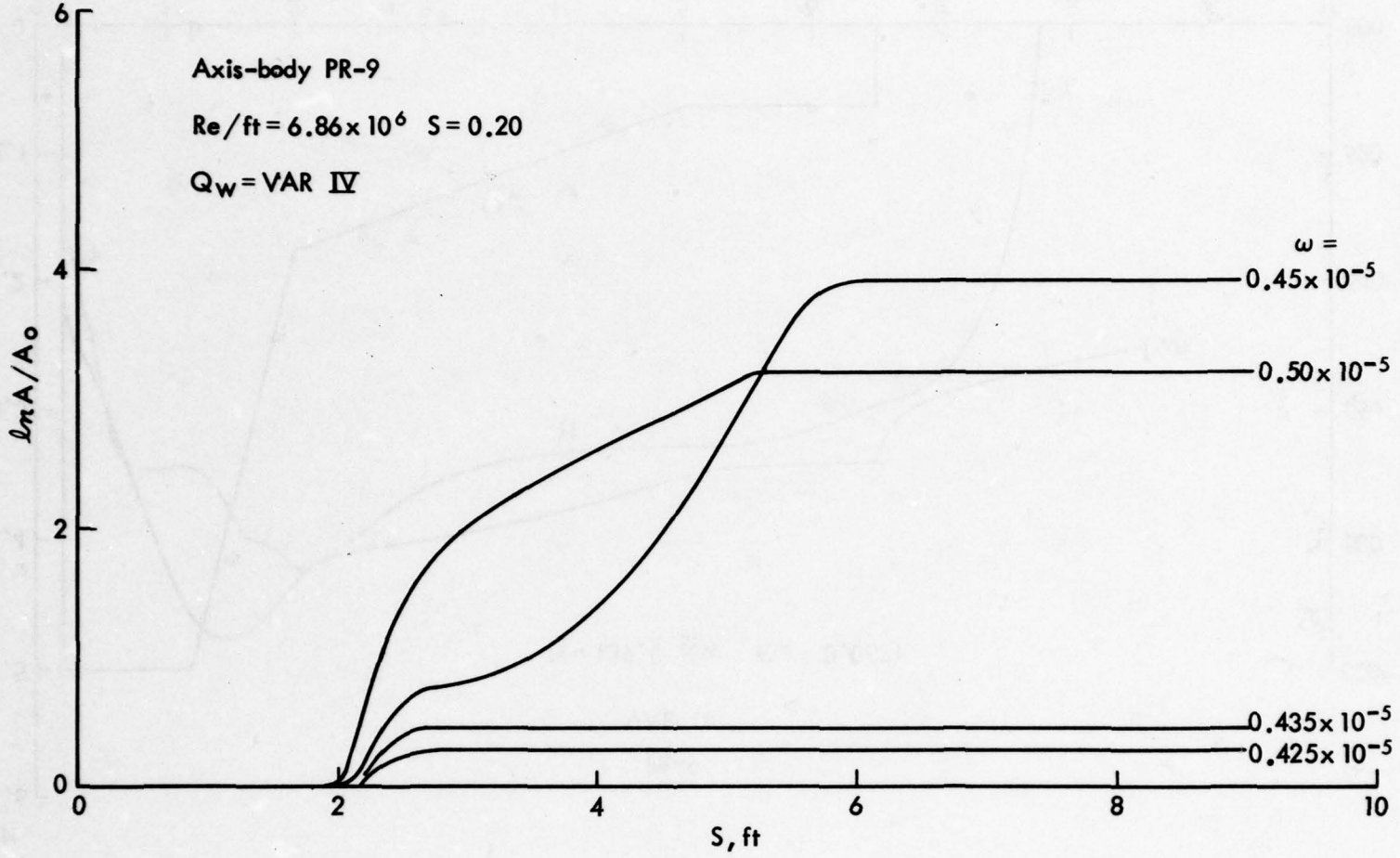
Axis-body PR-9
Re/ft = 6.86 x 10^6 S = 0.20
Q_W = VAR IV
ω =
0.45 x 10^-5
0.50 x 10^-5
0.435 x 10^-5
0.425 x 10^-5
ln A/A_o
S, ft
0
2
4
6
8
10

Fig. 18

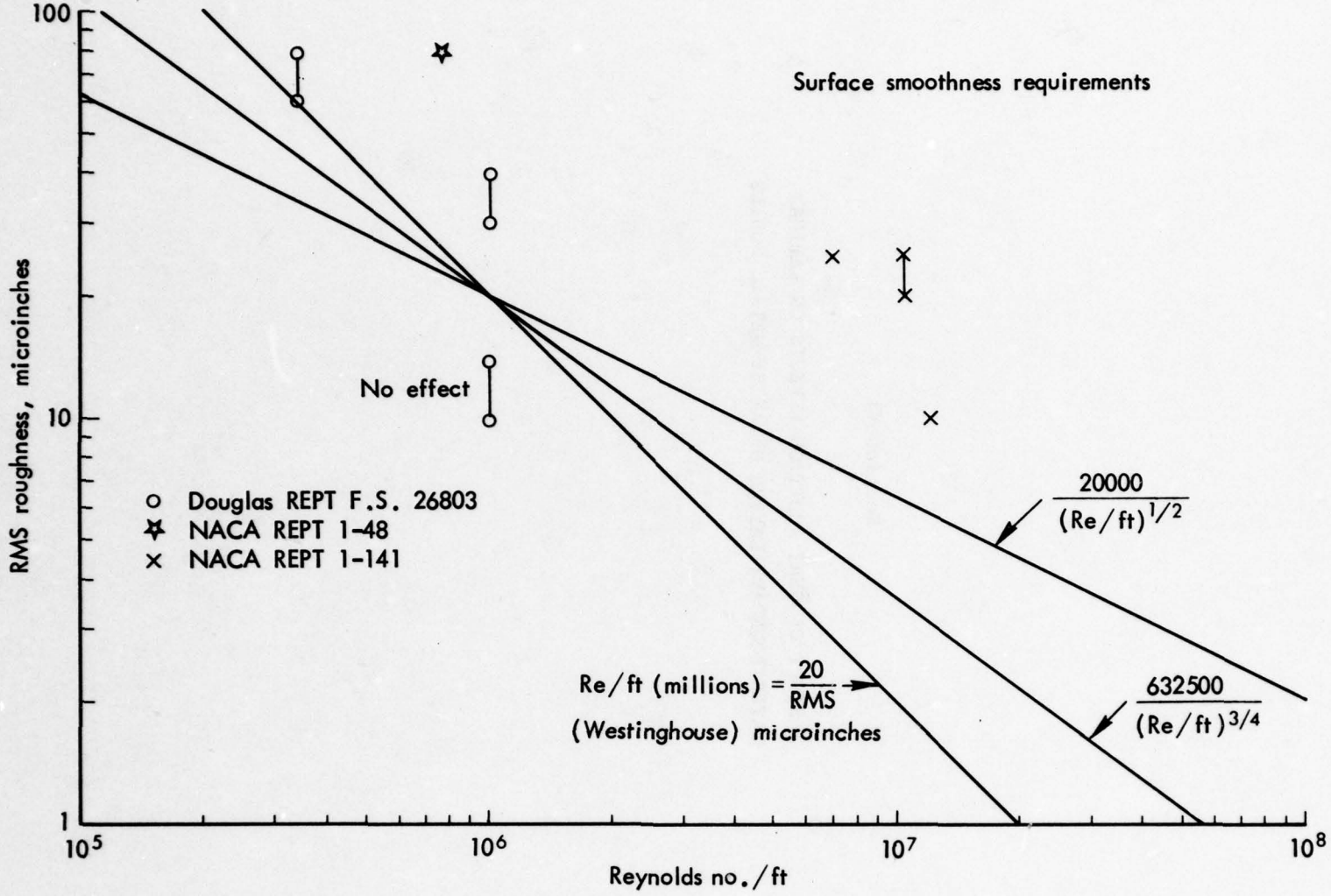
Surface smoothness requirements
100
10
1
RMS roughness, microinches
No effect
Douglas REPT F.S. 26803
NACA REPT 1-48
NACA REPT 1-141
20000 / (Re/ft)^1/2
632500 / (Re/ft)^3/4
Re/ft (millions) = 20 / RMS
(Westinghouse) microinches
10^5
10^6
10^7
10^8
Reynolds no./ft

Fig. 19

Section VI

A STUDY OF HEAT ADDITION EFFECTS ON LAMINAR WATER BOUNDARY LAYERS OF AXISYMMETRIC BODIES

VI-3 LOW-SPEED BOUNDARY LAYER TRANSITION WORKSHOP
(Sept. 13-14, 1976: Rand Corp.)

A STUDY OF HEAT ADDITION EFFECTS ON LAMINAR, WATER BOUNDARY LAYERS OF AXISYMMETRIC BODIES

by

Joseph J. Eisenhuth
Applied Research Laboratory
The Pennsylvania State University
P. O. Box 30
State College, PA 16801

Summary of Presentation

The presently popular subject of stabilizing boundary layers by the addition of heat at the wall has received attention at the Applied Research Laboratory (ARL), Penn State. The primary interest here has been in the prediction of the heat necessary, from a designer's point of view, to forestall transition on axisymmetric bodies and in the estimation of the accompanying mean-flow boundary layer characteristics that result. The focal point in this investigation has been the implementation of a code to provide a solution, by numerical integration means, of the boundary layer equations and in getting the kind of correlation of critical Reynolds number that would permit bypassing the very involved stability calculations in making simple estimates of transition.

Basic Equations and Computer Code

The basic boundary layer equations for axisymmetric flow are shown in Slide 1 and are derived for an incompressible flow with heat addition at the boundary. In the development of the equations, effects such as buoyancy and dissipation of energy by friction are ignored. The boundary conditions are shown at the bottom of the slide.

To put the equations in a form suitable for solution, a stream function, ψ, and a nondimensional normal distance, η, are defined in Slide 2. In addition, the M, R, and θ parameters, which will appear in the resulting equations, are also defined. M is the standard Falkner-Skan parameter, R is a radius gradient parameter which results from the axisymmetric case, and θ is just the normalized temperature difference.

The resulting equations with boundary conditions are shown in Slide 3. These ordinary differential equations are explicitly independent of x and the velocity and temperature profiles that result are given by similar type solutions. The primes indicate derivatives with respect to η; the bars over the physical quantities show normalization with respect to the free-stream quantities, P is the free-stream Prandtl number; C_p is the specific heat at constant pressure; k is the thermal conductivity.

The code for the solution of the two-dimensional version of the mean-flow equations appearing in Slide 3 is presented in Reference 1 as part of a more general computer code. In this solution the method of Nachtsheim and Swigert (Reference 2) was adapted for the numerical integration process and was found to be satisfactory. In the present study, the code for the two-dimensional equations was extended to the axisymmetric case and was further altered to provide certain boundary layer information that wasn't explicitly calculated in the original version.

Critical Reynolds Number Correlation

Stability information in terms of the critical Reynolds number, $R_{\delta^*_{crit}}$, is available for two-dimensional flow both for the case of the unheated boundary with pressure gradient and for the flow over a flat plate with heating at the wall. The results of the unheated case are found in Reference 3 as the critical Reynolds number versus the Pohlhausen parameter $\Lambda = \frac{\delta}{\nu} \frac{dUe}{dx}$, and the heated case

results were obtained from Reference 1 as critical Reynolds number versus temperature difference. Λ and ΔT were translated into the shape parameter $H = \delta^*/\theta$ so that in each case $R_{\delta^*_{crit}}$ could be plotted against H. The curves in Slide 4 are the result. It can be seen that the correlation is quite good, indicating that the stability of the laminar boundary layer is strongly dependent upon H, regardless of whether it is obtained by favorable pressure gradient or by heat. A similar correlation is reported in Reference 4.

This correlation provides the basis for the development of the type of design information which will be presented here. Although based on two-dimensional stability information, the correlation is considered valid for the axisymmetric case because the stability equations are the same for both cases.

Computed Results

There are a variety of ways to present results depending upon the user's needs. Slide 5 presents curves showing the effect of pressure gradient and temperature on the shape parameter for the two-dimensional case (R=0). If one wishes to obtain a certain shape factor, one need only interpolate between the curves of constant M to determine the temperature difference necessary to do so. If one would rather work in terms of an effective M, the additional curve of H versus M in Slide 5 could be used along with the idea of the shape factor-stability correlation to generate the curves shown in Slide 6. With the curves of Slide 6, one need only interpolate between curves to arrive at a temperature difference to produce a chosen effective pressure gradient parameter. In lieu of trying to work with temperature as an additional parameter, it was felt that the effective M could be used in some simplified transition prediction method. As an example of local shear stress and local heat flux values that result from a choice of stability level, Slides 7 and 8 are presented for the specific values of U_e = 50 ft/sec, x = 4.0 ft, and again the two-dimensional case. The values of shear stress and heat flux can be scaled from these curves for other values of x and U_e.

Slides 9 and 10 are presented to show the effect of having different ambient temperatures. The interest in this kind of effect stemmed from considerations of a water tunnel test program in which the Reynolds number range could be extended by heating the tunnel water. Slide 11 is developed to provide values of temperature difference to maintain a certain level of effective M. In this case the M_{eff} = 0.3 level represents close to the maximum heat that can be added before the critical Reynolds number will start decreasing.

Slides 12 and 13 are presented to show the difference between the two-dimensional and axisymmetric cases. Similar plots can be shown for other values of R. Slide 14 is similar to Slide 11 in that it shows the temperature difference necessary to maintain a certain level of stability, in this case for various values of R and M. The level chosen here was again close to the maximum heat that can be added before the critical Reynolds number will again decrease.

Laminar Separation Limits

An attempt was made to obtain some limits, with regard to the various parameters, beyond which laminar separation would occur. Slide 15 represents one way of presenting this information. Values of R and M below and to the left of the curves represent separated flows. Another presentation of this same information is found in Slide 16. It can be seen that temperature difference has relatively little effect on laminar separation. This is consistent with the calculations reported in Reference 5 for the two-dimensional case and are shown as the curve marked "Rand". Although showing slightly more effect of temperature, the Rand calculations also indicate the minor role of heating in the prevention of laminar separation.

Transition Criteria

A purpose in employing the $R_{\delta^*_{crit}}$ - H correlation was in being able to use the effective M to enter experimental transition curves based on unheated operation.

Presumably, theoretical stability information for the unheated case might also be reduced to a form that would make use of the effective Falkner-Skan parameter. Aspects of this work are still in progress, so only a first attempt at developing some simplified transition curves is presented.

It would seem logical that the parameters that affect H and thus $R_{\delta^*_{crit}}$, would also be controlling as far as transition is concerned. The first attempt therefore made use of the parameters M and R. Reference 6 provides transition information for several bodies over a range of Reynolds numbers. The geometric characteristics and the potential flow calculations for one of these bodies were used to generate R and M distributions along the body length. Combining this information with the experimental transition curve given for that body, a plot like the one shown in Slide 17 is possible. Very little variation of M along the body occurs and the major parameter appears to be R. This is similar to the kind of criterion used in Reference 7 except that instead of R a parameter, $(D/r)(dr/d\ell)$ is used. It is anticipated that M can be an equally effective parameter in influencing transition and that bodies with greater variations in M would show different trends. In other words, there should be some cross curves of constant M appearing in a general plot for all types of bodies.

References

1. Lowell, R. L., Jr. and Reshotko, E., "Numerical Study of the Stability of a Heated, Water Boundary Layer," Case Western Reserve University, FTAS TR 73-93, January 1974.

2. Nachtsheim, P. R. and Swigert, P., "Satisfaction of Asymptotic Boundary Conditions in Numerical Solution of Systems on Nonlinear Equations of Boundary-Layer Type," NASA TN D-3004, 1965.

3. Schlichting, H., "Boundary-Layer Theory," McGraw-Hill Book Company, 1968.

4. King, William S., "The Effect of Wall Temperature and Suction on Laminar Boundary-Layer Stability," Rand Report R-1863-ARPA, April 1976.

5. Aroesty, J. and Berger, S. A., "Controlling the Separation of Laminar Boundary Layers in Water: Heating and Suction," Rand Report R-1789-ARPA, September 1975.

6. Groth, E. E., "Boundary Layer Transition on Bodies of Revolution," Northrop Aircraft, Inc., Report BLC-100, July 1957.

7. Granville, P. S., "The Prediction of Transition from Laminar to Turbulent Flow in Boundary Layers on Bodies of Revolution,"

$$\frac{\partial(\rho r u)}{\partial x} + \frac{\partial(\rho r v)}{\partial y} = 0$$

$$\rho\left(u\frac{\partial u}{\partial y} + v\frac{\partial u}{\partial y}\right) = \rho U_e \frac{dU_e}{dx} + \frac{\partial}{\partial y}\left(\mu\frac{\partial u}{\partial y}\right)$$

$$\rho C_p\left(u\frac{\partial T}{\partial x} + v\frac{\partial T}{\partial y}\right) = -\rho u U_e \frac{dU_e}{dx} + \frac{\partial}{\partial y}\left(k\frac{\partial T}{\partial y}\right)$$

BOUNDARY CONDITIONS:

at $y=0$ $\quad u = v = o$

$\quad T = T_w$

at $y \to \infty$ $\quad u \to U_e$

$\quad T \to T_\infty$

SLIDE 1

$$\psi = (\rho_\infty \mu_\infty x U_e)^{1/2} \; f(\eta)$$

$$\eta = \left(\frac{U_e}{\nu_\infty x}\right)^{1/2} \int_0^y \left(\frac{\rho}{\rho_\infty}\right) dy$$

$$\theta = \frac{T - T_\infty}{T_w - T_\infty}$$

$$M = \frac{x}{U_e} \frac{dU_e}{dx}$$

$$R = \frac{2x}{r} \frac{dr}{dx}$$

SLIDE 2

$$(\bar{\rho}\,\bar{\mu}\,f'')' + M(1 - f'^2) + \left(\frac{M+R+1}{2}\right) ff'' = 0$$

$$P\bar{C}_P\left(\frac{M+R+1}{2}\right)\; f\theta' + (\bar{\rho}\,\bar{k}\,\theta')' = 0$$

BOUNDARY CONDITIONS:

at $\eta = 0$ $f' = f = 0$

$\theta = 1$

at $\eta \to \infty$ $f' \to 1$

$\theta \to 0$

SLIDE 3

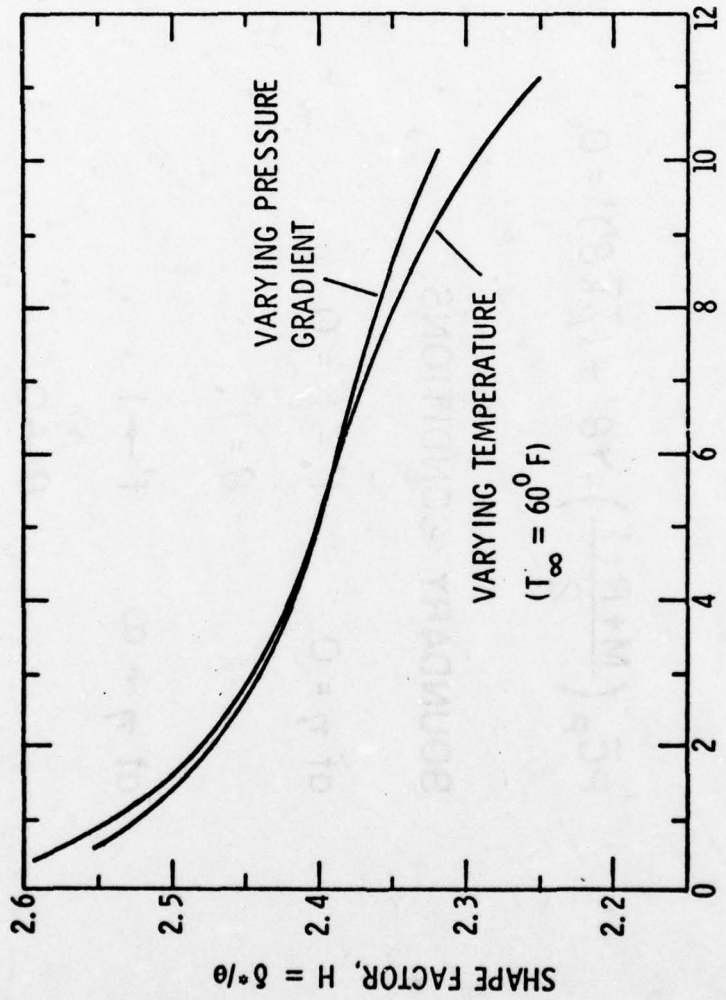
SHAPE FACTOR, H = δ*/θ
2.6
2.5
2.4
2.3
2.2
0
2
4
6
8
10
12
CRITICAL REYNOLDS NUMBER, R_{δ^*} crit X 10^{-3}
VARYING PRESSURE GRADIENT
VARYING TEMPERATURE
($T_\infty = 60^0$ F)

SLIDE 4

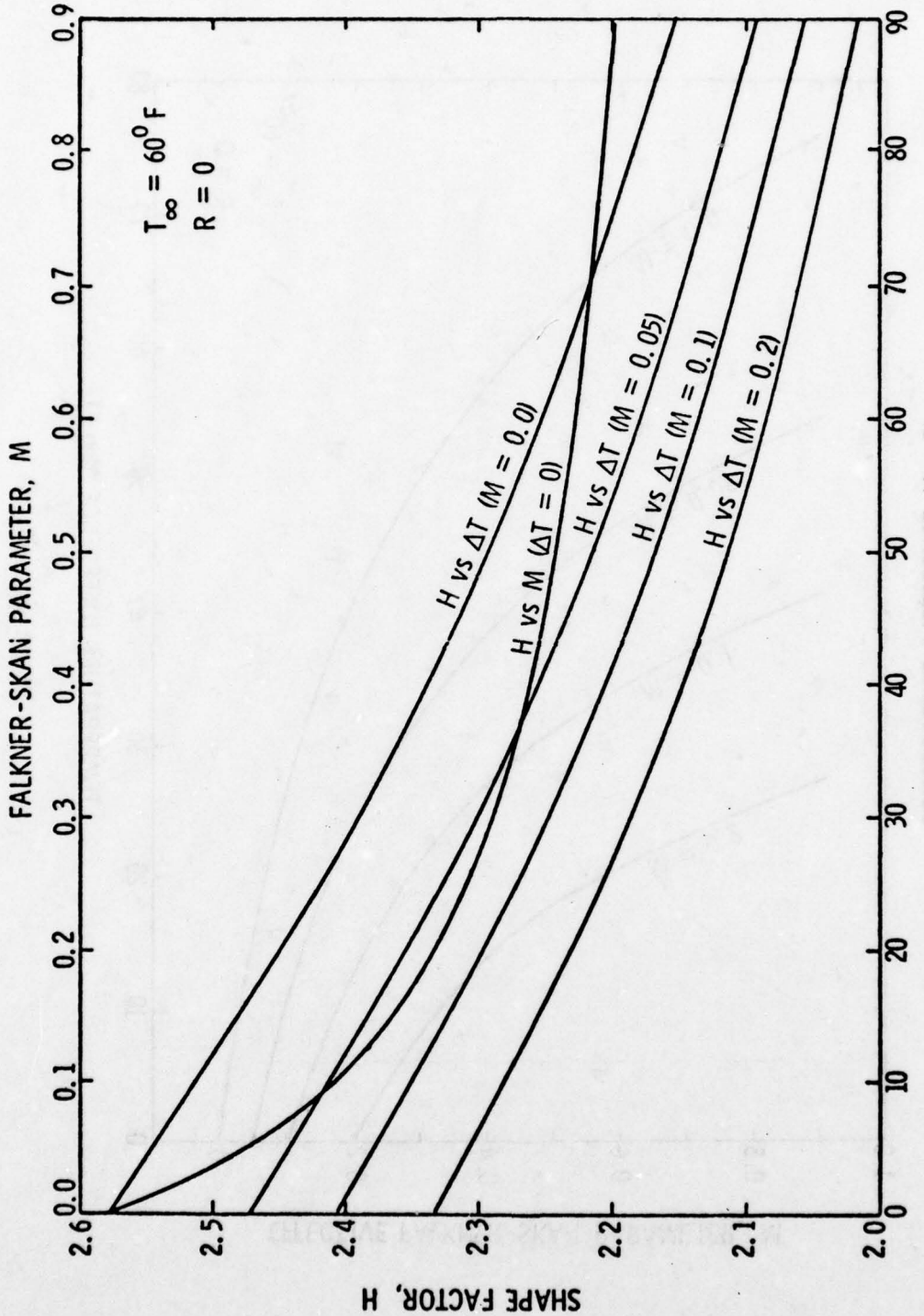
FALKNER-SKAN PARAMETER, M
0.0
0.1
0.2
0.3
0.4
0.5
0.6
0.7
0.8
0.9
$T_\infty = 60^\circ F$
R = 0
H vs ΔT (M = 0.0)
H vs M (ΔT = 0)
H vs ΔT (M = 0.05)
H vs ΔT (M = 0.1)
H vs ΔT (M = 0.2)
SHAPE FACTOR, H
2.6
2.5
2.4
2.3
2.2
2.1
2.0
TEMPERATURE DIFFERENCE (deg F)
0
10
20
30
40
50
60
70
80
90

SLIDE 5

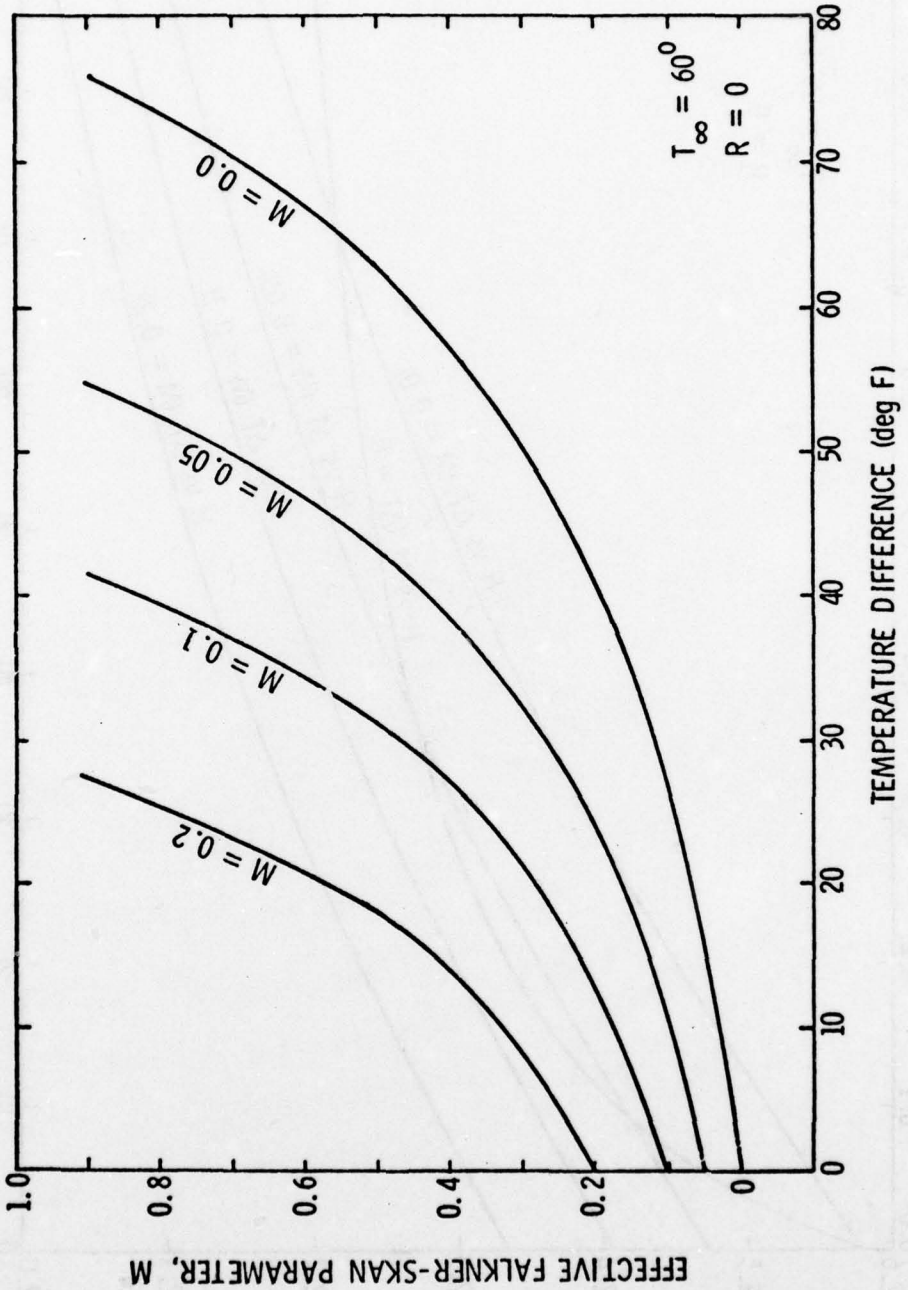
EFFECTIVE FALKNER-SKAN PARAMETER, M
1.0
0.8
0.6
0.4
0.2
0
TEMPERATURE DIFFERENCE (deg F)
0
10
20
30
40
50
60
70
80
$T_\infty = 60^o$
R = 0
M = 0.0
M = 0.05
M = 0.1
M = 0.2

SLIDE 6

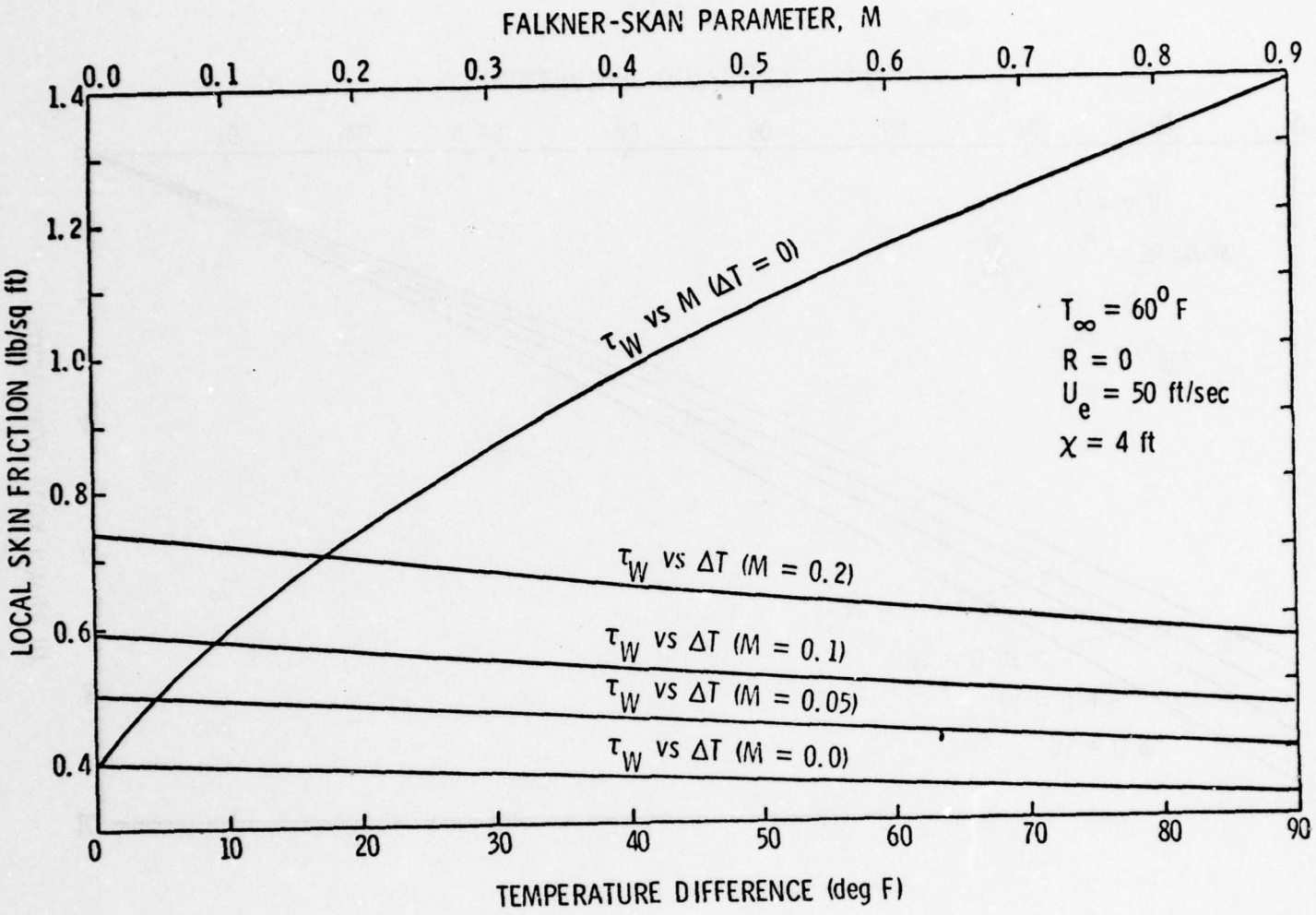
FALKNER-SKAN PARAMETER, M
0.0
0.1
0.2
0.3
0.4
0.5
0.6
0.7
0.8
0.9
LOCAL SKIN FRICTION (lb/sq ft)
1.4
1.2
1.0
0.8
0.6
0.4
τ_W vs M (ΔT = 0)
T_∞ = 60° F
R = 0
U_e = 50 ft/sec
χ = 4 ft
τ_W vs ΔT (M = 0.2)
τ_W vs ΔT (M = 0.1)
τ_W vs ΔT (M = 0.05)
τ_W vs ΔT (M = 0.0)
0
10
20
30
40
50
60
70
80
90
TEMPERATURE DIFFERENCE (deg F)

SLIDE 7

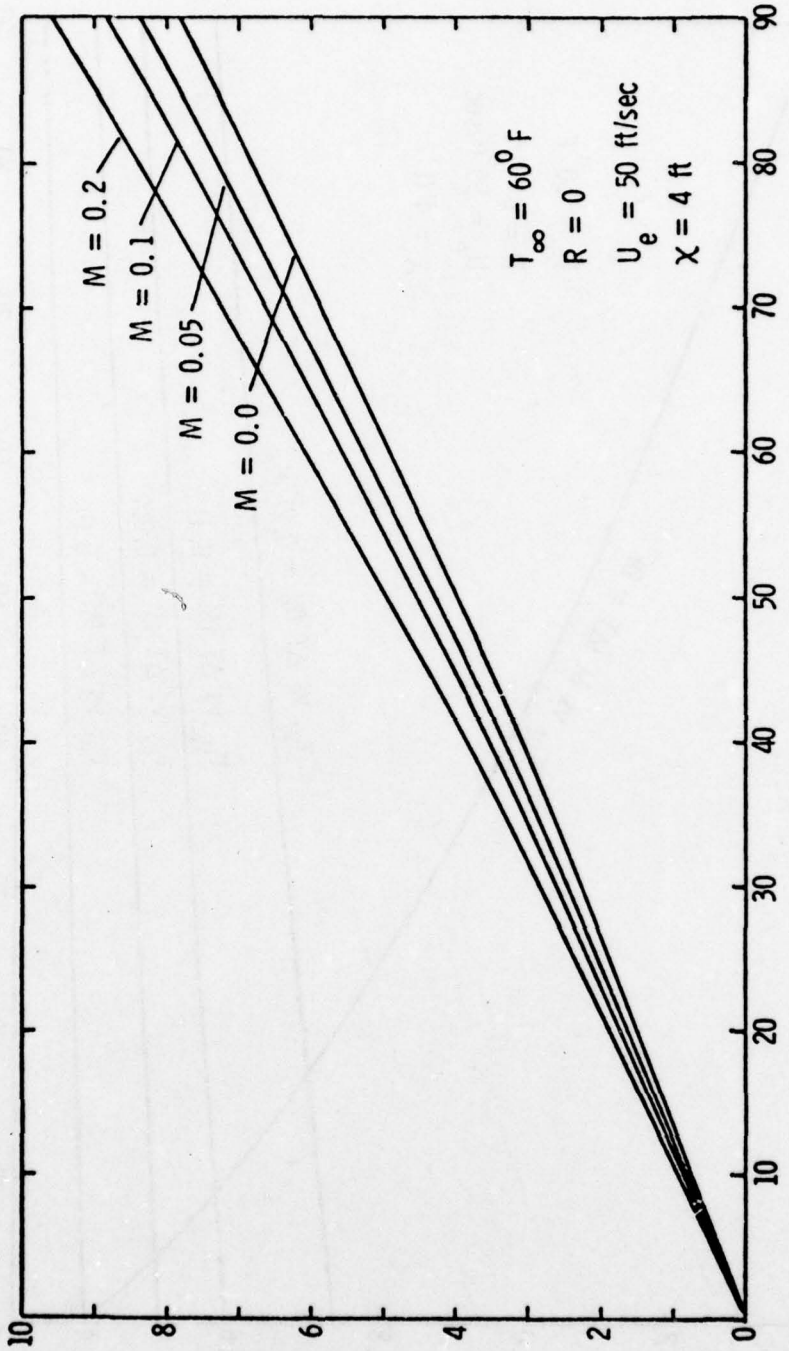
LOCAL HEAT FLUX (KW/sq ft)
TEMPERATURE DIFFERENCE (deg F)
M = 0.2
M = 0.1
M = 0.05
M = 0.0
$T_\infty = 60^0$ F
R = 0
U_e = 50 ft/sec
X = 4 ft
0
2
4
6
8
10
10
20
30
40
50
60
70
80
90

SLIDE 8

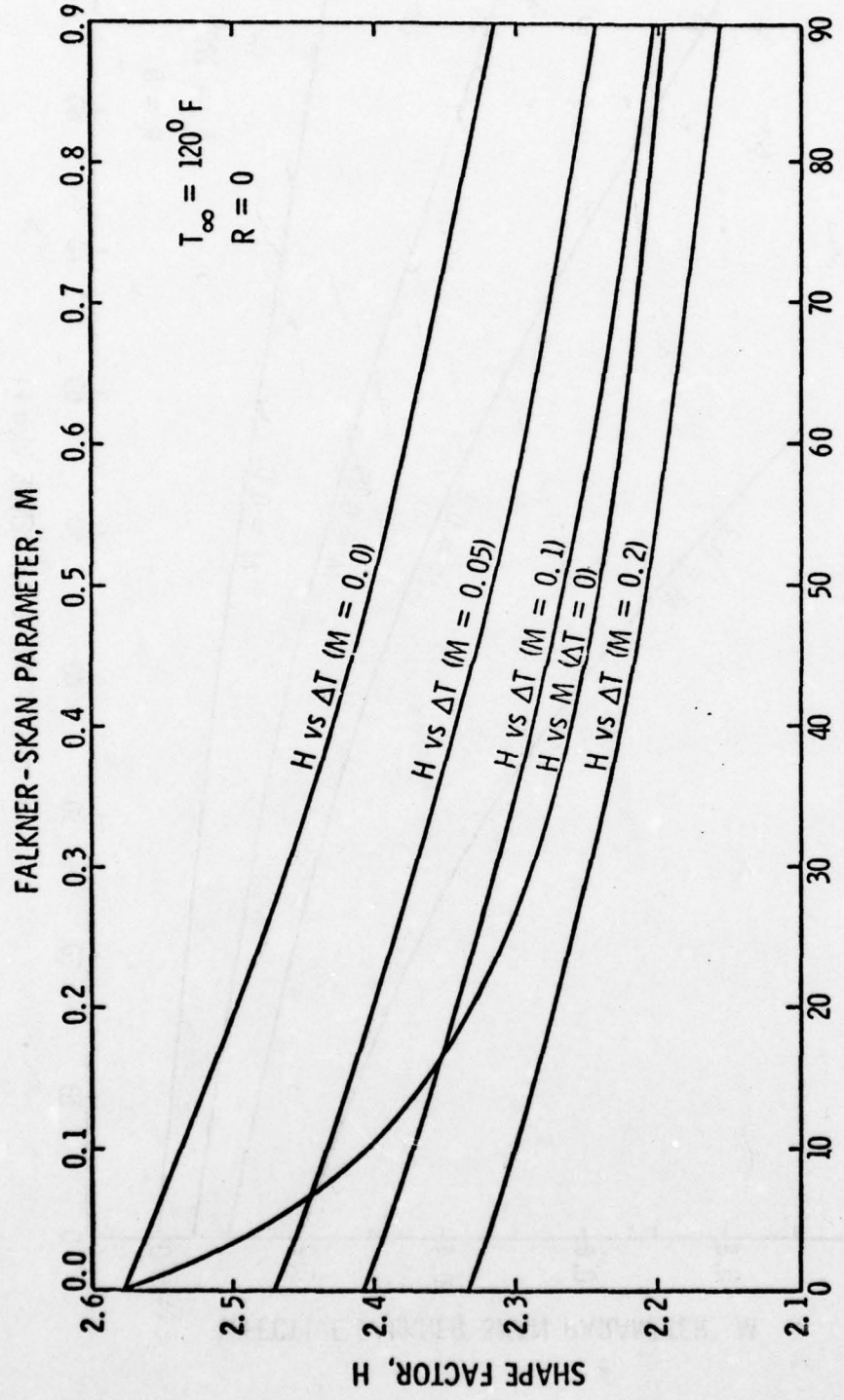
FALKNER-SKAN PARAMETER, M
0.0
0.1
0.2
0.3
0.4
0.5
0.6
0.7
0.8
0.9
$T_\infty = 120^0$ F
R = 0
H vs ΔT (M = 0.0)
H vs ΔT (M = 0.05)
H vs ΔT (M = 0.1)
H vs M (ΔT = 0)
H vs ΔT (M = 0.2)
SHAPE FACTOR, H
2.6
2.5
2.4
2.3
2.2
2.1
0
10
20
30
40
50
60
70
80
90
TEMPERATURE DIFFERENCE (deg F)

SLIDE 9

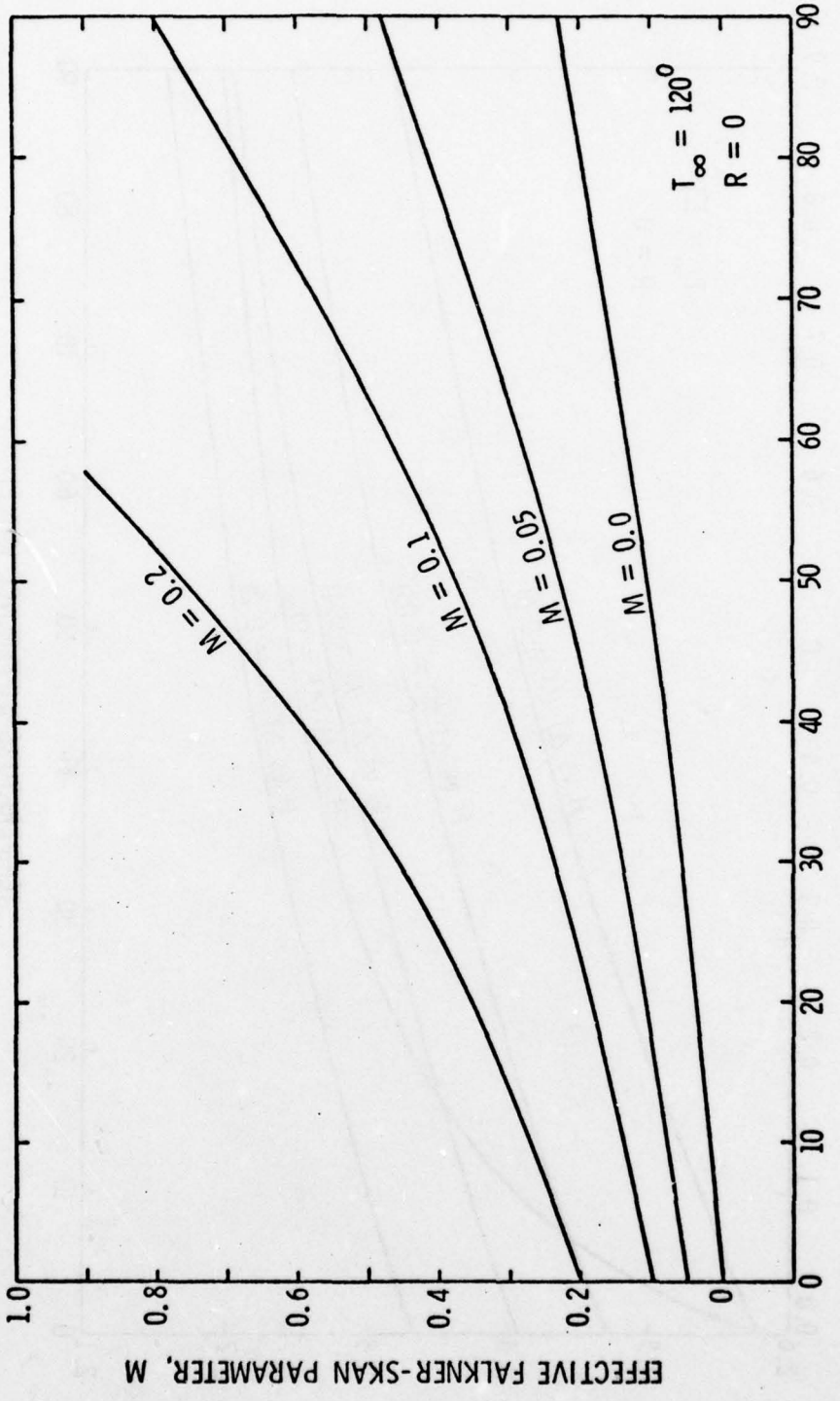
EFFECTIVE FALKNER-SKAN PARAMETER, M
1.0
0.8
0.6
0.4
0.2
0
0
10
20
30
40
50
60
70
80
90
TEMPERATURE DIFFERENCE (deg F)
M = 0.2
M = 0.1
M = 0.05
M = 0.0
$T_\infty = 120^o$
R = 0

SLIDE 10

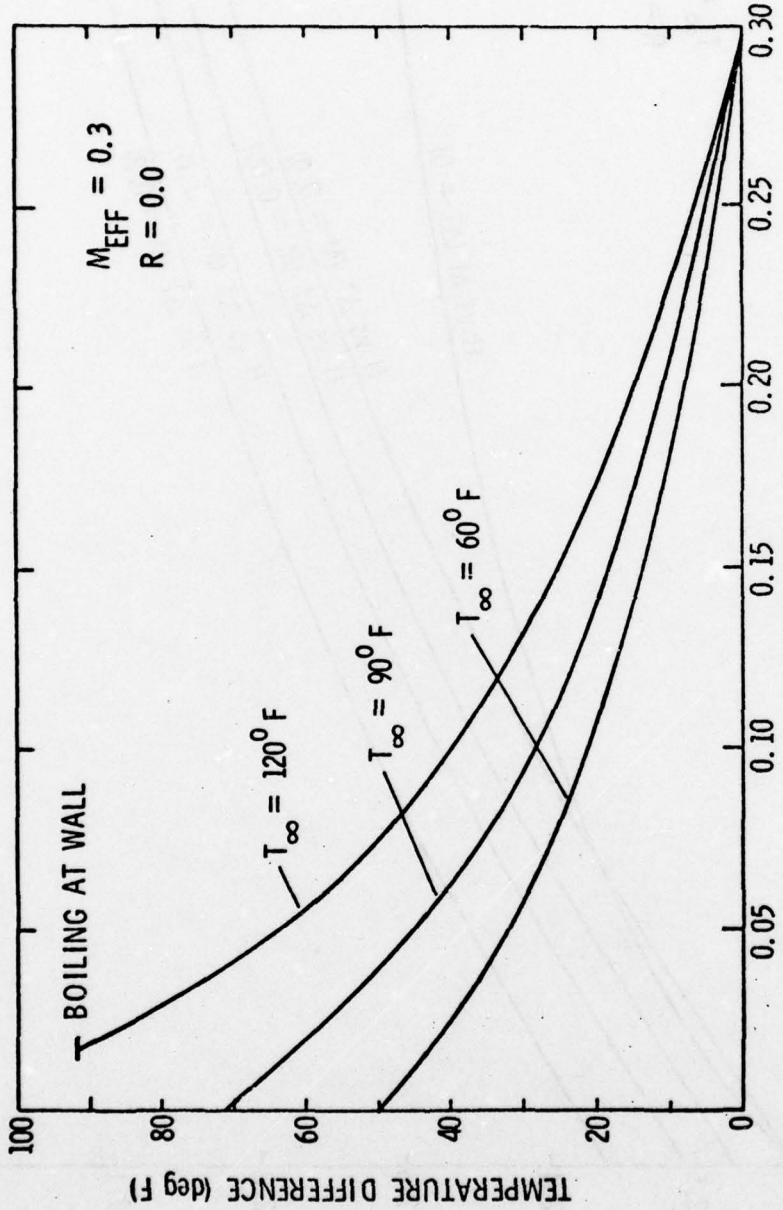
TEMPERATURE DIFFERENCE (deg F)
100
80
60
40
20
0
0.05
0.10
0.15
0.20
0.25
0.30
FALKNER-SKAN PARAMETER, M
BOILING AT WALL
$T_\infty = 120^0 F$
$T_\infty = 90^0 F$
$T_\infty = 60^0 F$
$M_{EFF} = 0.3$
$R = 0.0$

SLIDE 11

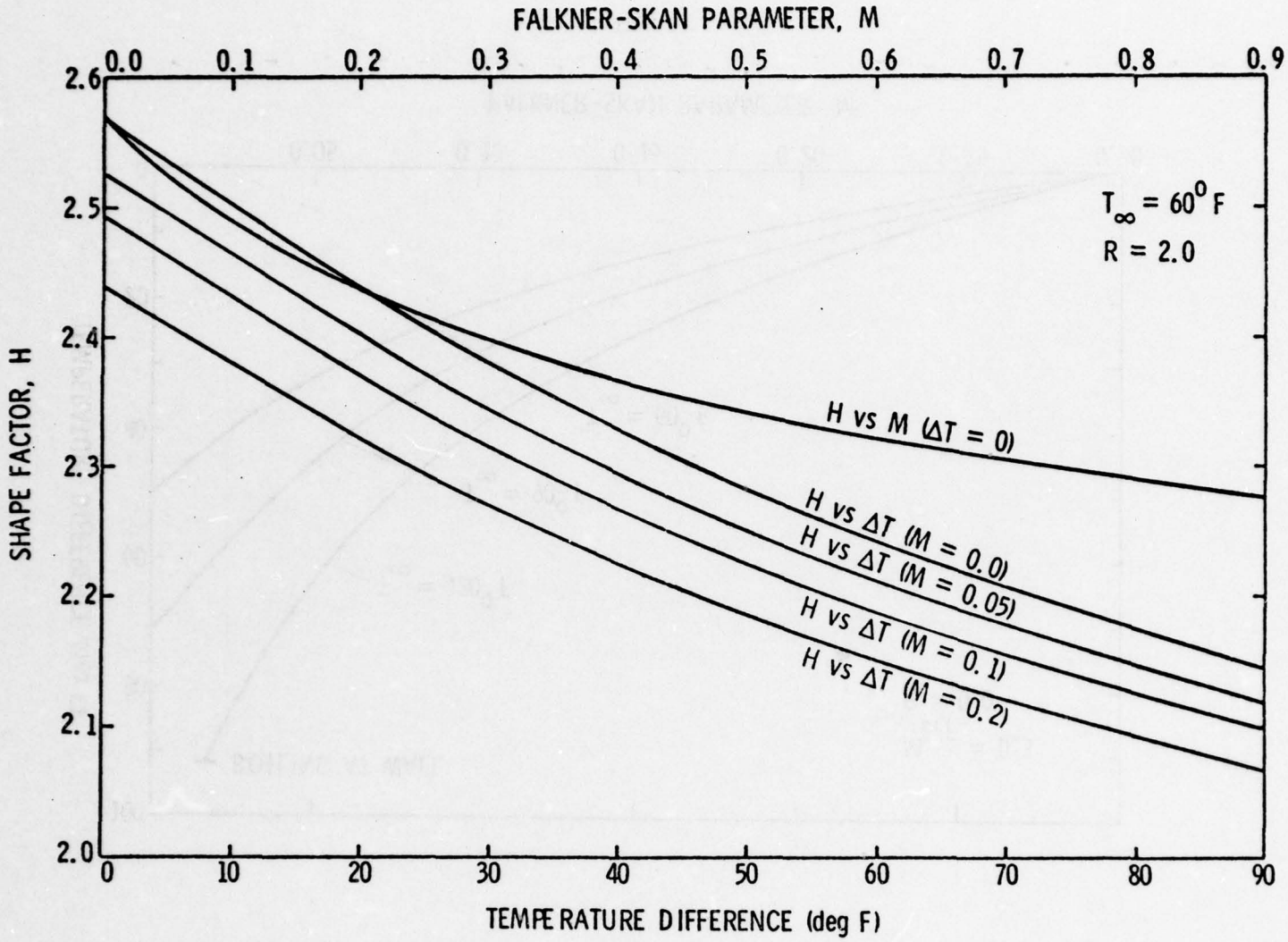
FALKNER-SKAN PARAMETER, M
0.0
0.1
0.2
0.3
0.4
0.5
0.6
0.7
0.8
0.9
2.6
2.5
2.4
2.3
2.2
2.1
2.0
SHAPE FACTOR, H
$T_\infty = 60^0$ F
R = 2.0
H vs M (ΔT = 0)
H vs ΔT (M = 0.0)
H vs ΔT (M = 0.05)
H vs ΔT (M = 0.1)
H vs ΔT (M = 0.2)
0
10
20
30
40
50
60
70
80
90
TEMPERATURE DIFFERENCE (deg F)

SLIDE 12

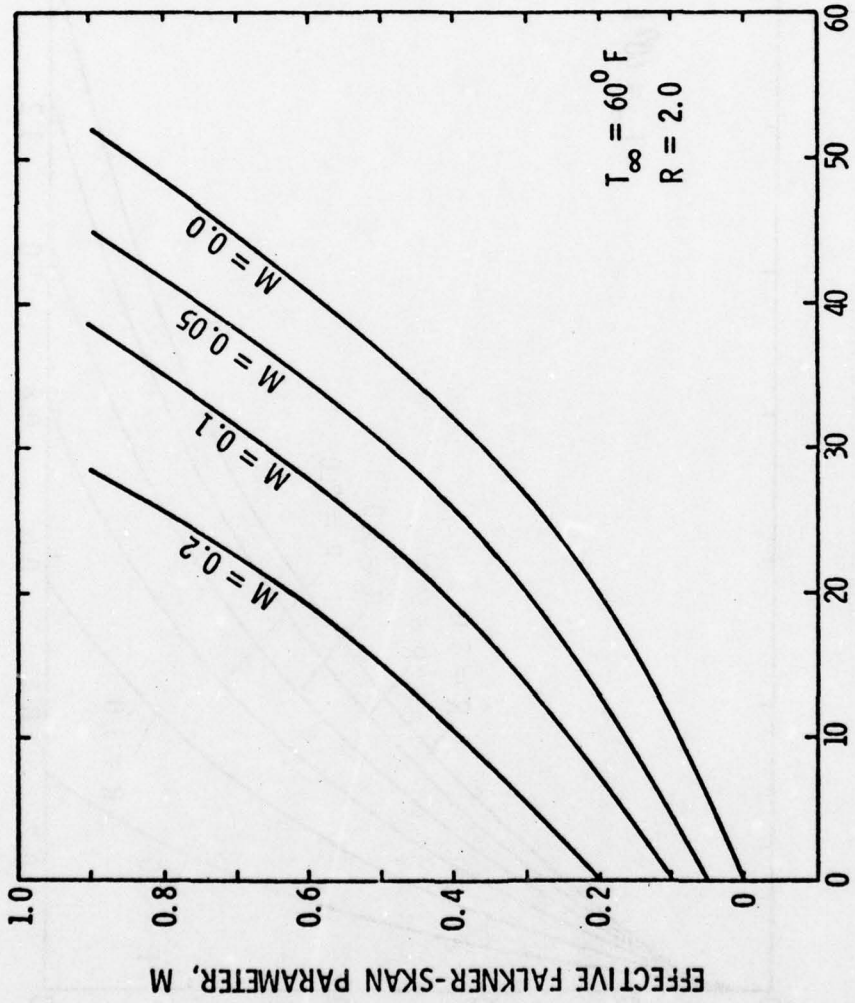
EFFECTIVE FALKNER-SKAN PARAMETER, M
1.0
0.8
0.6
0.4
0.2
0
0
10
20
30
40
50
60
TEMPERATURE DIFFERENCE (deg F)
$T_\infty = 60^0$ F
R = 2.0
M = 0.0
M = 0.05
M = 0.1
M = 0.2

SLIDE 13

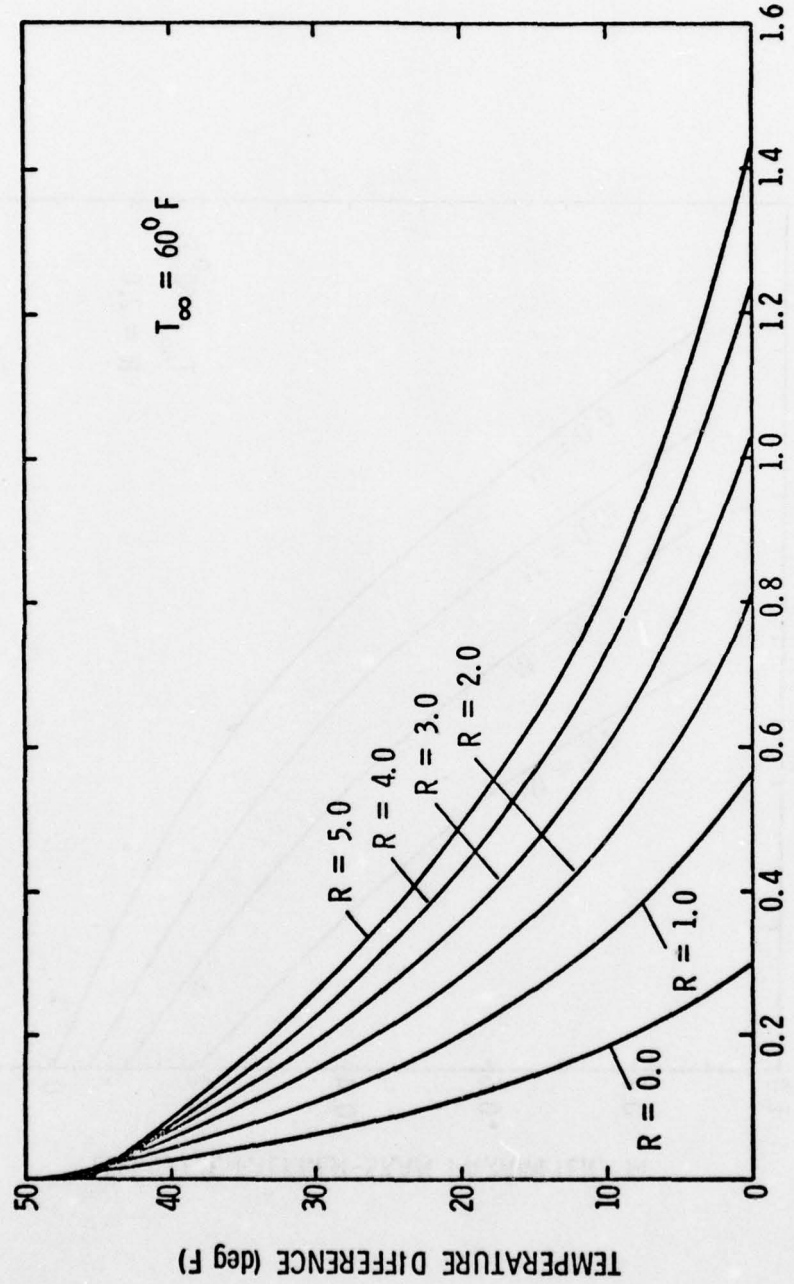
$T_\infty = 60^0 F$
R = 5.0
R = 4.0
R = 3.0
R = 2.0
R = 1.0
R = 0.0
TEMPERATURE DIFFERENCE (deg F)
FALKNER-SKAN PARAMETER, M
0
10
20
30
40
50
0.2
0.4
0.6
0.8
1.0
1.2
1.4
1.6

SLIDE 14

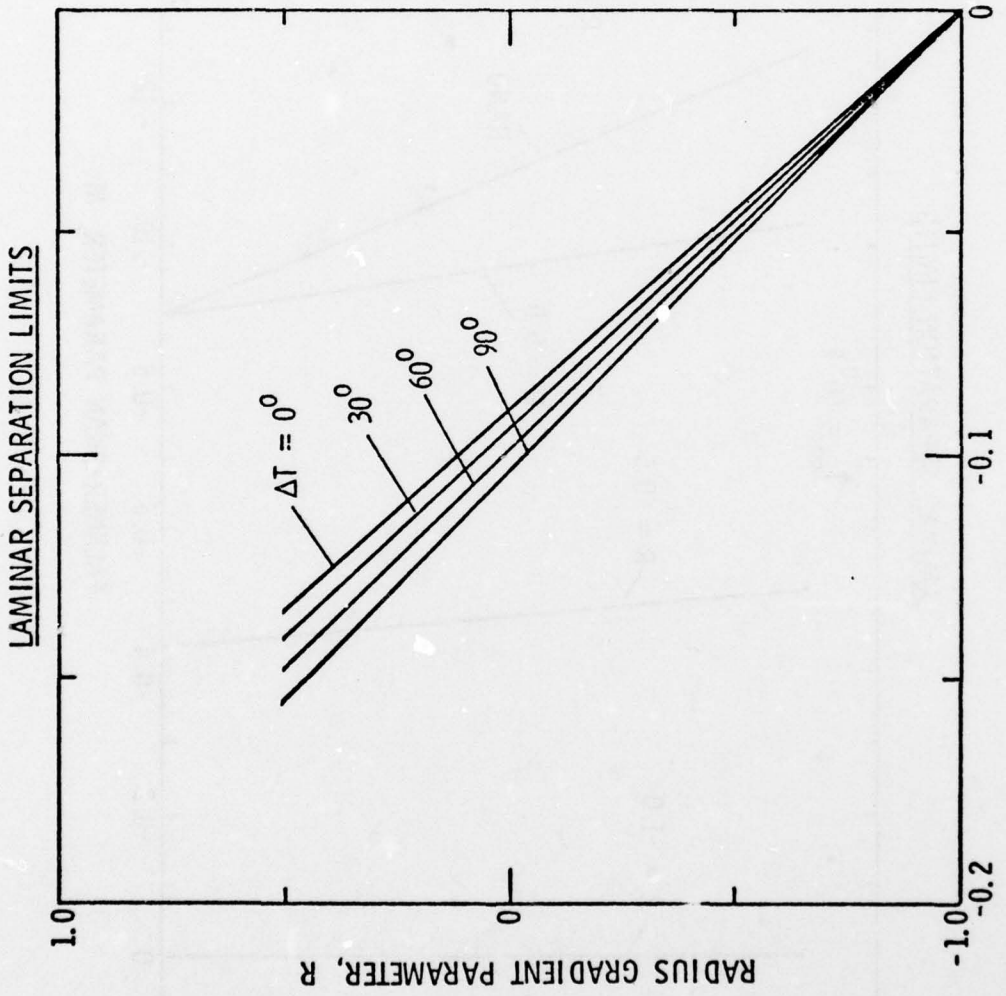
LAMINAR SEPARATION LIMITS
ΔT = 0°
30°
60°
90°
1.0
0
-1.0
0
-0.1
-0.2
RADIUS GRADIENT PARAMETER, R
FALKNER-SKAN PARAMETER, M

SLIDE 15

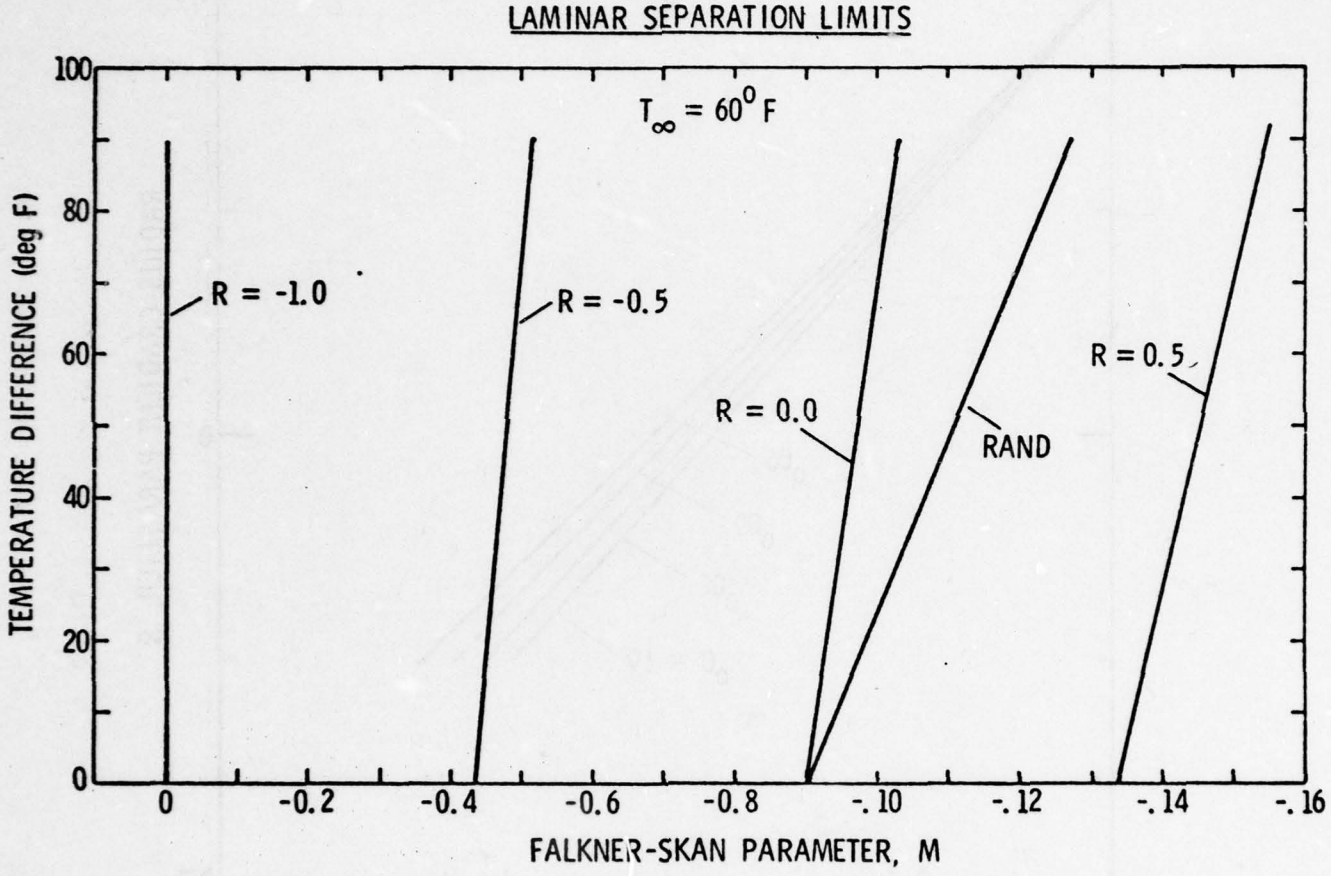
LAMINAR SEPARATION LIMITS
$T_\infty = 60^0$ F
TEMPERATURE DIFFERENCE (deg F)
100
80
60
40
20
0
R = -1.0
R = -0.5
R = 0.0
RAND
R = 0.5
0
-0.2
-0.4
-0.6
-0.8
-.10
-.12
-.14
-.16
FALKNER-SKAN PARAMETER, M

SLIDE 16

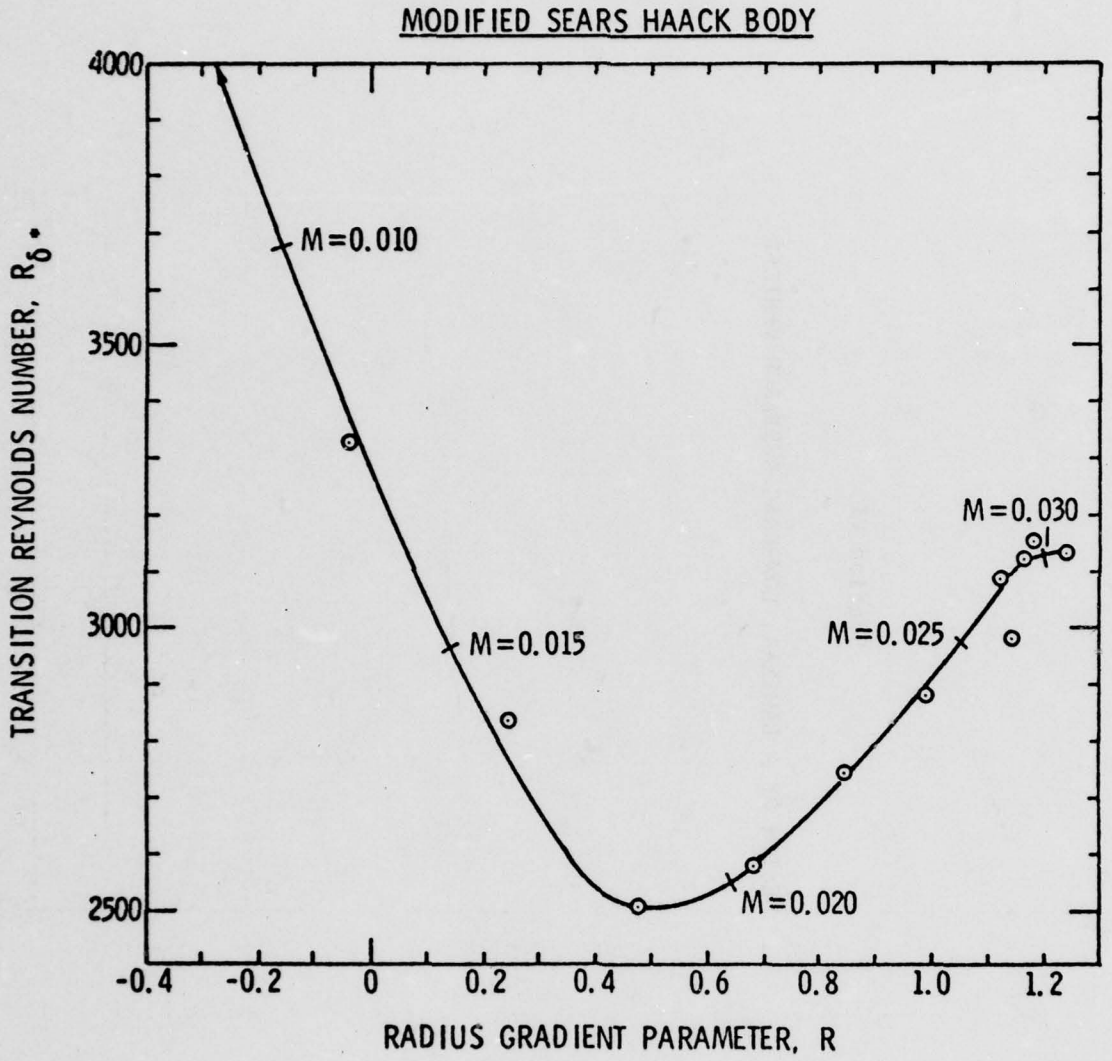
MODIFIED SEARS HAACK BODY
TRANSITION REYNOLDS NUMBER, R_{δ^*}
4000
3500
3000
2500
M=0.010
M=0.015
M=0.020
M=0.025
M=0.030
-0.4
-0.2
0
0.2
0.4
0.6
0.8
1.0
1.2
RADIUS GRADIENT PARAMETER, R

SLIDE 17

Section VI

DESIGN OF A LAMINAR, LOW-DRAG RESEARCH VEHICLE

VI-4 DESIGN OF A LAMINAR, LOW-DRAG RESEARCH VEHICLE

R. S. Scotti, B. H. Carmichael, and D. A. King,
Autonetics Group, Rockwell International, Anaheim, CA

An effort, sponsored by DARPA, is underway to perform the preliminary design of a low-drag research vehicle with a laminar forebody at a transition length Reynolds number to minimum pressure of 250 x 10^6. Boundary layer stability is to be maintained by exploiting the effects of favorable pressure gradient (shape) and distributed surface heating. The present level of understanding of these two effects, particularly in combination, does not allow for their simultaneous optimization without subjective inputs.

The accepted procedure for determining body shape to maintain (or stabilize) laminar boundary layer flow is one of iterative numerical computational trials. The flow field and corresponding stability characteristics must be computed for each trial shape. The addition of surface heating adds new dimensions to the task of optimizing vehicle contours by introducing several new variables such that the best unheated contour is probably not the best heated contour.

A numerical study is being performed at Autonetics following the above iterative approach. Guidance and overall direction is being provided by extensive experience with laminar flows possessed by the second author, by up-to-date results of laminar flow research, and by intuition. The following specific criteria in order of decreasing importance are applied in the process of evaluating candidate designs:

In regard to shape,

1. Primary objective is to achieve a transition Reynolds number (based on length and local free-stream velocity) of 250 x 10^6. Design is to be conservative as judged by all available transition predictive methods. "Conservative" is quantified by the next item.

2. Allow for flexibility of both vehicle operating conditions and test plan. The design must accommodate surface temperature distributions such that,

$$0 < \Delta T(x) \lesssim \Delta T_{max}(x)$$

where $\Delta T_{max}(x)$ is in excess of that predicted to completely damp growth of all small disturbances. Moreover, the design must allow for a progressive approach to the Re_T objective by means of a systematic variation of both vehicle speed and surface temperature field from lower operational transition Reynolds number to 250 x 10^6.

3. Maintain a prismatic coefficient which provides sufficient volume, particularly in the vehicle nose region, to practically accommodate the surface heat exchanger. Also, low sensitivity to angle of attack is to be sought in a rounded nose design.

In regard to size,

4. Maximize test time for a bouyancy-driven vehicle operating from a fixed release depth, while minimizing the effects of residual unsteadiness (acceleration) during "test" and the problem of broaching at the surface.

5. Minimize the effects of surface roughness and waviness within acceptable and reasonable (from the point of view of fabrication) limits.

6. Maintain contact with feasible/practical engineering practices in terms of

   -transportability

   -maneuverability

   -producibility

The stabilizing influences of a local favorable pressure gradient are controlled by vehicle contour and fineness ratio. Those of surface overheat are apparently controlled by both the magnitude and the gradient of the temperature field. In the present study all four variables, i.e., contour, fineness ratio, magnitude of and gradient of temperature are being investigated.

Results in the form of boundary layer flow and corresponding stability characteristics are presented for several promising shapes. These are compared to those of other, earlier conceptual designs in Figures 1 and 2--the first being a plot of some vehicle shapes and corresponding pressure coefficients, while the second displays the boundary layer shape factor, $H = \delta^*/\theta$, over the surface of several vehicles. Also shown in Figure 1 (in brackets) are the disturbance amplitude ratios as computed by Prof. F. Wazzan for the most amplified Tollmien-Schlichting waves in the boundary layer of each body. Indications are that a fair measure of boundary layer stability is provided by the magnitude and history along the vehicle surface of the shape factor H.

The vehicle contour designated as AH-12, which has a rounded nose like the AH-9 (as compared to the pointed AH-8) and a fineness ratio of 4.0 (as compared to 5.0 for the vehicles shown on Figure 1) apparently offers significant improvements in terms of the criteria listed above over others previously studied. Final refinement of this design is in process.

SHAPE AND PRESSURE COEFFICIENT COMPARISON

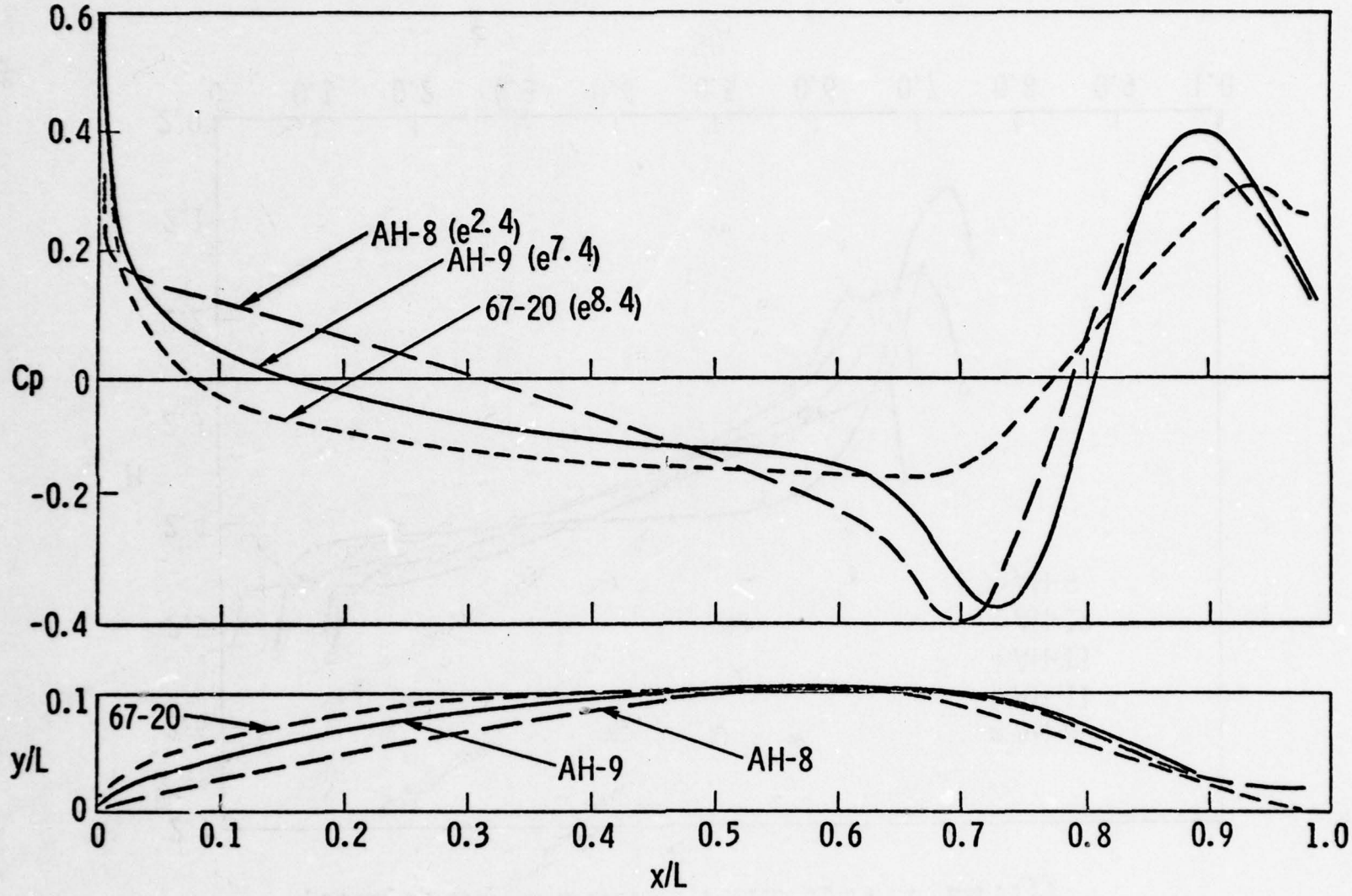

Figure 1.

Rockwell International

GS6-09088

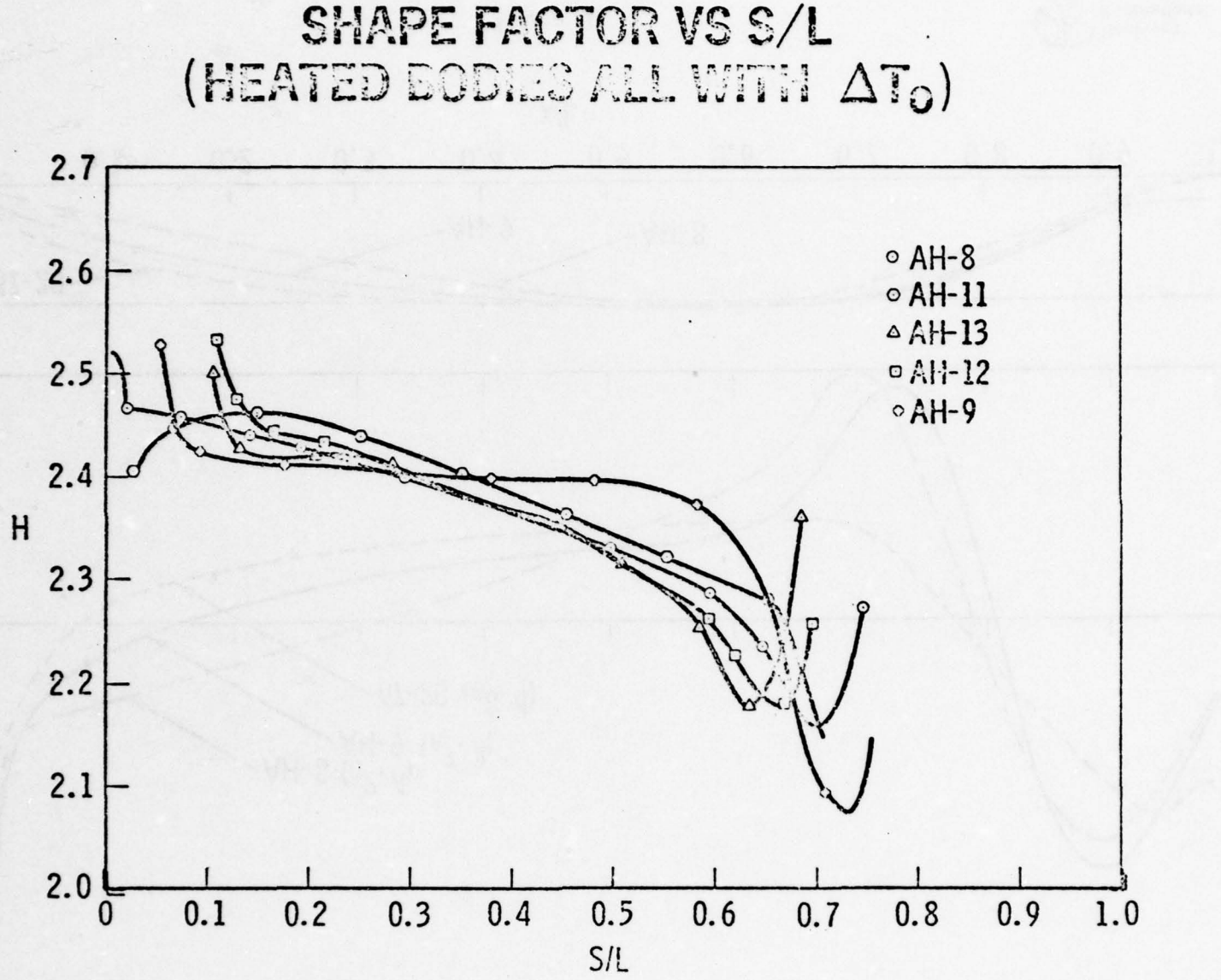
SHAPE FACTOR VS S/L
(HEATED BODIES ALL WITH ΔT_o)
2.7
2.6
2.5
2.4
2.3
2.2
2.1
2.0
H
0
0.1
0.2
0.3
0.4
0.5
0.6
0.7
0.8
0.9
1.0
S/L
AH-8
AH-11
AH-13
AH-12
AH-9

Figure 2.

Section VI

AXISYMMETRIC VEHICLE SYSTEM DESIGN FOR TOTAL PROPULSION POWER OPTIMIZATION

VI-5 AXISYMMETRIC VEHICLE SYSTEM DESIGN FOR TOTAL PROPULSION POWER OPTIMIZATION

F. R. Goldschmied
Westinghouse Research Laboratories
Pittsburgh, Pennsylvania 15235

The design objective is the power minimization for a given useful hull volume and operating speed, since it is the total propulsion-power of the underseas vehicle that is considered, rather than the drag of the bare hull. The design system optimization includes also the fins (to provide the desired degree of stability and maneuverability) with their drag and the propulsor with its efficiency.

Two design optimizations have been approached:

a) Utmost exploitation of laminar boundary-layers, whenever mission and economic constraints appear to allow it.

b) Assumed all-turbulent boundary-layers, when no useful laminar extent can be expected.

The design method is based on the optimum integration of hull design, boundary-layer control (single suction slot) and stern jet propulsion, as presented by Goldschmied.[1] A 60" test model is shown in the wind-tunnel in Fig. 1. Laminar transition is shown at 70% chord by the China Clay technique. The suction slot is visible at 83% chord; the BLC flow is ducted out through the hollow support strut. The experimental pressure distribution at $\pm 6°$ angle of attack is shown in Fig. 2.

The laminar/turbulent axisymmetric transition prediction method is that given by Goldschmied.[2]

At the length Reynolds Number of 10^7, assuming the same tail-fins drag $\Delta C_D = 0.003$ and the same propulsor efficiency of 85% for all cases, the following evaluation can be made:

a) Optimized theoretical all-turbulent Parsons/Goodson/Goldschmied[3]

I-36 body with tail fins and stern wake propeller: power coefficient C_{HP} = 0.0295 (Hull C_D = 0.022).

b) Wind-tunnel test of all turbulent vehicle, with tail-fins and ducted impeller: power coefficient C_{HP} = 0.0145.

c) Optimized theoretical laminar Parsons/Goodson/Goldschmied[3] X-35 body with tail-fins and stern wake-propeller: power coefficient C_{HP} = 0.0120 (Hull C_D = 0.0071).

d) Wind-tunnel test of laminar (72% length) vehicle, with tail-fins and ducted impeller: power coefficient C_{HP} = 0.0106.

It can be readily seen that the system design approach has yielded a 51% power reduction for the all-turbulent case and a 12% power reduction for the laminar case. Furthermore, it is quite significant that the all-turbulent vehicle requires only 21% more power than the laminar X-35 body. The power coefficients are plotted against length Reynolds number in Fig. 3.

Considerably better results may be obtained from a numerical optimization study; mathematical models are available for the hull geometry, the single suction-slot, the axial pump and the stern propulsive jet. For instance, five parameters may be allocated to the hull profile, two parameters to the suction slot, two parameters to the pump and one parameter to the jet; the ten parameters may then be simultaneously optimized by the methods of Ref. 3, subject to a set of suitable constraints.

References

1. F. R. Goldschmied, "Integrated Hull Design, Boundary-Layer Control and Propulsion of Submerged Bodies," AIAA Journal of Hydronautics, Vol. 1, No. 1, July 1967.

2. F. R. Goldschmied, "Transition Prediction Algorithm for Axisymmetric Submerged Bodies," U. S. Navy Sea Systems Command Hydromechanics Committee, 1974 Annual Meeting, Newport, Rhode Island, October 10, 1974.

3. J. S. Parsons, R. E. Goodson and F. R. Goldschmied, "Shaping of Axisymmetric Bodies for Minimum Drag in Incompressible Flow," AIAA Journal of Hydronautics, Vol. 8, No. 3, July 1974.

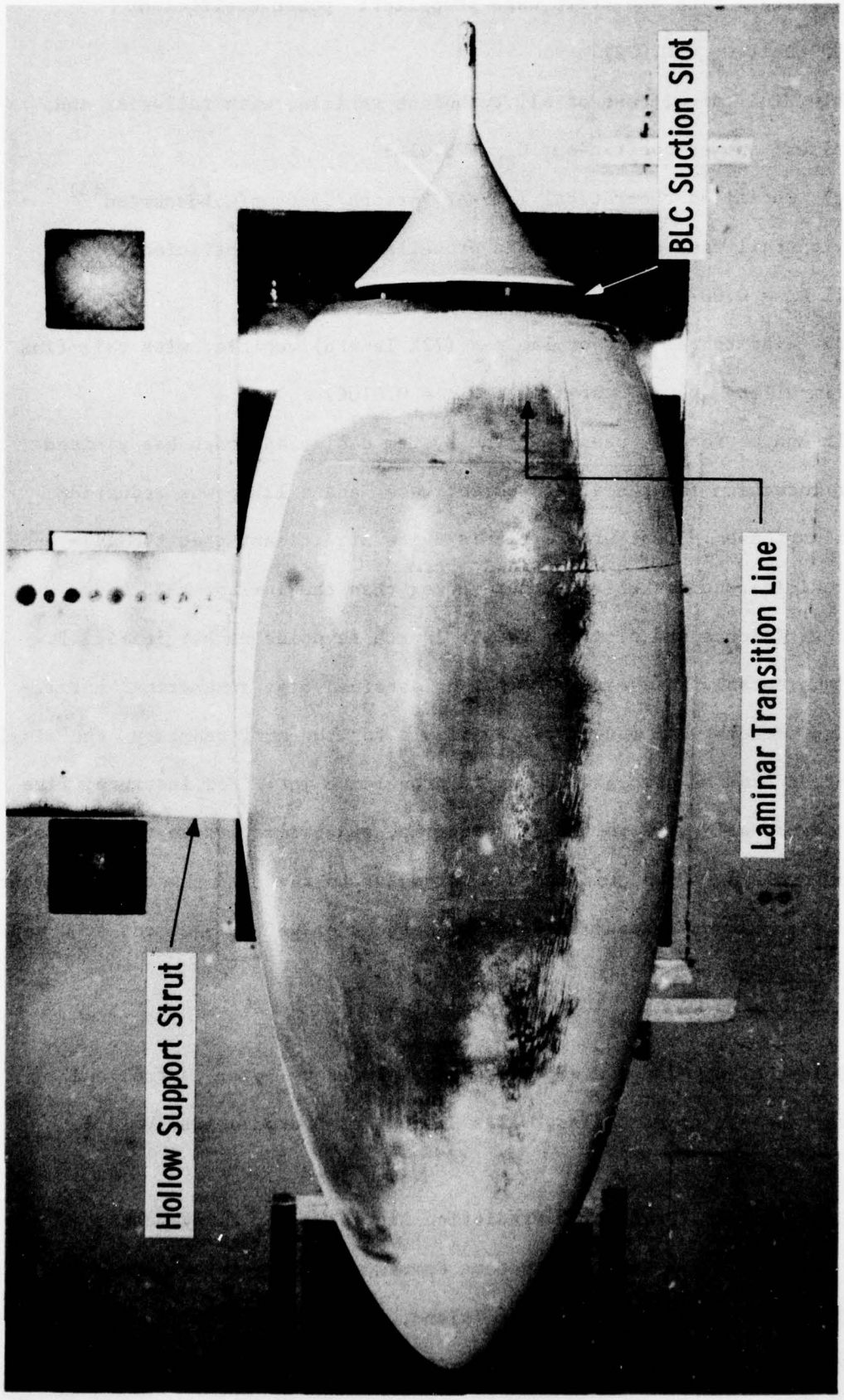

Fig. 1 — Photo of 60" test model in wind-tunnel

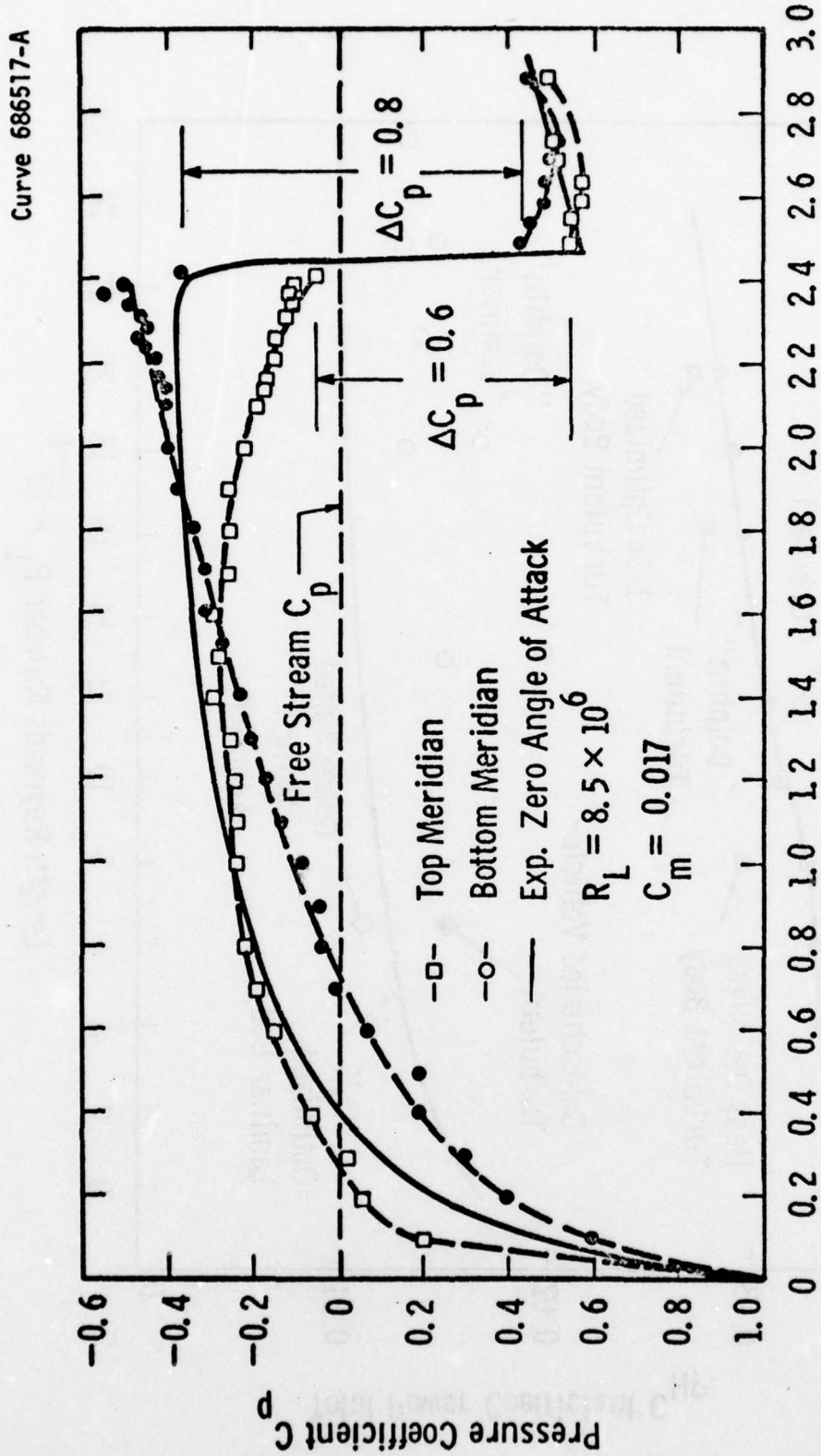

Fig. 2 – Experimental pressure distribution at 6° angle of attack

R. Goldschmied
m. s. - r. m. 8-18-76

Curve 686517-A

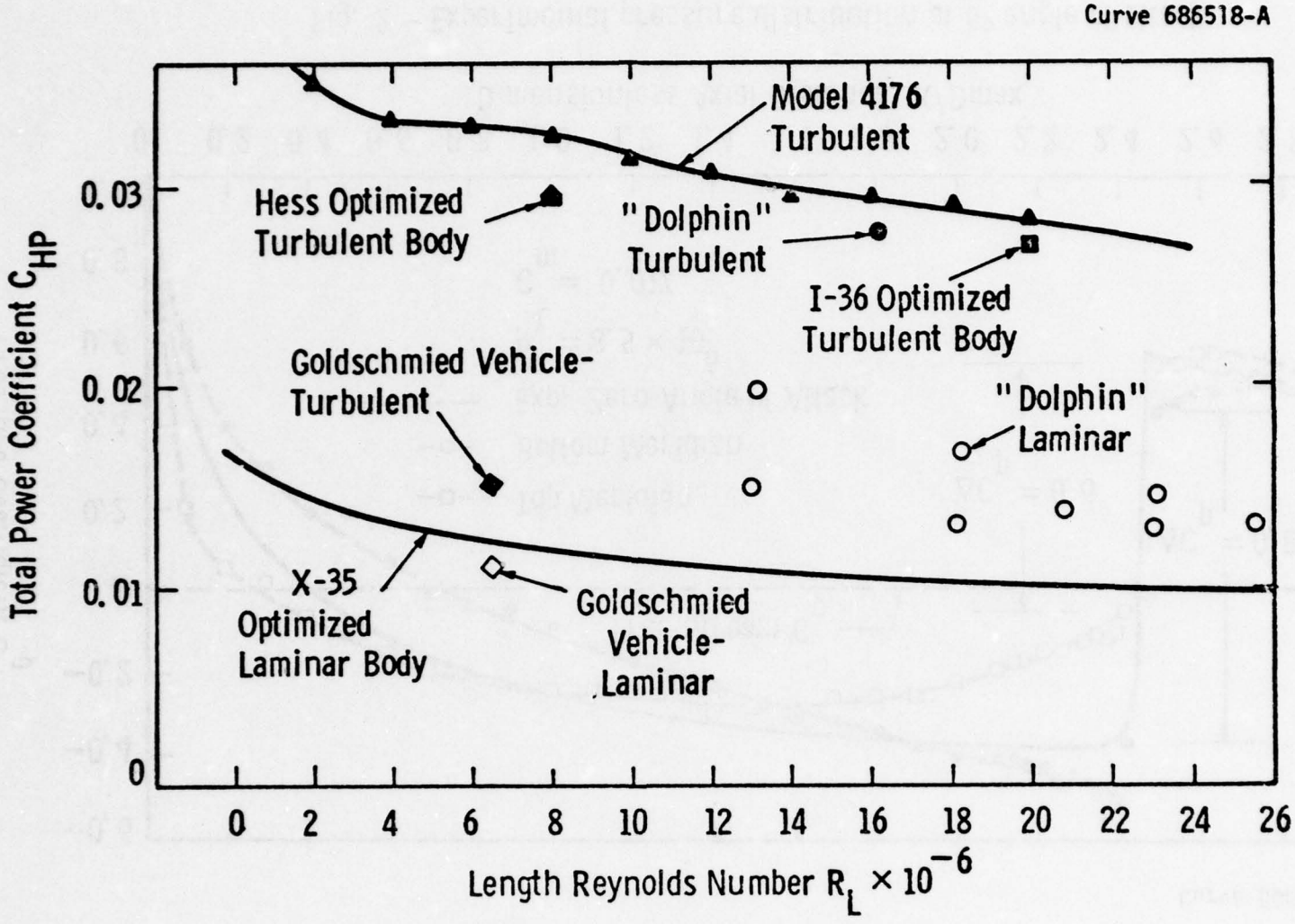

Fig. 3 — Power coefficients summary plot

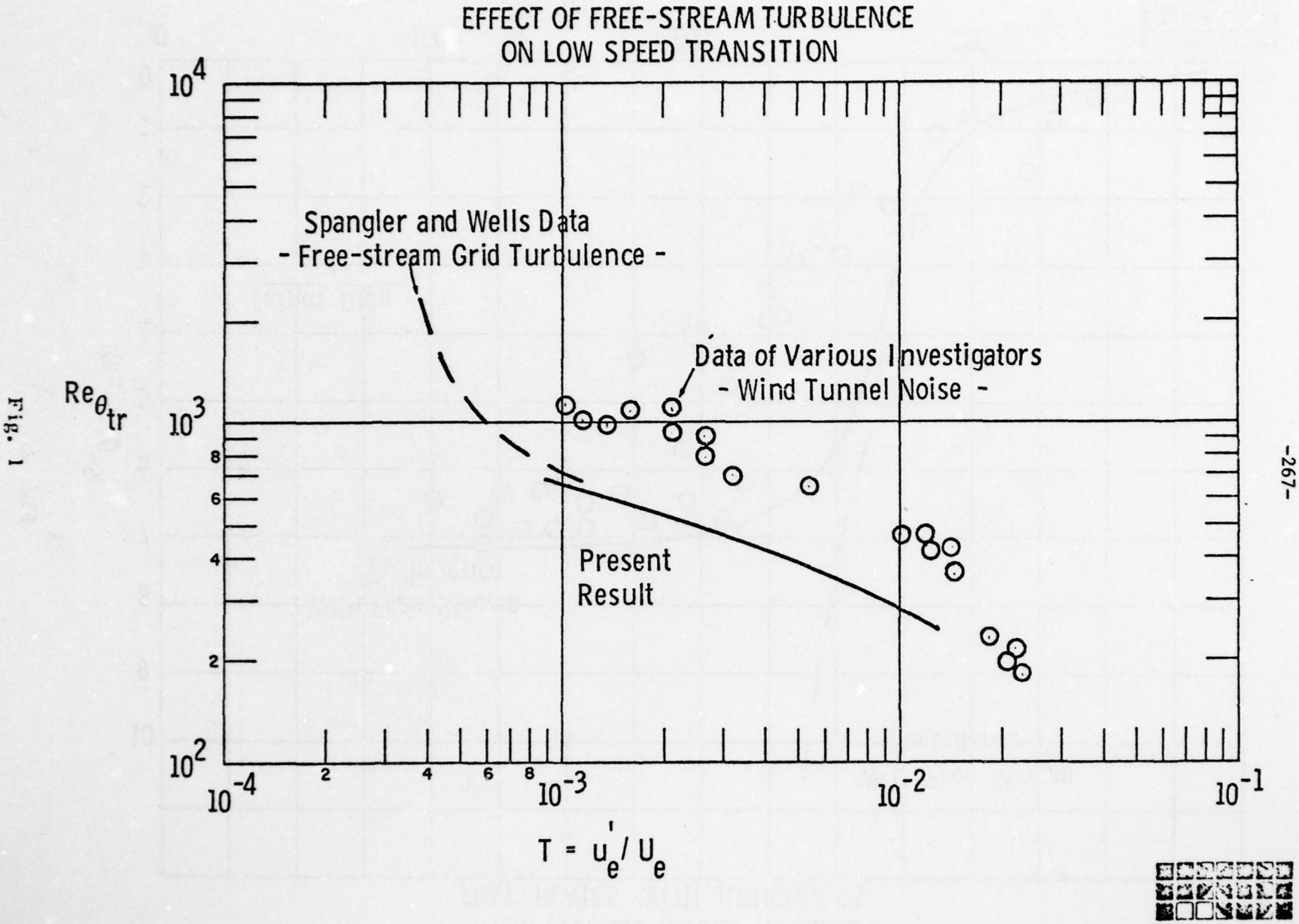
EFFECT OF FREE-STREAM TURBULENCE
ON LOW SPEED TRANSITION
Spangler and Wells Data
- Free-stream Grid Turbulence -
Data of Various Investigators
- Wind Tunnel Noise -
Present
Result
$Re_{\theta_{tr}}$
$T = u_e'/U_e$
10^4
10^3
10^2
8
6
4
2
10^{-4}
10^{-3}
10^{-2}
10^{-1}

Fig. 1

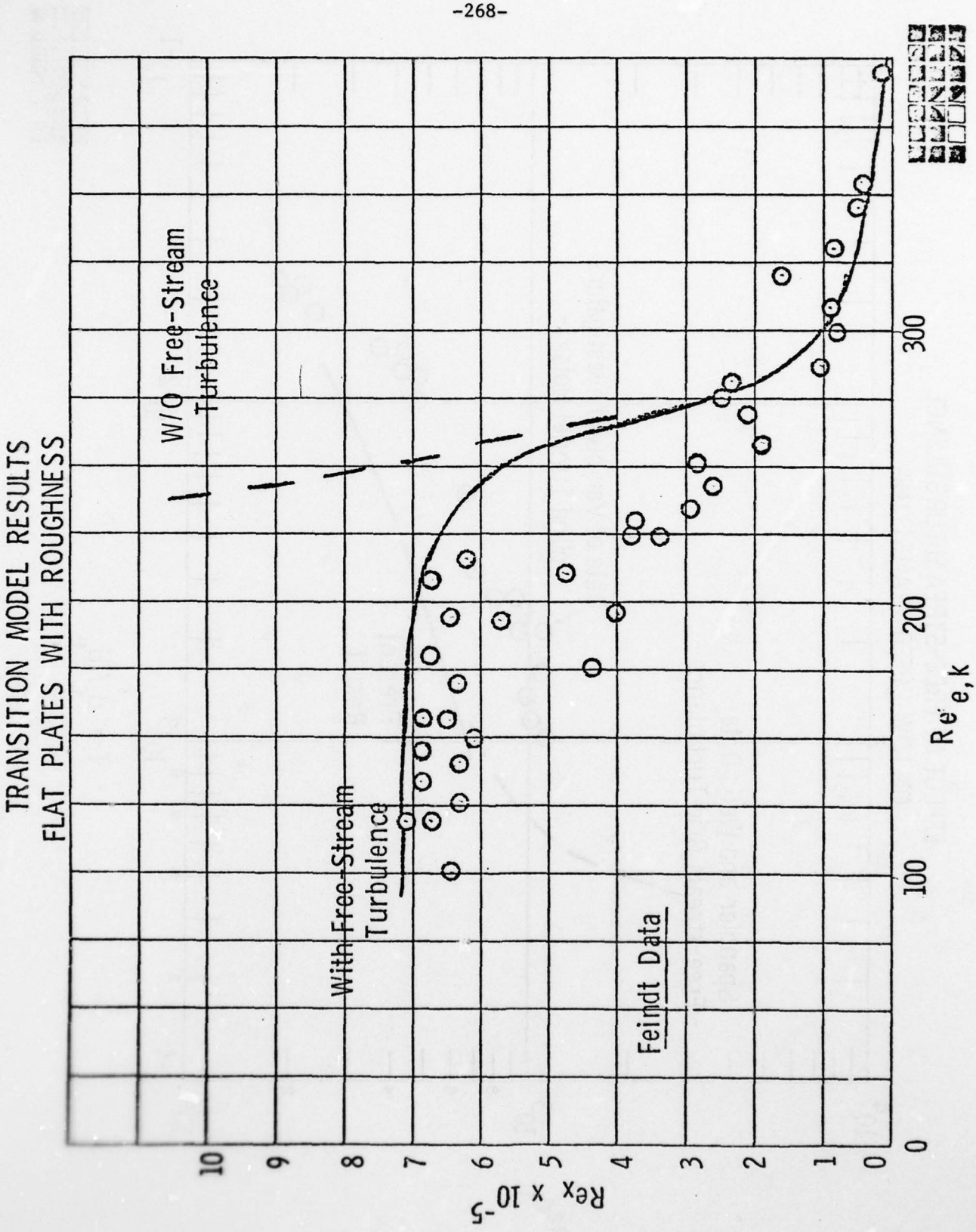
TRANSITION MODEL RESULTS
FLAT PLATES WITH ROUGHNESS
W/O Free-Stream Turbulence
With Free-Stream Turbulence
Feindt Data
$Re_{x} \times 10^{-5}$
$Re_{e,k}$
0
1
2
3
4
5
6
7
8
9
10
0
100
200
300

Fig. 2

INFORMAL PRESENTATIONS

SIMPLE RELATIONS FOR THE STABILITY OF HEATED LAMINAR BOUNDARY LAYERS IN WATER: MODIFIED DUNN-LINN METHOD

J. Aroesty, W. S. King, G. M. Harpole,
W. Matyskiela, A. R. Wazzan, C. Gazley, Jr.
The Rand Corporation
Santa Monica, California

ABSTRACT

We have developed a modification of Lin's method which can be used to estimate the minimum critical Reynolds number of a heated laminar boundary layer in water. This method is both simple and surprisingly accurate. As in Lin's original work, the method is most applicable when $c \to 0$, $\alpha \to 0$ and $\alpha Re \to \infty$. The internal details of the method do not agree entirely with exact analyses in other ranges of these parameters but the few required constants have been chosen so that predictions of minimum critical Reynolds number are consistent with results of more elaborate numerical integration of the Orr-Summerfeld equations (Fig. 1).

This method, which we have labeled the "modified Dunn-Lin method," can be used with confidence in engineering studies of laminar boundary layer control in water. The details of the method are reported in Ref. 1 and a summary of the equations used to estimate minimum critical Reynolds number is given below:

$$v(c)(1 - 2\lambda(c)) = .58$$

$$v(c) = \frac{\pi u''_c {}'_w}{u'^3_c}$$

$$\lambda = .4 \left\{ \left[1 - \frac{u'(c)}{u'(0)}\right] + .5 \left[1 - \frac{\mu(c)}{\mu(0)}\right] \right\}$$

$$(Re_{\delta^*})_{critical} \cong \frac{28u'(0)\mu(0)}{c^4}$$

The parameters v, λ, and Re_{δ^*} depend on the characteristics of the velocity profiles $u(\eta)$ and $u''(\eta)$ and the viscosity u evaluated at the wall and the critical layer.

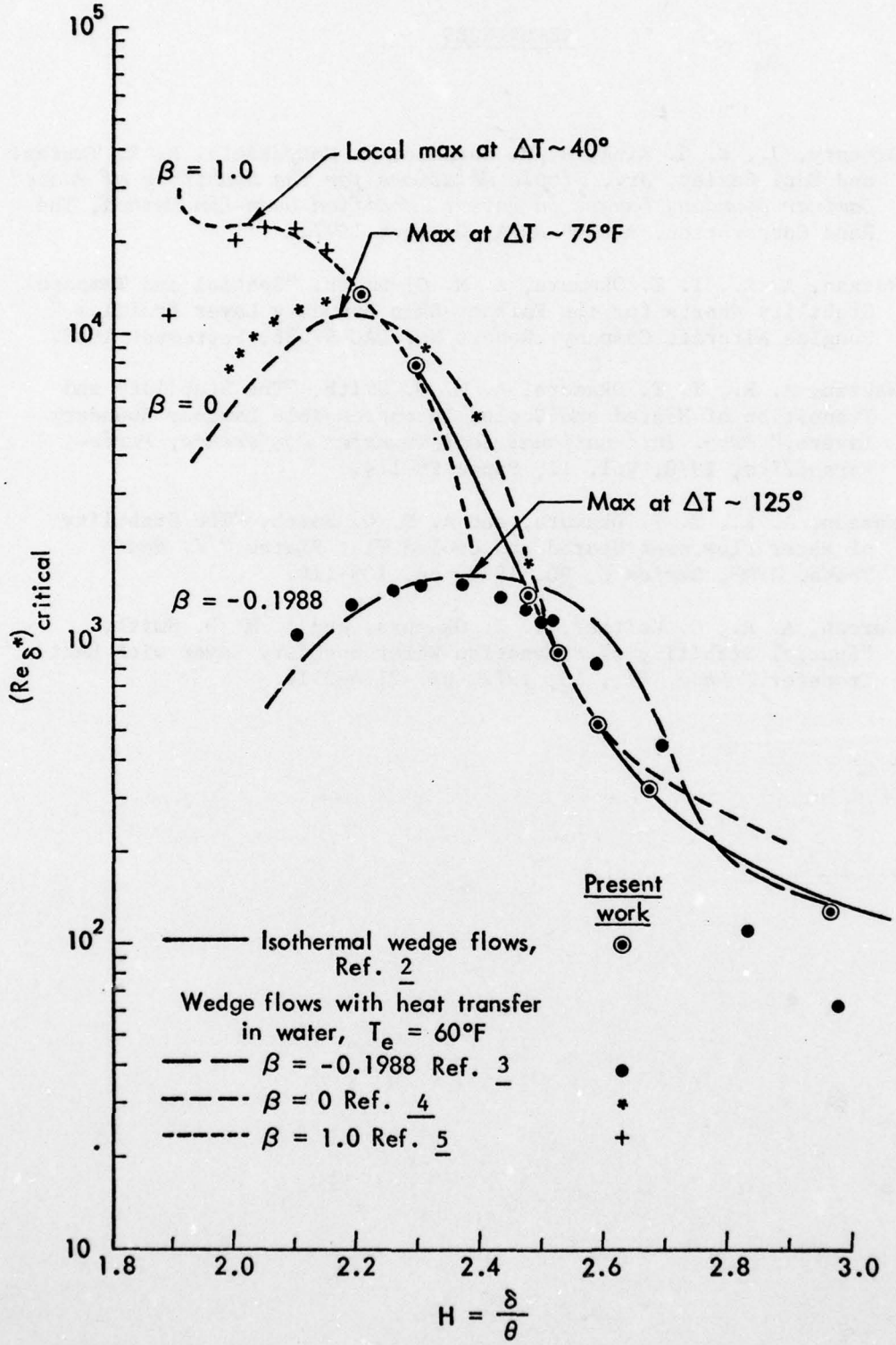

Fig. 1 — Comparison between modified Dunn-Lin method and numerical solution of the Orr-Sommerfeld equation

REFERENCES

1. Aroesty, J., W. S. King, G. M. Harpole, W. Matyskiela, A. R. Wazzan, and Carl Gazley, Jr., *Simple Relations for the Stability of Heated Laminar Boundary Layers in Water: Modified Dunn-Lin Method*, The Rand Corporation, R-2209-ARPA, October 1977.

2. Wazzan, A. R., T. T. Okamura, A. M. O. Smith, "Spatial and Temporal Stability Charts for the Falkner-Skan Boundary Layer Profiles," Douglas Aircraft Company, Report No. DAC-67086, September 1968.

3. Wazzan, A. R., T. T. Okamura, A. M. O. Smith, "The Stability and Transition of Heated and Cooled Incompressible Laminar Boundary Layers," *Proc. International Heat Transfer Conference, Paris-Versailles*, 1970, Vol. II, Paper FC-1.4.

4. Wazzan, A. R., T. T. Okamura, and A. M. O. Smith, "The Stability of Water Flow over Heated and Cooled Flat Plates," *J. Heat Trans. ASME*, Series C, 90, 1968, pp. 109-114.

5. Wazzan, A. R., G. Keltner, T. T. Okamura, and A. M. O. Smith, "Spatial Stability of Stagnation Water Boundary Layer with Heat Transfer," *Phys. Fl.*, 15, 1972, pp. 2114-2116.

Primary and Secondary Instabilities in Unstably Stratified Shear Flows

by

R.E. Kelly and R.M. Clever
Mechanics and Structures Department
School of Engineering and Applied Science
University of California, Los Angeles, Cal. 90024

It has been known for many years that instability in an unstably stratified shear flow (due, say, to heating from below) can occur in a manner quite dissimilar to that characteristic of the homogeneous case. For the latter case, Tollmien-Schlichting waves, which are two-dimensional in the plane of the flow, constitute the initial instability. For the unstably stratified case, however, disturbances can first appear which are periodic in a plane normal to the flow and which exhibit no streamwise waviness. These disturbances induce a distortion of the mean flow, however, and are therefore three-dimensional in this sense.

We call these buoyancy-driven instabilities longitudinal "rolls" or "vortices", in order to distinguish them from the hydrodynamically-driven waves. In appearance, they are similar to Görtler vortices, and so it was appropriate that Görtler wrote the first review paper on their occurrence (Ref. 1). This paper contains most of the references to the (mainly qualitative) experimental work on this instability done in the period 1920-1940. More recent experimental work concerns the case of a very large Prandtl number fluid (Ref. 2; the results are pertinent to convection in the earth's mantle), the effects of shear upon doubly-diffusive instability (Ref. 3), and convection in the thermal-entry flow (Ref. 4,5). However, analogous

work has been done in connection with free convection flows occurring on heated inclined surfaces, where similar rolls are observed for sufficiently large angles of inclination away from the vertical (Refs. 6-9). The experiments for fully developed flows indicate that the main effect of the shear, at least for low values of the Reynolds number (Re), is to organize the convection in the manner described above (i.e., as spanwise periodic longitudinal rolls).

This conclusion agrees with the theoretical results for fully developed flows, e.g., Couette flow (Ref. 10-11) and Poiseuille flow (Ref. 12). These analyses indicate that, for small amounts of shear, all disturbances are stabilized by the shear except for the longitudinal roll disturbance which, because it is independent of the streamwise coordinate, cannot be influenced by the shear. Thus, it will become unstable as soon as the Rayleigh number (Ra) exceeds the critical value ($Ra_c = 1708$ for a flow contained between two rigid horizontal surfaces). For such flows, therefore, only the Rayleigh number is important for finding the condition under which the flow becomes unstable due to buoyancy. The Reynolds, Froude, and Richardson numbers are not pertinent to predicting the onset of the longitudinal convective mode of instability for fully developed flows. Naturally, they are pertinent to predicting the onset of the two-dimensional shear instability which can occur at higher values of the Reynolds number with $Ra < Ra_c$.

Whether or not a similar conclusion holds for the case of an unstably stratified boundary layer still is an unanswered question (the experiments of Strazisar et al. (Ref. 13) concern a <u>stably</u>

stratified boundary layer). The theoretical analysis of the stability of such a boundary layer is complicated by the fact that nonparallel flow effects are likely to play an important role in determining the neutral stability curve of the longitudinal roll mode. Again, an analogy with Görtler vortices can be made, in which case the most critical disturbance on the basis of a parallel flow analysis turns out to have an infinite wavelength (see Fig. IX.4 of Ref. 14). This is in contrast to shear instabilities, partly because the longitudinal mode has no frequency and is therefore independent of time along the neutral curve. Thus, the parallel flow stability equation becomes purely diffusive at the edge of the boundary layer. By including one nonparallel flow term (corresponding to the vertical velocity) at lowest order for the heated inclined plate stability problem, Haaland and Sparrow (Ref. 15) were able to obtain a finite wavelength for the critical disturbance. Such a simple solution is unlikely for the case of a Blasius-like boundary layer because the vertical velocity at the edge of the boundary layer is in a direction opposite (outwards) to that of the free convection boundary layer (inwards). The importance of effects associated with streamwise variations might explain why the experimental critical Rayleigh numbers for the thermal entry flow as reported by Kamotani and Sparrow (Ref. 5) are so far above the theoretical predictions of Hwang and Cheng (Ref. 16), who did a "local" parallel flow stability analysis. If such effects are important at lowest order, then the Reynolds and Prandtl numbers will become important in determining the neutral stability of the rolls.

Other theoretical work on the problem of thermal convection in a shear flow has concerned the unstably stratified Ekman boundary layer flow (Ref. 17) in order to understand the "cloud band" structure often observed in the earth's planetary boundary layer (Ref. 18). Numerical work has been done which indicates how the rolls distort the mean velocity profile (Refs. 19-21) and how the disturbance field develops in time (Ref. 22).

At UCLA, our research has concentrated upon determining what happens to the rolls as the Rayleigh number increases beyond the critical value for the case of Couette flow (with a Prandtl number of 0.7). It is known for the case without shear (Ref. 23) that convective rolls can themselves become unstable and lead to three-dimensional and possibly unsteady flow as the Rayleigh number so increases. For the case when shear is present, the development of three-dimensionality (in the sense now that the roll becomes wavey in the streamwise direction) means that the perturbed roll can extract energy from the mean flow. Although the rolls occur originally due to buoyant effects, their secondary instability can be controlled by hydrodynamic effects and might lead therefore to a more severe disruption of the basic flow than provided by the rolls themselves. In this sense, the rolls can be viewed as introducing a "thermal roughness" into the flow, with possibly all the consequences that more ordinary roughness elements provide.

The analysis is a numerical one, based on use of the Galerkin method, as discussed in Ref. 23. It consists of the following steps: (1) Calculate the disturbance field associated with the rolls (including distortion of the mean velocity) for arbitrary Rayleigh

numbers;

(2) perturb the resulting (nonplanar) velocity and temperature distributions by a three-dimensional, time-dependent disturbance and find a neutral curve for the secondary instability as a function of the Rayleigh and Reynolds numbers;

(3) calculate the secondary disturbance energy equation so as to understand the mechanism causing the secondary instability.

The results will soon be submitted for publication and are not presented here in detail. However, they can be summarized as follows.

A secondary instability is possible which is very much dependent upon the Reynolds number. As Re increases to about 100, the value of $Ra - Ra_c$ at which the secondary instability occurs decreases to about 60, i.e., it occurs when Ra is about 3.5% above the critical value when $Re > 100$. The most unstable secondary disturbance travels with a wavespeed equal to the mean of the basic flow (for the antisymmetric Couette flow investigated, it was stationary). A second mode is possible which propagates relative to the mean of the basic flow, but it occurs only for larger values of $Ra - Ra_c$.

The eigenvalue calculations indicate therefore that shear can destabilize the rolls. The energy calculations indicate that distortions of the basic flow, both in the plane of the flow and normal to it, act as a major source for disturbance energy. Thus, the idea of the rolls acting as a source of "thermal roughness" seems to make sense. However, this does not imply that an immediate breakdown into turbulence would occur. An early observation

of wavey rolls in Poiseuille flow was made by Avsec (Ref. 24); the rolls are well-defined and are certainly not turbulent. For the case of free convection flow in an inclined, differentially heated box, Hart (Ref. 8) shows that the rolls must become quite distorted before "turbulence" occurs (see his Fig. 3; still, the turbulence occurs for values of Ra much less than those necessary for ordinary "turbulent" convection in a horizontal container). The situation there is probably similar to that observed in connection with Taylor vortices (Ref. 25), in which a sequence of states must be completed before the flow becomes turbulent. A similar sequence probably occurs for the kind of unstably stratified shear flows discussed here. However, the range of Rayleigh number necessary for the completion of the sequence might be very much dependent upon the Reynolds number. Thus, the neutral curves which define the sequence of states might bunch together as the Reynolds number increases, allowing transition to occur for very modest Rayleigh numbers at high enough Reynolds numbers. The best way to explore this possibility is by means of a carefully controlled experiment.

Acknowledgment

The research summarized at the end of this paper has been supported by the U.S. Army Research Office under Grant DA-ARO-D-31-124-72-G168.

References

1. Görtler, H., "Analogie zwischen der Instabilitäten laminaren Grenzschichtströmungen an konkaven Wänden und an erwärmter Wänden," Ingenieur-Archiv V. 28(1959), pp. 71-78.

2. Richter, F.M. and B. Parsons, "On the Interaction of Two Scales of Convection in the Mantle," J. Geophys. Res. v. 80 (1975), pp. 2529-2541.

3. Linden, P.F., "Salt Fingers in a Steady Shear Flow," Geophys. Fluid Dynamics v. 6 (1974), pp. 1-27.

4. Ostrach, S. and Y. Kamotani, "Heat Transfer Augmentation in Laminar Fully Developed Channel Flow by Means of Heating from Below," J. Heat Trans. (Trans. ASME, Ser. C), v. 97 (1975), pp. 220-225.

5. Kamotani, Y. and S. Ostrach, "Effect of Thermal Instability on Thermally Developing Laminar Channel Flow," ASME Paper 76-HT-R (1976).

6. Lloyd, J.R. and E.M. Sparrow, "On the Instability of Natural Convection Flow on Inclined Plates," J. Fluid Mech. v. 42 (1970), pp. 465-470.

7. Sparrow, G.M. and R.B. Husar, "Longitudinal Vortices in Natural Convection Flow on Inclined Plates," J. Fluid Mech. v. 37 (1969), pp. 251-255.

8. Hart, J.E., "Stability of the Flow in a Differentially Heated Inclined Box," J. Fluid Mech. v. 47 (1971), pp. 547-576.

9. Hart, J.E., "Transition to a Wavy Vortex Regime in Convective Flow between Inclined Plates," J. Fluid Mech. v. 48 (1971), pp. 265-271.

10. Deardorff, J.W., "Gravitational Instability between Horizontal Plates with Shear," Phys. Fluids v. 8 (1965), pp. 1027-1030.

11. Gallagher, A.P. and A. McD. Mercer, "On the Behavior of Small Disturbances in Plane Couette Flow with a Temperature Gradient," Proc. Roy. Soc. (A), v. 286 (1965), pp. 117-128.

12. Gage, K.S. and W.H. Reid, "The Stability of Thermally Stratified Plane Poiseuille Flow," J. Fluid Mech., v. 33 (1968), pp. 21-32.

13. Strazisar, A.J., J.M. Prahl, and E. Reshotko, Experimental Study of the Stability of Heated Laminar Boundary Layers in Water, Case Western Reserve Univ. Fluid, Thermal, and Aerospace Sci. Rep. FTAS/TR-75-113 (1975).

14. Rosenhead, L. (ed.), Laminar Boundary Layers, Oxford (1963).

15. Haaland, S.E. and E.M. Sparrow, "Vortex Instability of Natural Convection Flow on Inclined Surfaces," Int. J. Heat Mass Trans. v. 16 (1973), pp. 2355-2367.

16. Hwang, G.J. and K.C. Cheng, "Convective Instability in the Thermal Entrance Region of a Horizontal Parallel-Plate Channel Heated from Below," J. Heat Trans. (Trans. ASME, Ser. C) v. 95 (1973), pp. 72-77.

17. Asai, T. and I. Nakasuji, "On the Stability of Ekman Boundary Layer Flow with Thermally Unstable Stratification," J. Meteor. Soc. Japan v. 51 (1973), pp. 29-42.

18. Kuettner, J.P., "Cloud Bands in the Earth's Atmosphere: Observation and Theory," Tellus v. 23 (1971), pp. 404-425.

19. Ogura, Y. and A. Yagihashi, "A Numerical Study of Convection Rolls in a Flow between Horizontal Parallel Plates," J. Meteor. Soc. Japan v. 47 (1969), pp. 205-217.

20. Mori, Y. and Y. Uchida, "Forced Convective Heat Transfer between Horizontal Flat Plates," Int. J. Heat Mass Trans. v. 9 (1966), pp. 803-817.

21. Hwang, G.J. and K.C. Cheng, "A Boundary Vorticity Method for Finite Amplitude Convection in Plane Poiseuille Flow," Devel. in Mechanics v. 6 (1971), pp. 207-220.

22. Lipps, F.B., "Two-Dimensional Numerical Experiments in Thermal Convection with Vertical Shear," J. Atm. Sci. v. 28 (1971), pp. 3-19.

23. Clever, R.M. and F.H. Busse, "Transition to Time-Dependent Convection," J. Fluid Mech. v. 65 (1974), pp. 625-645.

24. Avsec, D., "Sur les Formes Ondulées des Tourbillons en Bandes Longitudinales," Comptes Rendus Acad. Sci. v. 204 (1937), pp. 167-169.

25. Coles, D., "Transition in Circular Couette Flow," J. Fluid Mech. v. 21 (1965), pp. 385-425.

ROUGHNESS EFFECTS ON TRANSITION ON AN ELLIPSOID
-PRELIMINARY RESULTS-

by

M. M. Reischman & G. L. Donohue
Naval Undersea Center
San Diego, California 92132

Presented at the RAND Low Speed Transition
Workshop
Santa Monica, CA

September 1976

The adverse effect of surface roughness on a stabilized boundary layer is well known, but quantitative data is lacking. The research discussed herein is centered on obtaining transition data on a constant-pressure body with wall heating and a variety of surface roughnesses. The transition location will be determined by laser anemometer measurements made in the NUC low-turbulence water tunnel, capable of a model length Reynolds numbers of $7X10^6$. Surface roughness of 8, 32, 64 and 120 micro-inch will be tested with surface overheats of 5 and 10^oF being applied. The purpose of this paper is to discuss the experimental facility being used and to present preliminary results of transition measurements performed on smooth and roughened, 9:1 ellipsoids of revolution at ambient wall temperature.

It is important that the experiments be carried out in a well-characterized experimental facility. The NUC water tunnel has a turbulence level of less than 0.2% over the entire speed range of 0-16 m/sec. Transition Reynolds numbers of approximately $2 - 3 \times 10^6$ are observed for this freestream turbulence level. The freestream velocity, acoustic and vibration variations have been well-characterized in terms of level and spectra. The test section configuration is an open-jet type, with a jet diameter of approximately 300 mm. The tunnel is a recirculating type with an essentially infinite run time.

Transition location is determined by analysis of laser anemometer measurements of velocity fluctuations made near the body surface at sequential arc length locations. Determination of the freestream velocity for each location (X/L_2) at which the turbulence level exceeds some prescribed value (~1%) defines the transition Reynolds number, R_{L_2}.

A nine-to-one ellipsoid of revolution (50 mm maximum diameter) was chosen as the basic test body due to its previously well-characterized behavior and its hydrodynamic simplicity. The body has an essentially zero pressure gradient history for a large portion of its length, with a minimal region of adverse pressure gradient over the afterbody. The confounding of transition delay due to pressure gradient with the effects of wall heating and roughness is minimized. Two models have been constructed thus far. The first is the baseline model. It is a smooth (surface roughness of 8 microinches rms) anodized aluminum body instrumented with internally-mounted thermistors for the measurement of the axial temperature distribution. The body is heated via an axisymmetric parallel-flow heat exchanger using hot water pumped in from outside the tunnel as the working fluid.

The temperature distribution can be controlled by varying the heating fluid mass flow rate, inlet temperature and flow direction. Figure 1 shows the model configuration. The second body is identical to the first except for material (stainless steel) and surface roughness. The first roughened model has a lath-machined 120 rms finish (two- dimensional distributed roughness). The succeeding models will have the same overall configuration but with 64, 32 and 16 rms microinch finishes.

Test results obtained thus far are preliminary in nature and do not include the effects of wall heating. Partial results of the flow field characterization measurements are shown in Figure 2, which also describes the body geometry. The calculated $Ue/U\infty$ and C_p as a function of x are done at a $Re_{L_2} = 6.5X10^6$, the measured data points were taken at $4.3X10^6$. Considering the Re difference, all measurements are within experimental error of the predicted values.

Transition measurements made thus far are summarized in Figure 3. The solid and dashed curves represent the transition measurements obtained in the NASA-Ames and Northrop Aircraft wind tunnels on a similar 9:1 ellipsoidal model. The turbulence level for those measurements was reported to be 0.02 and 0.12% respectively. The data points for a smooth body of revolution in the NUC water tunnel (turbulence level $\approx$ 0.2%) are in reasonable agreement with these data. A transition value predicted by an McDonnell-Douglas analysis using the Transition Analysis Program System (TAPS) code is also shown. This code uses a spatial linear stability analysis to predict transition.

The limited data taken on the roughened model under the same freestream conditions is described by the closed data points in Figure 3. The k/θ values at the measured transition point (X/L_2) range from .021 to .041 values smaller than one might expect to trigger transition according to Ko and Kosecoff (1). If one selects k/θ of 0.2 (see ref. (1)) as a value which will "tickle" a laminar boundary layer and ultimately result in transition, the corresponding axial locations are 3-7 mm from the nose. It should also be noted that the data reported here qualitatively agree with the surface smoothness data presented by Smith (2).

REFERENCES

1. "An Analytical Study of the Effect of Surface Roughness on the Stability of a Heated Water Boundary Layer", Ko, D.R.S. and Kosecoff, M., Presented at RAND Low Speed Transition Workshop, Santa Monica, CA, Sep 1976

2. "Laminarization of Water Boundary Layers over Bodies of Revolution", Smith A.M.O. and Wazzan, A.R., Presented at RAND Low Speed Transition Workshop, Santa Monica, CA, Sep 1976

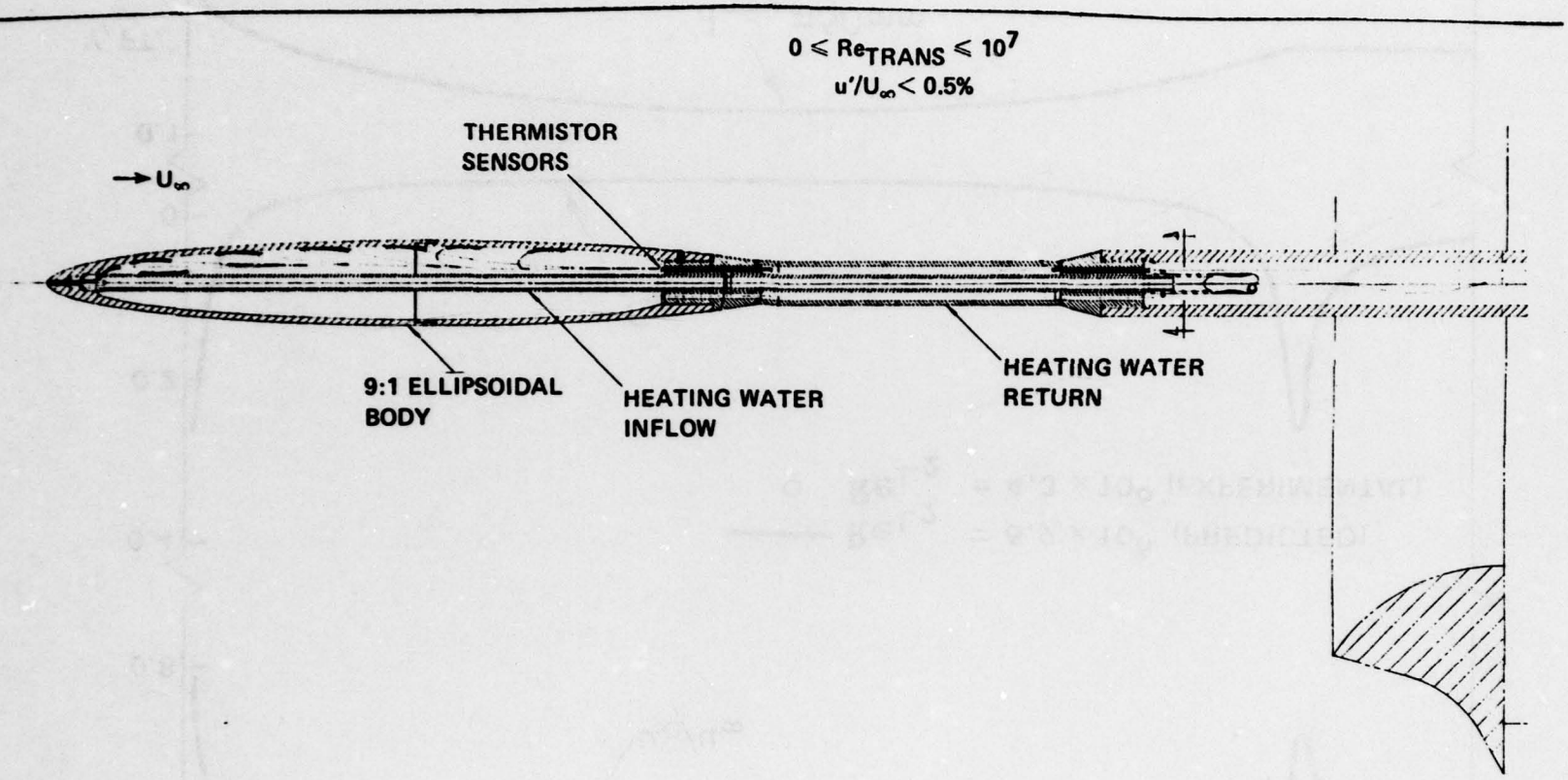

Figure 1. Schematic of thermally stabilized boundary layer transition study.

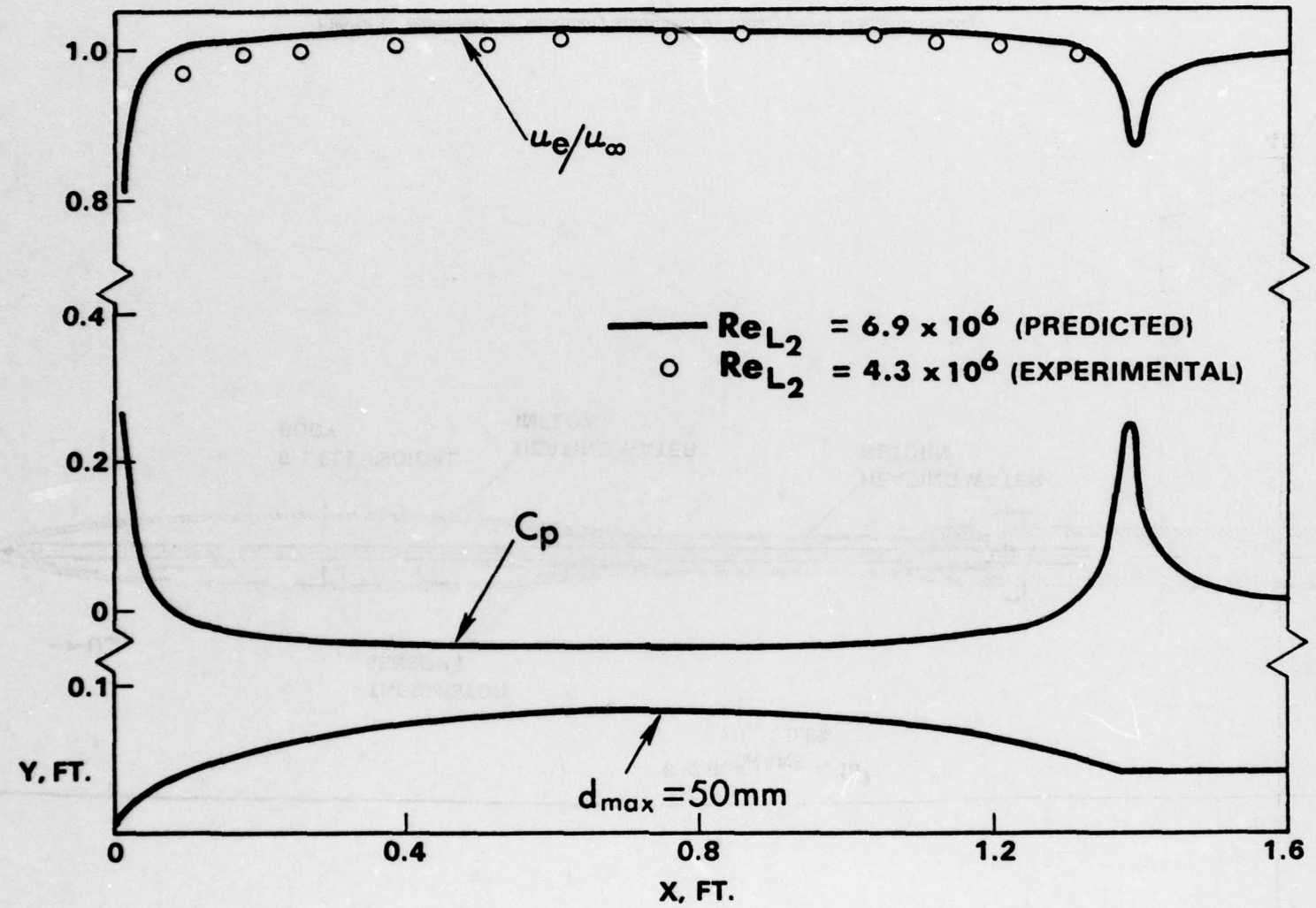

Figure 2. Flowfield characteristics of 9:1 ellipsoid.

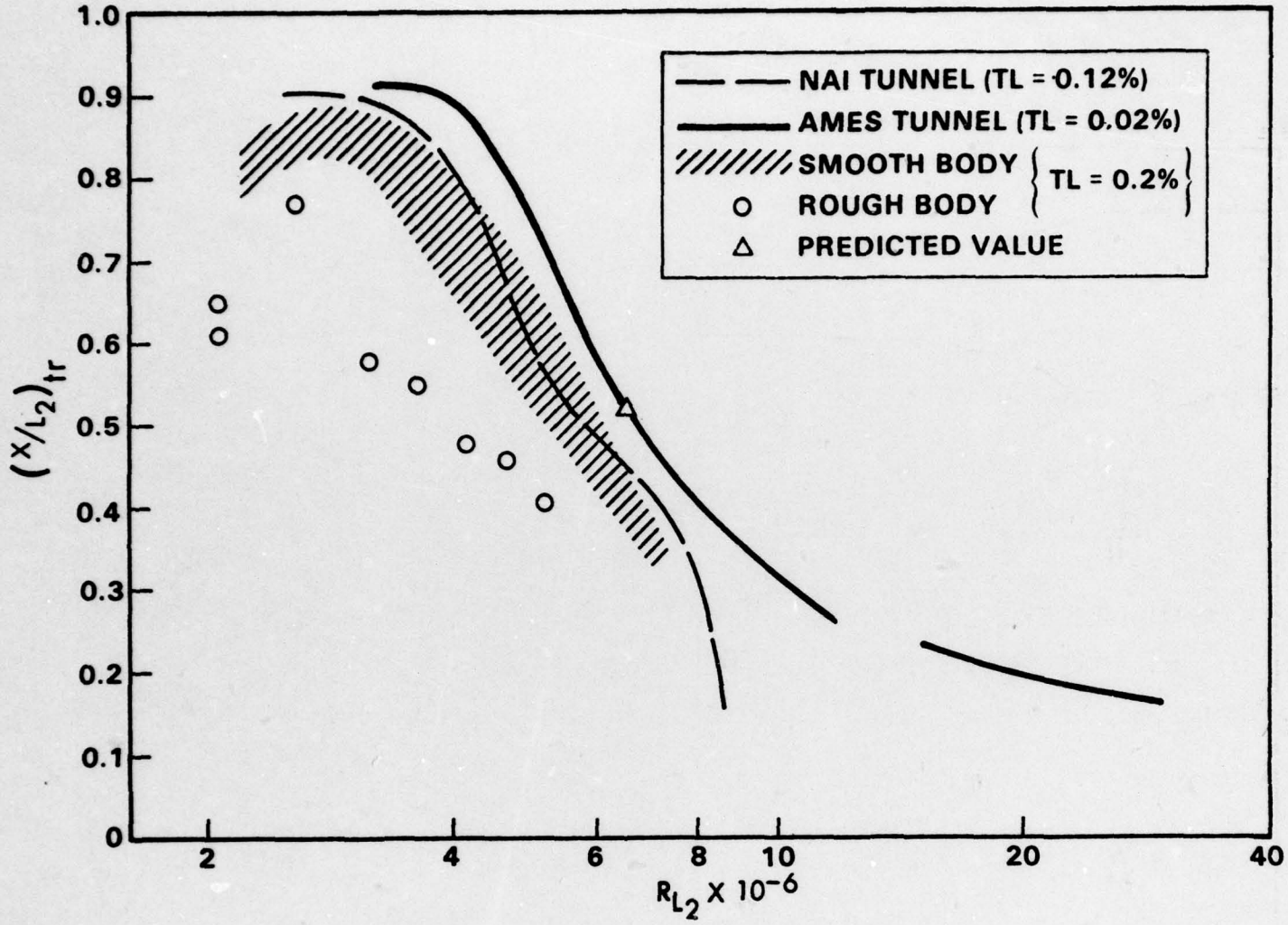

Figure 3. Transition data for smooth and roughened ellipsoids.